



**MONASH** University

**Changes to rainfall regimes in  
north-western Australia in observations  
and climate models**

**Scott William Clark**

BE (Hons), BSc

A thesis submitted for the degree of Doctor of Philosophy at  
Monash University

Submitted 2<sup>nd</sup> May, 2019

School of Earth, Atmosphere and Environment

---

## Copyright notice

©Scott William Clark 2019.

---

## Thesis including published works declaration

I hereby declare that this thesis contains no material which has been accepted for the award of any other degree or diploma at any university or equivalent institution and that, to the best of my knowledge and belief, this thesis contains no material previously published or written by another person, except where due reference is made in the text of the thesis.

This thesis includes 1 original paper published in a peer reviewed journal. The core theme of the thesis is changes to rainfall patterns over north-western Australia in current and future climates. The ideas, development and writing up of all the papers in the thesis were the principal responsibility of myself, the student, working within the School of Earth, Atmosphere and Environment under the supervision of Prof. Michael Reeder.

(The inclusion of co-authors reflects the fact that the work came from active collaboration between researchers and acknowledges input into team-based research.)

In the case of chapter 2 my contribution to the work involved the following:

Thesis Chapter	Publication Title	Status	Nature and % of student contribution	Co-author names, nature and % of co-author contribution	Co-authors Monash student (Y/N)
2	Rainfall regimes over north-western Australia	Published	Conducted research, wrote manuscript, 90%	1) Michael Reeder, supervision and editing, 5% 2) Christian Jakob, supervision and editing, 5%	No, No

I have renumbered sections of the published paper and added sections in order to generate a consistent presentation within the thesis.

**Student Name:** Scott W. Clark

**Student Signature:**

**Date:** 2/5/2019

---

I hereby certify that the above declaration correctly reflects the nature and extent of the student's and co-authors' contributions to this work. In instances where I am not the responsible author I have consulted with the responsible author to agree on the respective contributions of the authors.

**Main Supervisor Name:** Michael J. Reeder

**Main Supervisor Signature:**

**Date:** 2/5/2019

---

## Abstract

Rainfall over north-western Australia has been increasing since the 1950s. Recent research has focused on explaining the trend in terms of large scale modes of variability, however little research has focused on explaining the trend in terms of processes that cause rainfall. K-means clustering is applied to daily rainfall from observations to classify daily rainfall patterns into regimes, demonstrating their link to known synoptic structures and using them to explain the increasing trend in rainfall in the region. After removing tropical cyclones and assigning them to two regimes based on their location, six other regimes are identified. Aside from the two tropical cyclone regimes, the six regimes fall into three other groups: two regimes are associated with localised thunderstorms, two with monsoon lows and two with mid-latitude interactions. The increase in rainfall is dominated by an increase in frequency of tropical cyclones, monsoon lows and mid-latitude interactions at the expense of days with isolated storms, while changes to rainfall intensity associated with these regimes is less important.

The representation of observed rainfall regimes in CMIP5 models is analysed by developing and applying three regime assignment methods to the daily rainfall in the historical period from eight models. When considered together, the three methods allow the models to be ranked according to their ability to replicate the spatial pattern, intensity and frequency of the observed regimes. Models replicate most of the observed regime spatial patterns, but regimes associated with heavy rainfall produce a maximum intensity that is too high, and many models produce too little rainfall over inland parts of the study region. In addition, some models fail to replicate the synoptic patterns responsible for heavy rainfall in the region. The frequency and intensity of tropical cyclone-like vortices is also underestimated across most models.

The model ranking is employed to understand projections of rainfall under the RCP8.5 emissions scenario in CMIP5 models. The eight models used in this work produce differing projections of future rainfall, which does not depend on the model ranking. However, in most cases, changes to the frequency and spatial pattern of rainfall regimes rather than intensity are the main driver of a model's tendency toward wetter or drier conditions. Models are consistent in predicting an increase in intensity of heavy rainfall events, although for most models this is a smaller contributor to the projected trend than frequency changes. Changes to TC frequency and intensity tend to also be relatively minor contributors to the projected trend in each model.

---

## Acknowledgements

Thanks to my supervisors Prof. Michael J. Reeder and Prof. Christian Jakob for their support throughout the last four years, without which this work would not have been possible. I also acknowledge the support of Tony Rafter and Kevin Tory in providing cyclone tracks in CMIP5 models, without which a complete consideration of rainfall patterns in the models in Chapters 3 to 5 in this thesis would not have been possible.

Thanks also to Dr Bhupendra Raut for assistance with the clustering codes underpinning a large part of this thesis.

Thanks to the National Computing Infrastructure (NCI) for computing facilities and hosting data used throughout this work.

I acknowledge the World Climate Research Programme's Working Group on Coupled Modelling, which is responsible for CMIP, and I thank the climate modeling groups (listed in Table 4.1) for producing and making available their model output. For CMIP the U.S. Department of Energy's Program for Climate Model Diagnosis and Intercomparison provides coordinating support and led development of software infrastructure in partnership with the Global Organization for Earth System Science Portals.

This research was supported by an Australian Government Research Training Program (RTP) scholarship, with additional support from the ARC Centre of Excellence for Climate System Science.

Big thanks also to Dr Marc Cheong for going above and beyond in terms of support and guidance through the writing up stage.

Thanks to everyone in the School of Earth, Atmosphere and Environment, and in the Centre of Excellence for Climate System Science for help and support throughout this journey.

Finally, thanks to all friends and family along the way for their support through all of the ups and downs over the past four years.

---

# Contents

<b>1</b>	<b>Introduction</b>	<b>2</b>
1.1	Changes to rainfall in NWA . . . . .	2
1.2	Mechanisms of rainfall in NWA . . . . .	4
1.3	Model representation of rainfall in Australia . . . . .	6
1.4	Tropical cyclones in climate models . . . . .	8
1.5	Research aims . . . . .	9
1.6	Thesis outline . . . . .	11
<b>2</b>	<b>Observed rainfall over north-western Australia</b>	<b>13</b>
2.1	Methods . . . . .	14
2.1.1	Choice of dataset . . . . .	14
2.1.2	Considering tropical cyclones . . . . .	15
2.1.3	K-means clustering . . . . .	16
2.1.4	Composites . . . . .	17
2.1.5	Decomposition . . . . .	18
2.1.6	Extreme rainfall analysis . . . . .	19
2.2	Rainfall regimes . . . . .	19
2.2.1	Choosing the number of regimes . . . . .	19
2.2.2	The regimes in more detail . . . . .	21
2.3	Synoptic patterns . . . . .	26
2.4	Decomposition . . . . .	32
2.5	Sensitivity to TC separation . . . . .	35
2.6	Extreme rainfall . . . . .	37
2.7	Discussion and conclusions . . . . .	40

---

<b>3</b>	<b>Modelled rainfall over north-western Australia: Evaluating ACCESS1-0 against observations</b>	<b>43</b>
3.1	Introduction . . . . .	43
3.2	Methodology . . . . .	45
3.2.1	Rainfall regimes in CMORPH . . . . .	45
3.2.2	ACCESS1-0 and observation data . . . . .	46
3.2.3	Dry day and cyclone removal . . . . .	46
3.2.4	Clustering methods . . . . .	47
3.3	CMORPH rainfall regimes: comparisons to AWAP . . . . .	51
3.3.1	Spatial patterns . . . . .	51
3.3.2	Mapping to AWAP . . . . .	53
3.3.3	Frequency and contribution to total rainfall . . . . .	54
3.3.4	Synoptic patterns . . . . .	55
3.4	Rainfall regimes in ACCESS1-0 . . . . .	58
3.4.1	Assessing the climatology in ACCESS1-0 . . . . .	60
3.4.2	Method I: Projecting model rainfall onto observed regimes . . . . .	61
3.4.3	Method II: Independent clustering of model rainfall . . . . .	67
3.4.4	Method III: Clustering model and observations together . . . . .	77
3.5	Discussion . . . . .	79
3.5.1	Overall assessment of ACCESS1-0 . . . . .	79
3.5.2	Assessment and summary of the regime assignment methods . . . . .	80
3.6	Conclusion . . . . .	82
<b>4</b>	<b>Modelled rainfall over north western Australia: Comparing CMIP5 models to observations</b>	<b>84</b>
4.1	Introduction . . . . .	84
4.2	Data and methods . . . . .	85
4.2.1	Data . . . . .	85
4.2.2	Model assessment methods . . . . .	87
4.3	Results . . . . .	90
4.3.1	Climatological rainfall biases . . . . .	90
4.3.2	Method I: Projecting model days onto observed regimes . . . . .	95
4.3.3	Method II: Independent clustering of model rainfall . . . . .	104

---

---

4.3.4	Method III - Joint clustering of model and observed days . . . . .	119
4.4	Discussion: Overall model ranking . . . . .	125
4.5	Conclusion . . . . .	126
<b>5</b>	<b>Future projections of rainfall regimes over north-western Australia</b>	<b>128</b>
5.1	Introduction . . . . .	128
5.2	Data and methods . . . . .	130
5.2.1	Data . . . . .	130
5.2.2	Future regime determination . . . . .	130
5.3	Trends in mean climate under RCP8.5 . . . . .	132
5.3.1	Trend in the mean rainfall . . . . .	132
5.3.2	Trend in the mean flow . . . . .	133
5.4	Projecting RCP8.5 days to the historical model regimes . . . . .	135
5.4.1	Spatial patterns of projected future rainfall regimes . . . . .	135
5.4.2	Frequency and intensity of projected future rainfall regimes . . . . .	139
5.4.3	Decomposition of rainfall regimes . . . . .	143
5.4.4	Using decomposition to explain trend spatial patterns . . . . .	145
5.4.5	Changes to circulation patterns . . . . .	147
5.5	Independently determined rainfall patterns under a future climate . . . . .	149
5.6	Discussion and conclusions . . . . .	157
<b>6</b>	<b>Summary of key conclusions</b>	<b>160</b>
6.1	Observed rainfall regimes over north-western Australia . . . . .	160
6.2	Evaluating rainfall over north-western Australia in CMIP5 models . . . . .	162
6.2.1	Methods for assigning regimes to model rainfall . . . . .	162
6.2.2	Model evaluation . . . . .	163
6.3	CMIP5 rainfall over north-western Australia: Considering a future climate . . . . .	164
<b>A</b>	<b>CMIP5 historical regimes - full details of spatial patterns and wind fields</b>	<b>A.1</b>
A.1	Projected regimes (method 1) - Spatial patterns . . . . .	A.1
A.2	Projected regimes (method 1) - 850 hPa and 500 hPa wind fields . . . . .	A.4
A.3	Independently determined regimes (method 2) - 850 hPa and 500 hPa wind fields . . . . .	A.18
A.4	Tropical cyclone wind fields . . . . .	A.31

---

---

<b>B</b>	<b>CMIP5 RCP8.5 regimes - details of rainfall patterns and wind fields</b>	<b>B.32</b>
B.1	Projected future regimes - rainfall patterns . . . . .	B.32
B.2	Future regimes from projection method - wind anomalies . . . . .	B.35

## List of abbreviations

- AWAP: Australian Water Availability Project (rainfall dataset)
- CDD: CSIRO Direct Detection
- CMIP5: Coupled Model Intercomparison Project phase 5
- CMORPH: Climate Prediction Center (CPC)-morphing dataset
- ENSO: El Nino-Southern Oscillation
- MCS: Mesoscale convective system
- MME: Multi-model ensemble
- MSLP: Mean sea level pressure
- NWA: North-western Australia
- PV: Potential vorticity
- RCP8.5: Relative concentration pathway 8.5
- SST: Sea surface temperature
- TC: Tropical cyclone
- TCLV: Tropical cyclone-like vortex

# Chapter 1

## Introduction

### 1.1 Changes to rainfall in NWA

Annual precipitation over much of north-western Australia (NWA) has been increasing since the 1950s (Smith, 2004), in contrast with the rest of the continent which has a decreasing trend. Much of the trend in north-western Australia is associated with a statistically significant increase in precipitation over the summer months (Taschetto and England, 2009; Frederiksen and Grainger, 2015), which is when the majority of rainfall in the region is concentrated (Suppiah, 1992). Recent research has aimed to determine the factors influencing the trend in rainfall in this region, although few studies agree on the mechanisms affecting rainfall in NWA. A modelling study by Wardle and Smith (2004) suggested that changes to the land-sea temperature contrast is driving an overall increase in the strength of the monsoon, leading to higher rainfall. Taschetto and England (2009) note that the increasing trend over northern Australia in the summer months is due to enhanced vertical motion in the upper atmosphere, indicating a tendency toward deeper convection. In inland areas they also show that an increase in very heavy rainfall events is partly responsible for the increase in the mean. A study by Rotstayn et al. (2007) used a low-resolution version of the Mk3 CSIRO atmospheric general circulation model (GCM) to demonstrate that the increase in rainfall over the Australian continent is linked to increasing aerosol haze over south-east Asia. However, a later study by Shi et al. (2007) showed that the El Niño-Southern Oscillation (ENSO) relationship in the GCM extends too far west and produces an unrealistic relationship between northern Australian rainfall and SSTs in the Indian Ocean. As a result, the aerosol impact is exacerbated in the model by this unrealistic relationship. Shi et al. (2007)

also showed that the observed rainfall trend may be projected onto two modes of variability: firstly, anomalously low MSLP close to the coast causes an increase in moist air moving over the continent, leading to increased rainfall. Secondly, anomalously high MSLP over the continent causes diminished rainfall east of 130°E, but enhanced rainfall to the west. The sum of the patterns associated with these two modes explains the observed trend well. Feng et al. (2013) describe the anomalous MSLP over NWA as being influenced by anomalously high pressure over the southern Indian Ocean, mainly driven by enhanced SST gradient in the Southern Ocean.

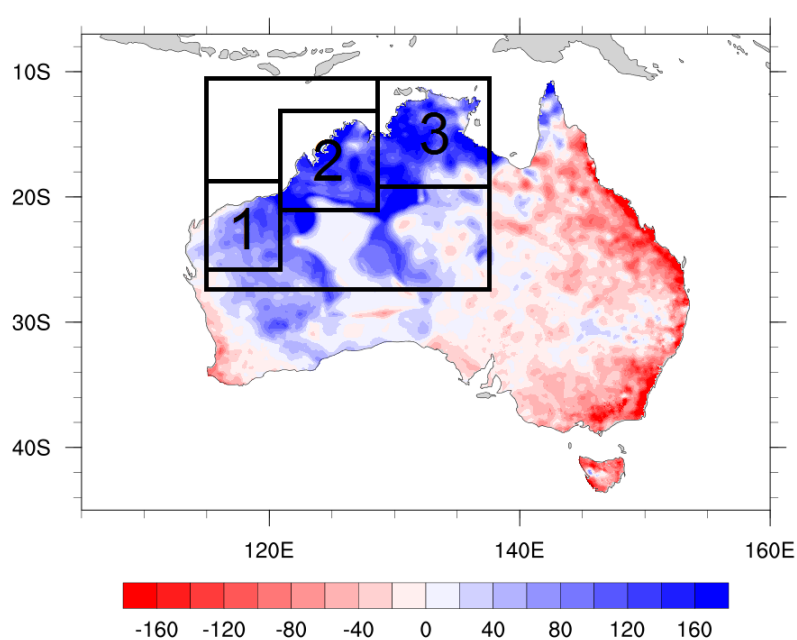


Figure 1.1: Difference in mean annual rainfall over the Australian continent for 1980-2009 vs. 1950-1979. The larger box indicates the study region used throughout this thesis. The numbered boxes indicate regions of interest: 1: Pilbara, 2: Kimberley, 3: Top End.

A study by Evans et al. (2014) showed no significant change in the length of the monsoon season in Darwin since 1979, with the observed trend explained by an increase in the number of active monsoon days at the expense of suppressed days. In contrast, Catto et al. (2012) found that changes in the atmospheric flow regimes over Darwin identified by Pope et al. (2009) have resulted in a lengthening of the wet season, and that changes in frequency of the wettest regimes are the greatest contributor. Emori and Brown (2005) decomposed the trend in modelled rainfall over the globe into dynamic and thermodynamic components, which represent changes in frequency and intensity of rainfall respectively. Over most tropical and subtropical regions where there is an upward trend in precipitation (includ-

ing north-western Australia), the changes are explained by an increase in the thermodynamic (intensity) component of rainfall. Smith et al. (2008) decomposed the total rainfall into rainy season length and average intensity, and arrived at a similar result. For many stations in north-western Australia, the average intensity of rainfall is increasing, with no significant trend in the duration of the wet season.

Overall, research to date provides contrasting evidence on how rainfall is changing in northern Australia. One aim of the work presented in Chapter 2 is to clarify how changes to frequency and intensity of rainfall affect the overall rainfall trend.

## 1.2 Mechanisms of rainfall in NWA

A number of mechanisms are responsible for rainfall in NWA. Even within the rainy season, rainfall is highly variable, with the summer monsoon season characterised by periods of active convection followed by suppressed or "break" periods, associated with changes to the flow associated with the monsoon trough, e.g. Davidson et al. (1983), Holland (1986). Generally, periods of active convection are associated with deep westerly winds over northern Australia, while break periods tend to have an easterly, less humid flow, e.g. (Davidson et al., 1983), (Murphy et al., 2016). Aside from changes to flow associated with the monsoon trough, other structured synoptic systems are responsible for producing rainfall over NWA. Warm cored synoptic systems such as tropical cyclones (TCs) and monsoon lows are some of the mechanisms responsible for rainfall in the region (Reeder and Smith, 1998). TCs are responsible for up to about 10% of the total rainfall in some parts of the region over land (Jiang and Zipser, 2010), although for some stations in NWA up to 40% of rainfall comes from TCs (Ng et al., 2015). In addition, up to half of extreme rainfall along the Pilbara coast is caused by TCs (Lavender and Abbs, 2013). TC frequency is strongly correlated with ENSO during the pre-monsoonal build-up (November-December), however the correlation is far weaker during the monsoon peak (Ramsay et al., 2008). There is conflicting evidence about whether TCs might contribute to the rainfall trend in NWA. Kuleshov et al. (2010) found no significant trend in total TC numbers in the Australian region from 1981 to 2006, nor a significant change in the number of intense TCs. In addition, Ren and Leslie (2015) found no significant trend in the number of TCs over the previous 50 years, although

Lavender and Abbs (2013) suggested that changes to TC numbers in the period 1989-2009 may partially explain the observed increasing trend in rainfall over NWA. Ng et al. (2015) suggested that there has been an increase in the fraction of rainfall from TCs from 1970-2007 at coastal stations, although the trend is not significant along the entire coast. In contrast, Dowdy (2014) found a significant decreasing trend in TC numbers over the Australian region once the effect of ENSO is removed from the data. The present work aims to resolve the discrepancy in changes to NWA TC frequency and intensity reported in the literature, and to determine if the rainfall trend is related to TCs.

Monsoon depressions are also responsible for rainfall in NWA, and together with TCs are special cases of a broader class of synoptic system characterised by coherent potential vorticity (PV) maxima (Berry et al., 2012). The structure of rainfall-producing monsoon depressions in northern Australia is similar to that of Indian monsoon lows, characterised by the PV maximum occurring at around 500 hPa and a warm core existing in the mid to upper levels (Hurley and Boos, 2015). Overall, coherent PV maxima may account for up to 50% of the climatological rainfall in north-western Australia (Berry et al., 2012), and almost all of the extreme rainfall (Hoang et al., 2016). Hurley and Boos (2015) suggested that up to 80% of rainfall occurs within 1000 km of a monsoon low. Coherent PV maxima may also display connections to mid-latitude weather. Wetter conditions over inland parts of NWA tend to be concurrent with negative geopotential height anomalies south of Tasmania (Berry et al., 2011). CMIP5 models also show a link between mid-latitude wave trains and certain phases of the Madden-Julian oscillation (Ackerley et al., 2015).

Mid-latitude Rossby waves also have an influence on the monsoon in northern Australia, initiating up to two-thirds of monsoon bursts in the region (Narsey et al., 2017). During the austral summer, cyclogenesis in the southern Indian Ocean can lead to north-eastward propagation of mid-latitude Rossby waves (Davidson et al., 2007). A trough associated with these waves produces a front-like feature, ahead of which low-level specific humidity increases. As this feature moves towards northern Australia, causing changes to circulation and moisture flux convergence (Narsey et al., 2017). The increased humidity raises CAPE, and thus induces widespread convection (Berry and Reeder, 2016).

The heat low that typically forms over NWA also regulates rainfall. Changes in low-level convergence around the heat low lead to a rainfall pattern characterised by a peak in rainfall rate during the afternoon near the coast, and an overnight peak in inland regions (Berry et al., 2011). Even in the absence of structured synoptic systems, convection also contributes to rainfall in north-western Australia even in the absence of strong synoptic systems. Convection can be isolated or organised into mesoscale convective systems (MCSs) such as squall lines (Reeder and Smith, 1998). MCSs may further organise into superclusters covering large areas (Mapes and Houze, 1992).

While tropical convection, coherent PV maxima and mid-latitude waves have been identified over the region and are known to contribute to the climatological rainfall, the proportions of these contributions have not been quantified. Moreover, the characteristic rainfall patterns resulting from these systems have not yet been determined.

### **1.3 Model representation of rainfall in Australia**

To understand how rainfall is expected to change with rising CO<sub>2</sub> emissions, it is a requirement that general circulation models (GCMs) accurately simulate the mechanisms leading to rainfall in NWA. There has been some focus on how CMIP5 models represent rainfall in the region. The multi-model ensemble for the 5th IPCC assessment report (using all CMIP5 models) shows a large positive bias in mean rainfall over the Maritime Continent, extending to ocean regions just north of the Australian continent (Flato et al., 2014). There is also a slight positive bias over northern and central parts of the Australian continent, although there is large variability between models on the magnitude and sign of the bias. Moise et al. (2015) suggest that CMIP5 models generally overestimate precipitation in inland areas of Australia, although the study region in this thesis only partially covers the sub-regions defined in their study. Krakauer and Fekete (2014) investigated global changes in precipitation over the 20th century in GPCC observations and a multi-model ensemble (MME), and find that over much of the globe including NWA, the sign of the observed trend is captured, but the magnitude is underestimated. Frederiksen and Grainger (2015) focused specifically on NWA due to the statistical significance of the observed rainfall trend, and use an analysis of covariance method on a smaller MME to show that models do capture the leading ex-

ternal modes of variability. However, despite multi-model means capturing observed climate and trends well, there is significant variability between individual models in their ability to simulate the observed climate (Jourdain et al., 2013), with the spread being largest between models from different institutions (Kumar et al., 2013). Models particularly have difficulty reproducing the seasonal cycle in monsoonal and subtropical regions. In central Australia, some models display a summer rainfall peak that is too intense, while others cause the peak to occur either too early or too late (Pascale et al., 2015). The seasonal distribution may also be poorly captured, with the monsoon onset in some models occurring too early and the monsoon retreat occurring too late (Jourdain et al., 2013).

Since there is a large spread in the ability of models to reproduce the observed climate, some models will tend to perform better than others in various locations. Globally, the pattern correlation of precipitation between observations and the GFDL and MIROC models has the highest statistical significance (Kumar et al., 2013). However, when smaller regions are considered and different metrics are used to assess model performance, other models may replicate the observed climate more closely. Over Australia, Moise et al. (2015) considered HadGEM2-ES and ACCESS1-0 to simulate an overall climate that is closest to observations in inland areas (referred to as "rangelands" in their study) based on a score combining surface temperature, precipitation and sea-level pressure. Grainger et al. (2014) utilised modes of variability in the 500 hPa geopotential height over the Southern Hemisphere to rank the models, while Jourdain et al. (2013) ranked the models by considering both their ability to replicate the monsoon rainfall rates in India and northern Australia, and how well the rainfall rates are coupled to ENSO. The use of different metrics across the literature results in different models being ranked highly. Thus the approach used for evaluating model performance and choosing the best models for future predictions should depend on the variables being tested.

In terms of future predictions, models tend to produce an increase in global mean precipitation less than that predicted by the Clausius-Clayperon alone (scaling of precipitation with increased humidity due to temperature increase), implying a weakening of circulation over the tropics (Held and Soden, 2006). However, in northern Australia there is significant variability among models in terms of future predictions of precipitation. A global study by

Knutti and Sedlacek (2013) using the RCP8.5 scenario for all CMIP5 models showed increased precipitation over northern Australia in the summer period by the end of the 21st century, although the trend is not robust. Christensen et al. (2014) summarises changes to Australian monsoon rainfall as small with substantial uncertainties, with little agreement in seasonality across models. Brown et al. (2016) also found little agreement across CMIP5 models, but find that spatial shifts in the circulation over northern Australia determines whether a particular model induces drying or wetting in a future climate. However, by using a subset of the best performing models, there is some consistency in the projected trend under the RCP8.5 scenario. Out of the ten best models determined by Jourdain et al. (2013), seven show significant wetting over northern Australia. In addition, Frederiksen and Grainger (2015) used the 11 best models from Grainger et al. (2014) to find wetting is due to enhanced north-westerly flow over northern Australia in the RCP8.5 scenario. Any trends in rainfall in the best ranked models are not statistically significant under the RCP4.5 scenario. Another aim of this research is to determine how typical rainfall regimes and their synoptic patterns are changing to explain the trend in the models.

## 1.4 Tropical cyclones in climate models

Tropical cyclones (TCs) are an important feature of the northern Australian climate. Most general circulation models have insufficient resolution to resolve the structure of TCs, however even coarse resolution models are able to produce TC-like vortices (TCLVs) (e.g. Manabe et al. (1970), Vitart et al. (1997)). TCLVs in GCMs are detected using a number of criteria including enhanced vorticity, wind and temperature fields consistent with a warm-cored structure and minimum wind speed (Bengtsson et al., 1995; Nguyen and Walsh, 2001). However, the observed wind speed threshold used to define a TC requires a tight pressure gradient that a coarse resolution GCM is unlikely to be able to produce (Walsh et al., 2004). The wind speed threshold for detecting a TCLV in a model must therefore depend on model resolution. The maximum wind speed threshold to define a TCLV has been found to be approximately linear with grid size (Walsh et al., 2007), with a horizontal resolution of approximately 60 km or better ideal for detecting TCs with the wind speed most closely resembling that of observed TCs (Murakami and Sugi, 2010). Most CMIP5 models have resolutions lower than this, therefore most TCLV detections require a resolution, and

therefore model, dependent threshold.

To simulate the number and strength of TCs in the present climate, recent studies have performed downscaled simulations of TCLVs. Earlier downscaled simulations show that model TCLV numbers depend strongly on the type of downscaling and model used (Lavender and Walsh, 2011), and thus there is some uncertainty in the ability of models to simulate current TC numbers. Studies have also projected TC activity in a future climate. Globally, there is expected to be a reduction in TC frequency, which is more robust in Southern Hemisphere basins, although there is likely to be an increase in rainfall intensity from each storm (Knutson et al., 2010). Knutson et al. (2015) found a statistically significant decline in the number of TCs in the South Indian Ocean region under the RCP4.5 emissions pathway, although near NWA the change in the number of storms is slightly smaller. They also find an increase in the frequency of high intensity (category 4-5) storms, however the increase is not statistically significant. Utsumi et al. (2016) suggested that TC genesis will decline greatly in the South Indian Ocean region in a future climate, although the contribution to rainfall per TC is expected to increase. Lavender and Walsh (2011) also noted that the number of TC days in the Australian region is expected to decrease by the end of the 21st century by using a downscaled model, and agreed that the frequency of the highest intensity storms is expected to increase slightly. Murakami and Sugi (2010) noted that changes to the number of TCs are not strongly resolution dependent, and therefore even low resolution ensembles may produce a reasonable estimate of changes to the number of TCs in a future climate. Conversely, downscaled simulations by Emanuel (2013) suggested that the number of TCs globally will increase in a high-emissions future scenario, with significant increases over parts of the South Indian Ocean, including near NWA. He also suggested that downscaled simulations may produce a differing result to low-resolution simulations. One aim of the present work is to determine how TCLVs contribute to simulated changes in rainfall in NWA.

## **1.5 Research aims**

This work focuses specifically over NWA due to the statistically significant increase in rainfall since the 1950s. While research has found that NWA rainfall has increased, and some synoptic systems responsible for rainfall have been identified, the connection between rainfall, the systems responsible for rainfall and the rainfall trend has not been established.

Investigations using CMIP5 models have shown differences in future projections of rainfall over NWA, which depend on changes in overall circulation patterns. However, these changes may also depend on changes to specific rainfall patterns and synoptic systems, which has not yet been established. To this end, it is also important to determine how well CMIP5 models replicate observed rainfall and synoptic patterns in the historical period.

The aims of this research are:

1. To determine the regimes and associated synoptic patterns responsible for rainfall over north-western Australia.
2. To attribute the observed rainfall trend over north-western Australia to changes in the observed rainfall regimes.
3. To determine how well climate models are able to replicate the observed rainfall regimes.
4. To determine how rainfall changes over north-western Australia in a future climate relate to changes in rainfall regimes.

The specific questions to address these aims are:

1. What are the patterns of typical daily rainfall over north-western Australia?
2. What are the synoptic patterns responsible for these rainfall patterns?
3. How do tropical cyclones contribute to the observed rainfall in NWA?
4. Which patterns have been changing in frequency and/or intensity?
5. How have changes to frequency and/or intensity affected the observed rainfall trend?
6. Which patterns are responsible for extreme rainfall?
7. How can we assign daily rainfall patterns in CMIP5 models to observed weather systems?
8. How well do CMIP5 models capture the observed rainfall patterns and weather systems over NWA?
9. How might rainfall over NWA change in a future climate in terms of frequency and/or intensity of rainfall and associated synoptic systems?

Research question 1 will be addressed by performing K-means clustering on gridded daily rainfall data for the period 1950-2010 from the Australian Water Availability Project (AWAP). The region chosen for this work is from 115-137°E and 10-28°S and is outlined in Figure 1.1. This region is chosen as it encompasses the majority of the AWAP is based on rain gauge observations which are only available over land and are sparse in inland parts of the study region, however it is chosen for its long record over spatial completeness in order to address questions 2 to 5. Question 2 will be addressed by calculating composites of low and mid level wind fields, specific humidity, K-index and potential vorticity for each pattern from ERA-Interim reanalysis data from 1979-2010.

Research question 6 will be addressed by comparing regimes determined in a single CMIP5 model, ACCESS1-0, to observed regimes determined from the Climate Prediction Center (CPC)-morphing (CMORPH) dataset. CMORPH data are available at 0.25 × 0.25 degree resolution from 1998-2016 and are based on satellite measurements, and are therefore spatially complete. Daily rainfall in ACCESS1-0 are assigned regimes using three methods: projecting model rainfall to observed regimes, independent clustering of model rainfall and combining model and observed rainfall into one dataset before clustering. The three methods provide different details about the spatial pattern, frequency and intensity of the model regimes which makes assessment of multiple CMIP5 models possible in order to answer question 7. Research question 8 is answered by using daily rainfall from the RCP8.5 scenario the same CMIP5 models, and using the first two regime assignment methods to indicate changes to frequency and intensity of the regimes in each model.

## 1.6 Thesis outline

Chapter 2 describes rainfall regimes in the observations and attributes rainfall changes to changes in the frequency and intensity of individual regimes. Much of the work in Chapter 2 forms the basis of Clark et al. (2018). K-means clustering is applied to daily gridded rainfall data spanning 60 years. The synoptic systems associated with the resulting rainfall regimes are determined and characterised, and the trend in rainfall is attributed to changes in the frequency and intensity of the individual regimes using a decomposition technique. A brief analysis of how extreme rainfall events are caused by specific regimes is undertaken.

In Chapter 3, three regime assignment methods are developed for the purpose of comparing rainfall regimes in CMIP5 models to the observations. We test the methods on the historical run in ACCESS1-0, and thoroughly analyse the ability of this model to replicate the observed rainfall regimes in the region. Biases relative to the observed climatological mean are considered in addition to changes to the frequency, intensity, spatial patterns and synoptic patterns of the regimes in ACCESS1-0 relative to the observations.

Chapter 4 utilises the three regime assignment methods to assess the performance in the region of seven other CMIP5 models. Metrics for comparing models are developed to provide a quantitative measure of the model performance in simulating the regime spatial patterns and frequency in replicating the overall observed climate. The ability of each model to reproduce the observed regimes with the correct frequency, intensity and low level winds is considered with the aim of informing future predictions.

In Chapter 5, NWA rainfall in the late 21st century under the RCP8.5 scenario is considered. Changes to mean rainfall and to rainfall regimes are determined using a similar decomposition technique to that used in Chapter 2. Changes to spatial patterns are also considered. Finally, Chapter 6 summarises the key findings of this thesis and suggests avenues for further research.

## Chapter 2

# Observed rainfall over north-western Australia

As discussed in Chapter 1, rainfall has been increasing over north-western Australia (NWA) since the 1950s, especially over the summer months (Smith, 2004; Taschetto and England, 2009; Frederiksen and Grainger, 2015). Recent studies have aimed to explain the increase in the region by considering mechanisms such as changes in overall circulation. These include changes to the land-sea temperature contrast (Wardle and Smith, 2004), and anomalously low mean sea level pressure (MSLP) over NWA (Shi et al., 2007) which may be linked to stronger high pressure systems over the southern Indian Ocean (Feng et al., 2013). Changes to the wet season length are also considered, with contrasting evidence regarding changes to the wet season length (e.g. Catto et al. (2012), Evans et al. (2014)). The key aim of this chapter is to explain the observed trend in rainfall in terms of typical rainfall patterns and synoptic regimes that cause rainfall in the region.

Mechanisms that cause rainfall in northern Australia have been documented. In the study region for this thesis, tropical cyclones (TCs) are responsible for around 10% of rainfall on average, but this fraction greatly increases in the Pilbara region (Lavender and Abbs, 2013). Coherent potential vorticity (PV) maxima, which include monsoon depressions and TCs, also contribute greatly to the total rainfall in the region (Berry et al., 2012), as does tropical convection which may be organised (Reeder and Smith, 1998; Mapes and Houze, 1992). Mid-latitude Rossby waves can also initiate rainfall in inland areas, and are a key influence on initiating active phases of the monsoon (Narsey et al., 2017). While mechanisms causing

rainfall over NWA have been identified, there is a need to quantify how they contribute to rainfall in the study region.

K-means clustering has been used in many previous studies to classify datasets into typical patterns. Raut et al. (2014) used K-means clustering on daily rainfall over south-western Australia to determine five typical rainfall patterns, and constructed composites of wind, mean sea level pressure and geopotential height fields to characterise the rainfall regimes in that region. A similar approach is taken in this chapter, with clustering performed on daily rainfall data in the region shown in Figure 1.1, and composites of important variables constructed for each resulting regime.

Section 2.1 discusses the data and methods used to determine the observed rainfall regimes, including how the influence of TCs is removed from the rainfall record to determine how other synoptic patterns initiate rainfall in NWA. In Section 2.2 we show how the regime patterns change between different choices of the number of clusters, before settling on a specific number and describing the spatial patterns in more detail. The synoptic patterns for the rainfall regimes are discussed in detail in Section 2.3. Changes to overall mean rainfall are attributed to changes in the frequency and intensity of individual regimes in Section 2.4. A brief overview of a similar analysis without TC separation is presented in Section 2.5, and extreme rainfall events in the region are linked to the regimes in Section 2.6. Finally, the results are discussed and summarised in Sections 2.7.

## **2.1 Methods**

### **2.1.1 Choice of dataset**

To determine the rainfall regimes over north-western Australia, firstly we need to investigate the patterns of rainfall typical of the region. Daily rainfall patterns may come from a range of datasets, which have different advantages and disadvantages. The Australian Water Availability Project (AWAP) (Jones et al., 2009) dataset contains gridded daily rainfall from 1900-2010 over the entire Australian land area at  $0.05 \times 0.05$  degree resolution, and is based on ground measurements. The high spatial resolution of the data is desirable for the precise determination of regimes, and the long period of coverage allows the entire increasing trend

to be examined. However, the ground-based nature of this dataset may cause problems as the study region contains areas with few observing stations. The sparse nature of the observing network may have a large effect on the validity of the dataset, especially when stations are added or removed from the observation network, and thus rainfall data in remote inland locations must be interpreted with care (King et al., 2013). A diamond-shaped region over north-western Australia centred around 22°S and 125°E appears to receive no rainfall over the entire 60 year period, producing a region of zero rainfall trend visible in Figure 1.1. This region contains no rain gauges, thus the data over NWA is spatially incomplete.

The Climate Prediction Centre (CPC) morphing (CMORPH) dataset provides daily rainfall from 1998-2016 using microwave satellite observations (Joyce et al., 2004). In this thesis, the raw data with no adjustment to gauge observations is used. As a result the data are available over all regions from 60°S to 60°N including over the ocean. This avoids the problem of using the land as an arbitrary boundary when considering synoptic systems, as well as allowing complete coverage of the entire land area in the study region. However, the data is of lower resolution (0.25 degrees) and covers a much shorter period which makes examination of long term trends since the 1950s impossible.

As the desired outcome is to create links between rainfall patterns and the rainfall trend, a longer record is of greater importance than a spatially complete record for the purposes of the work in this chapter. Thus for determining the observed rainfall regimes, AWAP has been chosen for the analysis throughout this chapter. As the upward rainfall trend has existed since 1950, this will be the starting point for the analysis giving 61 full years of daily rainfall data. Rainfall regimes in either dataset are mostly similar in spatial pattern, with some differences which may be the result of the missing data in AWAP. The differences between regimes determined from each dataset are discussed further in Chapter 3.

### **2.1.2 Considering tropical cyclones**

There are a range of synoptic systems that generate rainfall over north-western Australia (see Section 1.2). Tropical cyclones (TCs) are one such type of system which is responsible for over 20% of climatological rainfall in some parts of north-western Australia, especially near the Pilbara region (Jiang and Zipser, 2010). It is possible that the spatial rainfall pat-

terns created by TCs may resemble patterns created by systems other than TCs. As a result, the synoptic patterns associated with the rainfall regimes may consist of a combination of TC and non-TC characteristics. To separate the effects of these types of synoptic patterns, it is desirable to remove the influence of TCs from the rainfall record before finding regimes.

To this end, any day on which a TC is present anywhere in the study region is removed from the rainfall record used for clustering. This simple method may exclude days where the TC is far offshore, and thus unlikely to have an influence on rainfall over the land. While a more refined method may exclude TCs on basis of proximity to the coast, this may cause TCs to be included in the wind and PV composites produced later. As the aim is to be certain there are no TC days in the record, rather than inspect the TC days themselves in any great detail, the simple method is sufficient for the purposes of this study. TC tracks were taken from the International Best Track Archive for Climate Stewardship (IBTrACS) (Knapp et al., 2010) and are available at 6 hour resolution. The dates of any TC that occurs in the study region are taken, and the corresponding days in the AWAP rainfall record are separated, and sorted into two "TC regimes": a west and east regime depending on whether the cyclone is west or east of 126°E (a line dividing the study region in half). The cyclone regimes shown in Figure 2.2 are calculated as the mean of all rainy days in each TC regime. These are not regimes in the sense outlined in Subsection 2.1.3, however they can be used to assess how various synoptic patterns contribute to the total rainfall.

### **2.1.3 K-means clustering**

Following the separation of tropical cyclone days, the daily rainfall observations are further refined by removing dry days. This allows us to separate days with low precipitation from those which are effectively dry. A dry day was defined as per Raut et al. (2014), as a day on which the spatial average is less than 0.1 mm. The remaining daily rainfall observations are clustered using a K-means clustering algorithm. The algorithm partitions a set of vectors (the gridded rainfall data) into  $k$  subsets or clusters, where similar vectors will be placed in the same cluster as their Euclidean distance will be small. The mean of all vectors in a cluster produces a centroid, thus showing the average rainfall pattern for a regime. The number of clusters must be chosen with care: too many clusters tend to produce patterns

that are similar in spatial distribution, and may represent the same type rainfall event with different intensity or a slightly different position. Too few clusters will not capture all of the typical rainfall patterns that occur in the region. Once the regimes are identified from the clustering, the seasonal distribution and synoptic patterns can be identified from the regimes.

#### 2.1.4 Composites

Composites of various atmospheric variables are constructed to illustrate the synoptic patterns associated with each regime. The variables presented here are the wind at 900 hPa and 700 hPa, potential vorticity (PV) at 315 K, specific humidity at 900 hPa, 200 hPa meridional wind and K-index<sup>1</sup>. The K-index is defined by George (1960) as a measure of air-mass thunderstorm potential, and is defined by:

$$K = (T_{850} - T_{500}) + T_{d,850} - (T_{700} - T_{d,700}) \quad (2.1)$$

where the number in the subscript of each term denotes the pressure level and the subscript  $d$  denotes a dew point temperature. George (1960) defines an air mass thunderstorm as one "developing in areas of weak winds without apparent frontal or cyclonic influence". As will be discussed later, some of the regimes identified do involve cyclonic or frontal influence. The aim of using the K-index in this instance is to differentiate between regimes that do not have such an influence. Values of the K-index less than 20 are said to indicate no potential for thunderstorms, whereas values above 35 may result in "numerous, scattered thunderstorms".

The composites are produced from the ERA-Interim reanalysis dataset (Dee et al., 2011), available at  $0.75 \times 0.75$  degree resolution. The composite is calculated as the mean of a variable (e.g. wind) over all days in each regime. Dry days are composited separately and labelled as belonging to cluster 0. As the ERA-Interim dataset begins in 1979, only slightly more than half of the study period is covered, and thus the composites are an average of only all days in the regime that occur during or after 1979. Overall, each regime contains at least 200 days, and some regimes contain more than 500.

The 500 hPa wind and 315 K PV composites for 2 days prior (day -2) and 2 days following (day 2) a regime day are also calculated. As a given regime may persist for a number of

---

<sup>1</sup>The K in K-index has no relation to the K in K-means clustering.

days, the day -2 composites only include the days which are 2 days prior to the first day in a series of a particular regime. Similarly, the day 2 composites are calculated from the second day following a series of a particular regime. This prevents the composites from including days from the regime itself. For example, in a 7 day period, the corresponding sequence of regimes may be:

$$1, 2, 4, 4, 4, 2, 3 \quad (2.2)$$

For the composite for regime 4, day -2 will only include 2 days prior to the first day in regime 4 (that is, the first day in this sequence), and not 2 days prior to the second or third day in regime 4. Similarly, day 2 only includes the data 2 days after the last day in the sequence (ie. the last day the sequence, corresponding to regime 3.) As a result, the lag composites give an overview of the conditions leading up to and following a rainfall regime.

### 2.1.5 Decomposition

To link the clusters to rainfall changes, the total rainfall changes are decomposed into a change associated with a change in the frequency and a change associated with a change in the intensity of each cluster according to the expression:

$$\bar{P}_2 - \bar{P}_1 = \sum_{i=1}^N [(f_{2,i} - f_{1,i})P_{1,i} + (P_{2,i} - P_{1,i})f_{1,i} + (P_{2,i} - P_{1,i})(f_{2,i} - f_{1,i})] \quad (2.3)$$

where  $f_i$  represents the frequency of regime  $i$  and  $P_i$  represents its precipitation. The subscript  $i$  denotes the regime number, and  $N$  the number of clusters. The subscripts 1 and 2 represent the time periods 1950-1979 and 1980-2009 respectively, and overbars indicate time averages over these periods. The first term in the sum represents the change in precipitation associated with changes in the regime frequency, the second represents changes associated with changes in the regime intensity and the third is the cross term representing changes in precipitation due to changes in both frequency and intensity. This third term is usually small enough to ignore for small changes, and this is true in the case of this analysis. The size of the terms for each regime will identify which regimes contribute to the change in rainfall, as well as identify whether those contributions are due to changes in intensity or frequency (or both) of those contributing regimes.

### 2.1.6 Extreme rainfall analysis

To examine extreme rainfall, the threshold at which a rainfall occurrence can be considered extreme needs to be identified. It is standard practice to use a ranking system, where the top 5% or 1% (ie. 95th or 99th percentile) of occurrences is examined, however the definition of an occurrence must also be determined. An extreme occurrence is defined here as the 99.9th percentile of all non-zero points in the record of all wet days (defined in Section 2.1.3). An extreme day is defined as any day containing at least one extreme point within the study region, hence an extreme day may contain multiple points. Once the threshold is determined and extreme days determined, the trend in the number of days per year since 1950 is examined. The regime associated with each extreme day is also determined. Assignment of extreme days to regimes is done in two ways: first the regime each extreme fell into is determined, and the average number of extreme days in each regime per year is calculated. Second, the probability of a given regime producing an extreme day is calculated. The two distributions will be different as each regime contains a different number of days, and therefore a regime that does not occur often could be more likely to produce an extreme day than a common regime, even though they have the same number of extreme days per year.

## 2.2 Rainfall regimes

### 2.2.1 Choosing the number of regimes

Figure 2.1 shows the non-cyclone rainfall regimes produced from clustering. Each number represents the number of clusters set in the algorithm. The 4-cluster case produces a regime with light rainfall, and 3 regimes with heavier rainfall in different locations. As we progress to 5 clusters, one of the heavier rainfall clusters splits into a less heavy and a more heavy regime, with the more heavy regime similar in intensity to the other 2 heavy regimes. The less heavy regime is still higher in intensity than the light rainfall regime. When examining the 6-cluster case, a new heavy regime emerges in the western part of the study region, while the remaining regimes remain similar in shape.

The 7-cluster case produces another regime with a rainfall maximum in the northernmost part of the continent. As this looks similar to other regimes in this area, only distinguishing

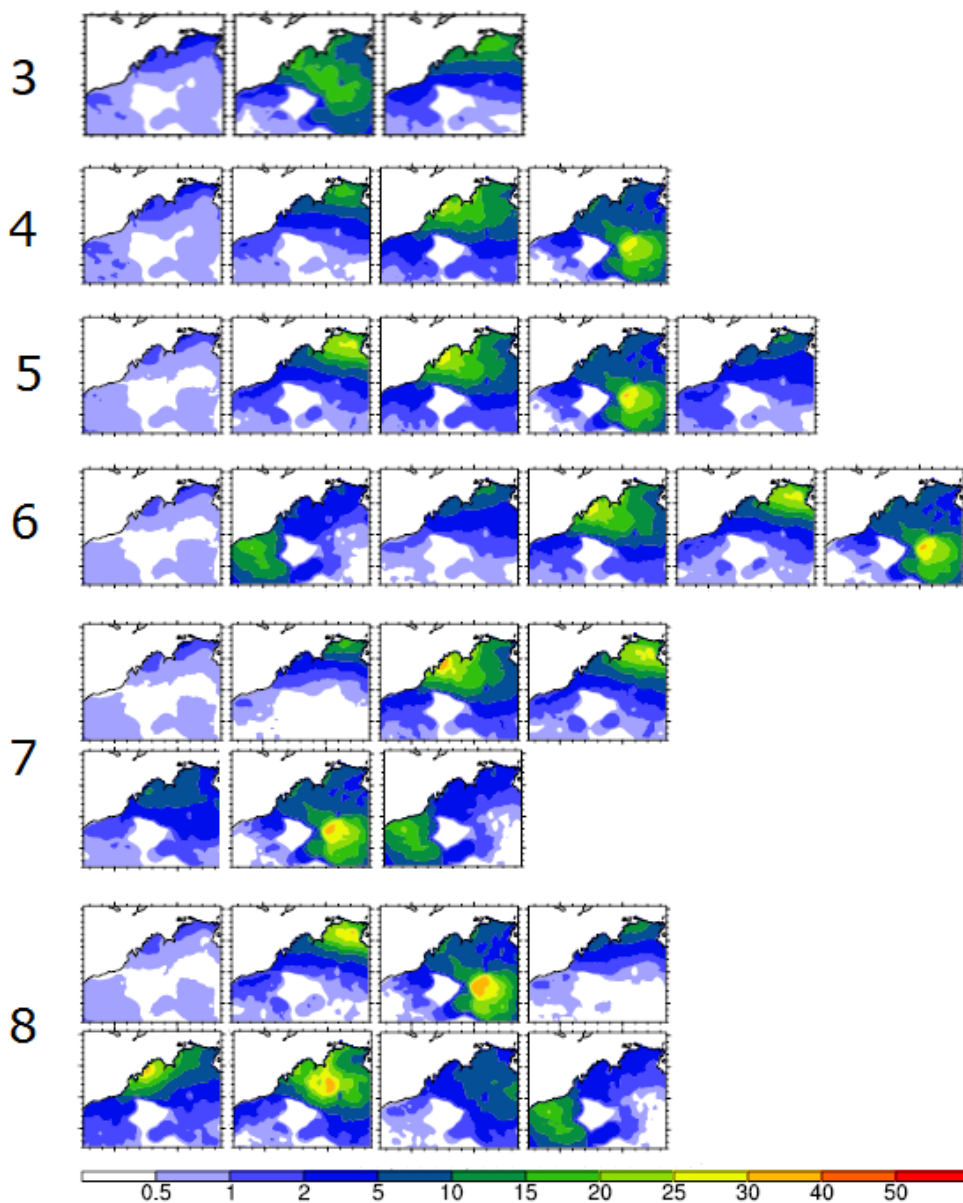


Figure 2.1: The rainfall patterns produced in AWAP from setting the number of clusters as 4 through to 8. Units are in  $\text{mm day}^{-1}$ .

itself by its intensity, this additional regime provides negligible additional information about the spatial nature of the rainfall regimes. Finally, the 8-cluster case appears to have split the inland regime into a heavier, further inland regime and a lighter regime in the far eastern end of the study region. This additional regime is also unlikely to provide extra information about the nature of rainfall in the region, thus this case also does not add much extra information relative to the previous cases.

As described in the methodology, the ideal number of regimes may be found by deter-

mining the largest number of regimes that look as different from each other as possible. Based on this criterion, the 6-cluster case will be used to describe the rainfall regimes and their synoptics over north-western Australia.

## 2.2.2 The regimes in more detail

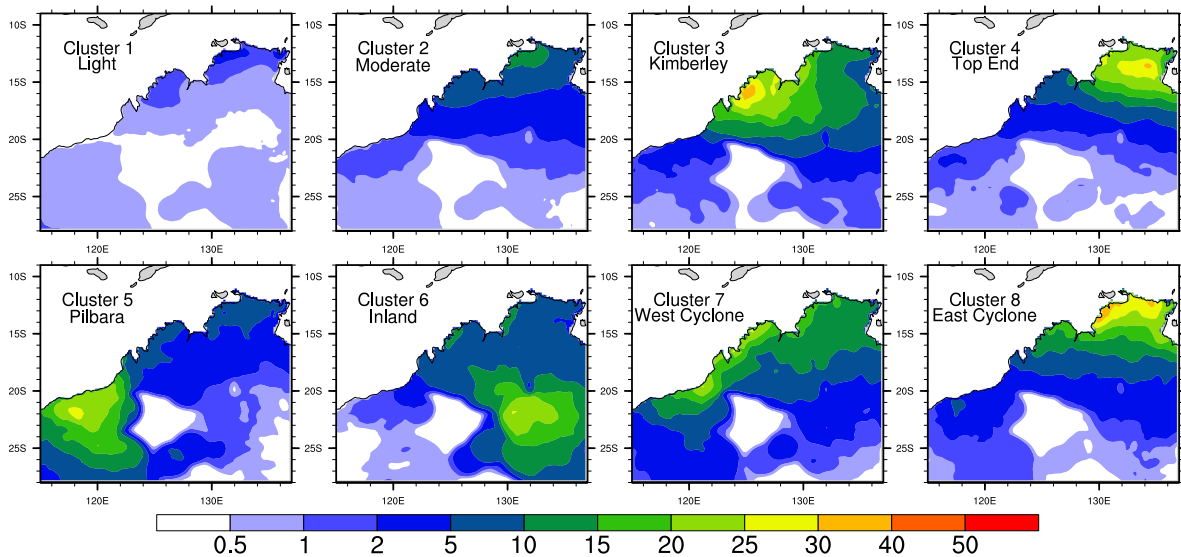


Figure 2.2: Centroids of the clusters corresponding to the rainfall patterns, plus the two TC regimes. Units are in  $\text{mm day}^{-1}$ .

The six cluster case outlined in the previous subsection, plus the two TC regimes calculated as per Subsection 2.1.2 make up the eight rainfall regimes shown in Figure 2.2. The first regime, to be referred to as the Light regime, represents 65% of all rainy days and is thus the most frequently occurring regime. The regime is characterised in the average map by light ( $< 5 \text{ mm day}^{-1}$ ) rainfall over far northern Australia and less than  $1 \text{ mm day}^{-1}$  over much of the rest of the region. However, typical days in this regime tend to consist of isolated patches of moderate ( $> 10 \text{ mm day}^{-1}$ ) rainfall which change location from day to day. These patterns usually correspond to the formation of isolated thunderstorms, which is a far more likely mechanism for rainfall in this region rather than widespread light rain as the map would suggest. Figure 2.3 shows the probability density function (PDF) of the fraction of the study region covered with rainfall greater than 1 mm in each regime. There is a sharp peak at approximately 0.05 for the Light regime, highlighting the isolated nature of the rainfall on most days in this regime. The map is an average of many (more than 5000)

such days, thus spreading the rainfall over a wider area in the average.

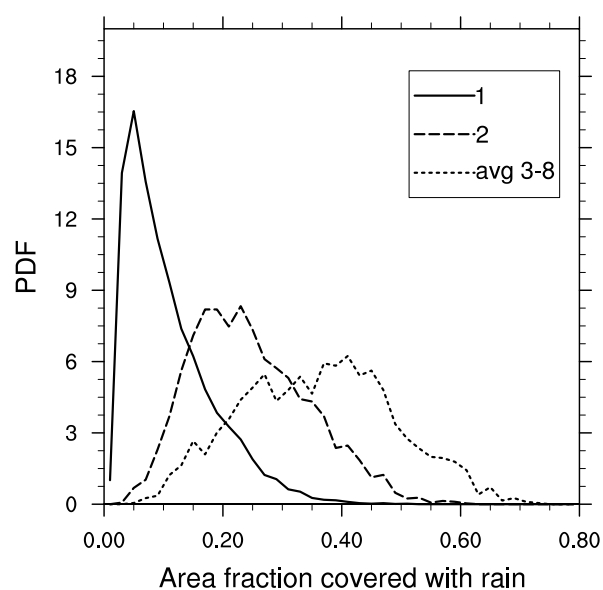


Figure 2.3: Probability density function of fraction of land area of region covered by rainfall under each rainfall regime.

The second regime, called the Moderate regime, occurs on 20% of all rainy days and has a spatial pattern characterised by larger totals (up to 15 mm), but the shape of the pattern is similar to the Light regime. Days in this regime tend to consist of slightly more widespread (though patchy) rainfall, though less widespread than in the remaining regimes, as may be seen in the PDF in Figure 2.3. This regime also consists of thunderstorms, although these are more widespread than the Light regime, and may lead to localised heavy totals. These may lead to extreme rainfall, which will be discussed in Section 2.6.

The PDFs of regimes 3-8 are similar, and thus Figure 2.3 shows their merged distribution for simplicity. The peak is broad, with a maximum at approximately 0.4, which demonstrates the widespread nature of rainfall in these regimes. The third, fourth and fifth regimes show strong rainfall maxima (up to 40 mm day<sup>-1</sup>), and lie close to the coast in the Kimberley region, over the Top End and in the Pilbara regions respectively. These regimes are thus called the Kimberley, Top End and Pilbara regimes respectively. The sixth regime has a rainfall peak slightly lighter than the preceding three regimes, although is unique in showing a rainfall maximum far inland. The regime is therefore called the Inland regime.

The west cyclone regime shows coastal rainfall along a long stretch of the Pilbara and Kimberley, although it is less than what might be expected from a TC (less than 30 mm day<sup>-1</sup>). TCs rarely make landfall at the same location, thus the average map for the west cyclone regime shown in Figure 2.2 may be regarded as an average across multiple landfalling locations, similar to the light regime being regarded as an average of numerous thunderstorms in different locations. The east cyclone regime may have also had a similar occurrence, although the rainfall maximum is higher in this regime. The rainfall pattern appears highly similar to the Top End regime, although the maximum is slightly higher (30-40 mm day<sup>-1</sup>) and occurs closer to the coast as would be expected when TCs make landfall.

Table 2.1 summarises the percentages of rainy days that each regime constitutes, and the contribution of each regime to the total rainfall of the region. Regimes 3-8 constitute less than 4% of rainy days each, and together comprise only around 14% of all rainy days. However, these regimes contribute around 45% of the total rainfall of the region. 12.2% of the total occurs when there is a TC in the region, despite accounting for less than 4% of rainy days. Taking the Light and Moderate regimes together, slightly more than half of the climatological rainfall arises from local scattered (or isolated) thunderstorms, with the remaining half arising from regimes producing widespread rainfall.

The seasonal frequency of the occurrence of all regimes is shown in Figure 2.4. The prominence of the wetter regimes over the austral summer is expected, as the majority of climatological rainfall occurs during this time. The prominence of dry days in the austral winter is also expected for the same reason. The light regime is more evenly distributed throughout the year, although there is a maximum in the austral spring corresponding with

Table 2.1: Summary of the proportion of rainy days and the contribution of each regime to the spatial average rainfall.

Regime	Proportion of rainy days	Contribution to rainfall
Light (1)	65.1%	27.1%
Moderate (2)	20.9%	27.9%
Kimberley (3)	2.9%	10.2%
Top End (4)	3.6%	8.8%
Pilbara (5)	1.5%	4.7%
Inland (6)	2.2%	8.1%
West cyclone	2.2%	7.5%
East Cyclone	1.6%	4.7%

the pre-monsoonal build-up. This suggests that either isolated thunderstorms are able to form during winter under the right conditions, or rainfall could occasionally move along southern parts from mid-latitude cold fronts.

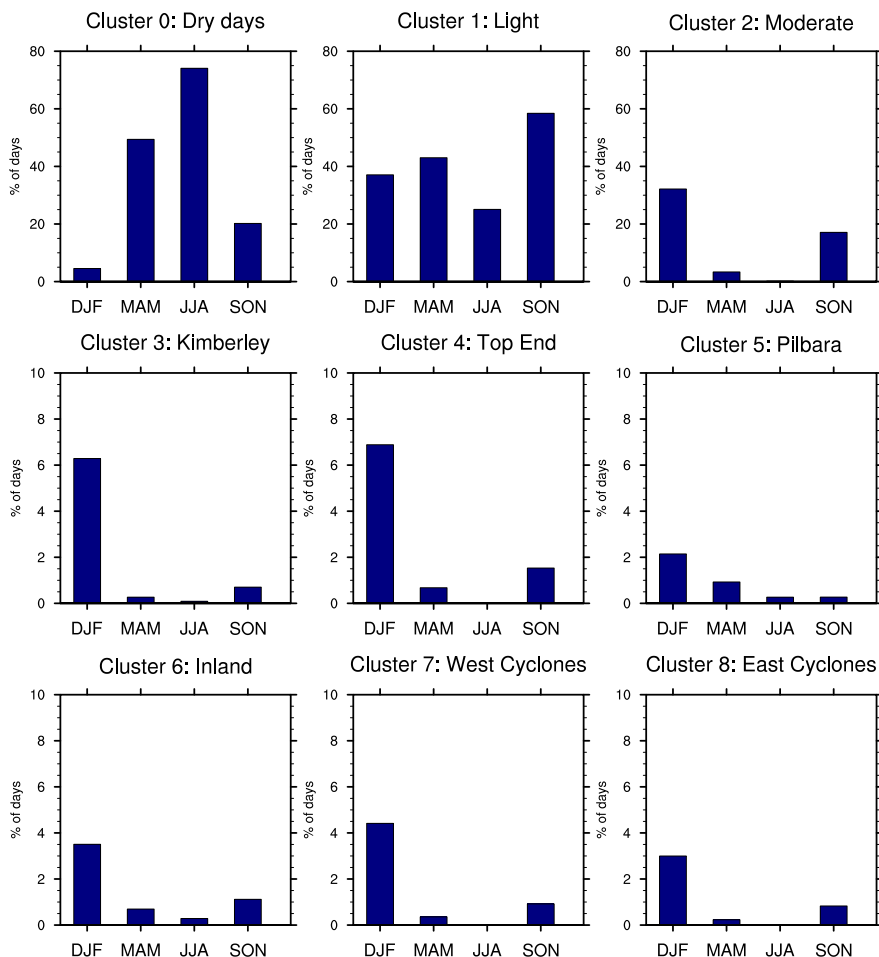


Figure 2.4: Distribution of the percentage of days in each regime occurring in each season.

It might be thought that the regimes presented thus far could be interpreted as movement of a single synoptic system between locations, causing heavy rainfall at different locations. For example, a synoptic system over the Top End causing heavy rainfall could readily move to the Kimberley, and thus be in a new regime. To test this idea and understand how regimes transition between each other, Figures 2.5 and 2.6 show the probability of transition to any regime after 2 and 3 days respectively, given any day in that particular regime. The figures show that after 2 days, a dry day will normally continue to be dry, followed by transitioning to the light regime. This is expected as most of the dry days are in winter, where there are lengthy periods without rain. Many dry days also occur in spring during the "build-up"

season, where it is possible that dry days and Light regime days may alternate in some way. The Light and Moderate regimes are most likely to transition within themselves after 2 or 3 days, indicating these regimes are typical of the majority of days over the build-up and summer monsoon season. Regimes 3-8 are also most likely to transition to the moderate or light regimes within 2-3 days, or to themselves. Transitions between regimes 3-8 are relatively unusual and random, thus indicating that the majority of heavy rainfall regimes may be initiated by synoptic systems that are relatively short lived, or move offshore rapidly. The synoptic patterns will be discussed in the next section.

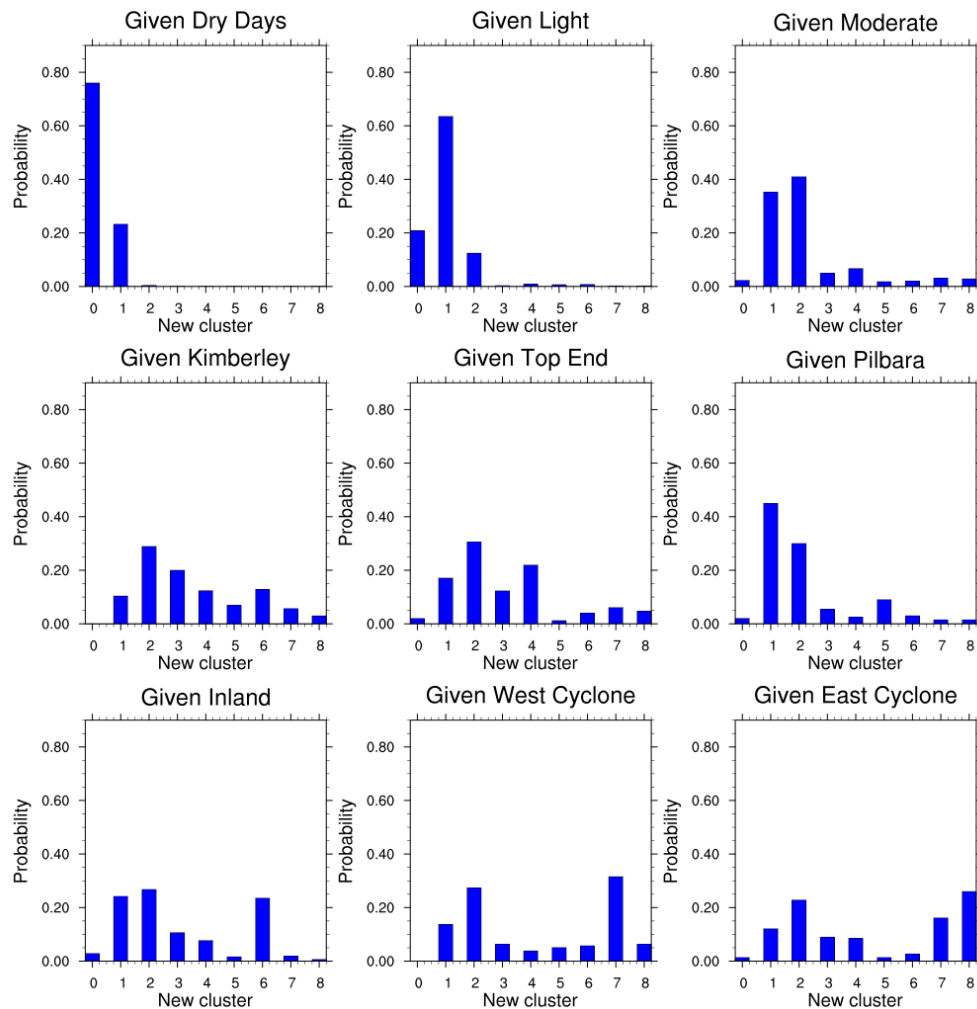


Figure 2.5: Probability of transitioning to another cluster after 2 days given a day in one cluster. The horizontal axis of each panel is numbered according to those given in Figure 2.2.

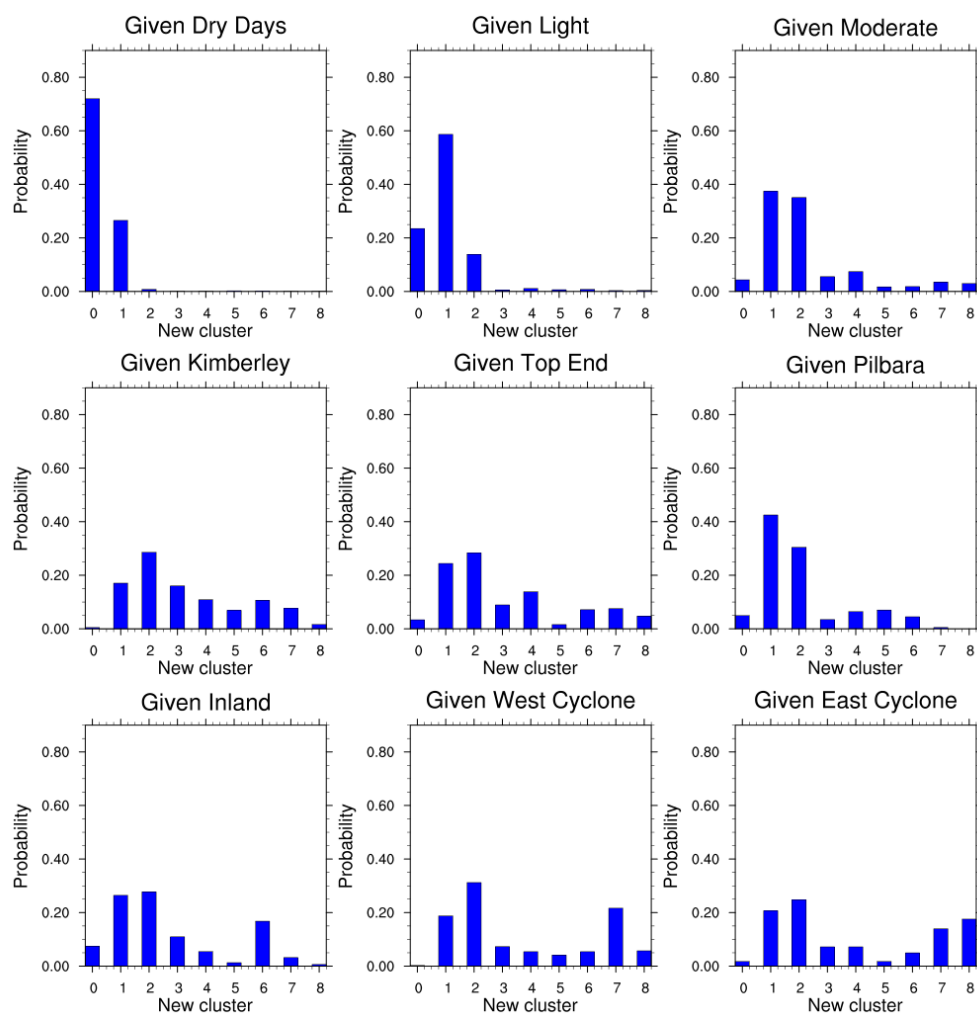


Figure 2.6: Probability of transitioning to another cluster after 3 days given a day in one cluster.

## 2.3 Synoptic patterns

Composites of the 900 hPa and 700 hPa wind for each regime are presented in Figures 2.7 and 2.10. In addition, composites of the 900 hPa specific humidity and K-index are presented in Figure 2.8. These composites together will build an understanding of the state of the atmosphere in each regime.

The dry days regime is characterised by low-level dry (less than  $8 \text{ g kg}^{-1}$ ) south-easterly winds up to  $12 \text{ m s}^{-1}$  across much of the Australian continent. As the atmosphere is dry, the K-index is less than 20 over the entire continent, indicating the lack of potential for convection resulting in dry conditions. The Light regime shows slightly weaker (up to  $8 \text{ m s}^{-1}$ ) winds in the region that tend more easterly. The low-level humidity in the region is higher than for dry days (up to  $12 \text{ g kg}^{-1}$ ) and the K-index is between 20 and 25 over much

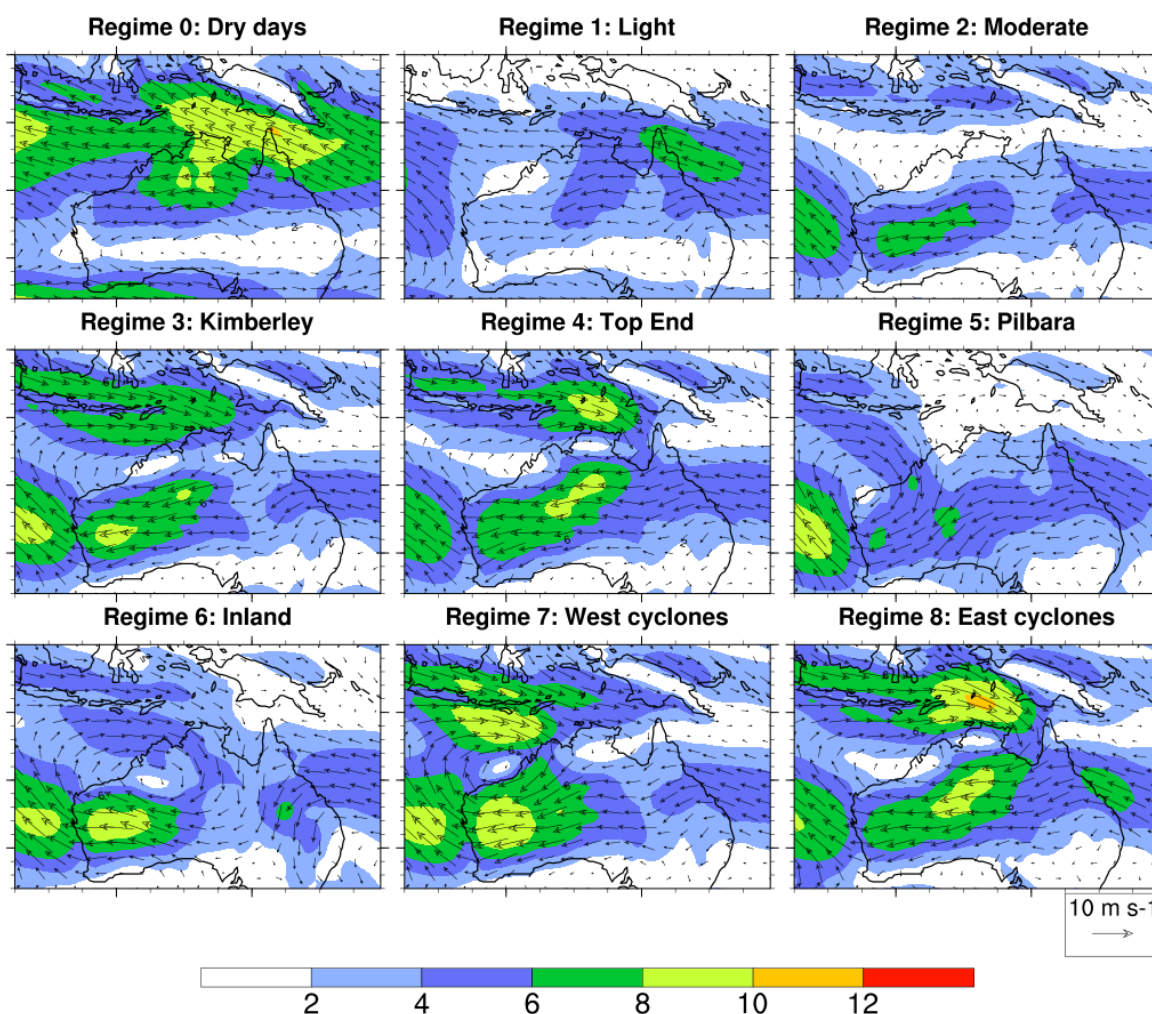


Figure 2.7: 900hPa wind composites for each regime. Shading indicates wind speed ( $\text{m s}^{-1}$ ).

of the study region, indicating the likelihood of isolated thunderstorm activity. As this regime peaks in frequency in the austral spring and autumn, these conditions are thus typical of the pre-monsoon "build-up" period and the end of the monsoon due to the composite being weighted to days in this time of year.

The Moderate regime composites show very light winds (less than  $4 \text{ m s}^{-1}$ ) and high specific humidity (greater than  $14 \text{ g kg}^{-1}$ ) over the study region. The high humidity results in a K-index greater than 30 over much of northern and north-western Australia, corresponding to a high likelihood of scattered thunderstorms explaining the larger average totals in the rainfall pattern in this regime. The Moderate regime peaks in frequency in summer; thus the Dry, Light and Moderate regimes are consistent with a gradual weakening of the easterlies over northern Australia in the lead-up to the monsoon.

The composites for all other regimes show low-level cyclonic winds with onshore winds near the rainfall maxima, with almost all regimes except the Pilbara regime having specific humidity greater than  $14 \text{ g kg}^{-1}$  at the rainfall peak. The widespread rainfall in these regimes is likely to contain embedded thunderstorms, as evidenced by the high K-indices for these regimes. The composites for the TC regimes show winds which are much lower than what would be expected for a TC (under  $12 \text{ m s}^{-1}$  in the composite). The reason is twofold: firstly, the composite is an average of multiple TCs centred in different locations, and thus the maximum winds are smeared over a larger area and tend to cancel out. Secondly, the ERA-Interim data may be unable to resolve the strong winds concentrated at the centre.

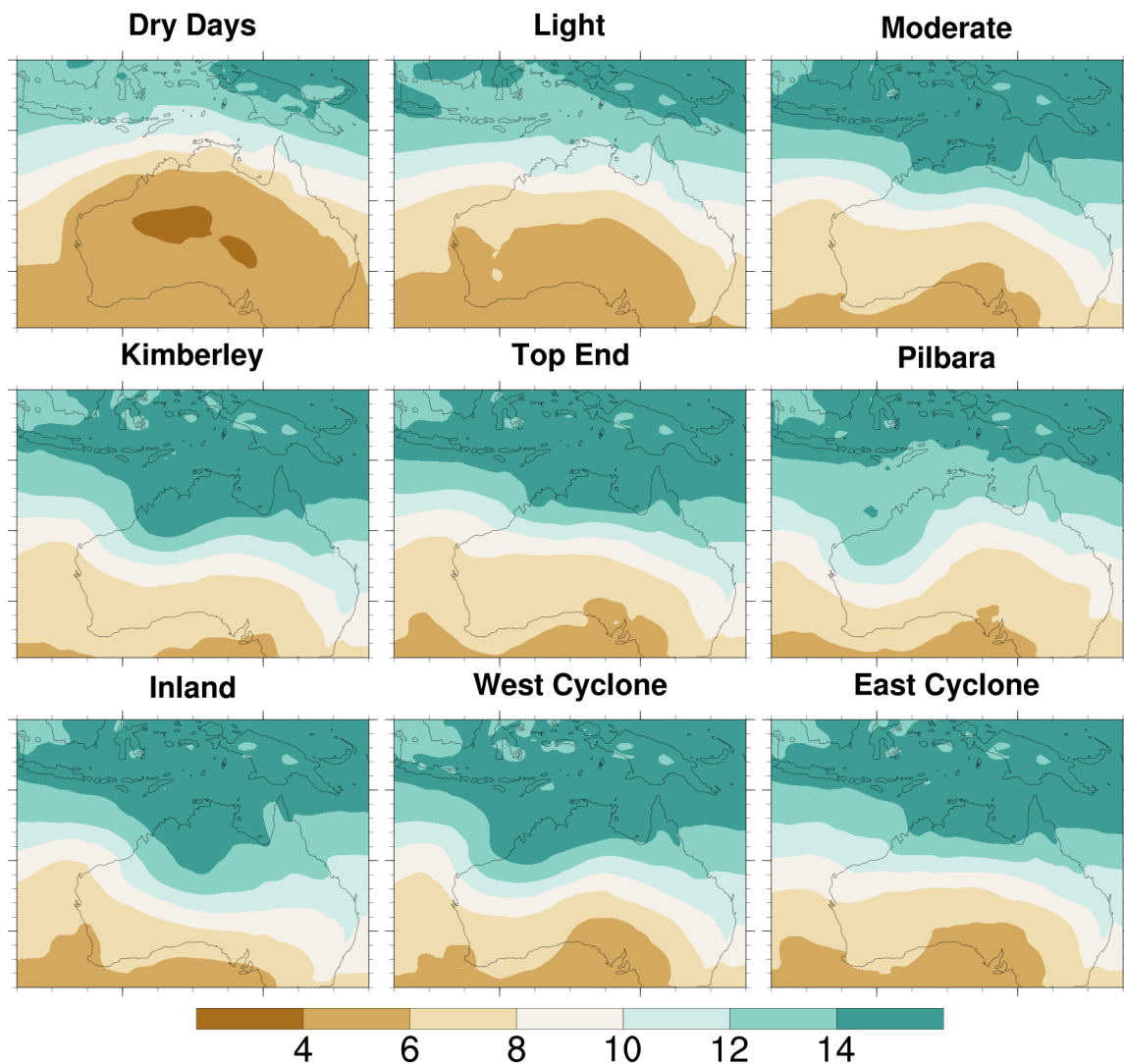


Figure 2.8: 900 hPa specific humidity composites for each regime (units  $\text{g kg}^{-1}$ )

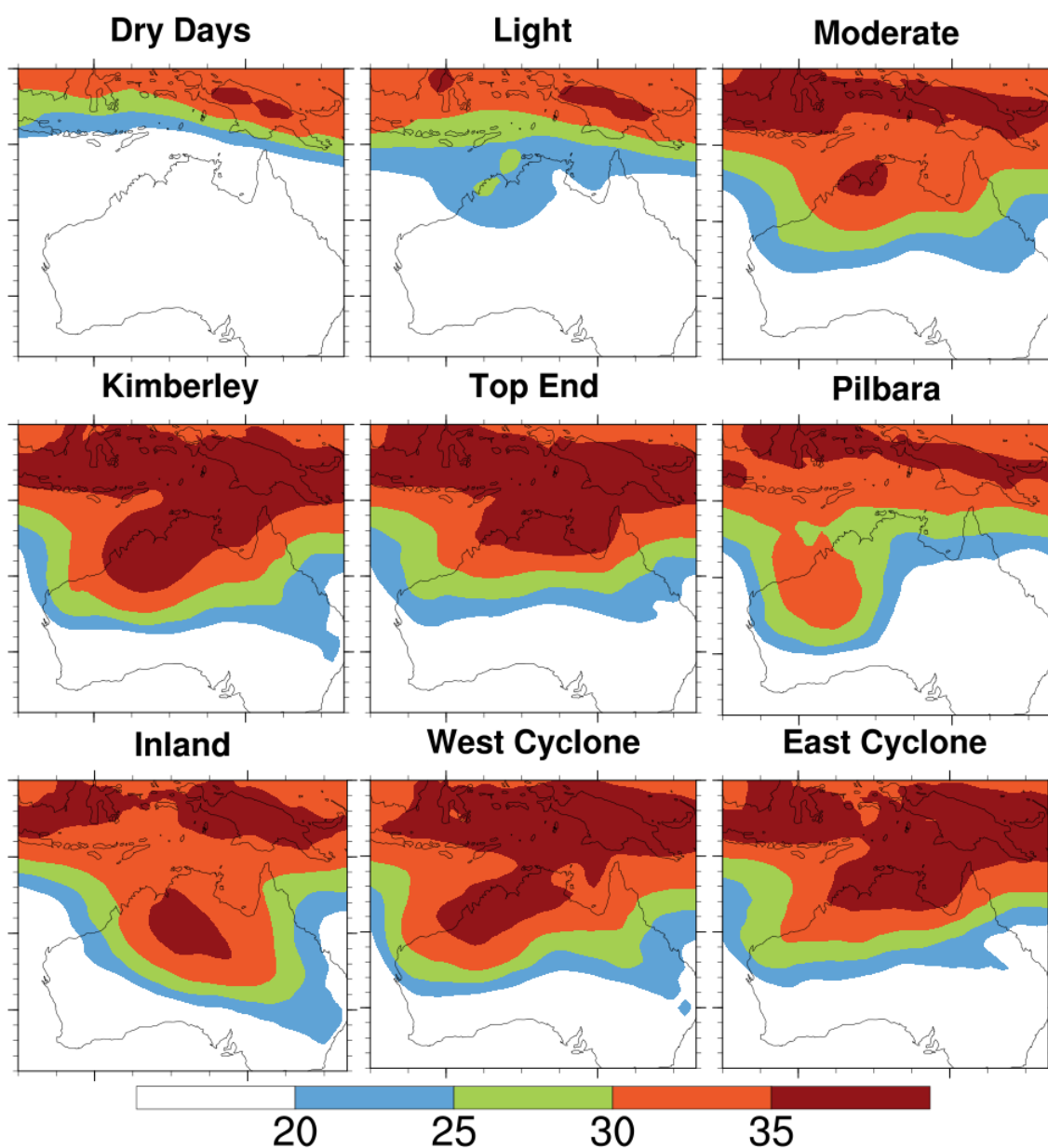


Figure 2.9: Composites of K-index (measure of instability) for each regime (dimensionless). A definition of K-index is provided in Section 2.1.4.

The 900hPa wind composites suggest that for all of the heavier regimes, there is a monsoon low present near the rainfall peak. As a result, the heavier rainfall regimes could be interpreted as the same type of synoptic system, although in different locations. However, the 700 hPa wind composites (Figure 2.10) and the 500 hPa wind and 315 K potential vorticity lag composites (Figure 2.11) highlight some differences in the heavier clusters. The Dry and Light regimes both show an anticyclone over NWA, and are highly similar to each other. The Moderate regime is also similar to the first two, although the anticyclone is further south. The Kimberley, Top End and the two cyclone regimes show cyclonic flow close to

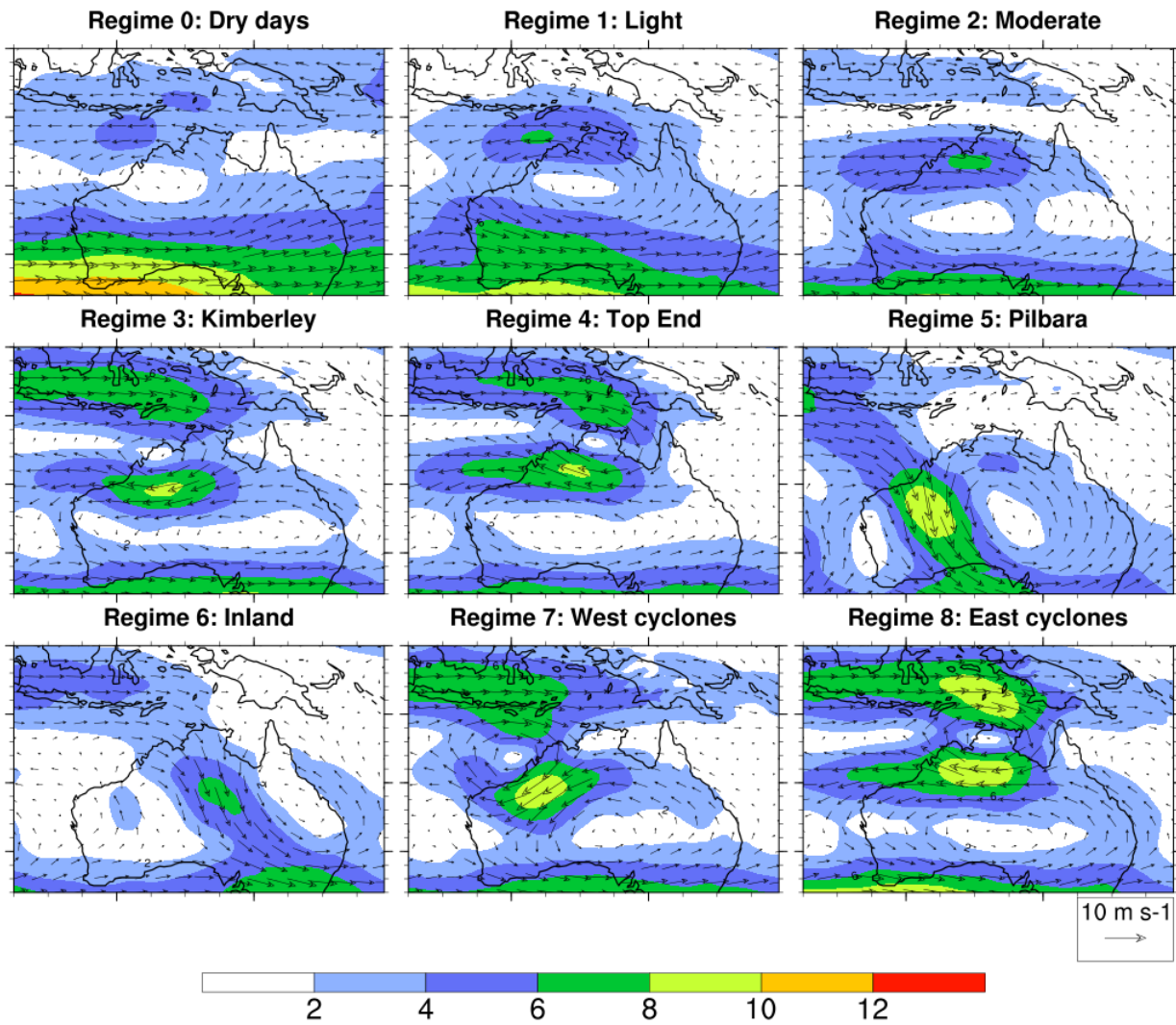


Figure 2.10: 700hPa wind composites for each regime (units m s<sup>-1</sup>)

the rainfall peaks, similar to Figure 2.10. However, the Pilbara and Inland regimes show evidence of a westerly trough, with strong (up to 10 m s<sup>-1</sup>) north-westerlies at the rainfall peak.

Figure 2.11 shows the lag composites of 500 hPa wind and 315K PV for regimes 3 to 8. These are shown to indicate the difference in the mid to upper level structure of regimes which cause heavier rainfall. The Kimberley and Top End regimes show an isolated, weak PV anomaly which strengthens over the area of maximum rainfall at day 0 before moving southward and weakening, with weakening occurring more rapidly in the Top End regime. Such weakening explains the lack of transitions between these two regimes outlined in Section 2.2, as the day 2 composite does not suggest a rainfall peak in a location corresponding to any other heavy regime. The composites for the Pilbara and Inland regimes show further

evidence of a mid-latitude trough over north-western Australia. The trough moves in an eastward direction and amplifies on day 0, initiating rainfall ahead of the trough. The two regimes are differentiated by the different zonal location of the amplified trough. Since the trough weakens and moves south in the Pilbara regime, it usually does not transition to the Inland regime, and as the dynamics of these two regimes are different from the monsoon low and TC type regimes, they are unlikely to transition between each other and explain the probabilities in Figure 2.5. The west TC regime lag composite shows a coherent PV anomaly strengthen in a similar fashion to the Kimberley regime, although stronger and offshore. The east TC regime also looks similar to the Top End regime, although the anomaly moves in a westerly direction and offshore.

Figure 2.12 shows the 200hPa meridional wind composites for regimes 3 to 8. For regimes 5 and 6 (Pilbara and Inland regimes), there is a clear propagating wave signal, showing these regimes are indicative of amplified mid-latitude Rossby waves. The remaining regimes show a significant pattern in the meridional wind, although this is not propagating, suggesting the existence of an upper level anticyclone over the continent.

Overall the eight regimes can be classified into four groups based on their synoptic pattern: a thunderstorm group (Light and Moderate), a monsoon low group (Top End and Kimberley), a midlatitude wave group (Pilbara and Inland) and the TC group. These groups are not the same as what would emerge from choosing three clusters rather than six when the clustering was carried out - note that the middle pattern in the 3 cluster case in Figure 2.1 shows a pattern that produces widespread rainfall from the Kimberley across to inland areas. Based on the synoptic patterns identified in this section, the composites for the three cluster case will produce a combination between a monsoon low and mid-latitude interaction. Choosing 6 clusters in this chapter allows the synoptic patterns responsible for the rainfall to be determined more clearly.

In the next section, the trend in mean rainfall will be decomposed into changes in frequency and intensity of rainfall associated with these synoptic patterns, to explain the trend in terms of changes to the identified rainfall regimes.

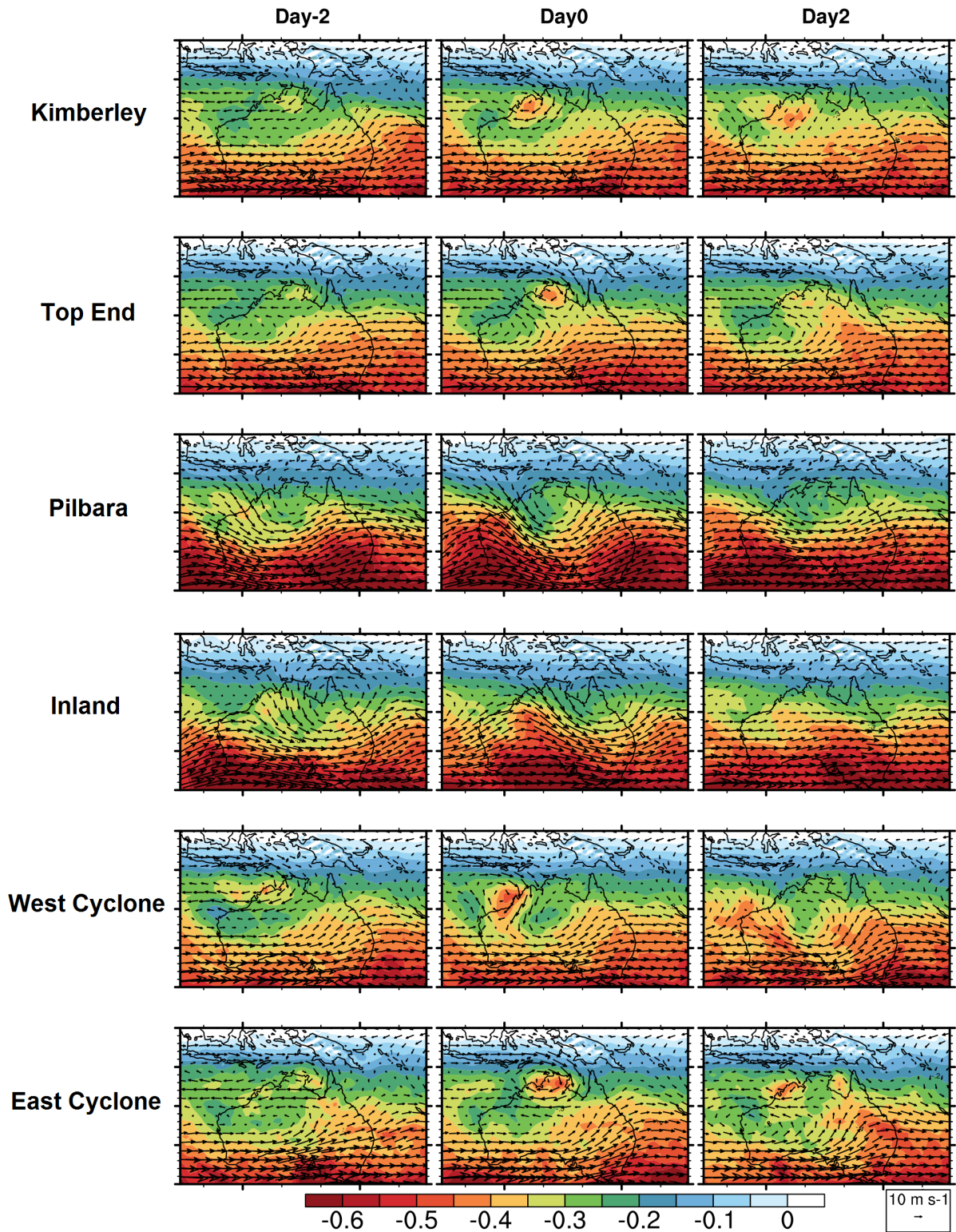


Figure 2.11: 315K PV (shading, units PVU) and 500hPa wind (vectors) lag composites for regime 3 to 8.

## 2.4 Decomposition

The previous two sections defined the rainfall regimes in terms of rainfall spatial pattern and synoptic structure. In this section, changes to the regimes between the periods 1950-

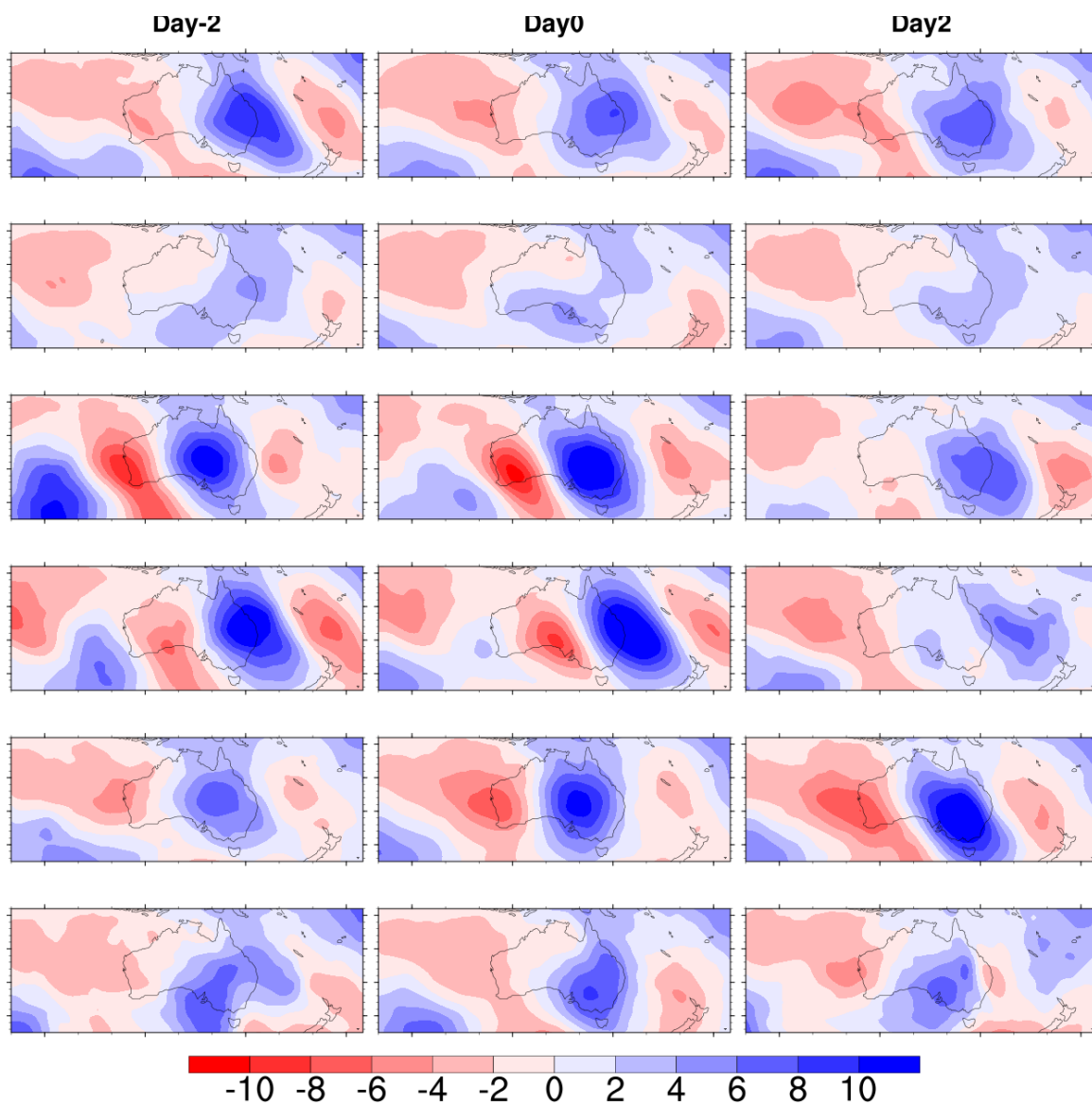


Figure 2.12: 200hPa meridional wind composites for regimes 3 (top row) to 8 (bottom row). Units are  $\text{m s}^{-1}$ .

1979 and 1980-2009 are analysed using the decomposition method outlined in Section 2.1. The method decomposes the change in mean rainfall between the two periods into changes in frequency and intensity of individual regimes. Figure 2.13 shows the results, and displays the frequency and intensity terms of the decomposition for each regime. The cross terms are small relative to each of the other terms and may safely be omitted. The size and sign of the frequency terms (left) relative to the intensity (right) terms suggest that most of the rainfall change between the two periods is due to changes in frequency rather than changes in intensity. By far, the largest single term in the decomposition is the frequency term for the west cyclone regime, which contributes an additional 24.4 mm per year to the rainfall

total in the second study period. However, the frequency terms of the remaining regimes are also significant and positive, except the Light and Moderate regimes. These terms add to a total contribution of 25.7 mm per year of additional rainfall. Thus, while an increase in the frequency of the West Cyclone regime contributes most strongly to the positive rainfall trend, changes in the frequency of many of the other regimes also contribute to the rainfall trend. There is also a minor positive contribution from the Light ( $6.4 \text{ mm year}^{-1}$ ) and Moderate ( $6.9 \text{ mm year}^{-1}$ ) intensity terms. There is a negative contribution ( $9.7 \text{ mm year}^{-1}$ ) for frequency in the Light regime, meaning changes in frequency contribute negatively to the overall rainfall trend. This implies there is a decrease in the number of days in the Light regime, compensating for the increase in frequency of the remaining regimes.

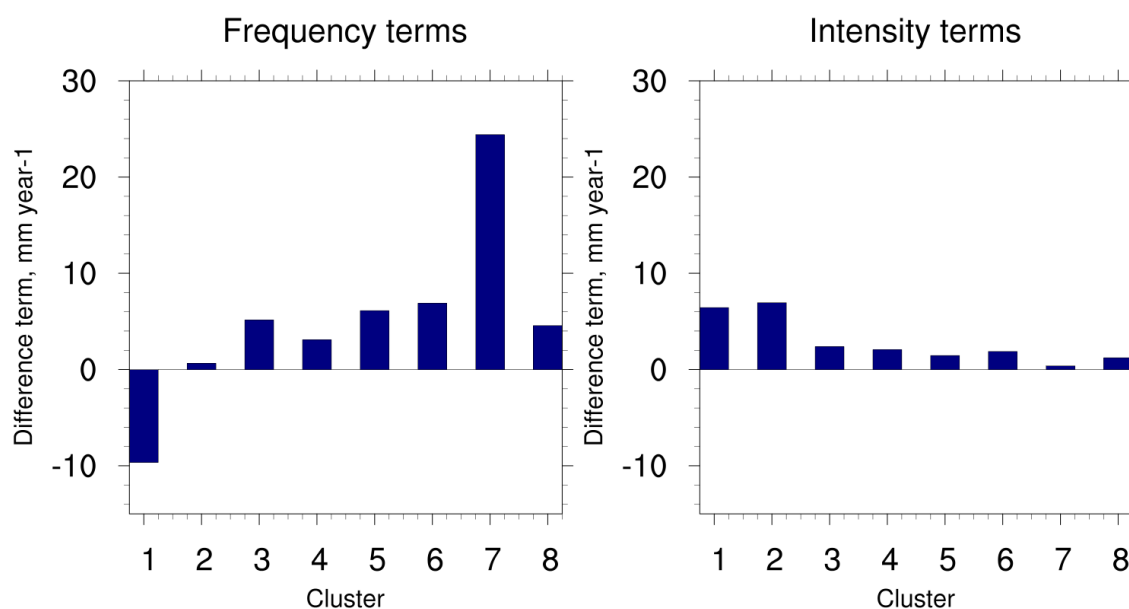


Figure 2.13: Decomposition of mean rainfall into changes in frequency and intensity of each regime. Left panel shows the frequency terms, right panel shows the intensity terms. Cross terms are omitted.

Changes in the absolute number of days in each regime between the two periods is summarised in Figure 2.14. There is an increase in the number of the days in regimes 3-8, with the largest increase in West Cyclone regime days, a similar result to the decomposition. This increase in frequency of the heavy regimes comes overwhelmingly at the expense of days in the light regime, rather than resulting in a much larger number of wet days. As the synoptic structures associated with the heavier regimes are most likely to occur in summer, they are unlikely to replace dry days as these do not occur regularly in summer. Thus they are

more likely to replace days in either the Light or Moderate regime, with the former being the case as shown here. The results reiterate that changes in the frequency of regimes associated with structured synoptic systems are the main driver of the observed rainfall trend.

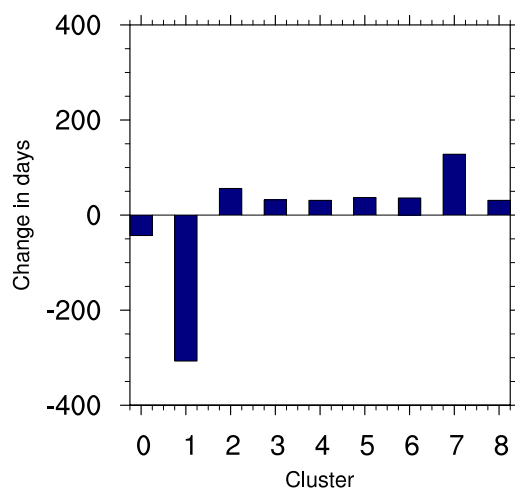


Figure 2.14: Difference in number of days in each regime between 1980-2009 and 1950-1979.

## 2.5 Sensitivity to TC separation

The removal of TCs prior to clustering highlighted that rainfall over parts of the study region may be influenced by TCs and other synoptic systems. To illustrate the necessity of first removing TCs from the record, the rainfall patterns produced from clustering the AWAP rainfall without separating TCs is given in Figure 2.15. All of the rainfall patterns look very similar to those in Figure 2.2, although there is a noticeable slight increase in intensity of the Top End and Pilbara regimes. The inclusion of TCs therefore has negligible bearing on the spatial rainfall patterns for each regime. The frequency and contribution to total rainfall of each regime has changed slightly with the heavier regimes, which is expected as the TC regimes must be absorbed into the remaining regimes.

The main issue resolved by removing TCs from the record is the interpretation of the PV fields. Figure 2.16 shows the PV lag composite for the Pilbara regime without TC separation. At day -2, there is an isolated PV minimum to the north of the Pilbara which is not present in Figure 2.11. As the difference in the members in the cluster can only be attributed to the presence of TCs, the PV minimum must correspond to a TC in the region. The composite then shows an interaction between the TC and a mid-latitude wave at day 0 before being

absorbed and moving south-west at day 2.

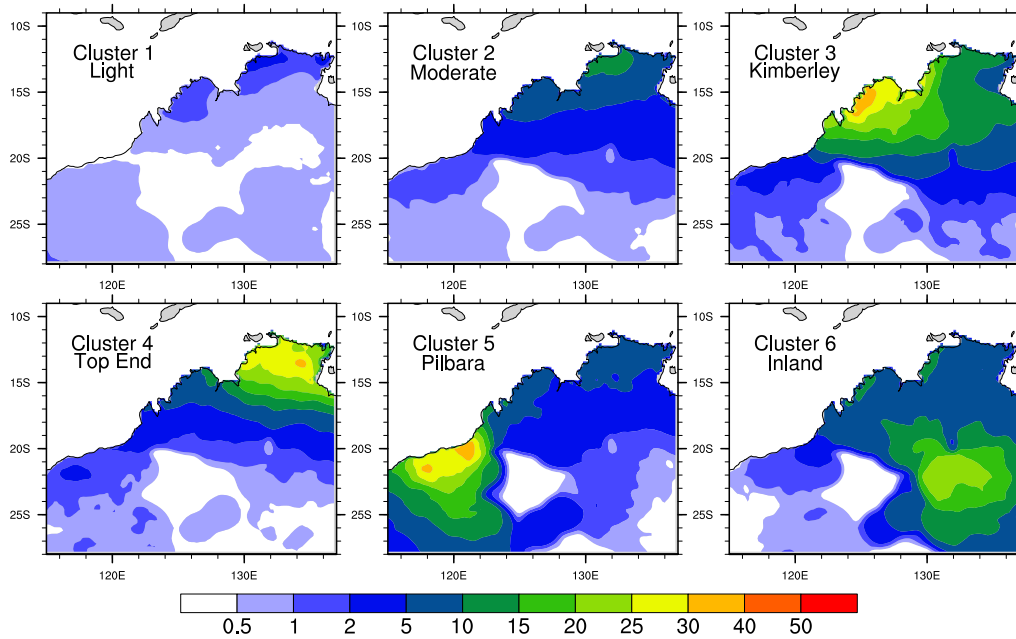


Figure 2.15: The rainfall regimes that would happen if cyclone days were left in the data set. Units are  $\text{mm day}^{-1}$ .

If cyclone days were not separated from the rainfall record, the progression shown in Figure 2.16 would appear to be reasonable, as it appears to show a strong monsoon low interacting with a mid-latitude trough. However, after TC separation, the spatial rainfall pattern for the Pilbara regime is unchanged (although marginally less intense), but the PV composite no longer contains a TC. Thus, the PV composite in Figure 2.16 can be considered to be an average of both TC days and mid-latitude interaction days, both of which result in a similar spatial rainfall pattern.

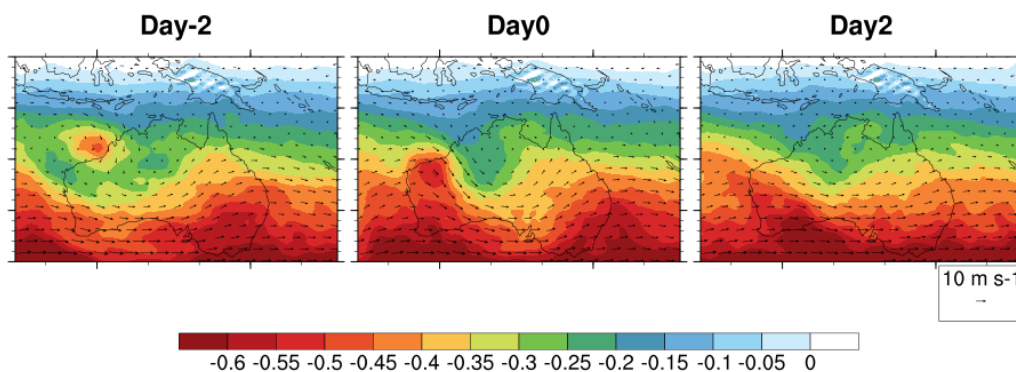


Figure 2.16: 315K PV and 500 hPa wind for the Pilbara regime without cyclone removal.

The decomposition of changes in the rainfall regimes without TCs in Figure 2.17 suggests that the main contribution to the rainfall trend is changes in the frequency of the Kimberley and Pilbara regimes. Based on the location of TCs in the West Cyclone regime, many of the TCs are absorbed into these two regimes. Thus, failing to remove TCs will result in the rainfall trend being falsely attributed to a strong increase in the Kimberley and Pilbara regimes. Separation of TCs is therefore important to accurately determine the synoptic systems responsible for rainfall in NWA, and to accurately attribute changes in rainfall to changes in the synoptic systems.

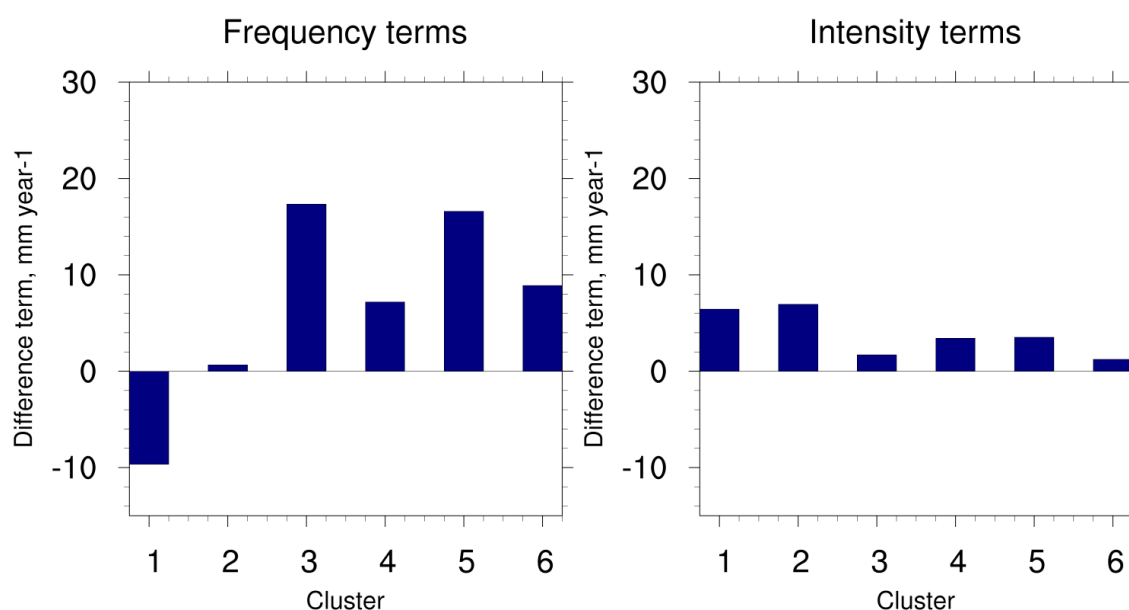


Figure 2.17: The decomposition of the regimes without removing cyclones.

## 2.6 Extreme rainfall

Contributions of each rainfall regime to the climatological mean and overall rainfall trend have been established in previous sections. This section discusses the how each regime contributes to extreme rainfall in NWA. As discussed in Section 2.1.6, an extreme day is defined as any day that contains at least one point above the 99.9th percentile of all rainy grid points, determined to be  $107.2 \text{ mm day}^{-1}$ . Figure 2.18 shows the number of days per year that are considered extreme. Similar to the overall trend in rainfall, the number of extreme days per year is generally increasing over the 60 year period. There is a significant decrease from the mid 1980s to the early 1990s, followed by a sharp increase and return to the general trend.

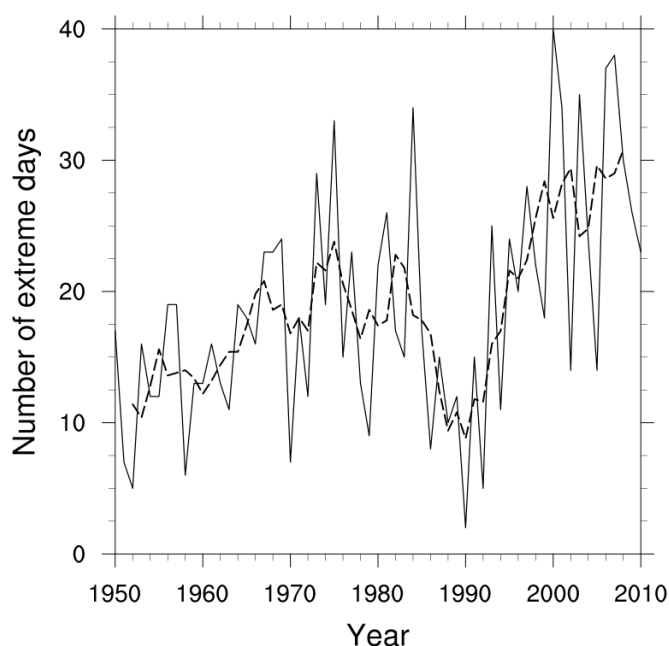


Figure 2.18: Number of extreme days per year from 1950-2010. The dashed line represents the 5 year moving mean.

The contribution of each regime to extreme rainfall will now be considered. Here we determine the total number of extreme days that fall into each regime, as well as the probability that a given day in the regime is extreme. The number of days per year that are considered extreme as a function of regime are shown in the left panel of Figure 2.19. Any of the regimes are capable of producing extreme rainfall, with the moderate, Kimberley, Top End, and West Cyclone regimes producing a similar number of extreme rainfall events per year. A slightly surprising result is that the light and moderate regimes also contain days that can be considered extreme. It is possible that thunderstorms occurring in these regimes produce isolated heavy falls which are above the threshold for extreme rainfall, albeit only over a small number of grid points. These heavy falls are likely to cause localised flooding, thus they are rightfully counted as extreme rainfall. Of the heavier regimes, the Pilbara and inland regimes cause relatively fewer extreme events per year, due in part to their lower frequency.

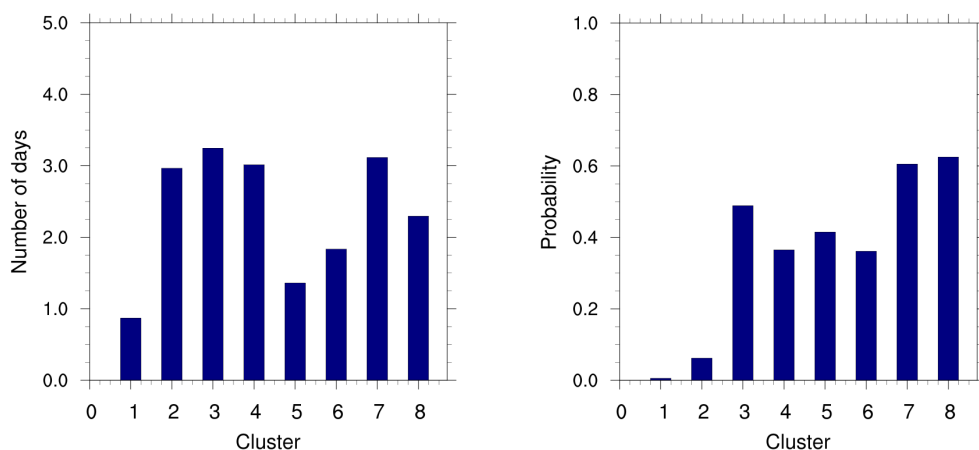


Figure 2.19: Left panel: number of days per year that are extreme in each regime. Right panel: probability that a day in a given regime is extreme. The numbering of the regimes is the same as that given in Figure 2.2.

The right panel of Figure 2.19 shows the probability of a day being extreme, calculated by dividing the number of extreme days in a regime by the total number of days in that regime. Tropical cyclone regimes have a more than 50% chance of producing extreme rainfall when they occur. The remaining heavy rainfall regimes have a slightly lesser chance of causing extreme rainfall, with the Kimberley regime being most likely to cause an extreme event. The remaining heavy regimes have a similar likelihood to each other of initiating an extreme event. As the Pilbara and inland regimes are less frequent than the other regimes (see Table 2.1), they constitute a smaller number of extreme days, although the likelihood of a day in these regimes causing an extreme event is similar to the Kimberley and Top End regimes. The increased frequency of regimes more likely to produce extreme rainfall can therefore explain the increasing trend in extreme days.

Figure 2.20 shows the spatial distribution of the extreme rainfall for each regime. For the heavy regimes, the typical location of the extreme rainfall points corresponds very closely to the location of maximum rainfall, although for most regimes the frequency of extreme events tends to decrease rapidly with distance from the coast, with the exception of the Inland regime. The decrease in extreme rainfall with distance inland is strongest for the Kimberley regime, suggesting the local topography may trigger convection on the western (windward) side resulting in a higher likelihood of extreme rainfall here. The Moderate regime also tends to produce extreme rainfall only along the coast, and especially at the coast of the Top End. The Light regime almost exclusively produces extreme events at two isolated

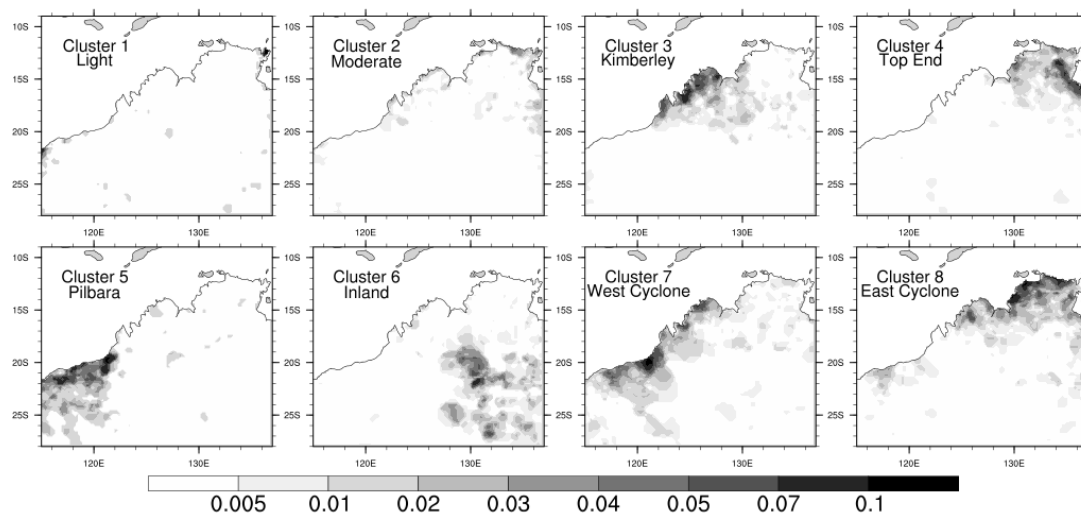


Figure 2.20: Spatial distribution of extreme points by regime. Shading indicates the fraction of extreme days in that regime that have an extreme point at that grid point.

points: on the coast in the far west of the study region, and in the far north-eastern corner of the region. It is possible that these heavy rainfall events are the result of monsoon lows or TCs that are only just outside the study region, rather than a tendency for extreme rainfall from thunderstorms to only occur in this region. Extreme rainfall caused by the Light regime is therefore likely to be overestimated, however based on the distribution for the Moderate regime, thunderstorms still occasionally produce extreme rainfall in that regime.

## 2.7 Discussion and conclusions

In this chapter, daily rainfall over NWA is classified into eight regimes which are characterised by observed synoptic patterns. The regimes can be divided into 4 groups: thunderstorms, monsoon lows, TCs and mid-latitude interactions. The monsoon lows often appear to be similar to the coherent PV anomalies described by Berry et al. (2012), highlighting the importance of these structures in the north Australian monsoon. The Pilbara and inland regimes constitute less than 4% of wet days, but they deliver much of the climatological rainfall to many inland desert regions of Australia. Regimes causing heavier rainfall (all except the Light and Moderate regimes) contribute almost half of the climatological rainfall of the region, despite only constituting 14% of wet days in the region, while the remaining half is caused by isolated or scattered thunderstorms not forced by a structured synoptic system.

Changes in the frequency of the heavy rainfall regimes (which includes TCs) account

for approximately 70% of the increase (Figure 2.13) in rainfall in 1980-2009 as compared to 1950-1979. This means that there is an increase in the frequency of formation of the weather systems that cause the heavy rainfall patterns. As these heavy regimes are already infrequent, small changes in the number of systems each year can cause a large change in rainfall in the region. The sharp increase in the frequency of TC days found in this study is in partially in disagreement with Ren and Leslie (2015), who suggested that there is no strong trend in the number of TCs, however it does support their conclusion that warming in the NWA TC basin has resulted in more favourable conditions for TC formation. The increase in frequency of TCs also disagrees with Lavender and Abbs (2013), who also did not observe a significant trend in TC number over NWA, however an increase in the frequency of monsoon lows associated with the Kimberley and Top End regimes does agree with Lavender and Abbs (2013). Although the results in this chapter show a strong increase in the frequency of TC days over north-western Australia, it is important to note that the TC track data includes tracks prior to the satellite era (before 1970). The trend in TC days, especially West Cyclone days may therefore be exaggerated, and could partially explain the difference in TC trend between this study and others (for example, Lavender and Abbs (2013) use TC tracks from 1970-2009 to avoid the pre-satellite era). The exaggeration of the trend in TCs should not affect the trend in other synoptic regimes responsible for rainfall in the region. The fact that the positive contribution from frequency changes for the monsoon low regimes is present regardless of TC separation highlights the robustness of the change in their frequency.

A trend associated with an increase in frequency of synoptic systems associated with heavy rainfall rules out a simple, direct effect of increases in SST on atmospheric moisture only, since such a simple effect would result in an increase in rainfall intensity with the frequency of these systems remaining the same. However, additional atmospheric moisture may explain the positive contribution of intensity for the Light and Moderate regimes. The result that frequency changes matter more than intensity changes disagrees with Emori and Brown (2005), who determined from examination of pointwise PDFs of model rainfall that frequency changes had no major effect on the rainfall trend. Emori and Brown (2005) used a small number of models in the Program for Climate Model Diagnosis and Intercomparison (PCMDI). The pattern for overall precipitation change in their study did not capture the observed positive trend in rainfall over NWA (see Figure 1.1), which suggests model biases

are a factor in their study.

The increase in the number of heavy rainfall days must be explained by a mechanism that creates more favourable conditions for the formation of the synoptic structures associated with these regimes. Sea surface temperatures are likely to still play an important role, since changes can affect the location and frequency of development of these structures. Future research should therefore focus on modelling and statistical studies aiming to determine the mechanisms responsible for regulating the frequency of these structures. The ability of CMIP5 models to replicate these mechanisms will be discussed in the next chapter.

## Chapter 3

# Modelled rainfall over north-western Australia: Evaluating ACCESS1-0 against observations

### 3.1 Introduction

Chapter 2 identified typical rainfall regimes over north-western Australia and their associated synoptic patterns, and described the observed rainfall trend in north-western Australia in terms of the changes to the frequency and intensity of these regimes. The next two chapters aim to determine how these rainfall regimes, and their associated flow patterns, are represented in the Coupled Model Intercomparison Project phase 5 (CMIP5) models with the ultimate aim of informing how the regimes will change in a future climate. Over the Australian region, there is generally a tendency for CMIP5 models to produce too much rain over northern Australia (Moise et al., 2015). As discussed in Chapter 1, the CMIP5 ensemble mean is able to capture the overall pattern of the observed global precipitation trend, however there is much variation among models in terms of regional trends (Kumar et al., 2013). Models generally have large variation in replicating observed precipitation over the Australian continent (Flato et al., 2014; Christensen et al., 2014). To eliminate some of the variation, some studies have selected subsets of CMIP5 models that replicate the observed climate well. Grainger et al. (2014) rank models based on their ability to replicate modes of variability in the 500 hPa geopotential height, while Jourdain et al. (2013) use rainfall rates in the Indian and Australian monsoon, and their coupling to ENSO as a basis for model

ranking. Moise et al. (2015) use a ranking based on temperature, rainfall and MSLP fields, and find that ACCESS1-0 performs best when the entire Australian region is considered, although other models perform better in other parts of Australia. Thus, ranking measures depend strongly on the metric, the region and the purpose of the ranking.

We now wish to use the regime-based approach developed in Chapter 2 to evaluate the ability of CMIP5 models to reproduce the observed rainfall patterns and synoptic patterns over north-western Australia. However, assigning regimes in models requires care, since defining model regimes based on observed regimes may not necessarily be the most accurate representation of how rainfall regimes behave in the model. However, directly clustering model data may result in regimes that are differently defined to the observations, making the comparison to observations less straightforward. Thus, it is desirable to develop a number of regime assignment methods that will take into account how the models change the frequency, intensity and spatial pattern of the rainfall regimes. This chapter will outline and test three regime assignment methods on one CMIP5 model, ACCESS1-0 (Bi et al., 2013), to both assess the ability of this model to reproduce the observed rainfall regimes with the correct spatial pattern, intensity and frequency, as well as identify a methodology that can be used to assess a larger set of models in Chapter 4. ACCESS1-0 was chosen to test these methods as it is one of the main Australian CMIP5 models.

Section 3.2 outlines the rainfall and TC track data in both observations and ACCESS1-0 that will be used in this chapter and the following chapters. The three regime assignment methods used to determine the model regimes will also be described in detail in this section. Section 3.3 describes the rainfall regimes determined from CMORPH observations and compares them to the regimes in AWAP from the last chapter. From this chapter onwards, the regimes determined from CMORPH are used as the observed regimes. Section 3.4 describes the climatological mean in ACCESS1-0, before applying the three regime assignment methods to rainfall in the model, providing detail on the spatial pattern, frequency and intensity of the regimes compared to the observations. An overall evaluation of the ability of ACCESS1-0 to replicate rainfall over north-western Australia, as well as a discussion on the merits of using each regime assignment method for a multi-model analysis is presented in Section 3.5.

## 3.2 Methodology

### 3.2.1 Rainfall regimes in CMORPH

In Section 2.1.1, the merits of using the AWAP and CMORPH datasets were briefly discussed. So far, the observed rainfall regimes were based on the AWAP dataset because of the much longer period the data covers, thus allowing the rainfall trend to be attributed to changes in the rainfall regimes. However, the region of missing data over inland parts of NWA in the AWAP dataset is problematic when comparing observations to model data. In addition, AWAP data are only available over land areas. For comparison to model data, it is more important for the observation dataset to be spatially complete than to have a long record. Thus, to allow model biases to be calculated and assessed more rigorously over the entire study region including over the ocean, the CMORPH dataset will be used in this chapter and following chapters for almost all analyses. However, differences in the trend in rainfall in the models relative to observations will continue to be evaluated against AWAP as the length of CMORPH is too short to discern the trend in rainfall. The CMORPH data are available from 1998-2016, and at 0.25 degree resolution. The rainfall regimes produced by the CMORPH dataset are first determined and compared to AWAP before being used for model evaluation.

Clustering on CMORPH data is carried out in the same manner as for the AWAP data (Section 2.1.3). As before, TC days and dry days (spatial mean  $<0.1\text{mm}$ ) are removed from the data before clustering. CMORPH data are available over both ocean and land regions, however the data over the ocean is masked out for the clustering to make the results comparable to the AWAP analysis. Ocean data is added back into the resulting regimes following clustering. As is discussed later (Section 3.3), the spatial completeness of the data results in seven clusters (rather than six as in Chapter 2) being an appropriate choice for clustering the CMORPH data. Since the regimes in Chapter 2 were determined from AWAP data using the period 1950-2010, there is an overlap in periods between 1998-2010. Thus, each day in this period will be associated with a cluster in both CMORPH and AWAP. This allows a comparison between the two datasets to highlight the similarities and differences between the two sets of regimes derived from them. The frequency and contribution to rainfall of each regime is also determined. Finally, the composites of the 500 hPa wind and 315K PV

are calculated to illustrate the synoptic systems associated with the regimes. The synoptic fields are calculated from ERA-Interim data as in Chapter 2.

### **3.2.2 ACCESS1-0 and observation data**

The Australian Community Climate and Earth System Simulator version 1.0 (ACCESS1-0) (Bi et al., 2013) has been chosen to test a set of methods to determine whether CMIP5 models are able to replicate the observed rainfall regimes. The historical run (forcing due to observed changes in greenhouse gases) for this model has a horizontal grid spacing of  $1.875 \times 1.875$  degrees in the horizontal. For determining the regimes, daily rainfall from the model years 1970-1999 was re-gridded to a  $2.0 \times 2.0$  degree spacing for comparison to other CMIP5 models in Chapter 4. The period was chosen due to availability of tracks of TC-like vortices (described later in this section). The CMORPH regimes described in Section 3.3 are also re-gridded to a spacing of  $2.0 \times 2.0$  degrees wherever they are compared to ACCESS1-0 and other CMIP5 models.

### **3.2.3 Dry day and cyclone removal**

As shown in Chapter 2, tropical cyclones (TCs) are an important feature in the climatology of NWA rainfall. Even coarse resolution GCMs are able to produce TC-like vortices (TCLVs) (Manabe et al., 1970), and thus they must be accounted for when considering rainfall regimes in the CMIP5 models. TCLVs are detected and tracked using the CSIRO Direct Detection (CDD) scheme (Nguyen and Walsh, 2001; Walsh et al., 2004) for model years 1970-1999, and days on which a TCLV is inside the study region are separated from the rainfall data as was done for observations in Section 2.1.2. Prior to using any of the three analysis methods described below, the TC days were separated into either a western or eastern TC regime based on the location of the storm centre, and thus the rainfall patterns are calculated independently of any of the methods outlined in the next section. The TC regimes will be presented with the rainfall patterns from all three methods, but the regimes are covered in more detail for Method II when the synoptic patterns in the model are described.

The cyclone detection scheme is based on a number of vorticity, temperature and wind

speed thresholds, the latter of which are resolution and model dependent (Nguyen and Walsh, 2001; Walsh et al., 2004). The criteria ensure that vortices that are tracked are warm-cored, closed lows with similar structural characteristics to a TC, and are as follows:

1. Vorticity must be greater than  $10^{-5} \text{ s}^{-1}$ .
2. There must be a closed sea level pressure minimum within 250 km of the vorticity maximum.
3. The sum of the tropospheric temperature anomalies at 700 hPa, 500 hPa and 300 hPa relative to the environment must be greater than zero.
4. The wind speed around the centre must be greater at 850 hPa than at 300 hPa.
5. The temperature anomaly at the centre must be greater at 300 hPa than at 850 hPa.
6. The wind speed at the outer core must be greater than a model-dependent threshold (for ACCESS1-0:  $8.5 \text{ m s}^{-1}$ ).

Once a TCLV fulfils all criteria for at least 24 hours, criteria 3, 4 and 5 are relaxed. These criteria characterise a storm as warm cored, and will no longer be true if a TC undergoes extratropical transition. A storm undergoing such a transition usually does not signify the end of a TC track. For the purposes of this work, a TCLV that transitions into a cold-cored system is viewed as having TC influence, and is therefore still removed from the rainfall data.

Following TC separation, dry days (defined as having a spatial mean  $<0.1 \text{ mm}$  as per Section 2.1.3) were removed from the model rainfall data. The frequency of dry days is also compared to the observations.

### **3.2.4 Clustering methods**

To determine the rainfall regimes in the model to compare them to the observations, three regime assignment methods are proposed. All three methods use daily, non-TC rainfall in ACCESS1-0. Regime assignment is carried out based on land data only, and ocean data is added back into the regimes following regime assignment.

### **Method I: Projection**

The first regime assignment method, referred to as the projection method, projects each day in the model to the observed CMORPH regimes. The Euclidean distance from a given day in the model to each of the observed regimes is calculated, with the day assigned to the regime associated with the smallest distance. Once all wet, non-TC days in the model are assigned to a regime, the model regimes are determined by taking the mean of all model days in each regime. This method is relatively simple and produces spatial patterns similar to the observations, since model regimes determined using this method are centred around the observed regimes. Since the regime spatial patterns by design do not vary significantly from those of the observations, this method allows the frequency and intensity of the model regimes to be calculated in a straightforward manner, and allows direct comparison to the frequency and intensity of the observed regimes. However, this method is unable to determine if the model produces rainfall spatial patterns that vary from those observed. Changes to frequency and intensity in the models determined from this method should be used in conjunction with changes in regime spatial patterns to evaluate the models. The following two methods are able to take spatial pattern differences into account.

### **Method II: Direct clustering**

The second assignment method clusters the model rainfall independently from the observations, and allows a set of model regimes to be determined. Ideally, the model should be able to reproduce all of the observed regimes without producing regimes not in the observations. Thus, we use seven clusters as was the case for clustering the CMORPH observations. As described in Sections 3.2.1 and 3.3, we choose seven clusters (plus the two cyclone regimes) for clustering in the observations from this chapter onward. If the most sensible number of clusters in the model is anything other than seven, this implies the model is either unable to produce some observed regimes (if less than 7), or produces regimes which are not in the observations (if more than 7). Choosing a different number of clusters for each model would make comparison to the observations difficult, especially for a large number of models as will be evaluated in Chapter 4. Thus seven clusters will be used in all model clustering. Using seven clusters allows the model regimes to be compared to the observed regimes in a 1:1 fashion.

The non-TC model regimes are mapped to the observed regimes by calculating a measure of similarity between each model regime and each observed regime. One measure of similarity is the Euclidean distance - the closer one spatial pattern is to another, the smaller the Euclidean distance. Thus, if a set of model regimes are arranged such that they are matched to an observed regime with a similar spatial pattern, the Euclidean distance between each pair must be small. Therefore the best pairing of a set of model regimes to observed regimes will have a small sum of Euclidean distances over all of the possible pairs. The best match is assumed to correspond to the smallest sum of the distances.

For illustrative purposes, Table 3.1 gives a set of 4 regimes, which are not based on any results. Each row represents one set of regimes (observations, for example) and each column a second set (model, for example). The table shows, for example, that the Euclidean distance from observed regime 1 to model regime 2 is 30. The sets of regimes may be paired to one another in many ways. One possible permutation of matching the regimes could be along the diagonal from top left. The sum of the distances would therefore be the sum along the diagonal, in this case 240. A new permutation could be along the diagonal from top right to bottom left, which gives a new total of 350. This higher total, indicating the matching is more distant than the previous example, is considered to be a poorer arrangement. By trialling every possible permutation, the arrangement highlighted in blue is found to produce the lowest possible sum of 180, and this is considered to be the optimum arrangement of model regimes to observed regimes in this example. The same approach can be repeated for other measures of similarity, such as pattern correlation which is also trialled below in Section 3.4.3. Mapping with pattern correlation can be carried out in the same way by calculating the correlation between each model and observed regime rather than the distance; however since a higher pattern correlation implies a more similar pattern, the sum of pattern

Table 3.1: Example of Euclidean distance mapping using two sets of 4 regimes. The highlighted cells show the optimal arrangement for matching the regimes.

		Model			
		1	2	3	4
Obs	1	40	30	100	60
	2	50	30	90	40
	3	80	100	70	40
	4	130	170	70	100

correlations is maximised rather than minimised.

Following mapping, the frequency and contribution to the total rainfall of each regime is also assessed. The model regimes determined by this method are used as a basis for determining the synoptic regimes associated with the model. Composites of wind at the 850 hPa and 500 hPa levels, as well as specific humidity at 850 hPa and meridional wind at 250 hPa are calculated for comparison with the observed regimes, and are calculated as an average across all days in a given regime, the same approach as used in Section 2.1.4.

### **Method III: Combining model and observed data**

The third assignment method takes an equal number of days from CMORPH and ACCESS1-0, and carries out the cluster analysis for both sets of days together. We choose daily rainfall from 1981-1999 in ACCESS1-0 to ensure that the atmospheric forcing is as close to the period in CMORPH observations as possible. Although the model and observed days are tagged before clustering, the algorithm is blind to these tags and therefore makes no distinction between a model day and an observed day. The clustering will only produce patterns based on the closeness of the daily rainfall patterns based on Euclidean distance. If the model produces rainfall patterns that do not resemble the observed regimes, the centroids of the resulting clusters will appear different to the observed regimes. If the model produces incorrect regimes, or produces regimes at the incorrect frequency, this can be determined by examining the fraction of model days in each cluster from this method. To demonstrate the level of perturbation from the observed regimes caused by the model days, seven clusters are used. As a point of comparison, any regime that consists of more than two-thirds observed days (thus a ratio of 2:1) is considered to be a regime the model fails to replicate. A regime that consists of a ratio of 2:1 in favour of model days is considered to be a regime that is incorrectly produced by the model. While this ratio is arbitrary, it is a useful start for model comparison as it is simple to compare the number of missed regimes or incorrect regimes across models.

The three regime assignment methods are assessed for their applicability to a larger number of models, with the aim of ranking them (in Chapter 4) for their suitability for making predictions of the regimes in a future climate in Chapter 5.

### 3.3 CMORPH rainfall regimes: comparisons to AWAP

#### 3.3.1 Spatial patterns

The spatial patterns for rainfall regimes in CMORPH are identified for comparison to those from AWAP, and as a reference for model evaluation. Clustering over land regions only was carried out for CMORPH data using the same method outlined in Section 2.1. The 6-cluster case (the number of clusters used in Section 2.2) plus the two cyclone regimes is shown in Figure 3.1. When the spatial patterns are compared to Figure 2.2, we note that all of the regimes identified in the previous chapter emerge from the clustering with the exception of the Pilbara and Moderate regimes. Two different patterns emerge - one additional pattern is centred between the maxima for the Kimberley and Top End regimes, and the second is centred between the coastal Top End and the maximum for the Inland regime. These are described in more detail below. Since two regimes that exist in AWAP are not present in CMORPH, the number of clusters is increased in order to determine whether more regimes present in AWAP will emerge from the clustering of CMORPH rainfall data. The number of clusters is now increased from 6 to 7.

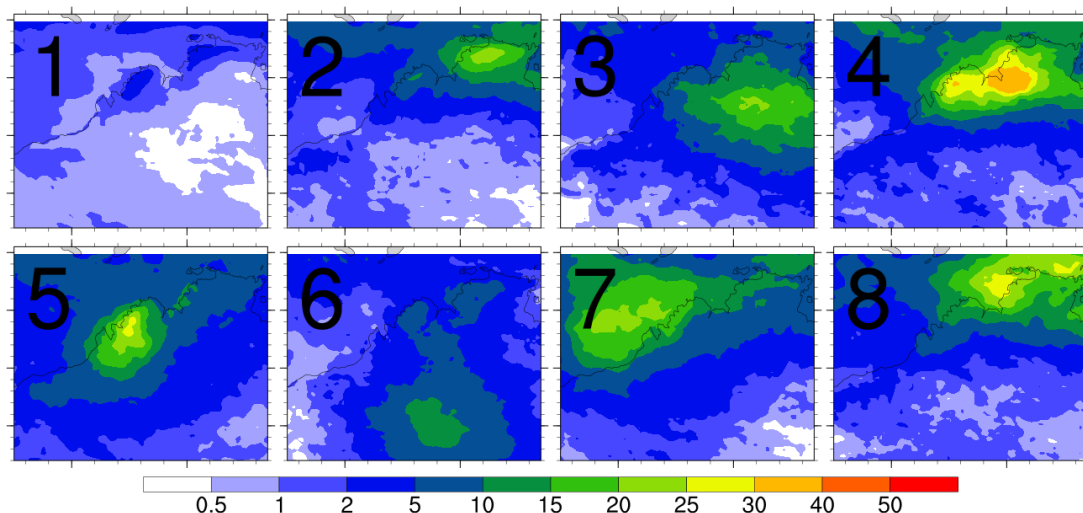


Figure 3.1: Rainfall regimes derived from CMORPH data - the 6 cluster case. Regimes 7 and 8 are TC regimes.

The 7-cluster case is shown in Figure 3.2. An additional regime that is identified in Section 2.2 emerges from the clustering here. There is a Light and Moderate regime present as regimes 1 and 2. Additionally, there is a Kimberley, Top End and Inland regime as clusters 3, 5 and 7 respectively. The TC regime patterns look similar in spatial pattern to those from

AWAP, which is expected as there is a relatively large number of cyclone days in each of those regimes (more than 200 each). There are two regimes present in the set of CMORPH regimes that are not present in the AWAP data. Regime 4 in CMORPH shows a maximum in rainfall located on the west coast of the Top End, extending toward the Kimberley region. This regime can be interpreted as being located geographically between the Kimberley and Top End regimes found in AWAP. This will be referred to as the Kimberley-Top End (KTE) regime. Regime 6 is characterised by a rainfall peak inland of the Top End, but further north than the Inland regime, and thus will be referred to as the Inland Top End (ITE) regime. The 7-cluster arrangement produces the highest number of clusters similar to AWAP, and thus this number (plus 2 cyclone regimes) is chosen as the optimal number of clusters for the CMORPH dataset.

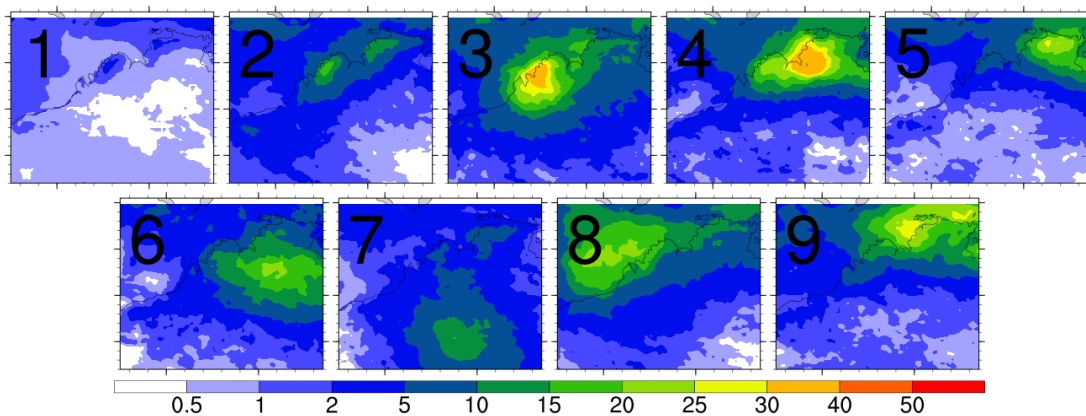


Figure 3.2: Rainfall regimes derived from CMORPH data - the 7 cluster case which will be used throughout the remainder of this thesis. Regimes 8 and 9 are TC regimes. Units are in  $\text{mm day}^{-1}$ .

The absence of the Pilbara regime in the CMORPH regimes suggests the regime is not present in the period 1998-2016. However, the location of the Inland type regime (Regime 7 in Figure 3.2) is slightly further west than in AWAP, and covers the area where there is missing data in AWAP. Thus, it is possible that CMORPH regime 7 is comprised of a combination of AWAP Pilbara and Inland regime days, and the presence of two regimes in AWAP rather than one in CMORPH is the result of the region of missing data in inland parts of the region. The combining of the two regimes is highlighted in the next subsection where days in each CMORPH regime are mapped to their equivalents in AWAP.

With the exception of the Pilbara regime, all of the regimes identified from AWAP are

present in CMORPH. Since there is no missing data regions over land, the CMORPH 7-cluster case is used from this point forward as the the reference observed regimes to which model patterns are compared. Changes to the mean of each cluster can affect the regime assignment of some days in the data, which can in turn affect the frequency and contribution to total rainfall. These changes will be discussed next.

### 3.3.2 Mapping to AWAP

Figure 3.3 shows how each day in each of the CMORPH regime is represented in the AWAP regimes. Each panel calculates the proportion of the assignment of each day in a CMORPH regime to each of the AWAP regimes, and presents it as a probability that a given day in a CMORPH regime is in each of the AWAP regimes. Regimes 0 (dry) to 2 map very closely to their equivalents in AWAP with a little crossover between the Light and Moderate regimes. The close mapping is expected as these have a high frequency of occurrence, and have a different average intensity compared to the other regimes.

However, the mapping is less clear when the heavy regimes (regimes causing heavier rainfall from monsoon lows, mid-latitude waves or TCs, in CMORPH these are regimes 3 to 7) are considered. Since the CMORPH regimes have slightly different spatial patterns and intensities to those AWAP, a given daily rainfall pattern which is only slightly closer to one regime may cross to the other with the change in spatial pattern. This threshold change also explains the significant change in frequency for each regime shown in Table 3.2. The heavy regimes are infrequent compared to the Moderate regime, so even if a small percentage of days from the Moderate regime in AWAP move to the heavy regimes in CMORPH, there will be a large contribution to the mapping from the Moderate regime. This explains the large contributions from the AWAP Moderate (2) regime noted for CMORPH regimes 3 to 7 in Figure 3.3.

The Pilbara regime (regime 5) in AWAP is captured by Regimes 2, 3 and 7 in CMORPH. Both Regimes 3 and 7 in CMORPH are located close to the missing data region in AWAP. It is therefore possible that when AWAP produces two separate regimes near the missing data region, CMORPH only produces one and shares some days with its Kimberley type regime. It is likely that the AWAP clustering artificially separates the Pilbara and Inland regimes due

to the existence of the missing data region.

### 3.3.3 Frequency and contribution to total rainfall

The frequencies and contribution to total rainfall for each CMORPH regime are given in Table 3.2. The spatial patterns for most of the regimes are similar to the patterns for the AWAP regimes, however the frequency and contribution to total rainfall is different to the AWAP regimes. Regimes 1 and 2 (equivalent to Light and Moderate) make up 64.3% of rainy days and contribute only 31.2% of the total rainfall, compared to 86% and 55% in AWAP respectively. The regimes derived from CMORPH produce heavy regimes (3 to 7) and TCs significantly more frequently than those using AWAP. The higher frequency of the heavier regimes may be the result of using a more recent time period, as heavier regimes are found to increase in frequency over time as per the result in Section 2.4. The lower rainfall maxima for some of the heavy regimes in CMORPH as discussed earlier may also contribute to the changes here.

To further illustrate the differences in frequency between regimes in CMORPH and AWAP, the frequency relative to all days rather than rainy days is presented in Table 3.3. Regimes 3 to 7 in CMORPH and 3 to 6 in AWAP are grouped into "heavy" regimes in order to give a general overview of differences in frequency where the number of regimes is not equal. The frequency of dry days changes little, however the frequency of light and moderate days is much lower in CMORPH, compensated by a large increase in the frequency of heavy rainfall

Table 3.2: Summary of the proportion of rainy days and the contribution of each regime to the spatial average rainfall for the CMORPH regimes

Regime description	Proportion of rainy days	Contribution to rainfall
Light (1)	51.5%	15.6%
Moderate (2)	12.8%	15.8%
Kimberley (3)	3.9%	10.4%
Kimberley/TE (KTE) (4)	3.7%	9.2%
Coastal Top End (5)	7.5%	10.0%
Inland Top End (ITE) (6)	4.5%	10.1%
Inland (7)	5%	9.1%
West cyclone	6.5%	11.6%
East Cyclone	4.6%	8.0%

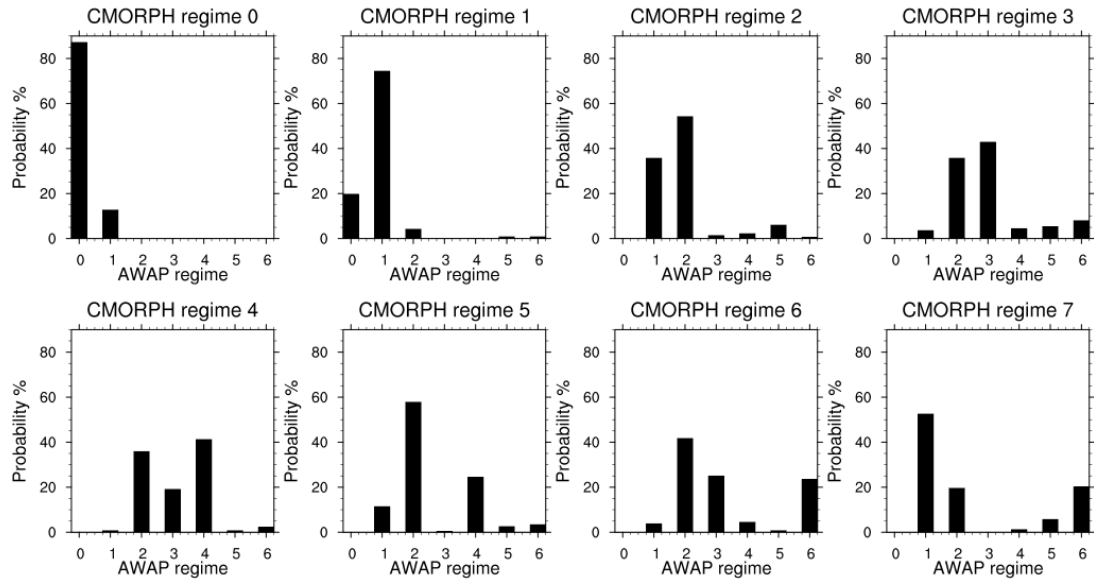


Figure 3.3: Probability of daily rainfall occurring in an AWAP regime given a certain CMORPH regime.

regimes and TCs. The differences could be due to the difference in time period used between AWAP and CMORPH, since the increasing trend over time means that CMORPH will have a higher mean over the region than the period for AWAP. These differences must therefore be taken into account when comparing the frequency of regimes in the models to the observed frequency. The difference in the observation methods used to produce each dataset could also contribute to the differences in frequency.

Table 3.3: Comparison of the fractions of dry, light, moderate, heavy and TC days between AWAP and CMORPH.

Regime group	AWAP frequency	CMORPH frequency
Dry	37.3%	35.4%
Light	40.8%	33.2%
Moderate	13.1%	8.3%
Heavy (non TCs)	6.4%	15.9%
TCs	2.4%	7.2%

### 3.3.4 Synoptic patterns

Composites of the 900 hPa wind fields for each regime in CMORPH are shown in Figure 3.4. When compared to Figure 2.7, the wind fields show little difference to those of the AWAP-based regimes, with the dry regime and Regimes 1 and 2 all closely resembling their counterparts (Light and Moderate for Regimes 1 and 2). The remaining heavy rainfall regimes, including the TC regimes, all show a closed low near the rainfall maximum in the

same manner as the composites when using AWAP. Regimes 5 and 7 have generally lower wind speeds than the equivalent Top End and Inland regimes from AWAP, however the shape of the circulation is preserved. The new regimes, 4 and 6, both show cyclonic circulation slightly west of the rainfall maximum resulting in moist onshore flow, which is a similar arrangement to the other heavy regimes.

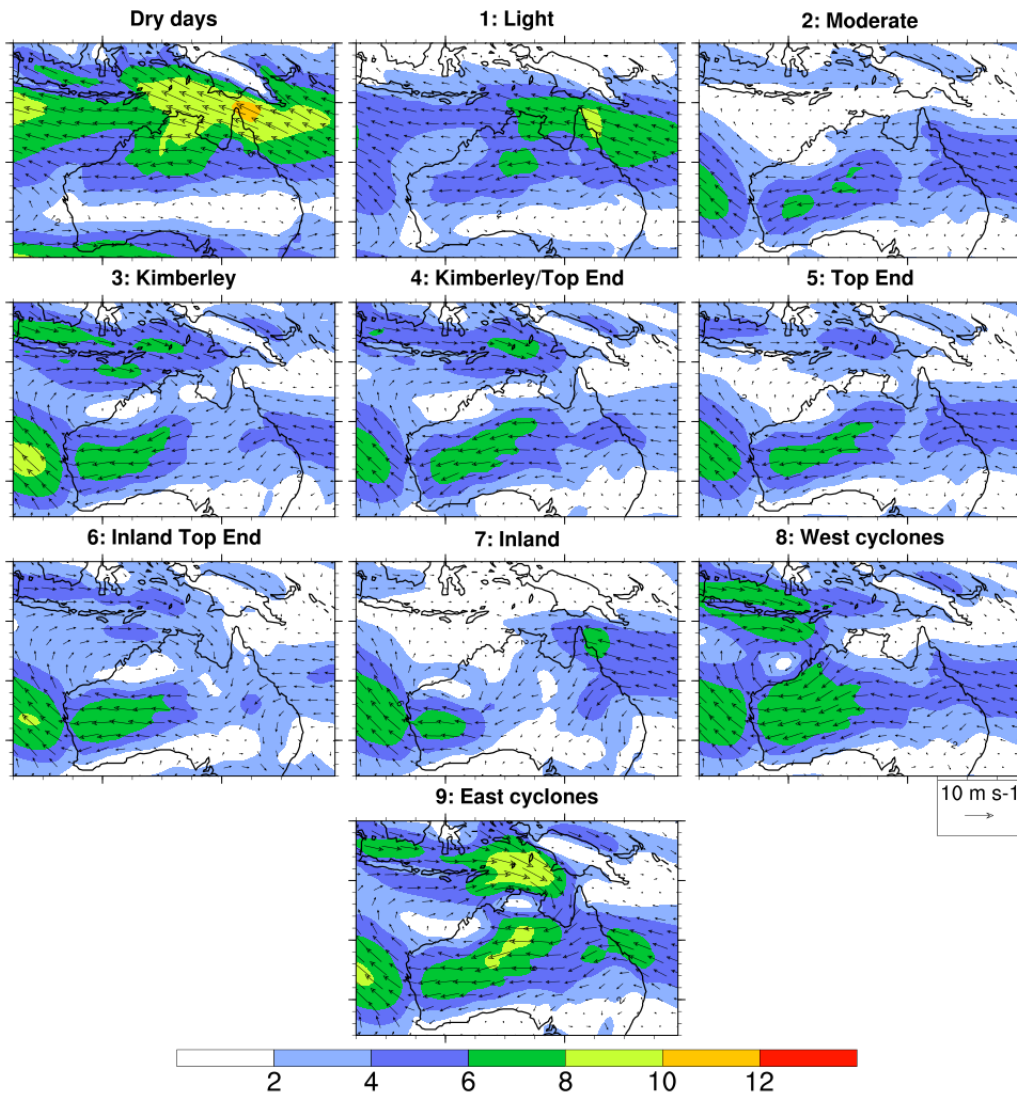


Figure 3.4: 900 hPa wind composites for the CMORPH regimes. Shading indicates wind speed in  $\text{m s}^{-1}$ .

The 850 hPa specific humidity composites for each regime are shown in Figure 3.5. A different level was chosen here compared to the 900 hPa level chosen in the last chapter as we are comparing low-level flow in models to observations later in this chapter, and the models to be evaluated do not provide output at 900 hPa. The patterns and values for specific regimes are very similar for the heavy regimes for both CMORPH- and AWAP-based

regimes despite the slight difference in levels, with regions above  $14 \text{ g kg}^{-1}$  present in the locations where the rainfall is occurring. The humidity is slightly lower for Regime 7, which is a similar result to the Pilbara regime in AWAP. As we progress from dry days to the Moderate regime, the humidity gradually increases over northern Australia from around  $6 \text{ g kg}^{-1}$  to around  $10\text{-}12 \text{ g kg}^{-1}$ . Overall, the intensity of the rainfall regimes is linked to the low-level humidity, similarly to the regimes based on AWAP.

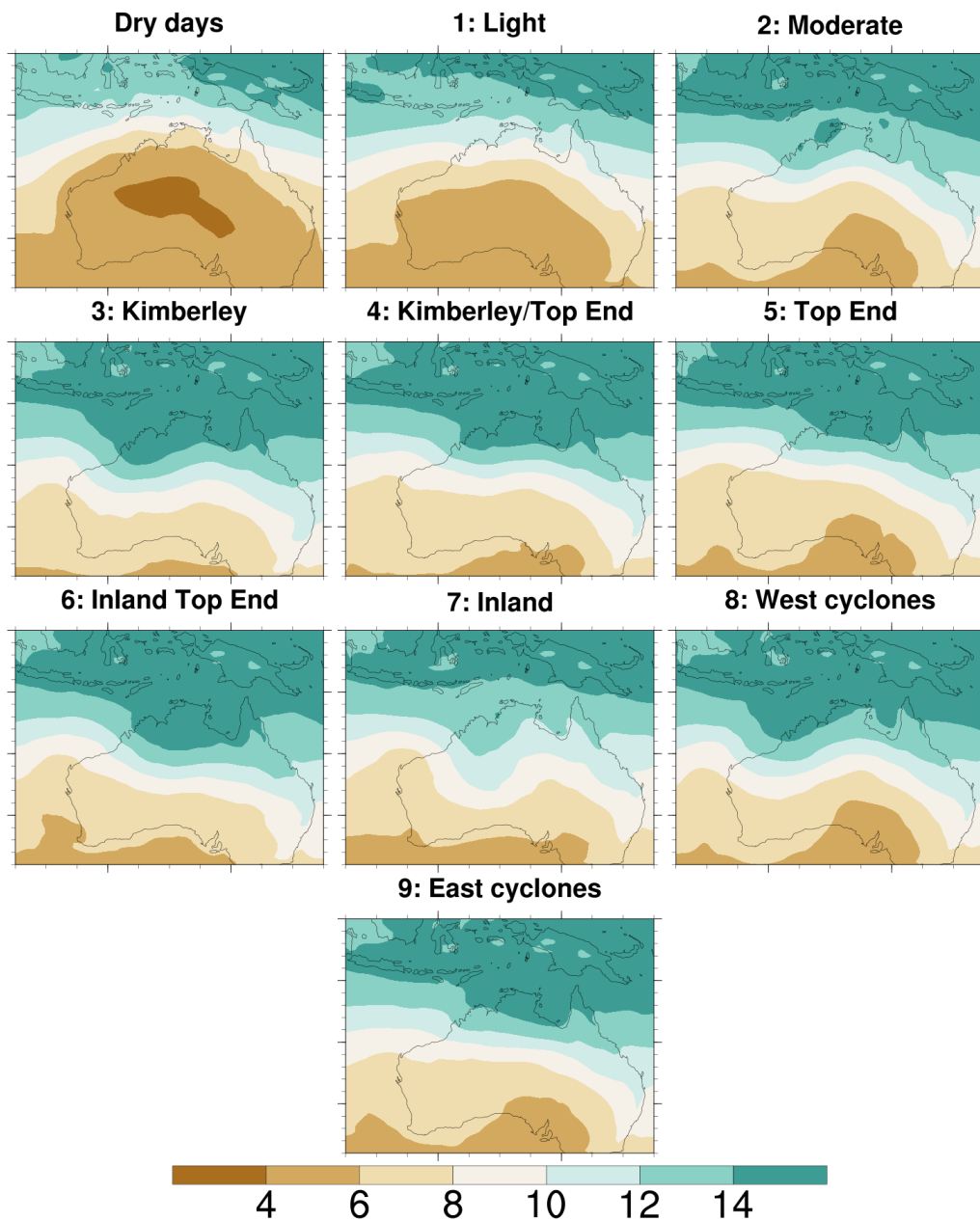


Figure 3.5: 850 hPa specific humidity composites for the CMORPH regimes. Units are  $\text{g kg}^{-1}$ .

Figure 3.6 shows the 500 hPa wind and 315K PV composites for CMORPH Regimes 3-9. Regimes 3 to 6 are associated with isolated PV anomalies centred over the region of maximum rainfall, although the signal is weaker than their equivalent patterns based on AWAP. It is likely that the weak signal is due to the much smaller sample of days in each regime rather than the average strength of the PV anomaly being weaker. The anomaly may be in a slightly different position on each day, which when averaged tends to blur out the actual strength of the anomaly, especially in smaller sample sizes. Regime 4 shows transport and slight strengthening of an isolated PV anomaly on the day of rainfall, and can therefore be characterised by a monsoon low highly similar to the AWAP-based Kimberley and Top End regimes. Regime 6 shows little evidence of an isolated PV anomaly, although the region of higher PV tends to extend westward at day +2, suggesting westward movement of a relatively weak disturbance. The CMORPH Inland regime (Regime 7) is able to capture the mid-latitude waves highlighted in Section 2.3, but the amplitude of the waves is weaker than for the AWAP regimes. The two TC regimes consist of isolated PV anomalies, similarly to the TC regimes in AWAP and what is expected for TCs.

Figure 3.7 shows the 250 hPa wind composites for Regimes 6 and 7. The wave pattern present in the AWAP Pilbara and Inland regimes is present in Regime 7, highlighting that this regime is also characterised by the influence of mid-latitude Rossby waves. Regime 6 has no such pattern, showing that the rain associated with this regime is unlikely to be influenced by mid-latitude interactions, and can be classified as another monsoon low-type system.

Overall, the CMORPH regimes strongly resemble the AWAP regimes in terms of spatial and synoptic patterns. Two additional regimes emerge, neither of which are associated with a new type of synoptic system. While the Pilbara regime does not emerge from the clustering, many of its days are absorbed into the new Inland-type regime (Regime 7). Since all of the major synoptic systems are represented by the CMORPH regimes, they may be adequately used as a real-world basis to which the CMIP5 models may be compared.

### 3.4 Rainfall regimes in ACCESS1-0

In this section, we begin to evaluate rainfall regimes in ACCESS1-0. Firstly, we determine how ACCESS1-0 simulates the mean rainfall over NWA before applying the three regime

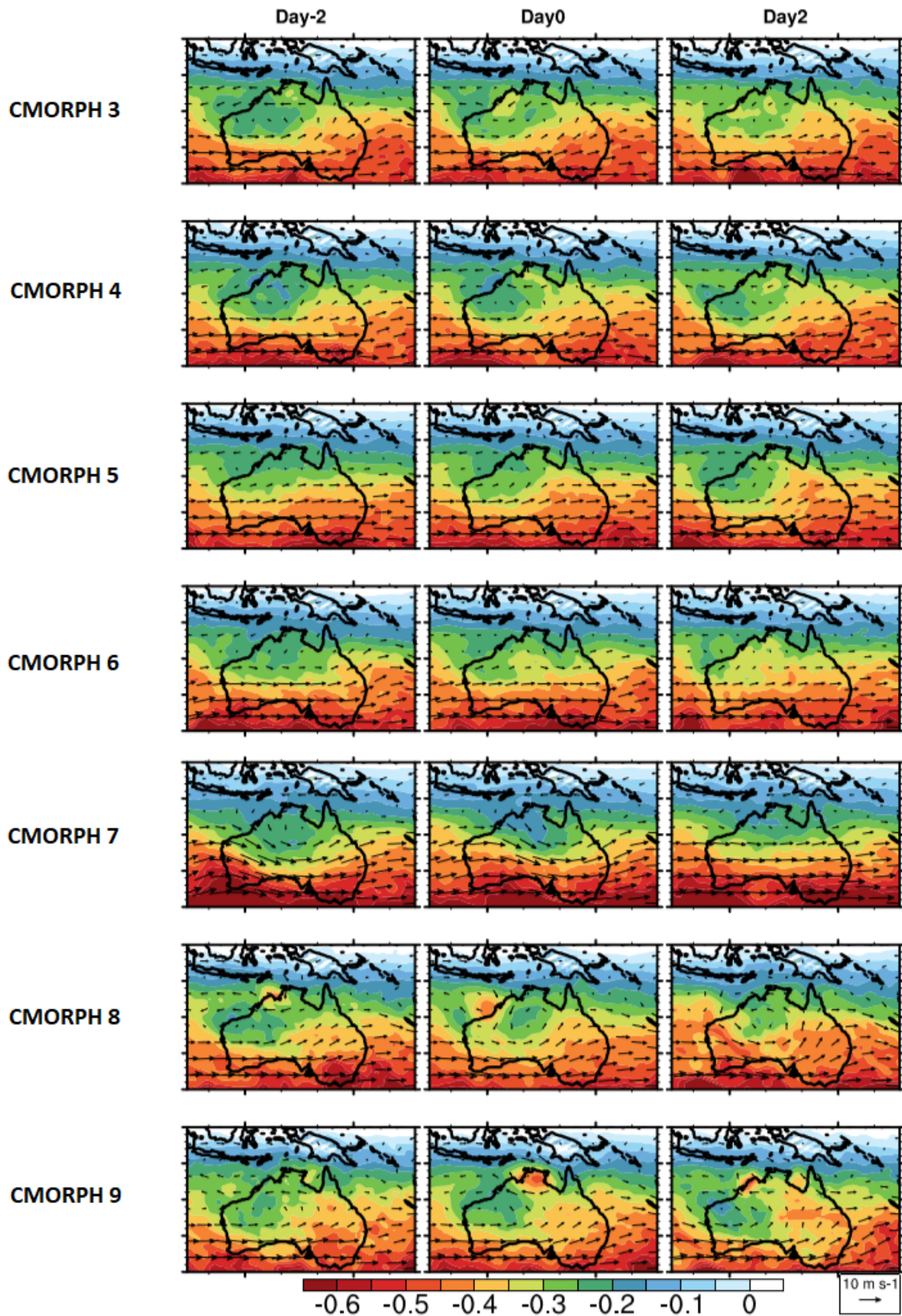


Figure 3.6: PV and 500hPa wind lag composites for CMORPH regimes 3-9. Composites indicate progression of systems 2 days prior, on and 2 days following a day in each regime. Shading units are in PVU.

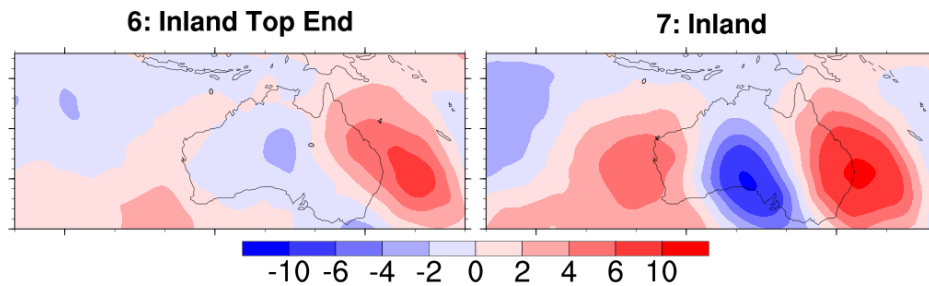


Figure 3.7: 250 hPa meridional wind composites for Regimes 6 and 7 in CMORPH. Units are  $\text{m s}^{-1}$ .

assignment methods to the model rainfall data. This section illustrates how each of the methods provides different information about the frequency, intensity and spatial patterns of model rainfall regimes, and provides an assessment of the ability of ACCESS1-0 to simulate the observed regimes.

### 3.4.1 Assessing the climatology in ACCESS1-0

The climatological rainfall in ACCESS1-0 is compared against the mean in the CMORPH observations to determine the nature of any precipitation biases. A secondary aim is to determine the biases over the neighbouring ocean regions, thus the choice of CMORPH rather than AWAP for this purpose. The mean rainfall is therefore taken over a much shorter and later period (1998-2016) than for AWAP (1950-2010). On the other hand, annual rainfall from 1970-1999 in the historical period are used to produce the mean in ACCESS1-0. Due to the observed increase in rainfall, the mean in CMORPH is likely to be higher than an observed mean from 1970-1999, however the observed change in rainfall over most of the study region from AWAP is approximately 20-30% inland, and closer to 10% near the coast (not shown), and thus biases in the model of more than 20%, especially near the coast, can be considered to be significant.

Figure 3.8 shows that there is a strong negative bias of more than 20% relative to the observations over most land areas within a few hundred kilometres of the coast; while the inland SE of the study region and ocean areas north of about  $12^{\circ}\text{N}$  show positive biases of over 20%, although the inland regions have small absolute changes due to the low mean (left panel of Figure 3.8). Negative biases exceed 600 mm, or 60% in small parts of the Kimberley region. From the positive bias over the ocean and negative over land, it is possible that

processes associated with the monsoon are unable to produce rainfall sufficiently southward. Changes to rainfall regimes could help understand how the bias in models occurs, so we will discuss these changes in the next section.

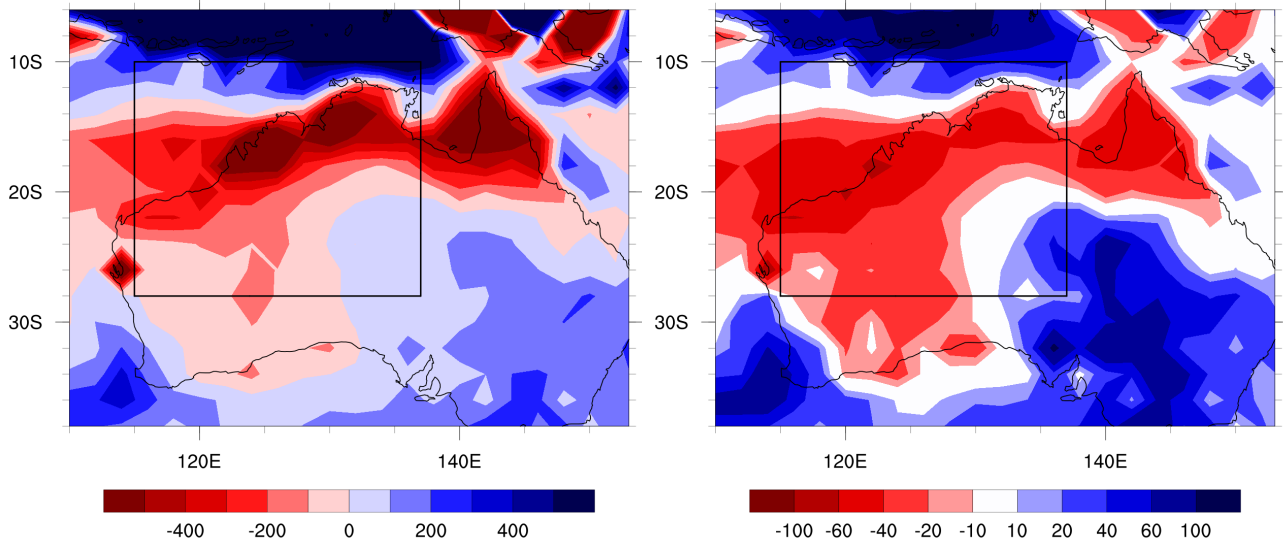


Figure 3.8: (left) Bias in annual mean rainfall in ACCESS1-0 historical run vs. CMORPH. Units are in  $\text{mm year}^{-1}$ . (right) As before, but expressed as a percentage of the annual mean in CMORPH. The box indicates the study region.

The seasonal distribution of rainfall over the land in the study region in ACCESS1-0 and in CMORPH shown in Figure 3.9. By comparing the two curves, we can determine the timing of biases in rainfall. The maximum rainfall in the model occurs a month later and is less than that of the observations. From October to December, rainfall in the model is significantly below that observed, in most months less than half of that observed. Thus, much of the negative bias in rainfall over land can be attributed to a reduction in spring and early summer rainfall. Austral winter rainfall is slightly higher in the model than in the observations, although still far lower than other months.

### 3.4.2 Method I: Projecting model rainfall onto observed regimes

In the previous subsection, we showed that there are significant biases in the representation of mean rainfall in ACCESS1-0. We decompose the model rainfall into regimes, starting with the projection method in this section, with the aim of explaining these biases in terms of changes to the regimes.

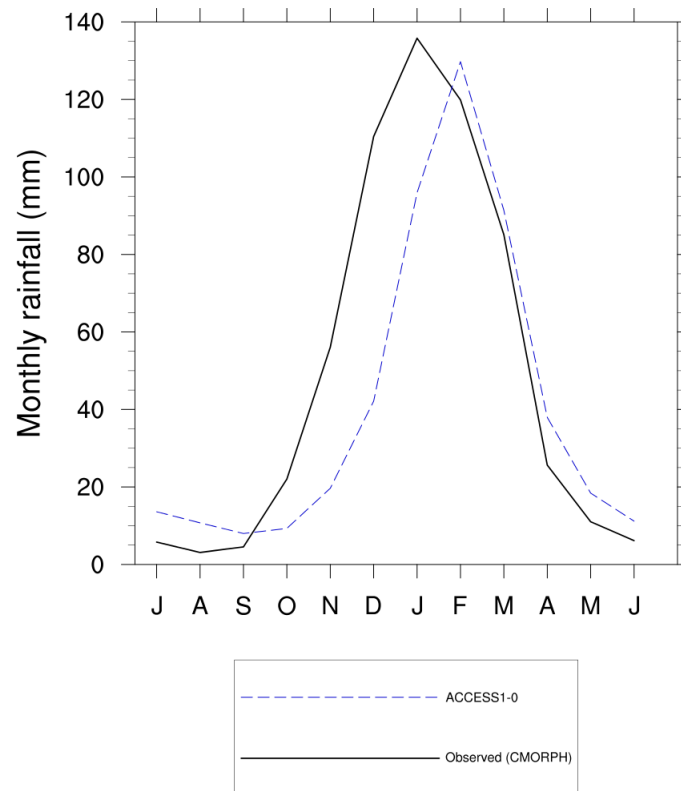


Figure 3.9: Monthly mean rainfall over the land ( $\text{mm month}^{-1}$ ) within the study region in CMORPH (solid black line) and ACCESS1-0 (dashed blue line).

### Spatial patterns and their frequency

Method I, also referred to as the projection method, determines rainfall regimes based on the mean of the closest (by Euclidean distance) model daily data to the observed regimes. Figure 3.10 shows the model regimes found when projecting model days onto the observed rainfall regimes in this way. The patterns are very similar in shape to the observed regimes as presented in Figure 3.2, and thus the regimes determined using this method may have the same number labels as for the observed regimes. Regime 2 has lost some of the detail in the spatial pattern along the coast, which is expected in lower resolution data. In addition, the maximum rainfall in most of the heavy regimes is more intense than in the observations. The maximum rainfall appears to be slightly shifted onto the coast or offshore, in the case of Regimes 3, 4 and 5 (compare Figure 3.10 to Figure 3.2). While this may initially appear to be an artefact of the low resolution in the model clustering, it fits with the bias in mean rainfall shown in Figure 3.8, as an offshore shift of the regimes associated in coastal rainfall agrees with the negative bias in the climatological mean. The similarity in the shape of the model rainfall pattern relative to CMORPH is an expected result, as this method forces the

model regimes to fit the observations. Of course, it is possible that the model produces regimes that do not match the observations. Therefore, this method is unable to identify whether model regimes have differing spatial patterns from the observations. Instead, the main information from this method is in the frequency with which each regime occurs.

Table 3.4 shows the frequency and contribution to total rainfall by the observed and model regimes. Relative to the observations, ACCESS1-0 rains more frequently, with 71.9% of all days being wet days, compared to 64.6% in CMORPH observations. The higher fraction of wet days in ACCESS1-0 is represented most strongly by a large fraction of light rainfall days (Regime 1) and a low fraction of heavy rainfall days. In ACCESS1-0, 52.1% of wet days fall into Regime 1, which contributes 29% of rainfall in the region, compared to 33.2% and 15.5% for the observations respectively. In contrast, ACCESS1-0 produces almost all of the heavy rainfall regimes far too infrequently, with regime 3 most poorly represented at slightly more than one-quarter of the observed frequency. Regime 5 is well represented in terms of frequency, but as previously mentioned the rainfall maximum has been shifted offshore and is more intense than observed. The maximum intensity of each of the heavy regimes is generally higher in the model than the observations, with Regimes 3 and 4 having maximum intensities of over  $50 \text{ mm day}^{-1}$ , as compared to around  $40 \text{ mm day}^{-1}$  in CMORPH. The maximum rainfall in the model for Regimes 6 and 7 are lower than observed, which when combined with the lower frequency, mostly explains the negative rainfall bias in inland areas. As the intensity of some of the heavy regimes in the model is higher than in the observations, their contribution to the total relative to their frequency is higher. For example, despite the Top End regime occurring at a similar frequency in the model compared to the observations, the contribution to the total from this regime is far higher than observed at 22%.

In summary, the projection method (method I) has shown that heavy regimes in the model occur too infrequently with rainfall that is too intense, and that the light regime occurs too frequently. However, the main drawback of the projection method is its assumption that the regimes in the model resemble the observed regimes. It is possible that the actual rainfall regimes produced by the model have spatial patterns which differ from the observed regimes. Method II, which is covered in the next section, produces model regimes independently of the observations, and therefore allows model regimes to differ from the observations more

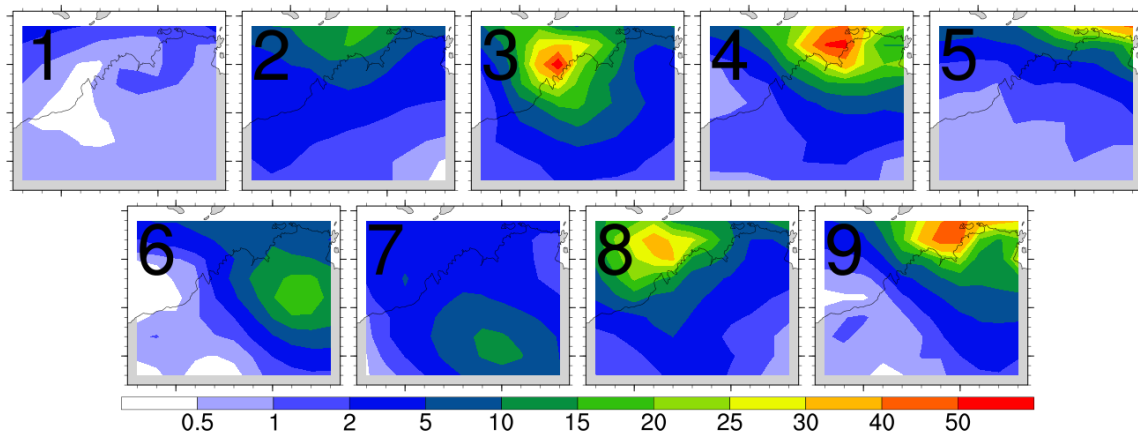


Figure 3.10: ACCESS1-0 rainfall regimes based on projecting model days onto observed regimes (Method I). The numbering for the regimes is the same as for the CMORPH regimes, due to the similarity of the spatial patterns.

Table 3.4: Frequency of days in each regime and the contribution of each regime to the total rainfall in CMORPH and ACCESS1-0.

Regime	% of rainy days		% Contribution to rainfall		Max. intensity (mm)	
	CMORPH	ACCESS1-0	CMORPH	ACCESS1-0	CMORPH	ACCESS1-0
<i>Wet days</i>	64.6	71.9	-	-	-	-
1	33.2	52.1	15.5	29.3	4.7	2.62
2	8.3	4.2	15.7	9.8	18.4	15.5
3	2.5	0.8	10.4	4.1	39.3	58.5
4	2.4	1.3	9.2	8.0	40.5	53.6
5	4.9	5.9	9.9	17.6	26.5	42.7
6	2.9	1.1	10.0	4.3	24.2	19.7
7	3.2	1.9	9	5.9	15.5	11.6
West TCs	4.2	2.5	11.5	8.9	21.3	31.4
East TCs	3.0	2.0	7.9	11.4	28.8	46.0

readily. The circulation patterns for the regimes developed from the projection method are discussed next.

### Synoptic structures of projected regimes

The winds at 850 hPa for each regime determined from the projection method are presented in Figure 3.11. Since these composites are derived from regimes that are forced to look like the observations, they are not necessarily the synoptic patterns that ACCESS1-0 typically produces. However, these composites can be used to interpret the type of synoptic systems that would be present if the model did produce the correct rainfall spatial patterns. The 850 hPa wind is used to investigate low-level flow here, since 900 hPa wind (as was used in Chapter 2 and Section 3.3) is not an output in the version of ACCESS1-0 used here.

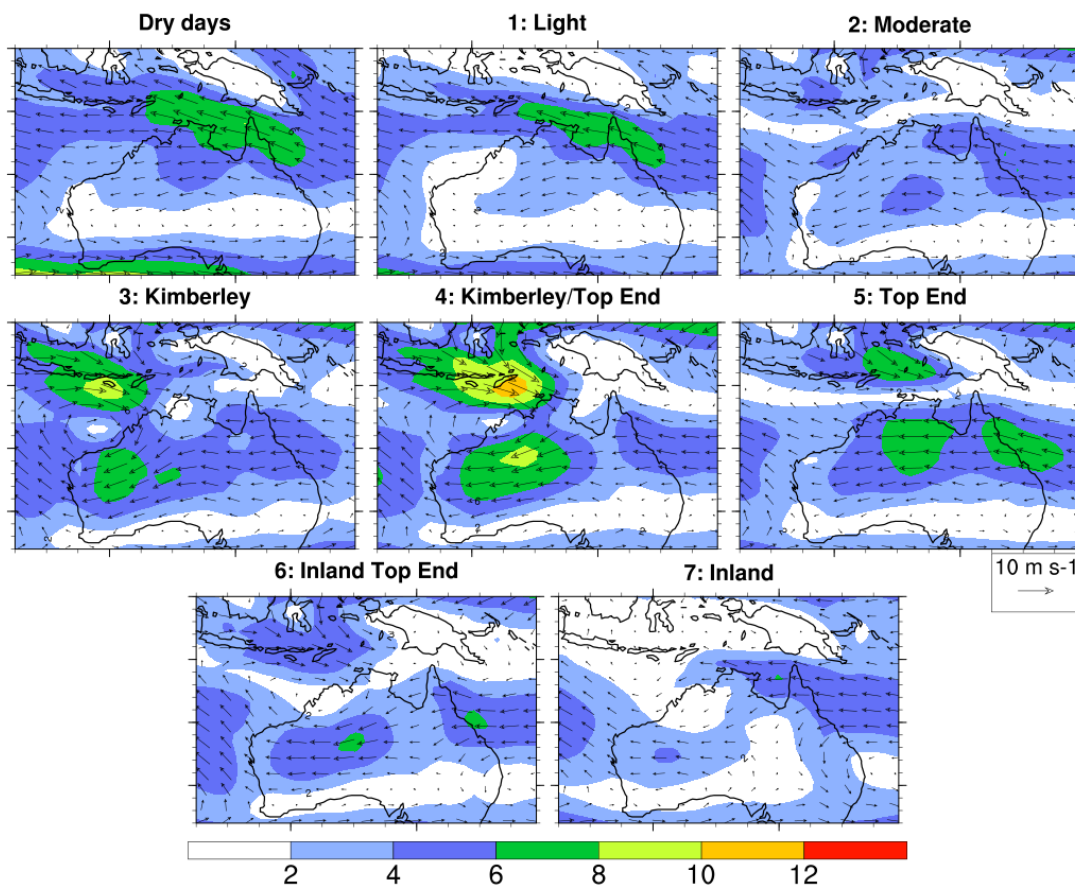


Figure 3.11: 850 hPa wind composites for the non-cyclone regimes in ACCESS1-0 derived from projecting to observed rainfall regimes (Method I). The cyclone regimes are equivalent in both Methods I and II, and are discussed in detail in Section 3.4.3.

The composites for dry days and Regimes 1 and 2 all appear similar to the CMORPH

low-level wind composites in Figure 3.4, with south-easterly winds over northern Australia in dry days, which tend more easterly and weaken in the transition through to Regimes 1 and 2. Regimes 3 to 6 all show cyclonic circulation near the regions of maximum rainfall in the same way as Regimes 3-6 in the observations, which suggests that the model produces rainfall in these regimes from monsoon lows in the same way as their counterparts in the observations.

Regime 7 in ACCESS1-0 only shows relatively weak circulation at 850 hPa. However, the regime producing inland rainfall in both CMORPH and AWAP is characterised by mid-latitude wave interactions, which are best identified by upper level wind patterns. Since both Regimes 6 and 7 in ACCESS1-0 are characterised by inland rainfall, meridional wind composites at 250 hPa are calculated and shown for these two regimes in Figure 3.12. The composite for Regime 7 (right) shows a mid-latitude wave pattern similar to the observations, although the magnitude of the winds is lower (max  $4 \text{ m s}^{-1}$  compared to  $10 \text{ m s}^{-1}$  in Figure 3.7) and the wave pattern is shifted significantly eastward. However, the general mid-latitude wave pattern is replicated in the model.

When the model does produce rainfall patterns in the region that are the same as observations, it does so with the correct synoptic patterns. However, the regimes defined using this method are not necessarily those the model produces naturally. The spatial patterns of regimes produced by the model can differ from the observations. The differences cannot be determined using the projection method, thus independent clustering shown in the next section allows these differences to be determined.

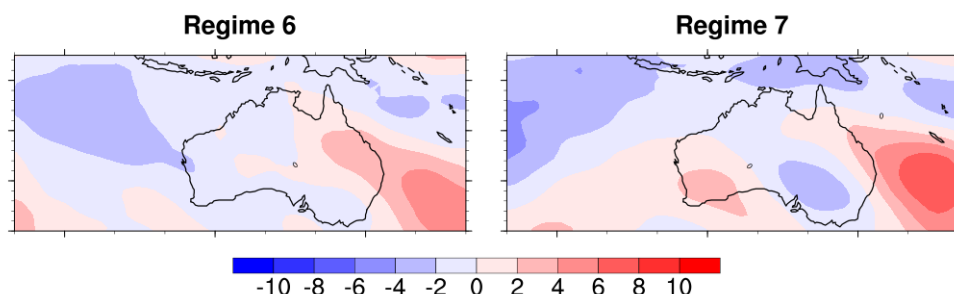


Figure 3.12: 250 hPa meridional wind composites for Regimes 6 and 7 in ACCESS1-0 derived from the projecting method (method I).

### 3.4.3 Method II: Independent clustering of model rainfall

#### Mapping the model clusters to the observed regimes

In this section, the regimes derived solely by clustering the model results are presented. As the clustering algorithm produces rainfall patterns in a random order, there is a need to objectively match the model rainfall patterns to the observed patterns. The matching involves calculating some measure of similarity from each model regime to each observed regime, and summing over all seven regimes for every possible arrangement of model to observed regimes. The measures of similarity used here are the Euclidean distance, where the sum across regimes is minimised, and the pattern correlation, where the sum is maximised.

A hypothetical example of this method was shown in Section 3.2.4. The matrix detailing the actual Euclidean distance between each ACCESS1-0 regime and each CMORPH regime is shown in Table 3.5. Note that the ACCESS1-0 regimes did not emerge from clustering in this order - the labels have been re-arranged for clarity. The cells containing blue shading show the mapping arrangement which gives the smallest possible sum of distances, and can be interpreted as the closest possible match between the model and observed regimes. The regimes in ACCESS1-0 are arranged according to this mapping, and are presented in Figure 3.13. The patterns themselves is discussed later in this section.

The Euclidean distance metric depends on both the spatial pattern and intensity of rainfall. As a result, it is possible that a model regime with a similar spatial pattern but a large intensity may have a larger distance from an observed regime than another which may have an incorrect spatial pattern. Pattern correlation may be used as another method of matching the model regimes to the observed regimes, which only takes into consideration

Table 3.5: The Euclidean distance between each CMORPH and ACCESS1-0 regime.

		ACCESS1-0						
		1	2	3	4	5	6	7
CMORPH	1	2.5	41.2	74.7	120.0	134.4	30.1	91.2
	2	32.7	35.6	54.0	98.0	119.9	28.1	88.5
	3	84.7	76.1	37.6	93.3	127.4	68.8	111.0
	4	88.7	72.5	76.4	68.2	105.3	71.2	107.8
	5	51.1	33.1	73.8	95.8	96.5	44.3	73.5
	6	61.7	60.0	69.7	96.7	124.8	35.4	102.0
	7	41.2	51.3	65.6	112.3	132.2	31.1	97.3

spatial pattern and not intensity. However, by considering only spatial pattern, there is a chance that regimes producing light and moderate rainfall, as well as regimes with a maximum over the Top End, may be incorrectly matched since their spatial patterns are similar to each other. Table 3.6 shows the pattern correlation matrix from matching ACCESS1-0 to CMORPH regimes. The ACCESS1-0 regimes along the horizontal axis are labelled in the same order they are labelled in Table 3.5 and Figure 3.13, with the blue text showing the optimum arrangement based on maximising the sum of the pattern correlations. Only one of the matches is the same as those produced from the Euclidean distance metric. Following the first row, the first (Light) regime in CMORPH is mapped to Regime 7 in ACCESS1-0, which has a very different and more intense spatial pattern than the least intense model regime. The first regime in ACCESS1-0 (taken as the "light" regime following the Euclidean distance method) is mapped to the seventh (inland) regime in CMORPH, which has a very different intensity and spatial pattern. These are examples of how the pattern correlation method does not reasonably map the model regimes to the observed patterns, so the Euclidean distance is preferred as an optimisation metric for mapping model regimes to the observations. The patterns resulting from the Euclidean distance mapping are covered in more detail next.

### The rainfall regimes in ACCESS1-0

Figure 3.13 shows the 7 rainfall regimes produced directly from ACCESS1-0 daily rainfall data, plus the two TC regimes derived from separating TC days from the data. The regimes have been ordered according to the mapping described earlier in this section, such that Regime 1 in ACCESS is equivalent to Regime 1 in CMORPH, and so on. By comparing

Table 3.6: The pattern correlation between each CMORPH and ACCESS1-0 regime. blue text shows the optimum mapping according to maximising the sum of the pattern correlation.

		ACCESS1-0						
		1	2	3	4	5	6	7
CMORPH	1	0.038	0.440	0.062	0.367	0.683	0.634	0.560
	2	-0.115	0.383	0.489	0.685	0.346	0.277	0.610
	3	-0.136	0.205	0.533	0.599	0.118	0.109	0.410
	4	-0.313	0.462	0.719	0.746	0.402	0.301	0.637
	5	-0.285	0.404	0.406	0.387	0.773	0.660	0.548
	6	-0.530	0.301	0.857	0.523	0.121	0.072	0.276
	7	0.312	0.275	0.121	-0.133	-0.195	-0.197	-0.159

this figure to Figure 3.2, we can see that the rainfall patterns associated with the observed Regimes 1, 4, 5 and the two cyclone regimes are replicated well in ACCESS1-0, since the spatial patterns generally match the observations; although in Regime 4 the maximum has shifted slightly offshore and is more intense than in the observations.

Compared to CMORPH, Regimes 2 and 3 have their maxima shifted offshore, with the latter regime having a less intense maximum compared to the observations. Regime 6 in ACCESS1-0 is significantly lighter than in the observations, and has an intensity more reminiscent of a Moderate type regime, however the location of the maximum is the same as the observed Regime 6. The regime corresponding to the observed Inland case is missing altogether, replaced by a regime with a large maximum offshore resembling CMORPH Regime 5 slightly. This regime is mapped to the observed regime with inland rainfall (Regime 7) because the other model regimes are a relatively good match to their respective observed regimes. Viewing along columns in Table 3.5, almost every model regime is mapped to the closest observed regime, except Regime 7 which is closer to CMORPH Regime 5 (Top End like). However, another model regime is already closer to the Top End regime, so it has been mapped to that space already, and thus Regime 7 is forced to map to the Kimberley regime as a leftover regime. Overall, the rainfall in most of the rainfall regimes in ACCESS1-0 is too heavy, and the maxima have been pushed offshore.

The rainfall spatial pattern of the regimes here, and in Figure 3.10, both suggest that ACCESS1-0 has difficulty replicating rainfall within a few hundred kilometres of the NWA coast, thus explaining the shape of the bias plot in Figure 3.8. As most heavy regimes are biased towards producing rainfall offshore rather than over land, there is less rainfall onshore resulting in the negative bias over inland coastal regions, and the positive bias offshore. ACCESS1-0 produces an inland regime (7) from the projection method, but fails to do so using the direct clustering method. The low frequency for Regime 7 in the projection method suggests that inland rainfall is produced at a low enough frequency that it does not emerge from direct clustering, instead being replaced by a second coastal maximum. The lack of an inland-type regime here suggests that the mid-latitude waves responsible for rainfall in this regime are not a significant driver of rainfall in ACCESS1-0.

The spatial pattern of the TC regimes appears as expected, with the rainfall maxima occurring over the western and eastern halves of the study region as expected. However, the intensity of the eastern TC regime is higher than the observed intensity, which is a similar result to the intensity biases noted in the other non-TC heavy regimes.

The presence of regimes that do not resemble the observations, or regimes that are missing in the model, will result in the sum of the distances over all matches being larger. Conversely, the closer the model regimes are to the observed regimes, the smaller the distance between them for the matched regimes, and the smaller the sum of the distances. As a result, the sum of the distances over all matches can be used as a metric to determine the closeness of model regimes to observed regimes. This metric can be used as a point of comparison to other models. While this simple measure is not able to detail specific differences between the model and observed regimes, it is able to provide a relative measure of a model's overall performance in reproducing the observed rainfall patterns.

### Frequency and intensity of ACCESS1-0 regimes relative to CMORPH

A comparison of the frequency of each of the regimes in both the CMORPH observations and ACCESS1-0 is presented in Figure 3.14. The figure presents the frequency relative to all days, as opposed to rainy days which has been previously presented in Chapter 2. Despite the differences in the spatial pattern of some of the regimes relative to the observations, the difference in the frequency of the model regimes compared to observations show a similar result to Method I. The model clustering method still results in ACCESS1-0 producing the

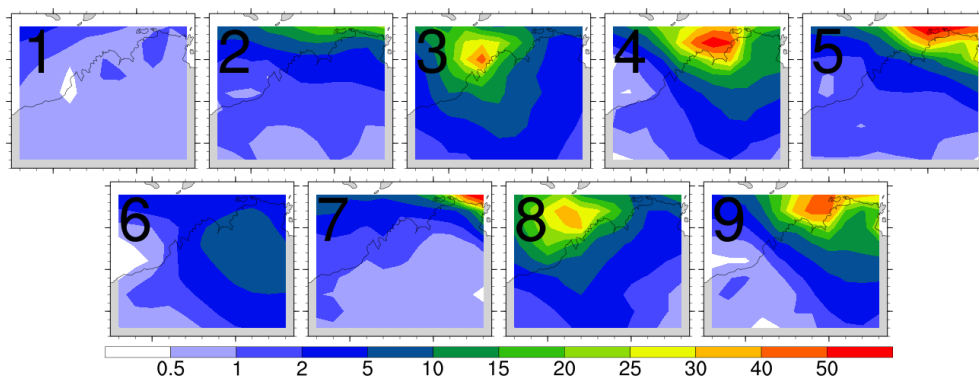


Figure 3.13: ACCESS1-0 rainfall regimes derived independently from the observations (method II).

light regime far too frequently, and almost all heavy regimes too infrequently, while Regime 5 has a frequency less than half of its equivalent in the observations. Only Regime 6 is more frequent than the observations, but this regime is far lighter and more closely resembles a Moderate regime based on its intensity, which may explain its higher frequency since lighter rainfall occurs more frequently than heavy rainfall. The two TC regimes are also at a lower frequency than observed TCs, although the difference in frequency is much smaller than for most of the other heavy regimes. Thus, based on the CSIRO Direct Detection scheme used to determine the TC tracks, ACCESS1-0 is able to reproduce TCs in the region with approximately the correct frequency.

For Regimes 2 to 5 and the TC regimes where the spatial patterns in ACCESS1-0 resemble those in CMORPH, the maximum intensity (defined as the maximum point in the regime centroid) for the regime centroid is much higher than that observed. These regimes generally consist of maxima which lie closer to the coast than in the observations, which explains the positive rainfall bias offshore in the climatological mean. Regime 6 consists of a much lower maximum than the equivalent in ACCESS1-0, suggesting the model has some difficulty in producing rainfall in inland areas. Regime 7, which has an isolated maximum of  $69 \text{ mm day}^{-1}$ , is the most intense regime in ACCESS1-0, although only produces this heavy rainfall in the corner of the region.

Generally, ACCESS1-0 produces heavy rainfall in coastal areas too infrequently with an intensity that is too high, compensated by an increase in the frequency and slight reduction of peak intensity of the Light regime. The synoptic structures associated with the remaining regimes will be assessed next.

### **Synoptic structures of the regimes in ACCESS1-0**

The winds at 850 hPa and 500 hPa for each ACCESS1-0 regime are presented in Figures 3.15 and 3.16. The 850 hPa wind is used to investigate low-level flow since 900hPa wind (as was used in Chapter 2) is not an output in the GCM version used here. The wind fields of the dry and Light (1) regimes appear similar in spatial pattern to the observed regimes shown in Figures 3.4 and 3.6. However, for the remaining regimes, some notable differences occur between ACCESS1-0 and the observed wind fields, although these differences are consistent

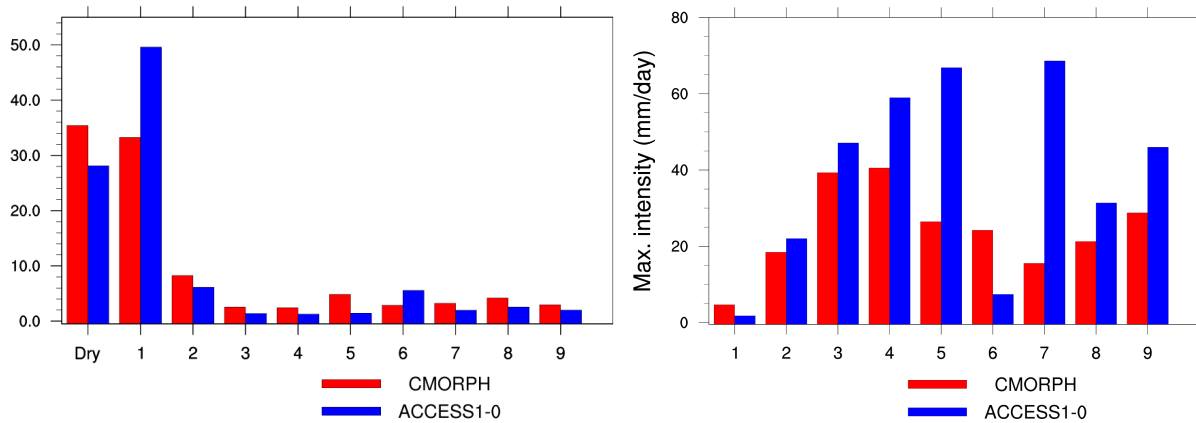


Figure 3.14: (left) Frequency of each regime in both CMORPH and ACCESS1-0, calculated relative to all calendar days. (right) Maximum rainfall for the centroid of each regime. The model regimes are numbered according to the mapping described in this section. Frequency in this plot is calculated relative to all calendar days.

with the differences in the model rainfall patterns relative to the AWAP observations. Looking at the 850 hPa wind composites, Regimes 2 and 7, which produce moderate rainfall and a sharp maximum in the corner of the Top End respectively, both show converging winds just north of the continent in a zonally oriented trough, consistent with offshore rainfall. Regimes 3, 4 and 5 are characterised a strong low pressure system in slightly different locations for each regime, which results in the heavy rainfall observed over northern Australia, consistent with the monsoon lows in the observations. However, the low centres are located further from the regions of maximum rainfall than in the observations. For instance, Regime 3 in CMORPH has a low centre almost directly on the coast, while the centre in ACCESS1-0 is located approximately  $5^\circ$  further west. In addition, the winds north of the continent for Regime 5 are stronger than any observed regime (up to  $14 \text{ m s}^{-1}$ ). Regime 6 shows no significant sign of a closed circulation causing rainfall, possibly as the rainfall in this regime is lower than other heavy regimes and is more likely to resemble the Moderate regime. The two TC regimes show circulation associated with the presence of the TCLVs, as expected since wind fields are used to identify the TCLVs in the first place.

To further characterise the regimes determined using Method II, 500 hPa wind composites for each regime are calculated and shown in Figure 3.16. Regimes 1, 2 and 6 show anticyclones near the regions of high rainfall, suggesting the systems responsible for rainfall in these regimes are shallow. Regime 3 has little signal aside from some weak onshore flow

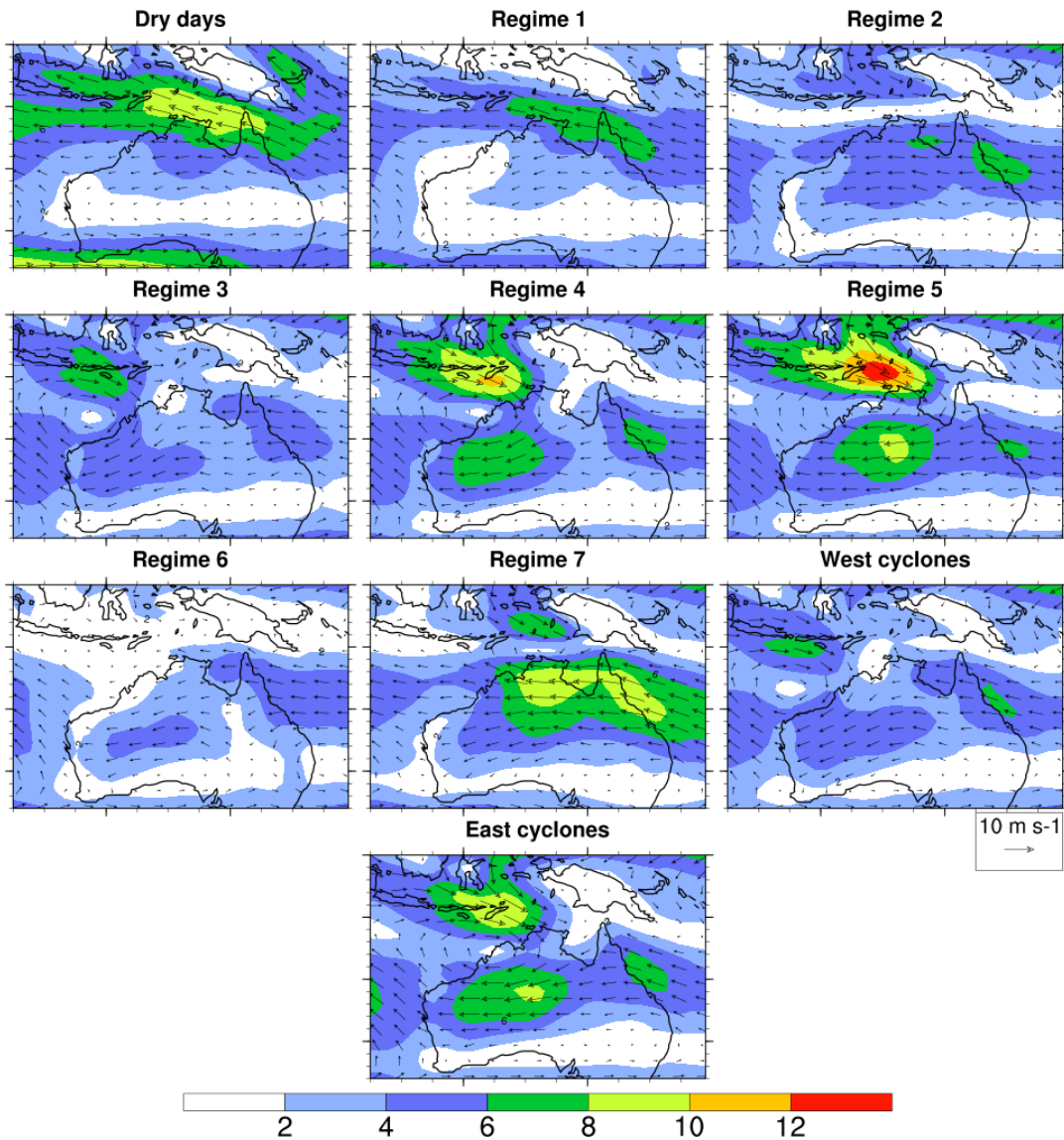


Figure 3.15: 850 hPa wind for each ACCESS1-0 regime (Method II). Shading indicates wind speed ( $\text{m s}^{-1}$ ).

over the region of maximum rainfall, suggesting the flow for this regime is also shallower than that observed. In contrast, Regimes 4 and 5 both have strong cyclonic circulation resembling that of monsoon lows, indicating these are relatively deeper systems. The East Cyclone regime shows a strong cyclonic circulation typical of TCLVs, however the West Cyclone regime shows a weak cyclonic circulation. No composite in Figure 3.16 shows evidence of mid-latitude waves, as opposed to the observations in Figures 2.11 and 3.6.

To further highlight the lack of mid-latitude waves in the Method II regimes in ACCESS1-0, Figure 3.17 shows the 250 hPa meridional wind composites for Regimes 3 to 7 (regimes causing heavy rainfall). Dry days and Regimes 1 and 2 are omitted, since these correspond to relatively lighter rainfall and have little forcing at lower levels (see Figures 3.15 and 3.16).

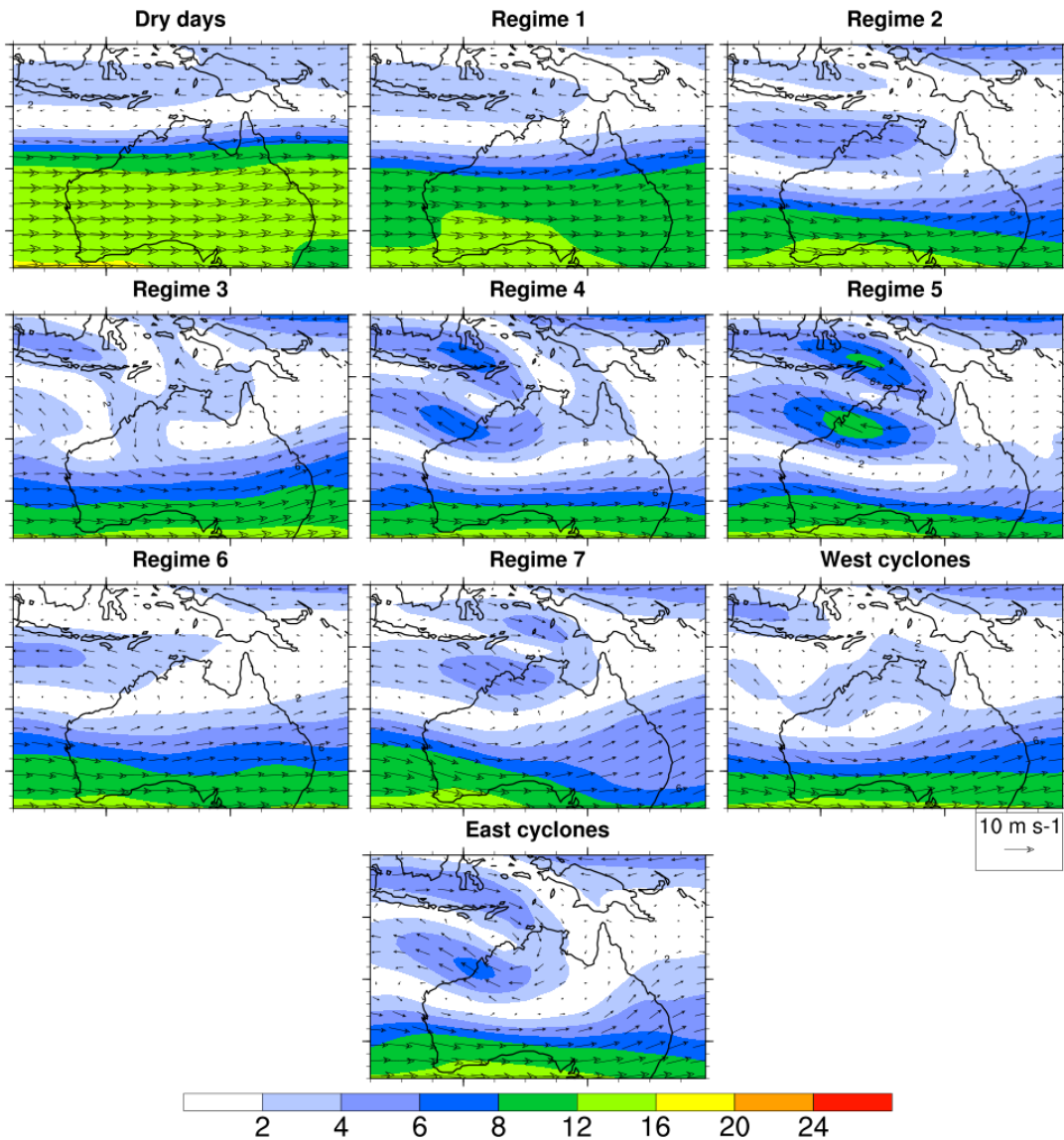


Figure 3.16: 500hPa wind for each ACCESS1-0 regime. Shading indicates wind speed ( $\text{m s}^{-1}$ .)

For Regimes 3 to 5, there is a weak northerly component over the western coast of Australia, and a weak southerly component over a broad region covering much of eastern Australia, which is consistent with an anticyclone over northern Australia rather than a mid-latitude wave pattern. Regimes 6 and 7 show very little pattern in the meridional wind composites, indicating that no regime produces a mid-latitude wave pattern.

Since most heavy rainfall maxima in the ACCESS1-0 regimes lie on the coast, and given that it is inland regimes with maxima further south that are usually influenced by the mid-latitudes, none of the model regimes produced by this method have maxima that are sufficiently far south or inland to be influenced by the mid-latitudes. An inland regime is produced

in Method I, however the frequency is much lower than in the observations. The presence of an inland regime in Method I, but not Method II suggests that mid-latitude waves cause rainfall in NWA so infrequently that it is not determined from the clustering.

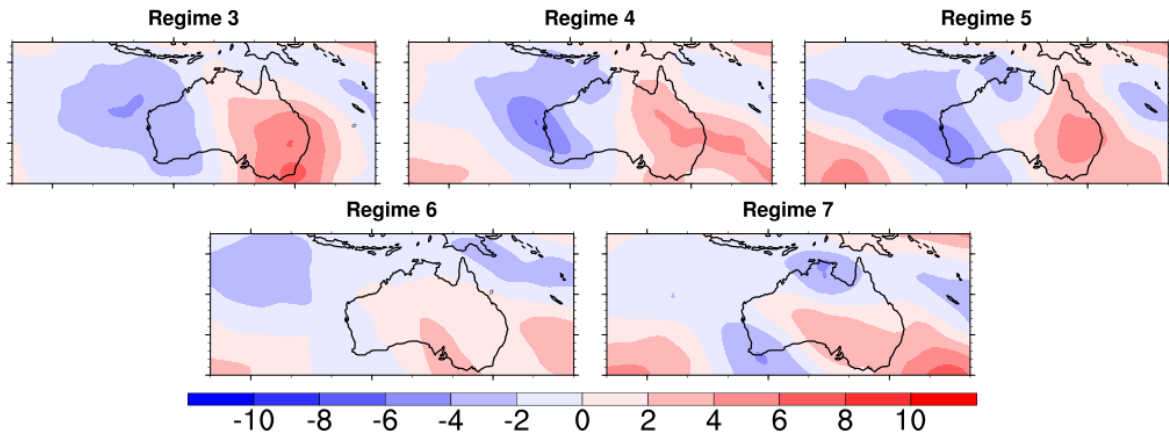


Figure 3.17: 250 hPa meridional wind for ACCESS1-0 Regimes 3 to 7 (Method II). Units are  $\text{m s}^{-1}$ .

The 850 hPa specific humidity composites for each regime are presented in Figure 3.18. Similarly to the observed regimes in AWAP, specific humidity over northern Australia gradually increases from around  $6 \text{ g kg}^{-1}$  to over  $10 \text{ g kg}^{-1}$  as we progress from dry days to Regimes 1 (light rainfall) then 2 (moderate rainfall). Regimes 3 to 5 also have high specific humidity close to the location of maximum rainfall, locally above  $12 \text{ g kg}^{-1}$ . Regime 6 has a region of specific humidity above  $12 \text{ g kg}^{-1}$  which is disconnected from the humid air over the Maritime Continent, while Regime 7 has the humid air ending further north than most of the other heavy regimes. The humid air is therefore generally in the correct location for rainfall to occur, and is consistent with observations, however the values are generally lower than those observed, with maxima for heavy regimes between  $12\text{-}14 \text{ g kg}^{-1}$  rather than above  $14 \text{ g kg}^{-1}$ .

Overall, the composites show that the Inland regime is missing from the model according to this method, and a regime corresponding to a monsoon trough causing heavy rainfall just offshore of the Top End has replaced it. Thus, all of the basic types synoptic systems responsible for rainfall in the region that were determined in Chapter 2 are captured by the model, with the exception of mid-latitude interactions. The model regimes which exhibit heavy rainfall do so with the correct circulation, although humidity in the lower troposphere

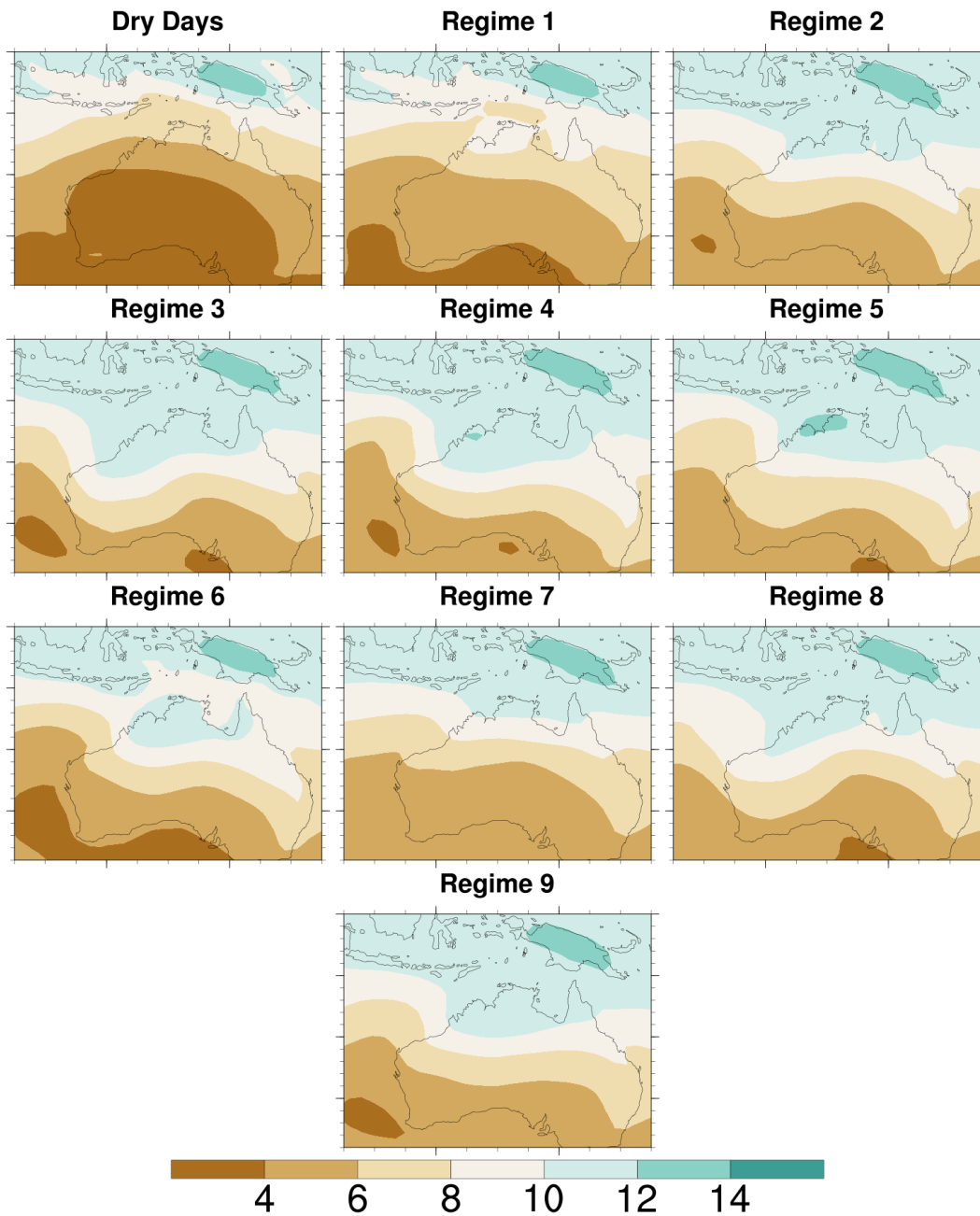


Figure 3.18: 850 hPa specific humidity for each ACCESS1-0 regime (Method II). Units are  $\text{g kg}^{-1}$ .

is usually underestimated. However, low-level convergence lines may erroneously produce rainfall offshore, thus moving the rainfall maximum northward toward the coast in some regimes. Thus, the model produces some rainfall from synoptic structures which are not identified in the composites associated with the observations.

The direct clustering method is able to determine and characterise rainfall regimes in the models without influence from the observations. Differences in spatial pattern, frequency,

intensity and synoptic patterns can be discussed in detail. Method III combines model and observed data into a single dataset for clustering, which summarises changes to regime spatial pattern and frequency in a concise manner, and is discussed in the next section.

#### **3.4.4 Method III: Clustering model and observations together**

This subsection presents and discusses the outcome from clustering model and observed data in a single analysis. TCs are removed prior to analysis, and are not included in this method since they are discussed in the previous method. Data from an equal number of observed (CMORPH) and model days are combined into a single dataset, before removal of dry days and clustering. The regimes produced from the 7 cluster case are shown in Figure 3.19. The regimes have been mapped to the CMORPH-only regimes using the same distance metric as outlined in Section 3.2.4 for Method II. As these regimes are at least partially based on the observed regimes, these are more likely to match the observations. By comparing Figure 3.19 to Figure 3.2, we note that the rainfall patterns are similar, and thus this method reproduces the basic patterns well with the exception of the Inland regime, which has already been noted in Section 3.4.3.

If there are differences in the location or intensity of the model regimes relative to those observed, the resulting clusters from this method will be different from the observations. As these patterns may be considered a hybrid of the observed and model patterns, the patterns themselves are difficult to interpret without information on the relative fraction of model and observed days in each regime. However, by considering this fraction of observed and model days in each regime, model performance can be evaluated in a relatively simple way.

Table 3.7 provides the percentage of cases in each regime that originated from model data. The percentage of observed cases is simply the remaining percentage to 100%. From this table, Regimes 3, 6 and 7 from this method are strongly biased toward containing observations, indicating that the model does not reproduce these regimes very well. These regimes strongly resemble the Kimberley, Inland TE and Moderate regimes respectively, despite the Moderate regime being mapped to the Inland regime in the observations. The addition of model data prevents the Inland regime from emerging from the observed data. The low fraction of model days in these regimes add evidence to the hypothesis that ACCESS1-0

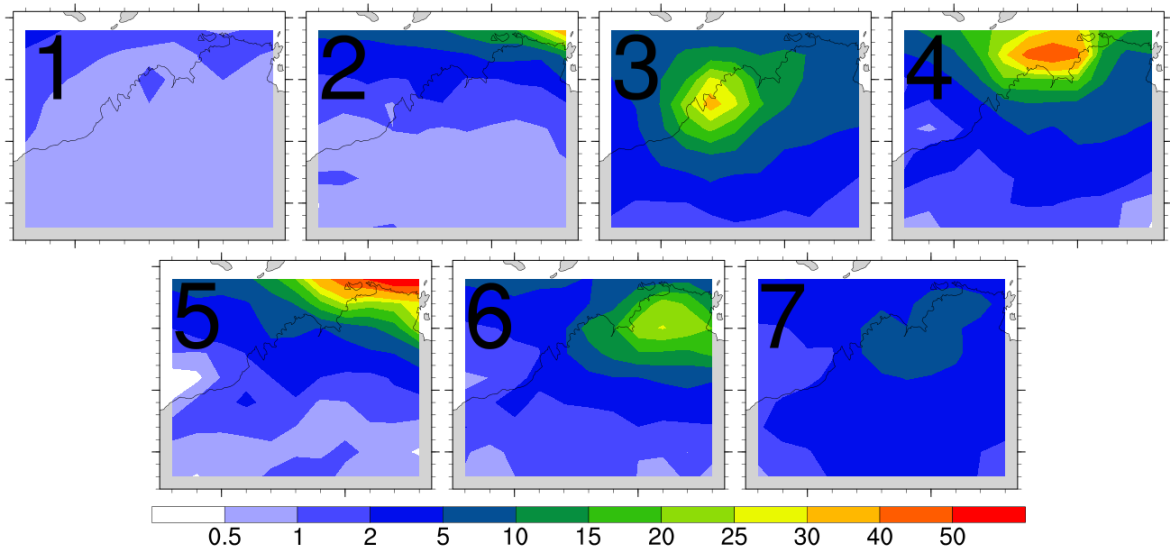


Figure 3.19: Combined model and observed clusters from Method III. Units are mm day<sup>-1</sup>.

does not move rainfall sufficiently inland to reproduce the Moderate and Inland TE regimes. Conversely, Regime 5 is strongly populated by model cases. The rainfall pattern in Regime 5 strongly resembles the erroneous heavy TE regime produced in Method II, which biases this regime toward heavier rainfall totals relative to the observations, especially given the large fraction of model days in this regime. The remaining clusters may be within the 2:1 ratio set as the threshold for a regime to be model or observation based, however there is still some bias toward model or observed days depending on the regime. As the Light regime has a very large overall population of days, the 40:60 ratio of observed to model days suggests the Light regime is produced far too often in the model, which agrees with the results from the previous two methods.

By determining the fraction of model (and by inference, observed) days in each regime from this method, it is possible to identify regimes in the model which do not exist in the observations. Thus, this method is effective as an additional tool to assess the ability of the

Table 3.7: Percentage of model days in each regime from the combined clustering method (Method III). The percentage of observed days in each cluster is equal to the remainder to 100%.

Regime	% model days	Regime	% model days
1	60.0	5	74.7
2	61.1	6	12.4
3	16.5	7	33.9
4	57.4	Total	53.1

models to replicate the observed regimes.

## 3.5 Discussion

### 3.5.1 Overall assessment of ACCESS1-0

This chapter has investigated the suitability of CMORPH for reproducing the observed rainfall regimes relative to AWAP, before comparing the CMORPH regimes with ACCESS1-0. Since CMORPH daily data fills in the regions for which AWAP has missing data, there have been minor changes to the regimes in CMORPH relative to those discussed in Chapter 2. There has also been an increase from 6 to 7 regimes when changing from AWAP to CMORPH observed data. The Pilbara regime in the AWAP based analysis has been eliminated and the cases belonging to it shared among remaining regimes, while two new regimes emerge: one with a rainfall maximum centred between that of the Kimberley and Top End regimes, and one centred in inland parts of the Top End.

Firstly, the ability of ACCESS1-0 to reproduce the annual mean rainfall is assessed. The model tends to underestimate precipitation over much of the land area of NWA and overestimate precipitation over the ocean. The strongest negative biases exist over the Kimberley and inland parts of the Top End within a few hundred kilometres of the coast. This is a result of the model tending to under-represent the frequency of heavy rainfall regimes, move the rainfall maximum offshore, and overestimate its intensity, a result consistent across all three regime assignment methods.

Both Methods I and II used to identify model regimes find that the model overestimates the number of rainy days as well as the number of days in regime 1 (light rainfall), and underestimates the number of heavy regime days significantly. In addition, the contribution of regime 1 to the total rainfall is greatly overestimated. These results agree with the general tendency of climate models to produce too much light rain in tropical regions (e.g. Stephens et al. (2010)).

The synoptic patterns associated with the heavy regimes in both Methods I and II (Figures 3.11, 3.15 and 3.16) mostly consist of monsoon lows, and thus their low frequency

suggests ACCESS1-0 has a bias toward producing fewer of these systems. Some of these systems are identified as TCLVs and are described as a separate system in this work, with their frequency only marginally lower than the observed frequency of TCs. This is somewhat surprising given the low model resolution, but it is a result of how rainfall is produced by the TC-like systems identified by the CDD method outlined in Section 3.2. Despite the lower frequency, the model is able to reproduce the basic structure of monsoon lows and TCLVs, with the wind speeds around the low centres slightly higher than in the ERA-Interim reanalysis, and the rainfall maxima located further from the low centre. The composite for regime 7 in Method I indicates that the model is able to produce rainfall in NWA from mid-latitude waves, but at a much lower frequency than observed. The low frequency explains why the regime does not emerge from clustering in Method II or III, and suggests the model does not produce a significant amount of rainfall in NWA from these systems.

The rainfall maxima in the regimes derived from Method II are generally located close to the coast or offshore, in contrast to the observed regimes where rainfall maxima are located slightly inland. The maxima are also much higher than those observed, partially explaining the offshore positive bias in the climatological mean rainfall. The negative bias over land areas can be explained by the shift of rainfall toward the coast, and the lower frequency of regimes causing heavy rainfall in the region.

From independent clustering (Method II), ACCESS1-0 is able to produce most of the rainfall regimes from the observations aside from those producing inland rainfall, and with the right circulation. However, there are slight biases in the location of the rainfall maxima, and more significant biases in the frequency of individual regimes, especially in regime 3. The bias in the model must therefore be explained by a mechanism that prevents rainfall from monsoon lows from moving further south, since regime 3, which has the strongest negative bias in frequency, is located further south than regimes 4 and 5. Future work in model improvement should aim to solve this bias in the historical period in the model.

### **3.5.2 Assessment and summary of the regime assignment methods**

The three regime assignment methods are assessed for their applicability to a multi-model comparison to be covered in the next chapter. The projection method (Method I) produces

regimes that have the same spatial pattern as the observations, thus allowing differences in frequency and intensity of each regime to be determined and interpreted in a straightforward manner. However, the assumption that the model regimes have spatial patterns equivalent to the observations has been shown to be false for ACCESS1-0, and is therefore potentially false for other models. Projection of model data onto observed regimes does not account for any differences in the spatial pattern of the regimes, and thus cannot be used to determine if differences exist. However, it provides the simplest comparison of differences in frequency and intensity of each regime, which will aid in determining this aspect of how the models differ from the observations and each other. Frequency and intensity comparisons determined using this method can be used to rank each model's ability to replicate the frequency of observed regimes, and thus partly explain climatological rainfall biases in each model. In addition, by fixing the rainfall spatial patterns of the regimes, the synoptic patterns in each model can be compared easily. Differences in the wind fields relative to observations can therefore only be explained by differences in the physical reasons for the model initiating rainfall, and not by differences in the rainfall spatial pattern.

Direct clustering (Method II) has the advantage of producing regimes directly from model rainfall, and thus it is possible to closely examine whether the typical rainfall regimes in the model differ in spatial pattern to the observations. In the case of ACCESS1-0, some of the spatial patterns and their intensity deviate from the observations, notably regime 7 which is characterised by a rainfall peak in the corner of the study region rather than an inland maximum. The location of the maximum is similar to that of regime 5, thus the two regimes can be considered to be similar. It is possible that a choice of using fewer clusters (for example, six) with this method could produce a set of regimes that are less similar to each other. However, choosing a new number of clusters for each model makes comparison across models difficult. If the model fails to produce certain regimes, or produces regimes that are not observed, the spatial patterns that emerge from the 7 cluster case are still likely to be different to the observed patterns. The differences can be quantified using the sum of distances from the mapping in this method.

The distance sum can be used as a metric by which to rank the ability of models in replicating the observed rainfall. However, it is more difficult to compare the frequency,

intensity and synoptic patterns of individual regimes to the observations since we will likely be making a comparison between differing rainfall patterns. As an example from Section 3.4.3, it is difficult to compare the frequency of regime 7 in ACCESS1-0 to the observations since the rainfall patterns (compare Figure 3.4 to Figure 3.2) are entirely different. Thus, Method II adds information about the spatial pattern of rainfall regimes rather than their frequency.

Method III provides similar information to Method II, since differences in the spatial pattern of the model regimes will be reflected in biases in the fraction of model days in a given regime. Bias in a Method III regime toward model cases may be interpreted as either over-representation of an observed regime in the model, or the spatial pattern being transformed into a pattern not occurring in the observations. The simple fraction measure in Method III is unable to distinguish between these two possibilities. However, any bias in a regime toward either observation or model days can be regarded as a shortcoming in the model, regardless of its cause. Thus, the fractions can be used as a concise way of showing differences in both frequency and spatial pattern in each model. Fractions that are significantly different from an equal mix of model and observed days imply a shortcoming in the model, thus the mean of the difference of fractions from 50:50 can be used to rank the closeness of model patterns and frequency to the observations.

The next chapter will assess the ability of a selection of other CMIP5 models in replicating the observed rainfall regimes. Information from all 3 methods will be used to determine how well a number of models are able to reproduce the observed rainfall regimes with the correct frequency, intensity and synoptic patterns. The ability of each model will be taken into account when investigating the future climate in Chapter 5.

## 3.6 Conclusion

This chapter outlined and tested the approaches to be used to compare the ability of a number of CMIP5 models to reproduce the observed rainfall regimes. The approaches were tested on a single CMIP5 model, ACCESS1-0, before further application to other models in the next chapter. Observed regimes were derived from CMORPH data rather than AWAP (Chapter 2) in order to use a spatially complete dataset. The change in observation dataset

resulted in two new regimes characterised by the presence of monsoon lows, and only one regime characterised by mid-latitude waves. Thus, a caveat to these results is that the choice of dataset can influence the rainfall spatial patterns of the regimes, although the same synoptic patterns are present in the regimes derived from both observed rainfall datasets used in this thesis.

Three regime assignment methods were developed: the projection method (Method I) assigns daily model rainfall a regime based on the minimum Euclidean distance to an observed regime. This method forces the model regimes to have the same spatial pattern as the observations, and therefore allows direct comparison of frequency and synoptic patterns. However, the method does not allow the possibility of the model to produce spatial patterns that differ from the observations. The direct clustering method (Method II) clusters model rainfall with no input from observations, allowing the typical rainfall patterns in the model to be determined. These may be different from observations, and depend on the model; thus the difference between the model and observed patterns can be used to rank the models. Method III clusters both model and observed data in one dataset, which concisely shows the differences in spatial pattern and frequency of model and observed regimes.

The ACCESS1-0 model is able to reproduce most of the observed rainfall spatial patterns over NWA with the correct flow pattern, however there are significant differences in the frequency and intensity of regimes responsible for heavier rainfall. In particular, the model does not simulate the frequency of rainfall over the Kimberley region well, or in the southern part of the study region. Differences in the frequency of the heavy regimes combined with offshore rainfall maxima led to significant dry biases over land areas, and wet biases to the north of the continent. The next chapter will use the regime assignment methods to rank the performance of ACCESS1-0 against a number of other CMIP5 models, with the aim of using the best performing models to understand projections of a future climate in the region.

## Chapter 4

# Modelled rainfall over north western Australia: Comparing CMIP5 models to observations

### 4.1 Introduction

In the previous chapter, three analysis methods to determine the rainfall regimes in climate models were developed and tested on a single model, ACCESS1-0. The work presented in this chapter uses these methods to assess the ability of a larger number of models in the Coupled Model Intercomparison Project phase 5 (CMIP5) to replicate the observed rainfall regimes. Together, the three methods build an understanding of the spatial patterns, frequency and intensity of the regimes produced by each model, with the aim of ranking them according to their ability to simulate the observed rainfall regimes before investigating rainfall regimes in a future climate in Chapter 5. In Chapter 2, the importance of considering TCs as a separate synoptic system over NWA was established, thus the model ranking will consider how TC-like vortices (TCLVs) are represented in the models. While TCLVs are produced by the models, tracks are only available for a set of 20 CMIP5 models and thus a subset of these with sufficient resolution over the study region are considered. Model ranking has been carried out in previous studies using a variety of metrics such as ability to reproduce geopotential height patterns Grainger et al. (2014) or MSLP patterns, Moise et al. (2015). The criteria used to rank the models varies, thus rankings for specific models will also vary across studies.

Section 4.2 outlines the data used in this chapter and gives an overview of the methods used. The methods used to determine the rainfall regimes are the same as those outlined in Section 3.2.4, however the results are used slightly differently as the aim of this chapter is to compare models rather than detail the regimes of individual models. Section 4.3 shows the results of the multi-model comparison by first discussing biases in the mean rainfall in each model, before applying the three regime assignment methods developed in Chapter 3 to a number of models. The synoptic patterns of model regimes are discussed in Subsection 4.3.2 to allow a fair comparison of the synoptic situation across models for a given rainfall pattern. An overall quantitative ranking of the models is presented in Section 4.4, while the final section summarises the key findings of this chapter.

## 4.2 Data and methods

### 4.2.1 Data

Daily precipitation was taken from the historical runs (using observed greenhouse gas concentrations) for eight CMIP5 models summarised in Table 4.1, to determine the rainfall regimes in each model and assess their similarity to the observations. Tracks for tropical cyclone-like vortices are available for a subset of 18 models. We consider only a subset of eight models for which TCLV tracks are available due to the resolution of the models. Due to the relatively small size of the study region, models with a native resolution coarser than  $2.0 \times 2.0$  degrees were considered too coarse to resolve the relatively localised nature of the rainfall regimes, and therefore they were not considered in this study. For consistency between models and comparing models to observations, the daily rainfall from each model was re-gridded to  $2.0 \times 2.0$  degree resolution. The model years 1970-1999 were chosen as in Chapter 3 due to availability of TCLV track data. The model data are compared to the observed regimes calculated from CMORPH daily rainfall, presented in Section 3.3. The observed regime spatial patterns are also re-gridded to  $2.0 \times 2.0$  degrees to allow the projection and clustering methods outlined in the next section to be utilised, and to allow fair comparison of intensity between observations and models. For each model, a single model realisation was used, with r1i1p1 chosen for all models except CCSM4, where r6i1p1 was used since the TCLV tracks are only available for this particular realisation. The two ACCESS models share parameterisation schemes for convection and cloud microphysics, while most

other models have reasonably independent convection schemes.

TC-like vortices (TCLVs) are detected and tracked using the CSIRO Direct Detection (CDD) scheme, outlined in Section 3.2.3. The wind speed threshold to classify a TCLV varies across the models considered in this chapter due to the differing native resolution of each model, with specific thresholds detailed in the second last column of Table 4.1. Similar to previous chapters, any day in which a TCLV is present in the region is defined as a TC day, and is separated into a TC regime based on the geographical location of its centre. Following TC removal, dry days are removed from the rainfall data in each model using the same threshold of 0.1 mm outlined in Section 2.1.3. Since TC days are separated prior to any regime assignment, the spatial pattern, frequency and rainfall intensity of TC regimes in the models are the same across the first two methods. Characteristics of the TC regimes are covered in more detail at the end of Method II. There is no need to define TC regimes in Method III (combining model and observed data) since any TC regime in this method would be a simple weighted average of the observed and model TC regimes, and differences in frequency and intensity are best compared directly.

Wind field composites associated with the observed regimes are calculated from the ERA-Interim reanalysis dataset as per previous chapters, available from 1979-2016 which covers all of the years that CMORPH covers.

Table 4.1: Summary of the eight CMIP5 models chosen in this chapter.

Model	Institution	Resolution (lat x lon)	TCLV wind speed threshold ( $\text{m s}^{-1}$ )	Reference
ACCESS1-0	CSIRO-BOM, Australia	$1.9 \times 1.2$	8.5	(Bi et al., 2013)
ACCESS1-3	CSIRO-BOM, Australia	$1.9 \times 1.2$	8.5	(Bi et al., 2013)
bcc-csm1-1-m	BCC, CMA, China	$1.1 \times 1.1$	10	(Xin et al., 2013)
CCSM4	NCAR, USA	$1.2 \times 0.9$	10	(Gent et al., 2011)
CNRM-CM5	CNRM-CERFACS, France	$1.4 \times 1.4$	10	(Voltaire et al., 2013)
CSIRO-Mk3-6-0	CSIRO-QCCCE, Australia	$1.9 \times 1.9$	9	(Rotstayn et al., 2010)
MIROC5	JAMSTEC, Japan	$1.4 \times 1.4$	10	(Watanabe et al., 2010)
MRI-CGCM3	MRI, Japan	$1.1 \times 1.1$	10	(Yukimoto et al., 2012)

## 4.2.2 Model assessment methods

The degree to which the models replicate rainfall over north-western Australia is assessed in multiple ways. A quantitative ranking is applied to the models in each method, and the sum of the ranks over the methods is used to produce an overall ranking. The metrics used for each ranking are outlined below, and summarised in Table 4.2. First, we assess how well the models replicate the observed rainfall distribution and the change in rainfall over Australia. Biases in the annual mean rainfall are calculated as a percentage difference between the mean in each model for the period 1970-1999 and the mean in CMORPH (1998-2016). We use CMORPH to determine mean rainfall despite its shorter period relative to AWAP to determine rainfall biases over the ocean in addition to those over land.

The model-simulated rainfall trend is determined using the difference in annual rainfall between the 25 year periods 1975-1999 and 1950-1974, similar to that in Figure 1.1 but with a shorter time span as the historical runs end in the year 2005. The rainfall trend is calculated at the model's native resolution. A metric for to the observed annual mean rainfall is calculated as follows: first, we take the absolute value of the percentage bias in rainfall over the region for each model, before taking the spatial average. This value for each model is ranked against the other models to produce a ranking of mean rainfall bias. Taking the absolute value avoids ranking a model well if there are positive and negative biases within the region that may average out to zero, and instead ranks a model better when a greater amount of the region is close to zero bias. A similar metric using the absolute changes in rainfall rather than the percentage change yields a very similar ranking for each model and does not change the overall rank.

Biases in the mean flow over the wet season (October to March) are also determined by calculating the mean of the 850 hPa wind fields for the period 1970-1999 in each model, corresponding to the same period for which the model rainfall is clustered. The mean flow in the observations is calculated from ERA-Interim data from 1979-2008. This period is chosen to maximise overlap of years between the CMIP5 and observations, while using the same time period length.

Secondly, the ability of the models to replicate the observed rainfall regimes is assessed.

In order to replicate the observed rainfall regimes accurately, the models must correctly produce the correct number of rainfall regimes in the correct location, with the correct frequency and intensity of rainfall. To assess the ability of the models to fulfil these criteria, the three methods developed in Chapter 3 are used to determine the ability of the models in producing the correct regimes. All three methods rely on separating dry and TC days in a similar fashion to that described in Sections 2.1.2 and 2.1.3 before any clustering method is applied. Following regime assignment using each method, the models are ranked according to a metric specific to the method being used. The metrics used for each method are summarised in Table 4.2. The synoptic patterns associated with the regimes in each model are also determined, however a ranking is only applied to wind fields determined from regimes in Method I to allow comparison of circulation between model and observed regimes that have the same rainfall pattern.

As described in Section 3.2.4, Method I (projection) projects the wet, non-TC days from each model onto the observed CMORPH rainfall regimes. To rank the models using this method, the absolute differences in frequency of regimes between each model and the observations for dry days, light, moderate, and grouped heavy regimes (same arrangement as in Figure 4.6) are calculated and summed. The sum of the differences is an indication of how well the models replicate the frequency of the observed regimes. This metric is more strongly influenced by high frequency regimes that vary greatly among models such as dry and Light days, however when combined with the metric from Method III, the overall ranking will include low frequency, high intensity regimes. The ability of the models to replicate the circulation patterns will also be ranked. The pattern correlation between the 850 hPa wind composite for each model regime and the composite for the equivalent observed regime is calculated. The ranking measure used for the 850 wind is the sum of the pattern correlations over all regimes in each model. The correlation for each regime is calculated as the mean of the correlation for the zonal component and that for the meridional component. The 850 hPa wind was chosen as differences between regimes and models are best characterised at this level, rather than at higher levels where it is more difficult to characterise differences in flow between regimes (see Appendix A).

The direct clustering method (Method II) calculates clusters from the model rainfall inde-

pendently from the observations, and allows a set of model regimes to be determined. Ideally, the model should be able to reproduce the observed regimes without producing regimes that are not observed. Thus, the same number of clusters used for clustering the CMORPH data (7) was used for each model. The non-TC model regimes are then mapped to the observed regimes in a 1:1 fashion, by finding the sum of the Euclidean distances over all regimes, for every possible permutation of model regimes to observed regimes (see Section 3.2.4 for more details). The permutation corresponding to the minimum sum is taken to be the best match of the model regimes to the CMORPH regimes. The minimum sum itself is taken as a metric with which to compare and rank all the models. If a model produces incorrect rainfall regimes or regimes with a significantly different intensity to the observations, its distance sum will be larger than a model producing regimes that are closer to the observations.

As described in Section 3.2.4, Method III (combined clustering) takes an equal number of days from CMORPH and one model, and calculates clusters for a dataset containing both model and observed days. Following clustering, the relative fractions of model days in each cluster (regime) are calculated. To determine significance of the model bias in regimes, uncertainty in the fraction of observed regimes was calculated by randomly halving the observed data and determining the fraction of the first half of the data in each regime, repeating 10000 times and producing a normal distribution of fractions. A threshold of 2 standard deviations of these distributions was used as the uncertainty bound for the observed fractions. If the fraction of model days is above the uncertainty bound, the regime can be considered to be a regime the model overproduces. Conversely, a model can be regarded to fail to produce a regime if the fraction is below the uncertainty bound. The model fractions can also be used to develop a simple ranking. In this case, the magnitude of differences between the model fraction and 0.5 (ie. 50/50 split) are summed across all regimes for each model. This is another metric for assessing frequency of regimes and spatial pattern. This metric is more strongly influenced by infrequent (heavy) regimes, since the model fraction is sensitive to smaller changes in frequency in the model as the total number of days in each regime is small relative to the entire period.

Each of the metrics provides an individual ranking for each model. An overall ranking is determined by summing the number ranks across each method. The main objective of

Table 4.2: Summary of the ranking methods used for each method in order to produce an overall ranking for the models.

Method	Calculated metric for ranking
Overall mean	Spatial average of the magnitude of percentage change from observations
Projection method (I)	Size of total frequency differences from observations, based on dry, light, moderate and summed heavy regimes (see Figure 4.6)
Synoptic patterns from projection method (I)	Sum of pattern correlation between model and observed 850 hPa wind composites across all regimes
Direct clustering (II)	Euclidean distance sum over all regimes
Combined clustering (III)	Total deviation from 50:50 model:observations over all regimes
<b>Overall rank</b>	<b>Sum number ranks from all methods with equal weighting</b>

using these ranks is to provide a general overview of the ability of each model to replicate the observed climate in the study region.

## 4.3 Results

### 4.3.1 Climatological rainfall biases

#### Biases in annual mean precipitation

To provide a general overview of the ability of each model to replicate the observed rainfall patterns over the Australian region, the percentage difference between the annual mean rainfall in each model and the observed mean from CMORPH is calculated and presented in Figure 4.1. The model rainfall is calculated from 1970-2000, whereas the observed rainfall is calculated from 1998-2016. Using 1998-2016 to calculate the observed mean will cause a higher mean than for 1970-2000 as noted previously, however the magnitude of the percentage change in observed rainfall over this period (approximately 20%) is lower than that of the percentage biases in most models.

Almost all individual models analysed here show location-dependent annual rainfall biases over north-western Australia. CCSM4 and MIROC5 on average are far too wet, in many locations more than doubling the observed rainfall. On the other hand, the ACCESS models show dry biases over most land-based areas of the region, with wet biases offshore. Of the remaining models, there are dry biases located over the Kimberley and inland Top End locations, with wet biases offshore and in central Australia (south-east corner of the study

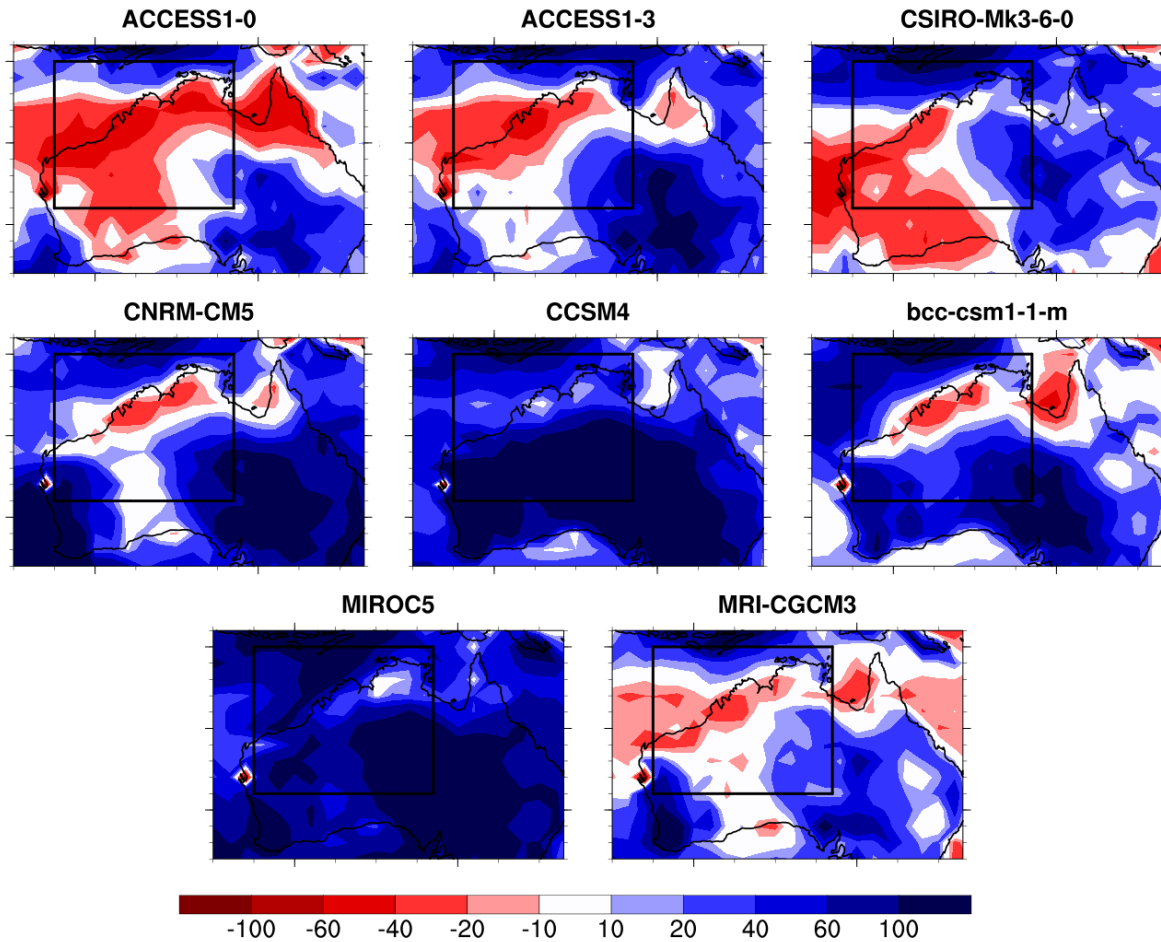


Figure 4.1: Percentage bias of yearly average rainfall relative to the mean in CMORPH. The box indicates the study region.

region). Overall, the biases are smallest for the MRI model, although almost all models tend to be drier over the Kimberley and Top End regions over land - these regions either display negative biases or, in the case of the wetter models, a weaker positive bias relative to surrounding regions. Almost all models produce positive biases over central Australia, agreeing with previous studies, e.g. Moise et al. (2015).

The ranking of each model based on the the magnitude of the percentage change across the study region is shown in Table 4.3. MRI-CGCM3 and the two ACCESS models are the best ranking models based on magnitude of biases. The biases are relatively weak for MRI-CGCM3, and are much larger for bcc-csm1-1-m, MIROC5 and CCSM4 due to the presence of regions of very strong positive bias within the study region. These ranks, and those of following sections are taken into account for the final ranking at the end of this chapter.

Table 4.3: Mean of magnitude of percentage error in annual rainfall for each model, and associated ranking.

Model	Mean mag. % diff	Rank	Model	Mean mag. % diff	Rank
MRI-CGCM3	22.1	1	CNRM-CM5	36.5	5
ACCESS1-3	26.8	2	bcc-csm1-1-m	47.0	6
ACCESS1-0	27.2	3	MIROC5	94.8	7
CSIRO-Mk3-6-0	34.7	4	CCSM4	96.5	8

### Biases in the seasonal rainfall distribution

Examining the seasonal distribution of rainfall in the models further identifies biases in the mean rainfall in each model. The monthly distribution of rainfall averaged over the study region for each model is presented in Figure 4.2. As described in Section 3.4.1, ACCESS1-0 has a rainfall maximum later in the wet season, and produces too little rainfall in the build-up during the austral spring. ACCESS1-3 and MRI-CGCM3 show a similar pattern, although MRI-CGCM3 has a higher peak rainfall during the wet season, partially compensating for the dry bias in spring and resulting in a weaker overall bias in rainfall. For most of the remaining models, the wettest months are far wetter than the observations. Aside from MIROC5 and CSIRO-Mk3-6-0 which have peak rainfall in December, the other models peak in the same month as the observations. Most of the models produce too much rainfall during the spring build-up, with MIROC5 and CCSM4 producing approximately double the observed monthly rainfall from October to December.

Overall, the seasonal distribution for CNRM-CM5 and bcc-csm1-1-m appear to most closely resemble the observations. While most models are able to produce the correct timing of maximum rainfall, many produce too much rainfall early in the wet season. The next section will determine how well the rainfall regimes are reproduced by the models using the three regime assignment methods from the last chapter.

### Model rainfall trends

The trend in rainfall for each of the models is shown in Figure 4.3, with the observed trend in AWAP shown for reference. Similar to Figure 1.1, the trend is presented as a difference in annual rainfall between two periods. In this case the periods 1950-1974 and 1975-1999

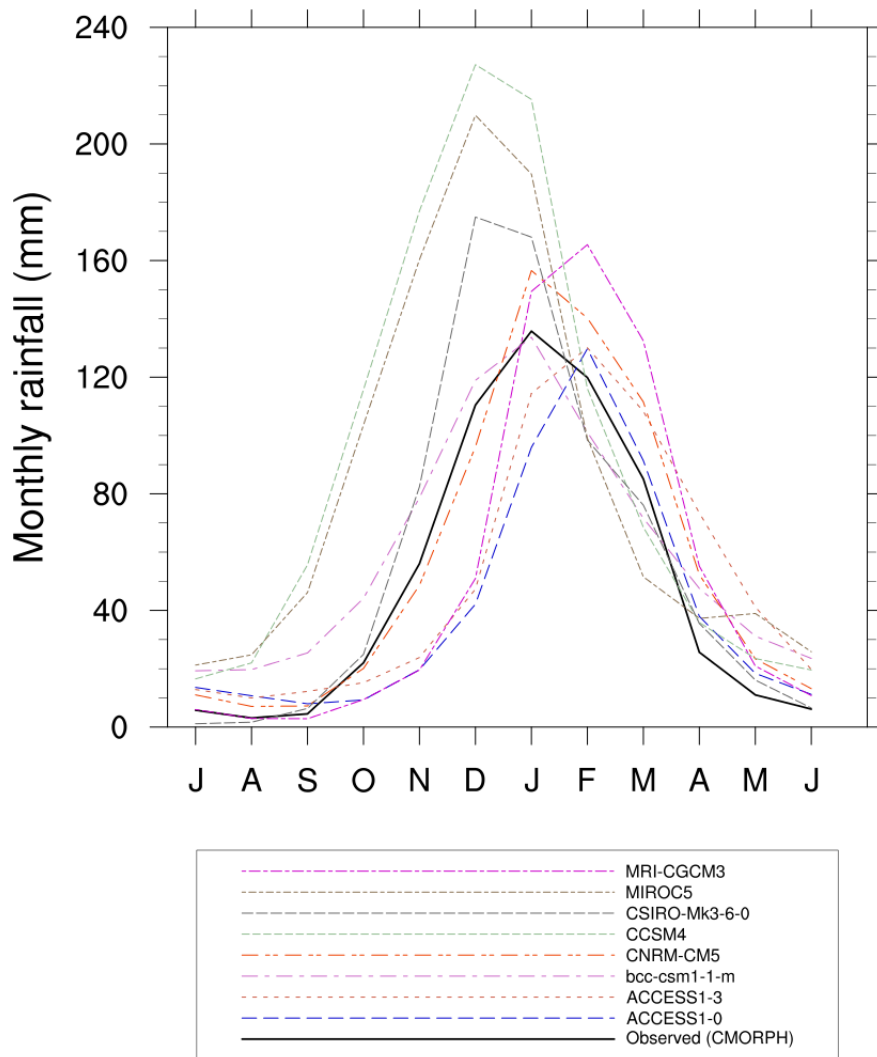


Figure 4.2: Distribution of mean monthly rainfall in the observations (solid black line) and in each of the CMIP5 models considered in this chapter (coloured lines).

are chosen instead of the 30 year periods used previously since many historical model runs end around 2005, and thus there is little overlap with the period used in CMORPH. Note that the trend plot in AWAP across the southern part of the study region contains some circle-shaped artifacts due to sparse coverage of measuring stations. Most of the models show an increase in rainfall in some part of the study region, although the pattern over the entire Australian continent varies by model. The study region was originally chosen due to the observations indicating increased rainfall inside the box, and generally decreasing rainfall outside. This pattern is replicated more closely by ACCESS1-0 and MRI-CGCM3 compared to other models. The remaining models either produce drying in some areas of the study region that have not occurred in the observations (CSIRO-Mk3-6-0, CCSM4), or produce wetting in eastern Australia that has not occurred (MIROC5). Most models produce

some wetting within the study region, however the pattern is not consistent among models, indicating that few are able to reproduce the observed rainfall trend. This agrees with Moise et al. (2015).

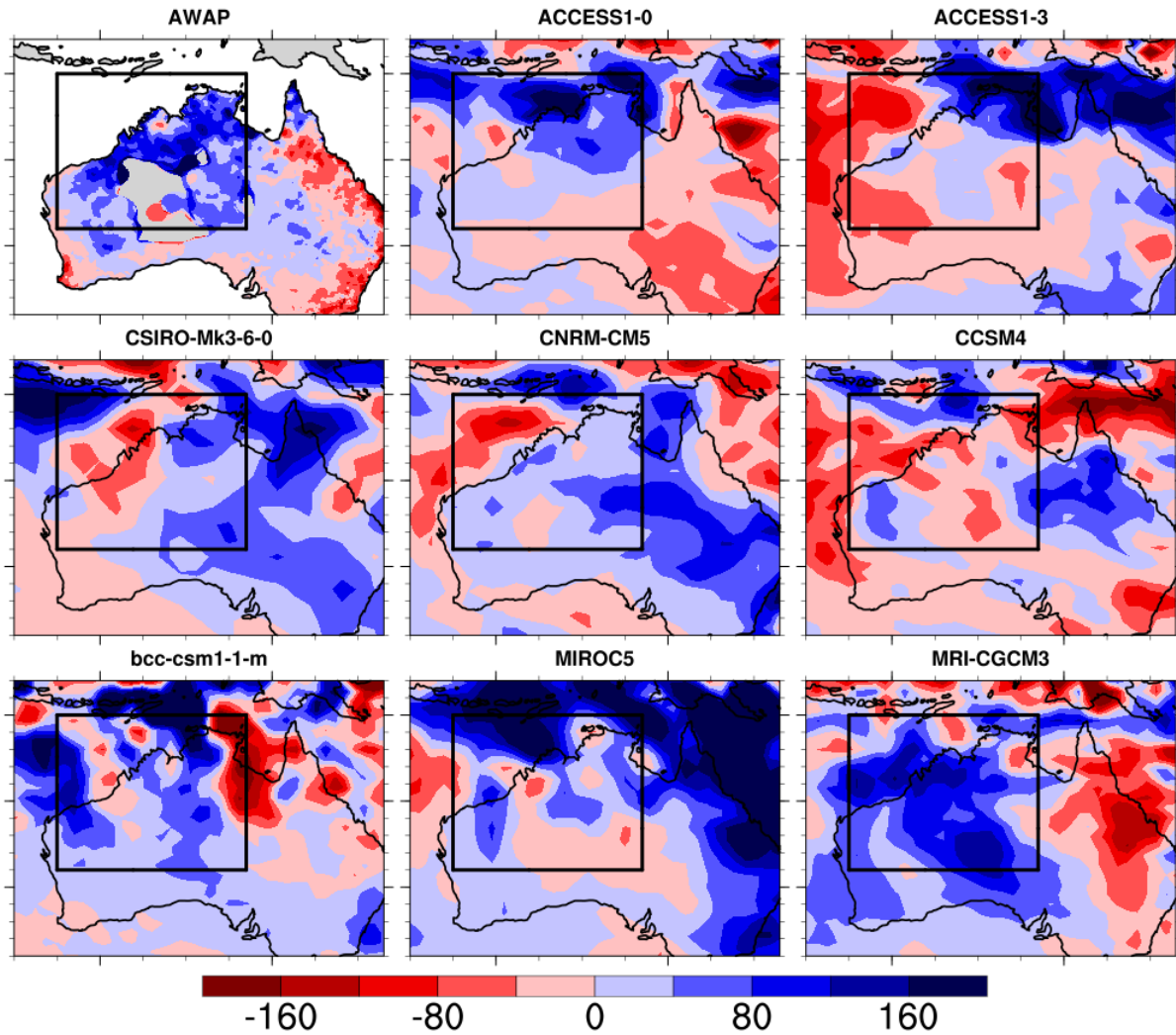


Figure 4.3: Change in annual precipitation (mm) between the periods 1975-1999 and 1950-1974 for AWAP observations and the historical run of the nine CMIP5 models considered in this chapter. The box indicates the study region. Note the periods used are different from those used in Figure 1.1.

### Biases in the mean winds

In order to indicate biases in how the models represent flow during the austral summer monsoon season, the mean flow across all days from October to March in a 30 year period is

calculated in the ERA-Interim reanalysis and in the eight models considered in this chapter. The anomaly between the model and ERA-Interim winds at 850 hPa is shown in Figure 4.4 to show differences in the low level flow. The general shape of the flow pattern at low levels is replicated well in all models (see Appendix A), although there are some biases in the strength of winds and location of convergence. The two ACCESS models show stronger easterlies over northern Australia and weaker westerlies over the Maritime Continent, suggesting an overall northward bias of the monsoon. bcc-csm1-1-m, CNRM-CM5, CCSM4 and MIROC5 all show anomalously strong westerlies over the Maritime Continent, with weaker easterlies over the Australian continent in the latter two models. This is consistent with enhanced convergence over the continent, resulting in the positive bias in climatological rainfall shown in Figure 4.1. CSIRO-Mk3-6-0 shows enhanced north-westerlies over the eastern part of the study region, but enhanced south-easterlies in the south-western part, which may partly explain the enhanced (reduced) rainfall in the eastern (south-western) part of the study region. There is relatively little bias in MRI-CGCM3.

Differences in the flow can partly explain the climatological rainfall biases evident in the models. The differences in mean flow are likely to be the result of differences in the frequency, spatial pattern and synoptic structure of model rainfall regimes. These model regimes are determined from the three regime assignment methods discussed in Section 4.2.2, and presented in the next three sections.

### **4.3.2 Method I: Projecting model days onto observed regimes**

This subsection describes projecting the wet days from each model onto the observed rainfall regimes from CMORPH, and produces model regimes from the days that are closest to the observed regimes. In Chapter 3, we determined that the projection method produces regimes that do not significantly differ from the observed regimes, although there are minor changes in intensity. Figure 4.5 shows the projected spatial patterns for Regimes 3 and 7 for all models as an example. The spatial patterns for the other regimes are shown in Appendix A. The spatial patterns for the regimes in each model look highly similar to the observations, although the maximum intensity for Regime 3 in bcc-csm1-1-m and MIROC5 is slightly higher than observed. When compared to the differences among models in the independently determined regimes discussed later and presented in Figures 4.11 to 4.13, the patterns can be regarded to be equivalent to the observations.

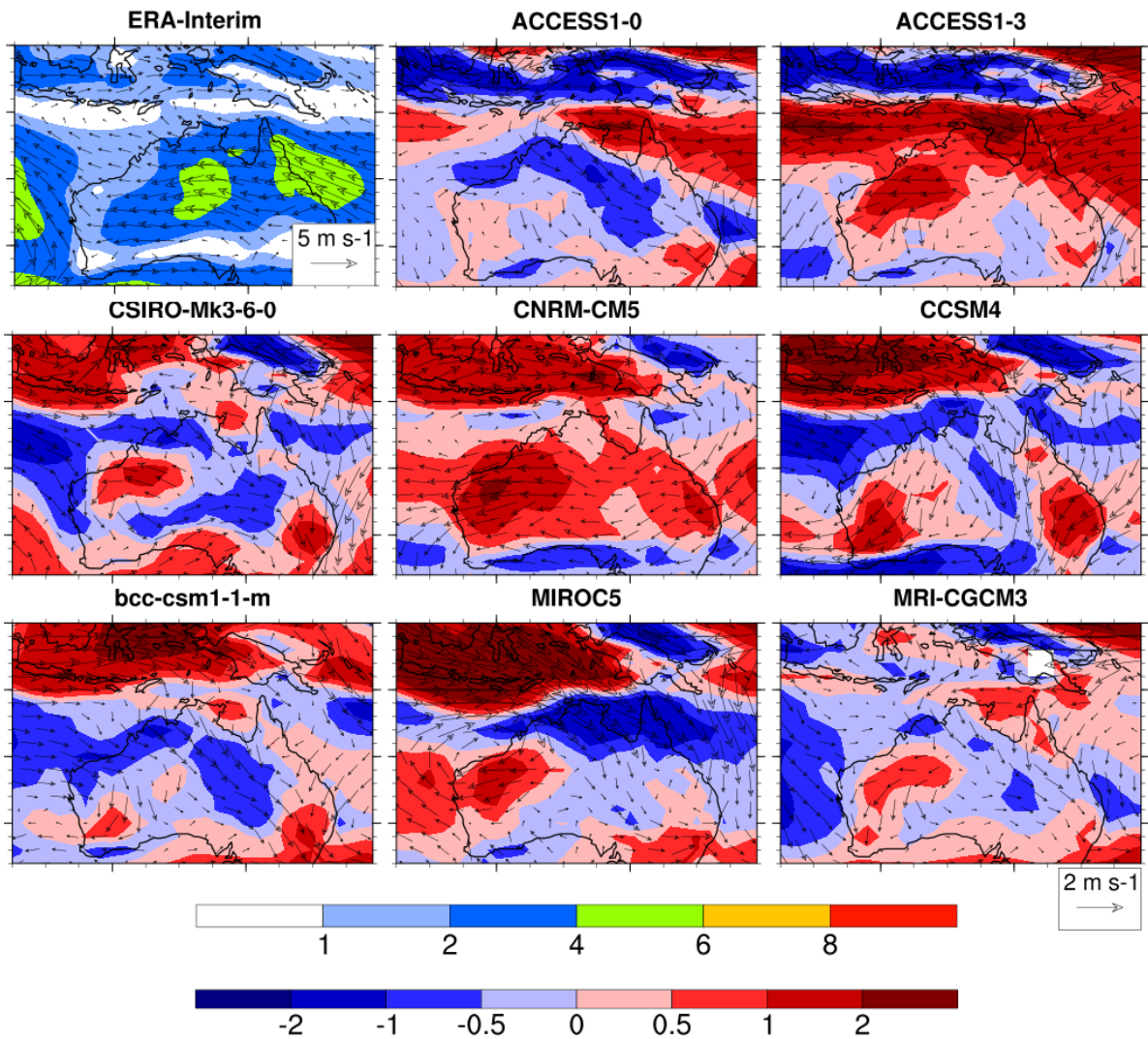


Figure 4.4: 850 hPa wind errors relative to ERA-Interim for each model averaged from October to March. Blue shading indicates weaker wind speeds in the models, while red shading indicates higher wind speeds. Units are in  $\text{m s}^{-1}$

Figure 4.6a and b show the frequency of the regimes in each model after projecting wet days to the observed regimes shown in Figure 3.2. From Figure 4.6a, we see that most models underestimate the number of dry days, or produce rainfall too often. The two ACCESS models produce a number of dry days similar to the observations, while CSIRO-Mk3-6-0 and MRI-CGCM3 produce too few wet days. In contrast, all remaining models produce too many wet days, with bcc-csm1-1-m having almost 90% of days as wet days in the region. In contrast, all models with the exception of the CSIRO and MRI models produce too many Light regime days. Representation of the Moderate regime varies across models, with three models underestimating the number of days in this regime (ACCESS1-0, ACCESS1-3 and

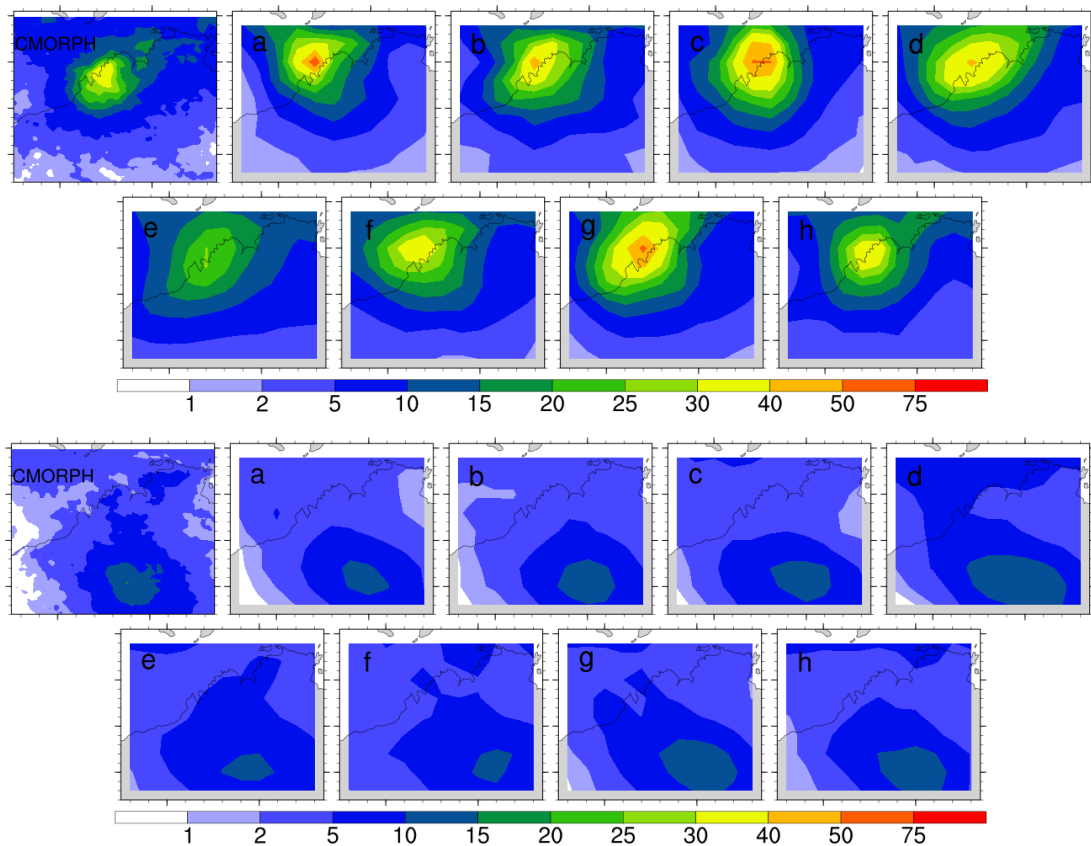


Figure 4.5: Spatial patterns for Regimes 3 (top) and 7 (bottom) from the projection method (Method I). The first panel shows the spatial pattern for Regime 3 or 7 in CMORPH, and the subsequent panels show each model. Labelling is as follows: a) ACCESS1-0, b) ACCESS1-3, c) bcc-csm1-1-m, d) CSIRO-Mk3-6-0, e) CCSM4, f) CNRM-CM5, g) MIROC5, h) MRI-CGCM3. Note the change in colour scale relative to figures in Chapter 3. Units are in  $\text{mm day}^{-1}$ .

bcc-csm1-1-m), and two overestimating the number of days (CCSM4, CNRM-CM5).

Figure 4.6b shows that representation of the heavy rainfall regimes varies greatly among models, with a number of models producing approximately the correct fraction of heavy rainfall days, such as bcc-csm1-1-m, CSIRO and MRI. However, when this is broken down to the fraction of each regime as shown in Figure 4.6b, the models that produce the correct frequency of heavy regimes generally may produce differing frequencies of each specific regime. For instance, bcc-csm1-1-m greatly overestimates the fraction of Top End (Regime 5) and Inland (Regime 7) days. In addition, the frequency of the Kimberley regime is underestimated in almost all models except CCSM4 and MIROC5, which produce too much rainfall generally as discussed previously. Most models also underestimate the fraction of TCs, with only bcc-csm1-1-m and MIROC5 producing more TC days than the observations.

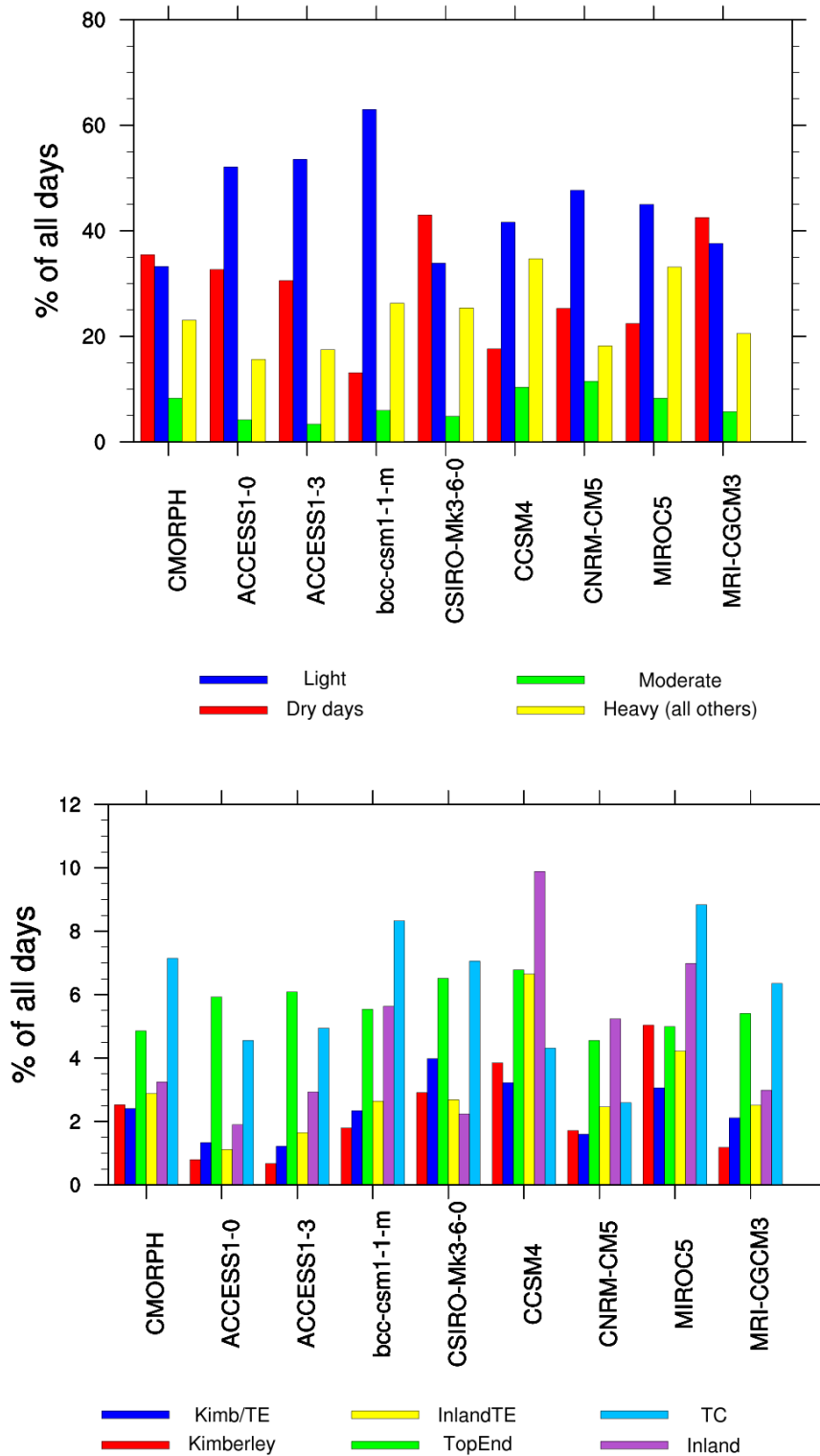


Figure 4.6: Frequency of the regimes in each model after projecting the wet days in each model to the observations. The top panel (a) shows the frequency of dry, light and moderate days, and the sum of all other (heavy) regimes. The bottom panel (b) breaks down the frequency of each regime responsible for heavier daily rainfall. All frequencies are calculated relative to all days.

Overall, no model is able to reproduce both the total frequency of all heavy regimes and the frequency of each individual heavy regime. The differences in frequency will be further discussed in more detail in the next section, after the differences between the model and observed spatial patterns have been determined.

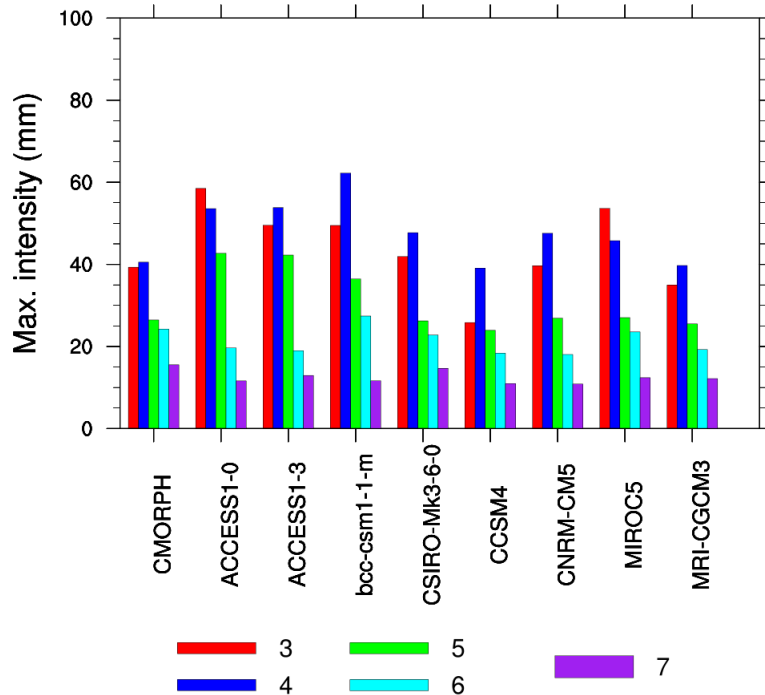


Figure 4.7: Maximum intensity of Regimes 3 to 7 (heavy, non-TC regimes) in each model produced using the projection method (Method I).

The maximum intensity of Regimes 3 to 7 is shown in Figure 4.7. The maximum intensity is defined here as the rainfall amount corresponding to the maximum point in the regime. Across models, the maximum intensity in Regimes 3 and 4 tend to be overestimated, with maxima above  $40 \text{ mm day}^{-1}$ . Conversely, the maximum of Regime 7 tends to be slightly underestimated, with maxima between  $10\text{-}15 \text{ mm day}^{-1}$ . From this method, the ACCESS models, bcc-csm1-1-m and MIROC5 produce the greatest intensity biases relative to other models. These biases become far more evident when the intensity of independently determined regimes from Method II are considered later in this chapter.

### Synoptic patterns

The synoptic patterns associated with the projected regimes are determined by calculating composites of 850 and 500 hPa wind fields for each regime. The synoptic patterns shown here can be viewed as those that force the model to produce the observed rainfall patterns, which may not necessarily be those the model typically produces. A selection of fields for Regimes 1, 3 and 7 are presented in this chapter for brevity. The full set of wind fields for each model are provided in Appendix A.

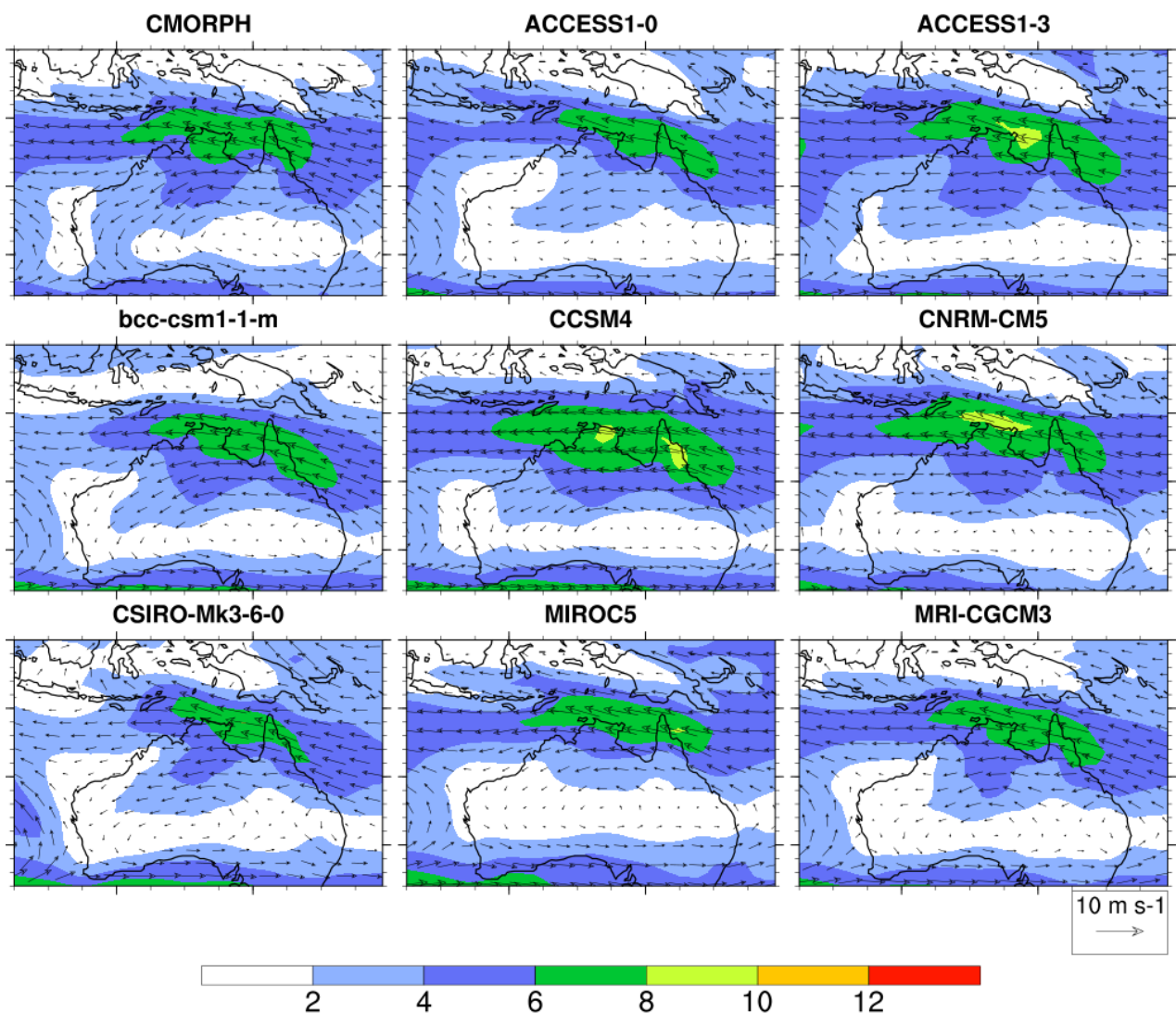


Figure 4.8: 850hPa wind composites for Regime 1 derived from the projection method in all models considered in this chapter. Shading indicates wind speed in  $\text{m s}^{-1}$ .

Figure 4.8 shows the 850 hPa wind composite for Regime 1, corresponding to the Light regime. In the composites for the CMORPH and AWAP (see Section 2.3) observations, the

low-level winds over northern Australia are easterly, typical of the build-up to the monsoon. All models are able to replicate the observed low-level wind fields, with only minor deviations in wind strength. The wind fields are also replicated well for dry days (see Appendix A), showing the models are able to replicate the general atmospheric flow as most days of the year are in either the dry or light regime. However, when heavy rainfall regimes are considered, significant model biases emerge.

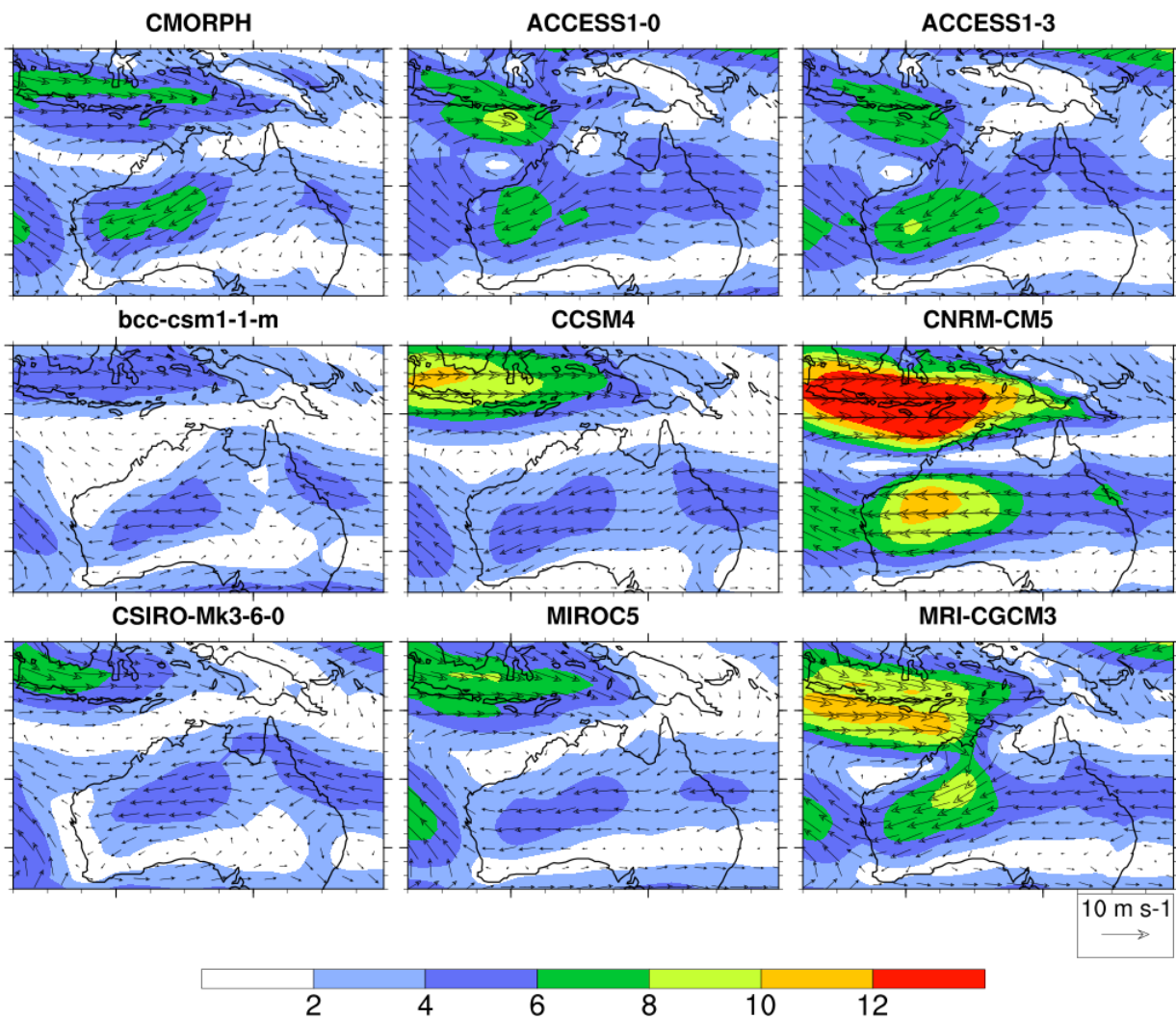


Figure 4.9: 850 hPa wind composites for Regime 3 derived from the projection method in all models. Shading indicates wind speed in  $\text{m s}^{-1}$ .

Figure 4.9 shows the 850 hPa wind composite for Regime 3, corresponding to a rainfall

maximum located in the Kimberley region in the observations. In both CMORPH and AWAP, the regime is characterised by a closed circulation corresponding to a monsoon low located near the region of maximum rainfall. The two ACCESS models similarly show a closed low near the rainfall maximum, and thus reproduce the synoptic conditions well. However, in ACCESS1-3 the rainfall is erroneously associated with a wave-like pattern at 500 hPa (see Appendix A). An elongated low centre is present in MRI-CGCM3, with winds surrounding the low much stronger than the observations. The low centre in CCSM4 and MIROC5 is broad with winds that are far weaker than those observed. CNRM-CM5 shows an elongated monsoon trough with winds that are far too strong. CSIRO-Mk3-6-0 and bcc-csm1-1-m show virtually no signal. In the cases of other projected heavy regimes (4-6) that are the result of a monsoon low, the biases in each model are similar to that for Regime 3, where bcc-csm1-1-m and CSIRO-Mk3-6-0 show little signal, and CNRM-CM5 shows a strong monsoon trough rather than a closed low. The majority of models therefore produce the rainfall patterns associated with this regime without the correct flow pattern.

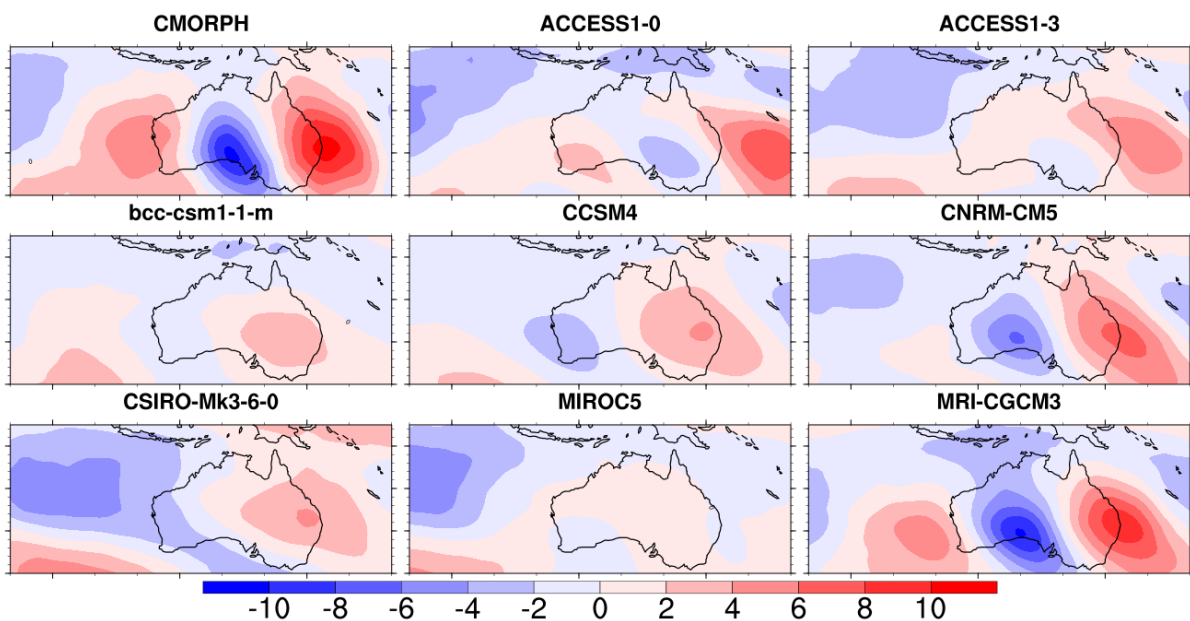


Figure 4.10: 250 hPa meridional wind composites for Regime 7 in all models and the observations. Units are  $\text{m s}^{-1}$ .

Regime 7 corresponds to a rainfall maximum located inland as shown in Figure 4.5, and is caused by the equatorward refraction of mid-latitude Rossby waves as discussed in Chapters 2 and 3. Mid-latitude Rossby waves are best characterised by calculating composites of 250

hPa meridional wind. These composites are calculated and presented in Figure 4.10. Only MRI-CGCM3 is able to replicate the observed wave-like pattern with a similar strength to the observations. CNRM-CM5 is also able to replicate the wave pattern, although the winds are weaker than those observed. ACCESS1-0 is able to produce a weak wave pattern, however the trough is positioned further east than observed. CCSM4 produces a similar pattern, but the trough is too far west. CSIRO-Mk3-6-0 incorrectly associates the rainfall with a broad ridge rather than a narrow trough. The remaining models show virtually no sign of a wave pattern in the Australian region, suggesting the rainfall in this regime is produced by convective activity that is not forced by a structured synoptic system.

To show the similarity of each model's synoptic patterns to the observations, the pattern correlation between the 850hPa wind composite for each model regime and the ERA-Interim equivalent is calculated, and averaged across all regimes in each model. A higher mean pattern correlation for a given model suggests the wind patterns for all regimes are generally better captured by the model. The pattern correlation was chosen for assessing the closeness of the model wind composites to the observations rather than the Euclidean distance in order to avoid penalty toward a model that reproduces the correct spatial pattern with wind speeds that are too strong or weak. The mean pattern correlation for each model is provided in Table 4.4.

When averaged over multiple regimes as presented in the table, the mean pattern correlation falls within a relatively narrow range. As discussed previously, MRI-CGCM3 produces wind speeds in heavy regimes that are too high, however the shape and location of the systems responsible for rainfall are correct. Two of the models which provide little signal in the heavy regimes, MIROC5 and CSIRO-Mk3-6-0, rank poorly. Despite what appears to be the correct shape of the monsoon low at 850 hPa, the ACCESS models perform relatively

Table 4.4: Mean pattern correlation across all regimes for the 850 hPa wind fields.

Model	Mean pattern corr.	Rank	Model	Mean pattern corr.	Rank
MRI-CGCM3	0.815	1	bcc-csm1-1-m	0.711	5
CCSM4	0.795	2	ACCESS1-0	0.689	6
ACCESS1-3	0.745	3	CSIRO-Mk3-6-0	0.669	7
CNRM-CM5	0.724	4	MIROC5	0.646	8

poorly, possibly due to the location of the low centre being too far west in the heavy regimes.

The regime frequency, intensity and synoptic patterns show errors relative to the observations, despite daily rainfall being constrained to have a spatial pattern similar to the observed regimes. The next section determines how rainfall regimes emerge in the models independently of observations, and ranks models according to the similarity of the independent regimes to the observed regimes.

### **4.3.3 Method II: Independent clustering of model rainfall**

#### **Rainfall spatial patterns**

As described in the previous chapter, the main drawback of Method I is its inability to determine if regimes have different spatial patterns relative to the observations. This section describes a ranking using direct clustering (Method II) from the previous chapter to determine changes to regime spatial patterns in the models relative to the observations. Firstly, daily, non-TC rainfall from each of the models is clustered, then matched to observed regimes using the minimum Euclidean distance method outlined in Chapter 3. The minimum Euclidean distance method determines the sum of Euclidean distances across all regimes for every possible permutation of model to observed regimes, and the permutation corresponding to the minimum sum is taken as the best possible match of model to observed regimes. In Section 3.4.3, we show that this method results in the possibility of a model producing regimes that are different to the observations. This is further highlighted in Figures 4.11 to 4.13, which present the spatial patterns for each regime in each model. The panels are arranged by regime rather than by model to show how each regime varies across models.

Regime 1, corresponding to light rainfall in the observations, is replicated well in the sense that all models produce a light regime, although bcc-csm1-1-m and MIROC5 extend light rainfall much further inland than the observations, and CCSM4 produces light rainfall along the south of the study region in addition to the north, but almost no rainfall in between. Regime 2, which corresponds to moderate rainfall, tends to have a maximum located just north of the Top End in almost all models except MIROC5, rather than onshore in the observations. MIROC5 places a large maximum in rainfall near the Pilbara for Regime 2, although Regime 5 for this model shows a pattern and intensity very similar to the observed Regime

2. The land-based maximum for Regime 3 is poorly replicated by ACCESS1-0 and CCSM4. The remaining models reproduce the pattern for Regime 3 well, although the maximum is too intense in most cases, especially in MIROC5. For Regimes 4 and 5, the position of the rainfall maximum is replicated relatively well by most models, however the rainfall maximum is too intense and located slightly offshore, which partially explains the positive mean rainfall biases north of the continent in most models. A Pilbara maximum does not exist in the CMORPH regimes, so the mapping has placed the Pilbara type model regime in Regime 2 rather than Regime 5 to minimise a relatively large distance sum, as is discussed later.

The spatial pattern for Regime 6 is replicated well by all models except ACCESS1-3 and CNRM-CM5, although ACCESS1-0 and bcc-csm1-1-m produce maximum intensities that are too low and too high respectively. The two ACCESS models fail to produce an inland maximum in the spatial pattern for Regime 7, with the maxima located close to the Top End coast. Most other models produce rainfall maxima for Regime 7 at approximately the correct intensity, but the location of the maximum varies greatly. bcc-csm1-1-m, CSIRO-Mk3-6-0, MIROC5 and MRI-CGCM3 all produce the peak too far west, resembling the Pilbara regime determined from AWAP (see Figure 2.2).

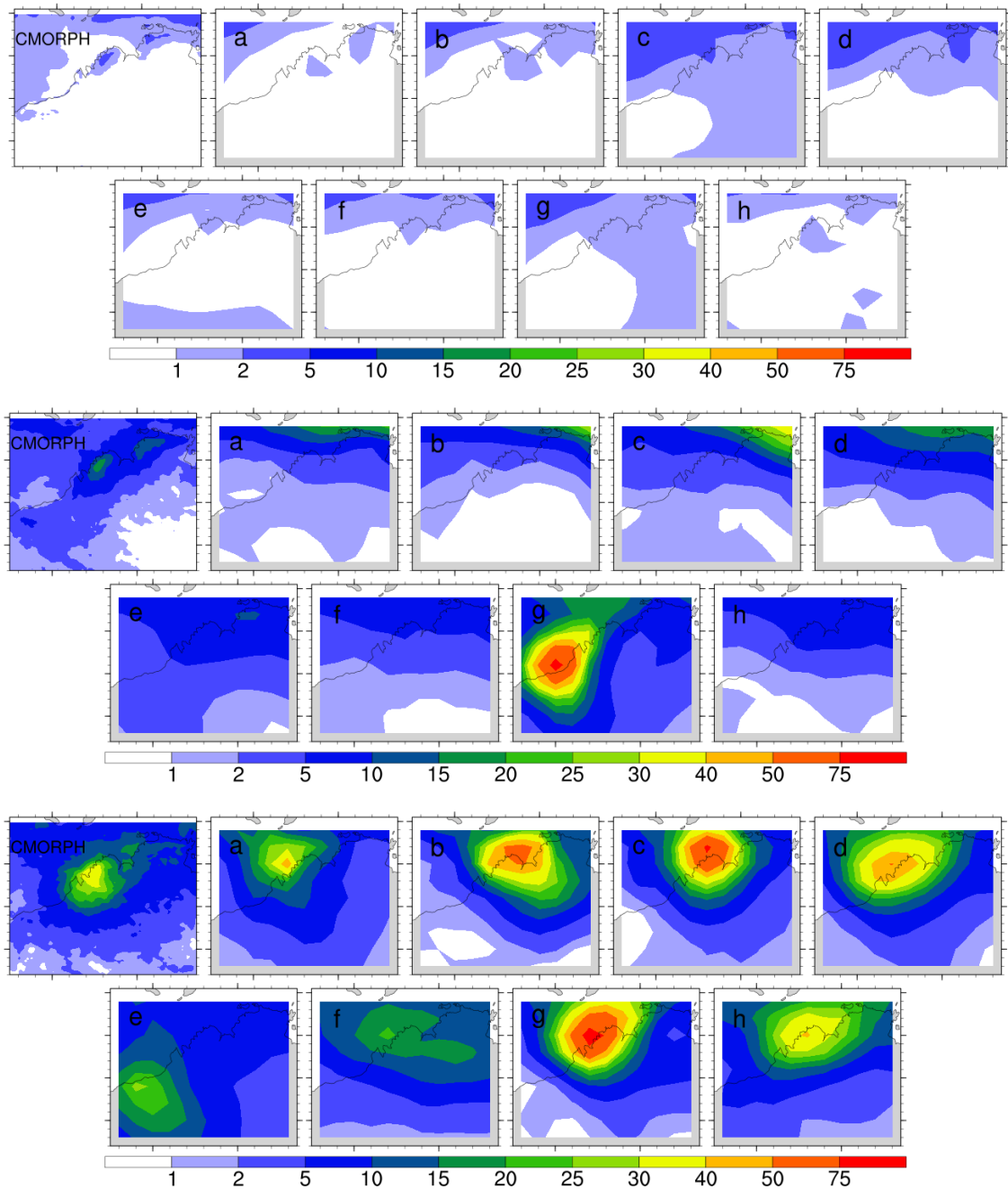


Figure 4.11: Spatial rainfall patterns for Regimes 1 (top) to 3 (bottom) produced by the CMIP5 models in Method II after matching. The first panel shows the regime in the observations, while the panels labelled a-i indicate the pattern assigned to the particular regime in each of the models. Labelling is as follows: a) ACCESS1-0, b) ACCESS1-3, c) bcc-csm1-1-m, d) CSIRO-Mk3-6-0, e) CCSM4, f) CNRM-CM5, g) MIROC5, h) MRI-CGCM3. Units are  $\text{mm day}^{-1}$ . Note the change in colour scale relative to figures in Chapters 2 and 3.

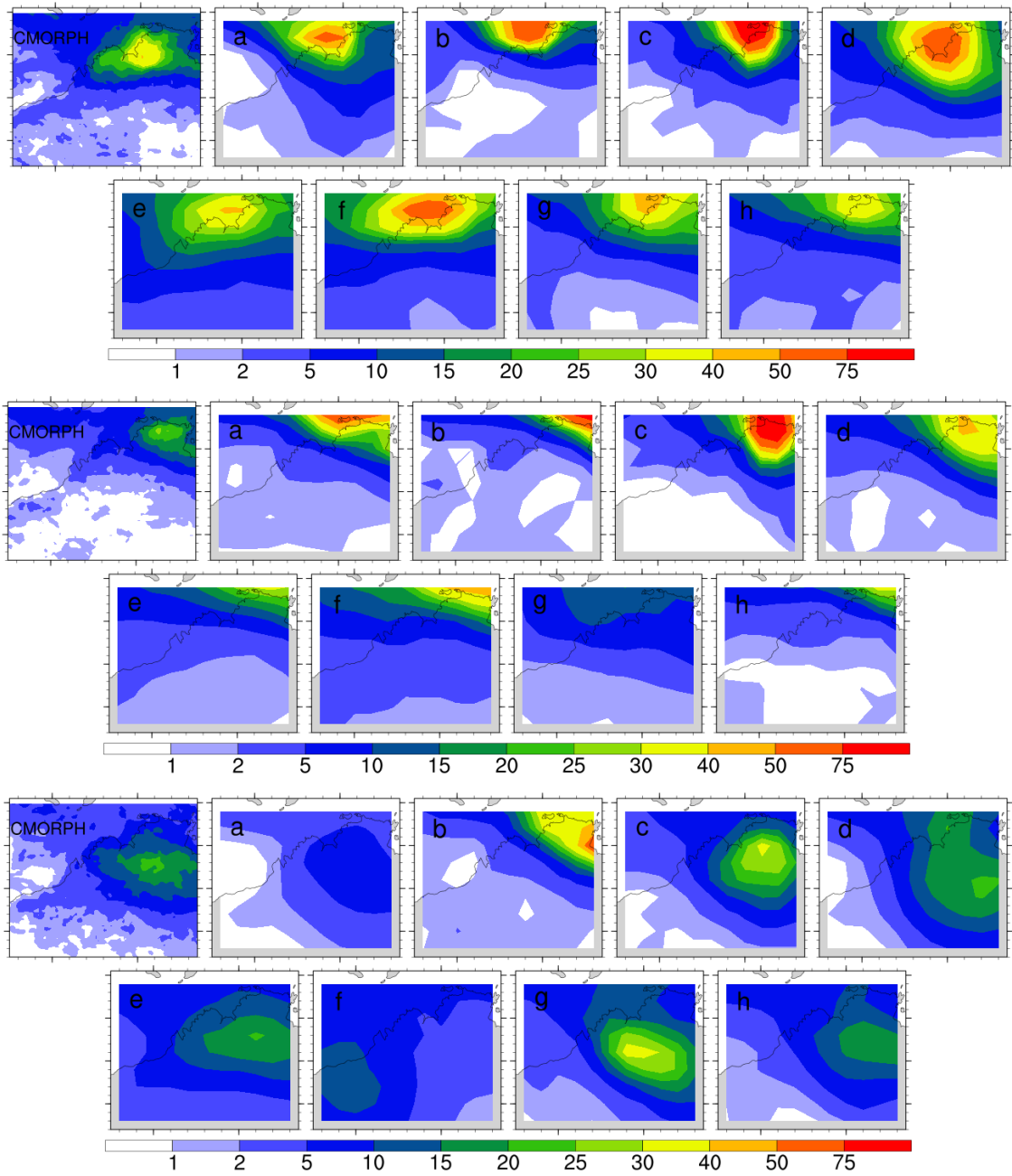


Figure 4.12: Spatial rainfall patterns for Regimes 4 (top), to 6 (bottom) produced by the CMIP5 models in Method II after matching. The first panel shows the regime in the observations, while the panels labelled a-i indicate the pattern assigned to the particular regime in each of the models. Labelling is as follows: a) ACCESS1-0, b) ACCESS1-3, c) bcc-csm1-1-m, d) CSIRO-Mk3-6-0, e) CCSM4, f) CNRM-CM5, g) MIROC5, h) MRI-CGCM3. Units are  $\text{mm day}^{-1}$ . Note the change in colour scale relative to figures in Chapter 3.

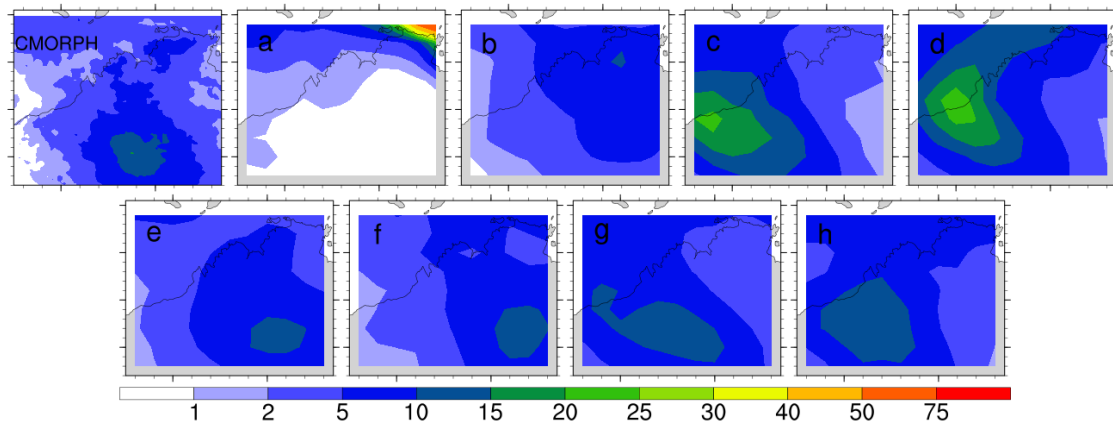


Figure 4.13: Spatial rainfall patterns for Regime 7 produced by the CMIP5 models in Method II after matching. The first panel shows the regime in the observations, while the panels labelled a-i indicate the pattern assigned to the particular regime in each of the models. Labelling is as follows: a) ACCESS1-0, b) ACCESS1-3, c) bcc-csm1-1-m, d) CSIRO-Mk3-6-0, e) CCSM4, f) CNRM-CM5, g) MIROC5, h) MRI-CGCM3. Units are  $\text{mm day}^{-1}$ . Note the change in colour scale relative to figures in Chapter 3.

Independent clustering highlights differences in the model rainfall regimes relative to the observed regimes. Most models are able to replicate the spatial patterns of Regimes 1, 4 and 5 well with intensities that are generally too high, while patterns in models assigned to Regimes 6 and 7 vary most from the observations. As described in Section 3.4.3, differences in the spatial patterns between the model and observed regimes result in a higher Euclidean distance between them. The sum over all regimes gives a measure of how similar the model regimes are to the observed regimes. The distance sum is thus used as a ranking measure next.

### Distance sums

The sum of the Euclidean distances across all matched regimes is used as a metric to determine how well the observed regimes are replicated in each model. An example of how distances are calculated and minimised for ACCESS1-0 was shown in Section 3.4.3. A smaller sum means that regimes are closer to the observations, since once the model regimes are matched to the observed regimes, a model regime's deviation in spatial pattern and intensity from an observed regime will manifest as an increase in the distance for that regime. Summed over all 7 regimes, greater deviation over multiple regimes will increase the distance sum, and as a result the size of the distance sum can be used as a measure to show how much the spatial patterns of a particular model's set of regimes have deviated from the observations.

The distance sums are shown in Table 4.5.

CNRM-CM5, CCSM4 and MRI-CGCM3 are the three models with the smallest sums, and thus the rainfall spatial patterns are most likely to resemble the observations. However, although the rainfall patterns are most closely resembling observations than other models, there are still some biases in the regimes. CCSM4 (model e in Figures 4.11 to 4.13) reproduces all observed spatial patterns well with the exception of Regime 3 (maximum over Kimberley), which has a maximum further south-west and less intense than observed. CNRM-CM5 has a similar problem to ACCESS1-0 where rainfall maxima for the coastal heavy regimes tend to be located offshore (see model f in the top panel in Figures 4.11 to 4.13), thus producing a similar bias pattern in the climatological rainfall to the ACCESS models. In addition, CNRM-CM5 produces a spatial pattern similar to the Pilbara regime in AWAP instead of the spatial pattern associated with CMORPH Regime 6. However, the maximum intensity of the regimes are much closer to the observations, so the distance of each regime (and therefore their sum) is lower. MRI-CGCM3 (see model h) in top panel of Figures 4.11 to 4.13) again has a similar problem with moving the rainfall maxima slightly offshore, but the onshore biases in the climatological rainfall are much weaker resulting in the lowest distance sum of the models presented here.

The full set of regimes in MRI-CGCM3 is shown in Figure 4.14. When the regimes in this model are compared to the observed regimes (see Figure 3.2), they have an average intensity closer to the observations than many of the other models, highlighting that this model is able to reproduce the rainfall regimes most accurately. bcc-csm1-1-m and MIROC5 have the highest scores, and thus have the poorest representation of the observed regimes. bcc-csm1-1-m tends to produce rainfall maxima that are far more intense than the observations (model c in top and middle panels of Figures 4.11 to 4.13), and the location of the maxima

Table 4.5: Distance sum for the best arrangement of model regimes to observed regimes, by model.

Model	Sum	Model	Sum
MRI-CGCM3	223.5	CSIRO-Mk3-6-0	387.8
CCSM4	240.5	MIROC5	448.6
CNRM-CM5	309.0	ACCESS1-3	490.2
ACCESS1-0	373.2	bcc-csm1-1-m	616.7

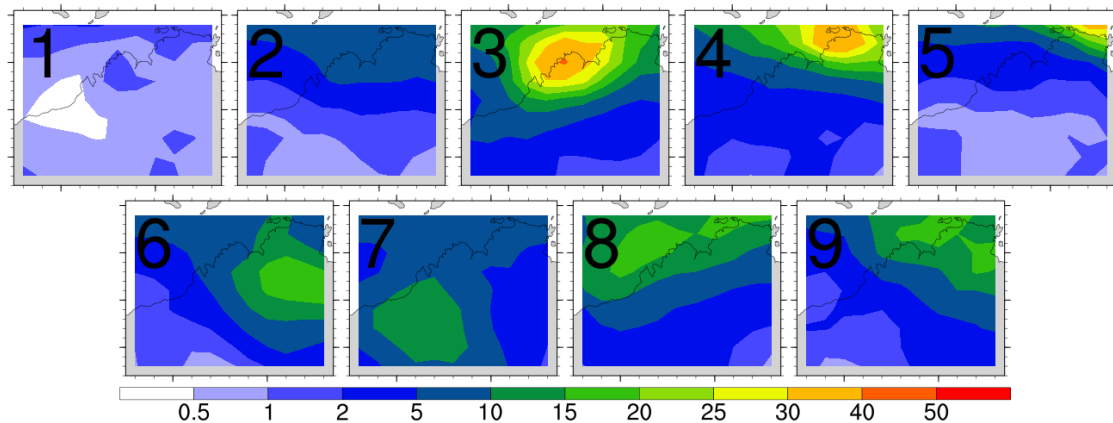


Figure 4.14: Rainfall regimes in MRI-CGCM3, with the final two regimes the west and east cyclone regimes respectively. These are the same patterns as for model h) in the previous regime plots, and are presented here to highlight the similarity to the observed regimes in Figure 3.2. Units are  $\text{mm day}^{-1}$ .

differ from the observations slightly. Although some models may appear to reproduce some regimes with the correct frequency when investigated with Method I, this method shows that the spatial patterns that some models are producing are different to the observations, thus these models are unable to replicate the observed rainfall regimes accurately.

### Robustness of independently determined regimes

To investigate the robustness of the rainfall regimes produced by each model, cluster analysis is performed on subsamples of model rainfall, and the resulting clusters are compared to the regimes produced by the whole dataset. A set of 30 subsamples are produced by sampling half of the wet days in each model randomly, and a set of 30 subsampled sets of regimes are produced by separately clustering each subsample. The Euclidean distance of the resulting clusters to each model's original regimes is calculated, and averaged over the 30 sets of subsamples to provide a measure of variability in the model regimes. The mean distance over the subsamples in each model is summarised in Table 4.6.

The mean distance sum of the model subsamples to the original model regimes is always smaller than the distance between the model regimes and the observations, although since the scores are non-zero, there is some difference between the subsamples and the original clusters. However, these differences are likely to be minor. For example, a distance sum of around 200 occurs between the MRI-CGCM3 regimes and the observed regimes, and the

Table 4.6: Average Euclidean distance sums across the 30 subsamples for each model.

Model	Min distance to obs	Mean distance across subsamples	Standard deviation of distances
ACCESS1-0	373.2	145.3	63.7
ACCESS1-3	490.2	282.1	88.3
bcc-csm1-1-m	616.7	347.4	78.4
CNRM-CM5	309.0	179.5	54.4
CCSM4	240.5	129.9	28.9
CSIRO-Mk3-6-0	387.8	195.8	71.1
MIROC5	448.6	236.0	97.5
MRI-CGCM3	223.5	168.8	72.2

spatial patterns in these two cases appear similar. Thus, the models for which the subsample mean is less than 200 can be assumed to have subsamples with similar spatial patterns to the original model regimes. The main exceptions to this are ACCESS1-3, bcc-csm1-1-m and MIROC5, with subsamples that deviate more from the original clusters. Inspection of subsamples in ACCESS1-3 (not shown) suggest some differences in the spatial pattern and formation of Moderate and Inland type regimes, resulting in large distances. Most of the subsamples in bcc-csm1-1-m and MIROC5 generally deviate greatly in terms of intensity but not spatial pattern, which explains the large distance in those models.

Some of the original regimes in both the models and observations have intense rainfall, but are infrequent. A subsample of half the model rainfall contains only 15 years of data, thus with infrequent regimes some difference in the spatial patterns is likely to occur. The subsampling method shown here is likely to show a higher level of uncertainty in the model spatial patterns than the original model regimes, since it is only possible to use half of the data for subsampling rather than the entire set. However, since the subsamples generally show distances that are low enough to be considered similar to the original model regimes, the spatial patterns produced in Method II are relatively robust.

### **Frequency and intensity of independently determined regimes**

The frequency of each model regime after mapping is shown in Figure 4.15. Since the spatial patterns of individual regimes may differ from the observations, it is not always possible to directly compare their frequencies. However, it is possible and useful to examine the frequency of the dry and light regimes in isolation, and by considering TC regimes and other heavy regimes respectively as groups of regimes. The percentage of dry days for each

model show that every model has a greater percentage of wet days than the observations, although CSIRO-Mk3-6-0 and MRI-CGCM3 are closer to the percentage of dry days in the observations compared to the other models. Despite the large number of wet days, most models overestimate the percentage of days in the Light regime, agreeing with the result of overestimation of the Light regime in Method I, which is expected given most climate models are known to initiate drizzle too often, e.g. Stephens et al. (2010). The number of TC days varies between models, with MRI-CGCM3 and CSIRO-Mk3-6-0 producing close to the correct number of TCs in the region, while CNRM-CM5 and CCSM4 are among those which underestimate the number of TCs. Conversely, MIROC5 strongly overestimates the number of TCs. As TCs are shown to be an important driver of the overall rainfall trend (see Section 2.4), the ability of a model to replicate the correct TC frequency is important, and thus this must be taken into account when assessing the models. A breakdown of the frequency and intensity of separate TC regimes is covered in more detail later in this section.

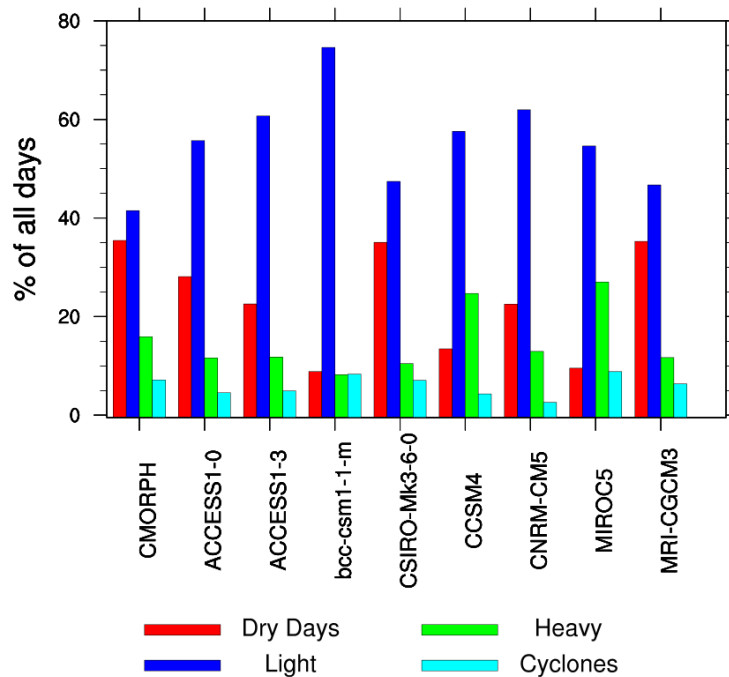


Figure 4.15: The percentage frequency of a number of regimes in observations and each CMIP5 model. The "heavy" regimes bar shows the frequency of all wet regimes excluding the Light regime and TCs.

With the exception of CCSM4 and MIROC5, the models underestimate the frequency of the heavy regimes. Here it is assumed that Regimes 3-7 in each model are heavy regimes,

which is true for most (though not always all) regimes in every model, despite some of the maxima being located on the coast or offshore. In most cases, the heavy regimes in the models are associated with either a surface low or upper level trough. Although these structures may not necessarily be the same as observed structures, their frequency of formation or lack thereof adds insight to the nature of the models' ability to replicate rainfall over NWA. Most CMIP5 models are unable to produce heavy rainfall regimes at the same frequency as the observations, leading to a negative bias in rainfall onshore in many cases. The higher frequency in CCSM4 and MIROC5 leads to the strong positive rainfall biases observed in Figure 4.1.

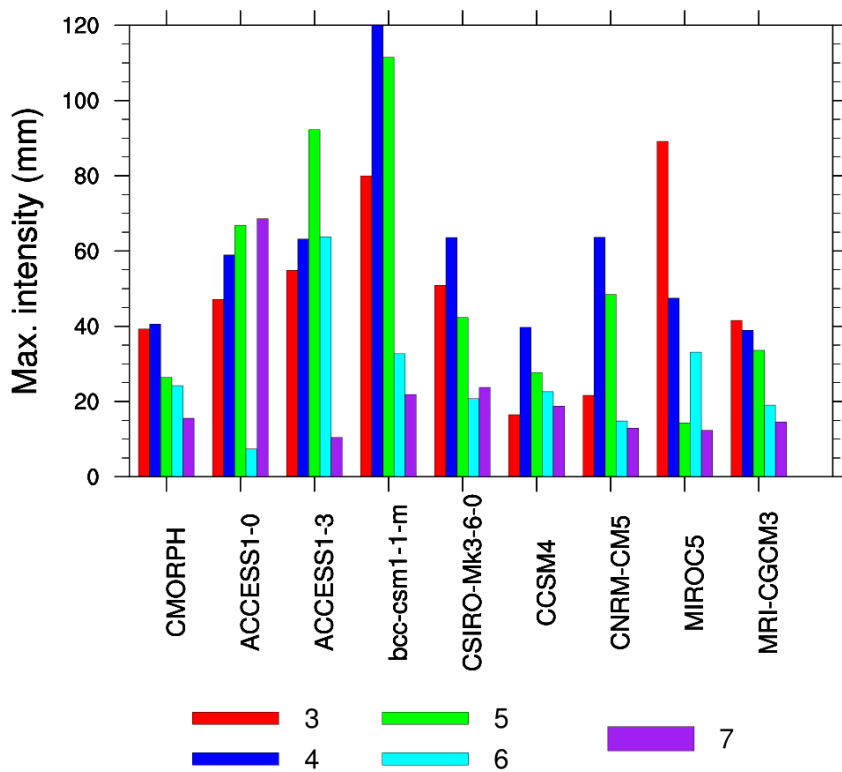


Figure 4.16: Intensity of Regimes 3 to 7 (heavy regimes) in each model's independently determined regimes.

Figure 4.16 shows the maximum intensity of Regimes 3 to 7 (considered the heavy regimes) and the TC regimes in each model, calculated as the value of the point of maximum intensity for each regime in each model. As previously discussed, most models do not reproduce every spatial pattern, although most are able to reproduce Regimes 4 and 5. Aside from CCSM4 and MRI-CGCM3, each model produces at least one regime with an

intensity above  $60 \text{ mm day}^{-1}$ , compared with the observed typical rainfall of around  $30\text{-}40 \text{ mm day}^{-1}$ . bcc-csm1-1-m produces mean maxima for Regimes 5 and 4 that are greater than  $100 \text{ mm day}^{-1}$  and  $120 \text{ mm day}^{-1}$ , the latter of which is above the threshold for an extreme day presented in Section 2.6. The ACCESS models and CNRM-CM5 overestimate the intensity of TC rainfall, while the remaining models predict an intensity that is too low. No model significantly underestimates the maximum intensity of all heavy regimes, but some models tend to underestimate the intensity of inland based regimes such as 6 and 7, and TC rainfall intensity is usually underestimated. The high intensity maxima of the regimes combined with the low frequency shows that models may be more sensitive to changes in the frequency of these regimes than the real-world climate.

### **Synoptic patterns of independently determined regimes**

Composites of the 850 hPa wind and 250 hPa meridional wind fields for each regime are calculated for each model. Some independently determined regimes are very similar to the observations, and thus similar to those determined from the projection method. The fields for Regimes 4 and 7 are presented in this chapter for brevity, and for comparison to the future rainfall regimes presented in the next chapter. The full set of wind fields for each model are provided in the Appendix A.

Figure 4.17 shows the 850 hPa wind composites for Regime 4, corresponding to a rainfall maximum between the Kimberley and Top End regions in the CMORPH observations. In the observations (both CMORPH and AWAP), the regime is characterised by cyclonic flow directly over the region of maximum rainfall. Among the models, there are different biases in the synoptic systems responsible for the rainfall. The two ACCESS models and MRI-CGCM3 produce a closed cyclonic circulation corresponding to a monsoon low similar to the observations, although the wind speeds are much stronger with a maximum above  $10 \text{ m s}^{-1}$  in both ACCESS models, compared to around  $6 \text{ m s}^{-1}$  in the observations. MIROC5 also shows a cyclonic circulation, although the centre is located too far west and the wind strength is too weak. CNRM-CM5 produces a convergence line over the region corresponding to a monsoon trough, with wind speeds on either side being far too strong ( $<12 \text{ m s}^{-1}$ ). CCSM4 shows a similar monsoon trough pattern, but the wind speeds are too weak over land. The remaining models (bcc-csm1-1-m, CSIRO-Mk3-6-0) show almost no sign of any structured

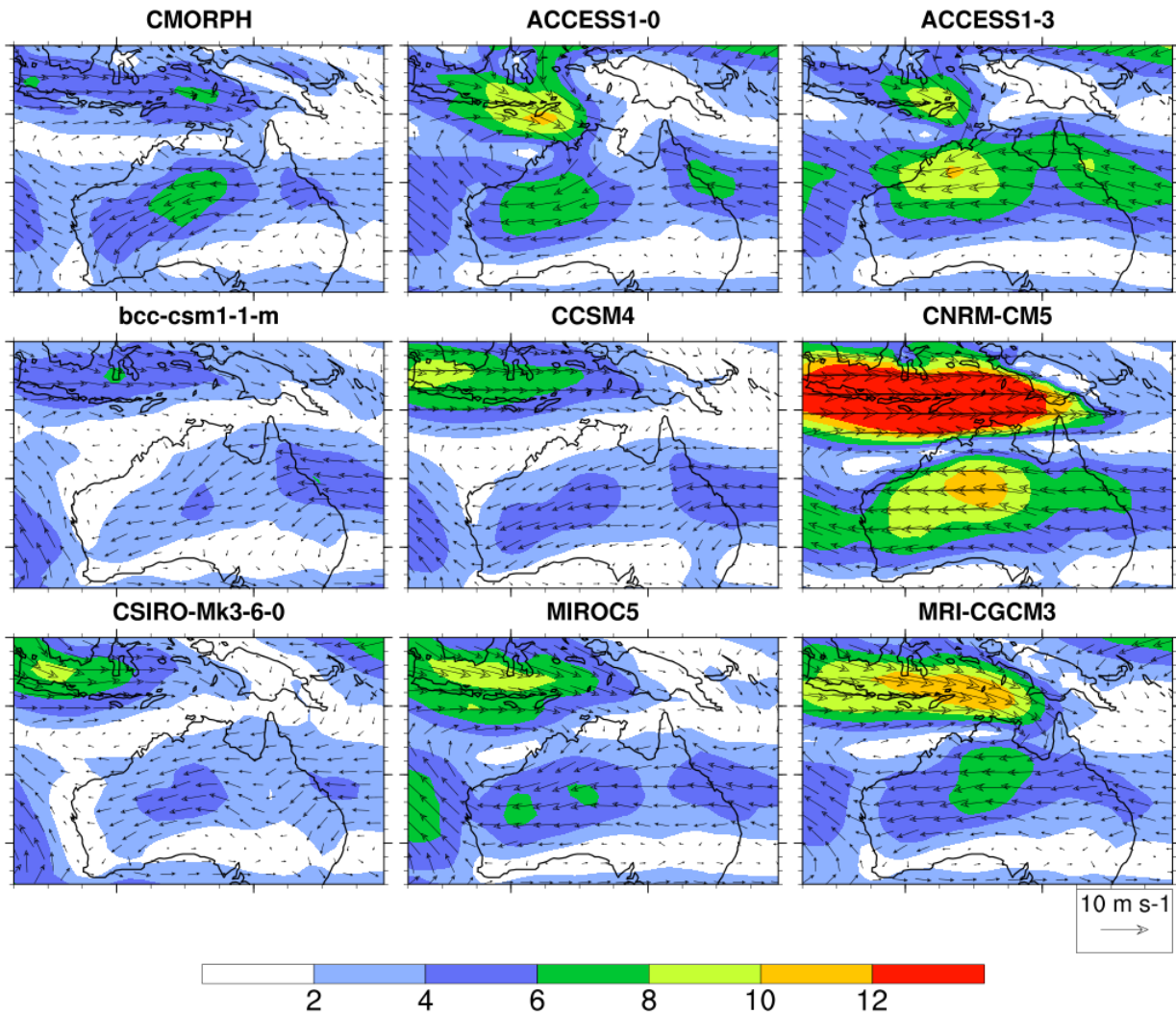


Figure 4.17: 850hPa wind composites for Regime 4 from direct clustering (Method II) in all models considered in this chapter. Shading indicates wind speed in  $\text{m s}^{-1}$

synoptic system near the rainfall maximum. There is also a lack of structure in the 500 hPa composites for these models (see Appendix A). Each model also presents similar problems in replicating the observed synoptic patterns for Regimes 3 and 5, where CNRM-CM5 produces a strengthened monsoon trough, the ACCESS models produce realistic circulation similar to the observations, CCSM4 and MIROC5 produce weak circulation systems and bcc-csm1-1-m and CSIRO-Mk3-6-0 show very little evidence of structured synoptic systems. The biases for this regime are overall similar to that described for Regime 3 in Section 4.3.2, indicating that models produce similar biases for similar regimes relative to the observations.

Figure 4.18 shows the 250 hPa meridional wind composites for Regime 7, which corresponds to an Inland regime in the observations. The observed rainfall pattern in Regime 7

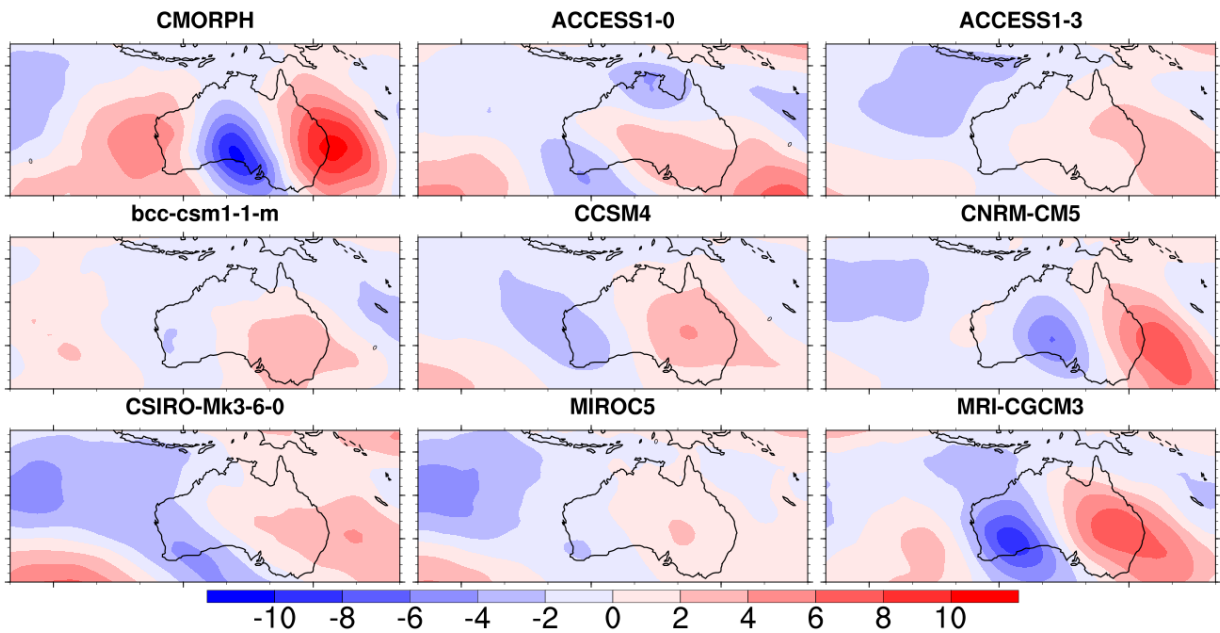


Figure 4.18: 250hPa meridional wind composite for Regime 7 in all models. Units are  $\text{m s}^{-1}$

is the result of the presence and equatorward refraction of mid-latitude Rossby waves. Only CNRM-CM5 and MRI-CGCM3 are able to replicate the observed wave-like pattern, although MRI-CGCM3 has shifted the pattern slightly westward due to the location of the rainfall maximum (see Figure 4.13). The ACCESS models do not produce a wave like pattern for Regime 7 from this method, since their rainfall spatial patterns for this regime are close to the northern coast and not inland as in the observations. The remaining models produce rainfall patterns either like the Inland or Pilbara regime, however the composites do not have a wave-like pattern, which highlights the difficulty of the models to replicate the synoptic patterns responsible for rainfall in this part of the study region.

### Description of TC regimes

In Chapter 2, TCs were shown to provide a significant component of the observed climatological rainfall over NWA, and found to be a significant driver of the overall rainfall trend. The spatial patterns, frequency and intensity of TCLVs in the models are now shown here. The spatial patterns of TCs are shown in the middle and bottom panel of Figure 4.19. For the West Cyclone regime, observed spatial patterns are relatively well replicated by the two ACCESS models, CNRM-CM5 and MRI-CGCM3, although in ACCESS1-0, offshore maximum intensities are higher than that observed. The same models also reproduce the general spatial pattern of the East Cyclone regime well, with the rainfall maximum occurring

just offshore of the Top End. The maximum rainfall intensity in ACCESS1-0 is again too high relative to observations, while MRI-CGCM3 has a maximum intensity point lower than that observed. For both cyclone regimes, The other models produce mean rainfall that is too light compared to the observations, with no strong onshore spatial pattern relating to TC rainfall.

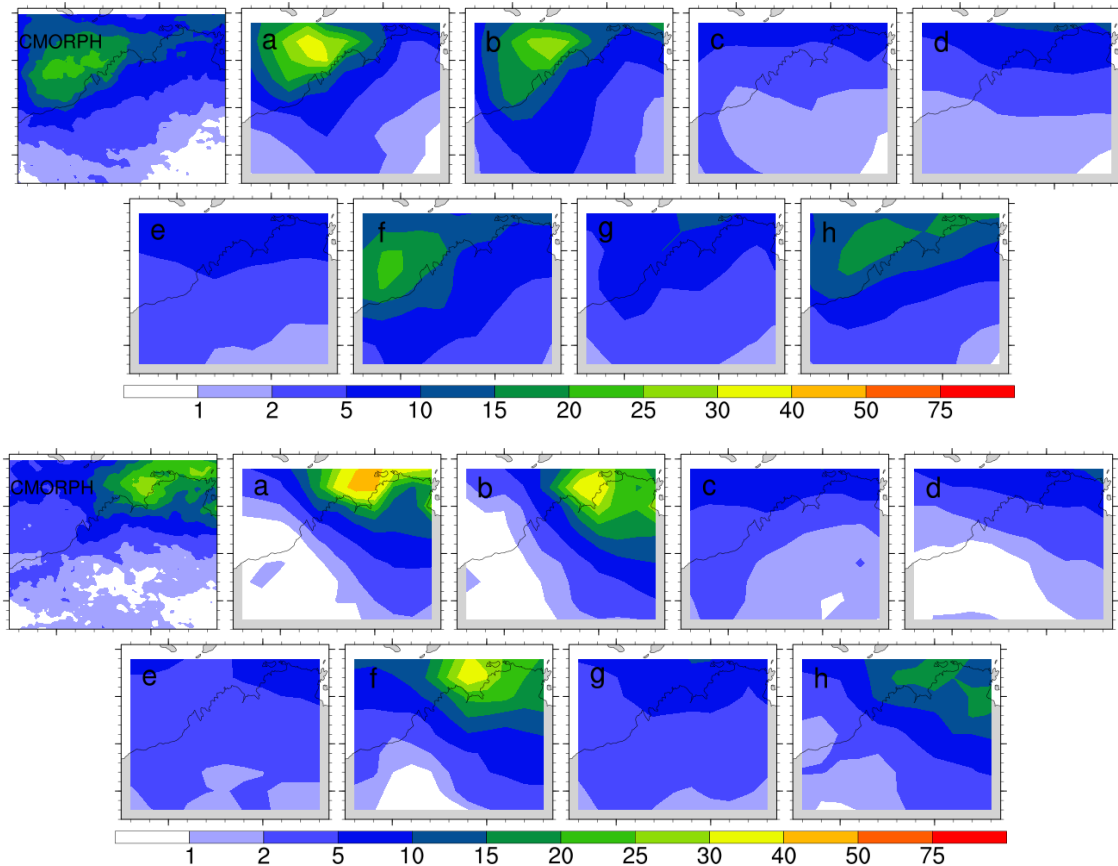


Figure 4.19: Spatial rainfall patterns for the two cyclone regimes produced by the CMIP5 models. The first panel shows the regime in the observations, while the panels a-i indicate the pattern according to each model. Middle set of patterns correspond to the West Cyclone regime, bottom is the East Cyclone regime. Labelling is as follows: a) ACCESS1-0, b) ACCESS1-3, c) bcc-csm1-1-m, d) CSIRO-Mk3-6-0, e) CCSM4, f) CNRM-CM5, g) MIROC5, h) MRI-CGCM3. Note the change in colour scale relative to figures in Chapter 3.

Figure 4.20 shows the frequency of each TC regime in each model, relative to all days. In observations, there are slightly more TC days in the eastern half of the study region (East Cyclone regime). As discussed earlier in the section, MRI-CGCM3, bcc-csm1-1-m and CSIRO-Mk3-6-0 produce approximately the correct frequency of TCs, however they both underestimate the number of TCs in the western half of the study region. Conversely, ACCESS1-3, CCSM4 and CNRM-CM5 produce too many TC days in the western half of the

region, and too few in the eastern half. ACCESS1-0 produces only slightly too few TC days (as per Section 3.4.3), while MIROC5 produces far too many TC days.

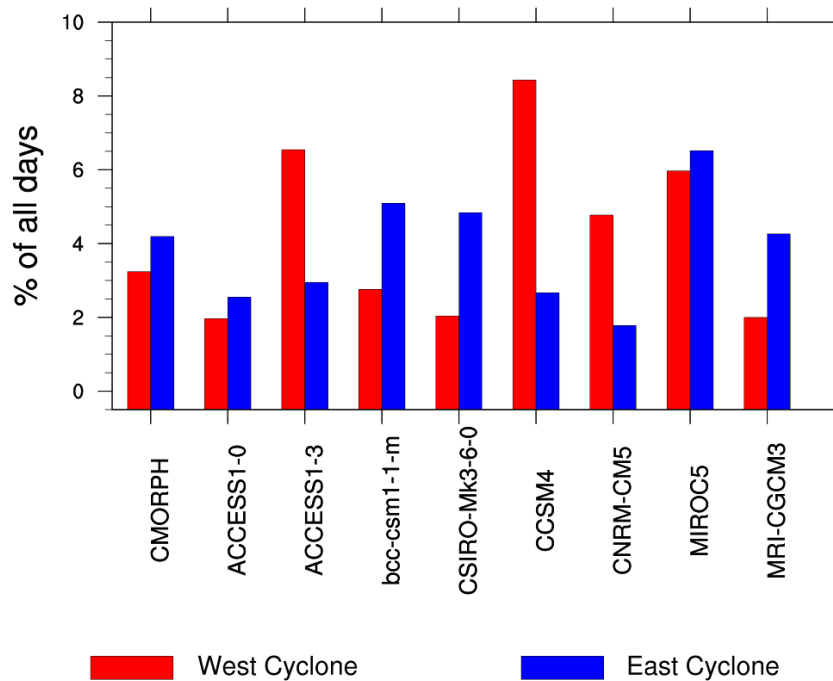


Figure 4.20: Percentage frequency of the two TC regimes in observations (far left) and each CMIP5 model considered in this study.

The 850 hPa wind fields for the East Cyclone regime in each model is given in Figure 4.21. The biases in each model for the TC regimes are the same as those for Regimes 3 to 5 in both the projection and direct clustering methods, with the ACCESS models and MRI-CGCM3 showing closed circulations for both TC regimes, and CNRM-CM5 showing stronger winds on the northern and southern side compared to the western and eastern sides. The remaining four models show almost no sign of a closed circulation, despite being defined as such by the CDD algorithm. One potential explanation for this is that individual vortices in these models tend to be relatively small and asymmetric. A system centred just to the north of a given point will produce strong easterlies, while a different system located to the south will produce strong westerlies. Thus the mean of multiple such systems centred in different locations tends to wash out to the mean flow, leaving little signal in the composites presented here.

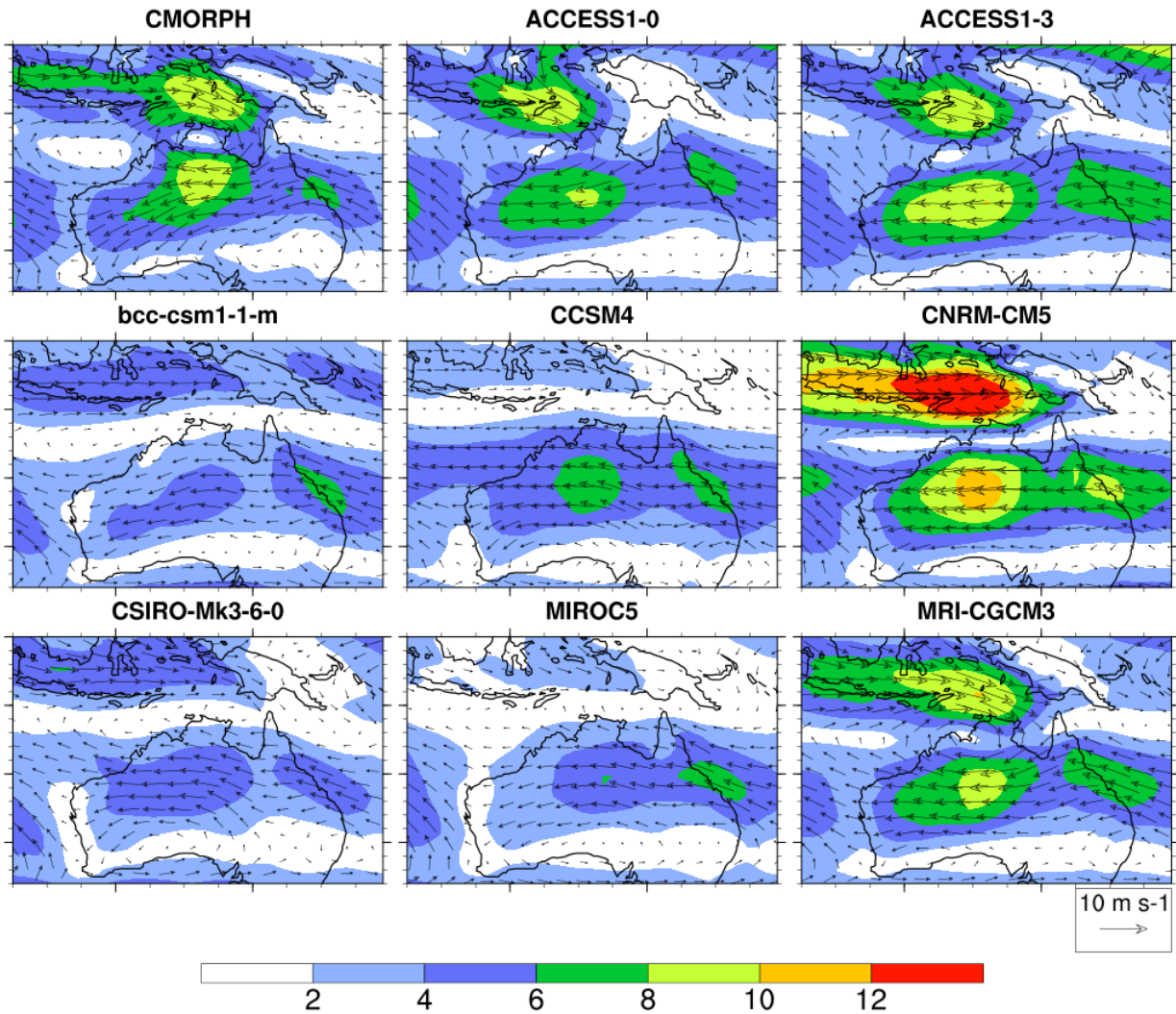


Figure 4.21: 850hPa wind composites for the East Cyclone regime in each model.

Overall, the rainfall pattern and associated synoptic pattern are replicated well by the ACCESS models, MRI-CGCM3 and CNRM-CM5. Of these, ACCESS1-3 and CNRM-CM5 produce too many TC days in the western half of the region, thus the distribution of storms is different to that observed. The remaining models poorly reproduce observed rainfall and synoptic patterns of TCs, possibly to large variation in tracks of relatively small storms.

#### 4.3.4 Method III - Joint clustering of model and observed days

This section assesses the models using Method III, described in Section 3.2.4 and tested in Section 3.4.4. For each model, a dataset containing an equal number of CMORPH and model days is built before dry days and TCs are separated, and the remaining days are clustered. Method III may alter the spatial patterns of the observed regimes due to the presence of model data. Similarly to Method II, the resulting regimes have spatial patterns that do not

necessarily appear the same as the observations. However, due to the presence of observed data the regimes produced from this method are closer to the observed regimes than those produced from Method II, since the spatial patterns produced will lie somewhere between purely model patterns and purely observed patterns rather than purely model patterns as in Method II.

The two parts of Figure 4.22 show the regimes for each model. The patterns are grouped by regime number rather than by model, similar to that done for Method II. Similar to the other methods, a light regime is produced with a spatial pattern that is very similar to observations with only slight variation in spatial pattern. Regimes 3, 4, 5 and 6 are all produced with a very similar spatial pattern to the observations, however the intensity is much higher for some models. For Regime 3, the intensity is too high for the combined regimes from MIROC5, CSIRO-Mk3-6-0 and bcc-csm1-1-m, while the combined Regime 5 in the ACCESS models are too intense. The representation of Regime 2 in this method is poor in MIROC5 and bcc-csm1-1-m where a sharp maximum occurs in the Pilbara, a similar result to the direct clustering (Method II). For Regime 7, the patterns are more similar to the observations for the ACCESS models, but are poorer for bcc-csm1-1-m and CSIRO-Mk3-6-0 with the rainfall maximum located further north-eastward along the coast. However, generally the presence of the observed days in the clustering produces a set of regimes which are closer in spatial pattern to the observations compared to the independent clustering discussed earlier.

For each model, each regime contains various fractions of model and observed days. A summary of the fraction of model days (the observed days make up the remainder) is given in Figure 4.23. As detailed in Chapter 3, regimes from this method that contain a large fraction of model days do not occur in the observations. Hence, the fraction of model days can still be used as a measure of the closeness of the model regimes to the observations, and can be used to assess performance between models. The error bars in the figure indicate a 95% confidence interval obtained by randomly halving the wet days in the observations and determining the fraction of days in one half of the split. Comparing the model fraction to this uncertainty bound allows the deviation from an even split between model and observed data for a given regime to be more clearly determined. Some regimes occur more frequently than others, so a regime with a low frequency of occurrence will have greater uncertainty in

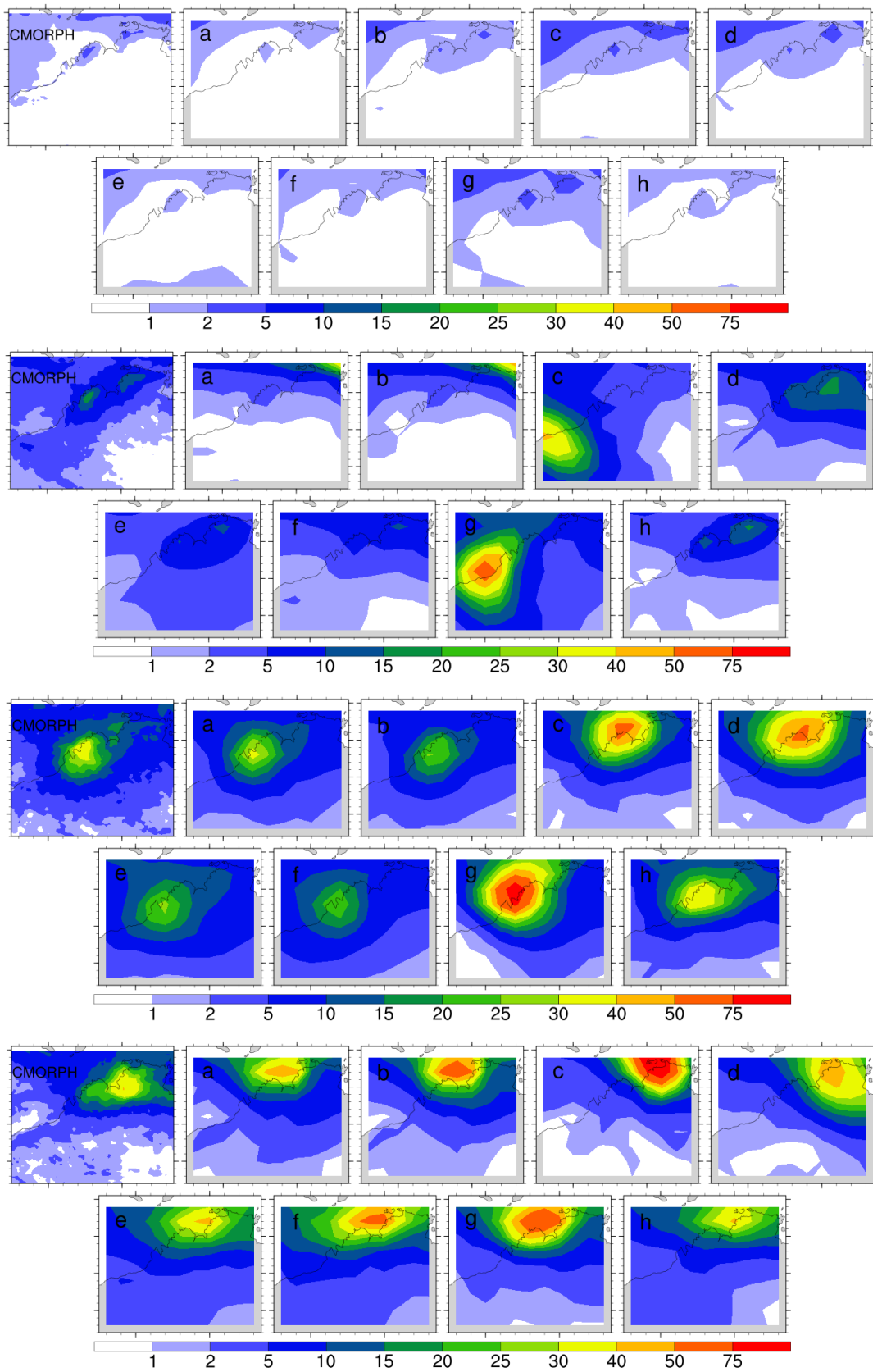


Figure 4.22a: As for Figure 4.11, but for Method III (combined clustering) and Regimes 1 to 4.

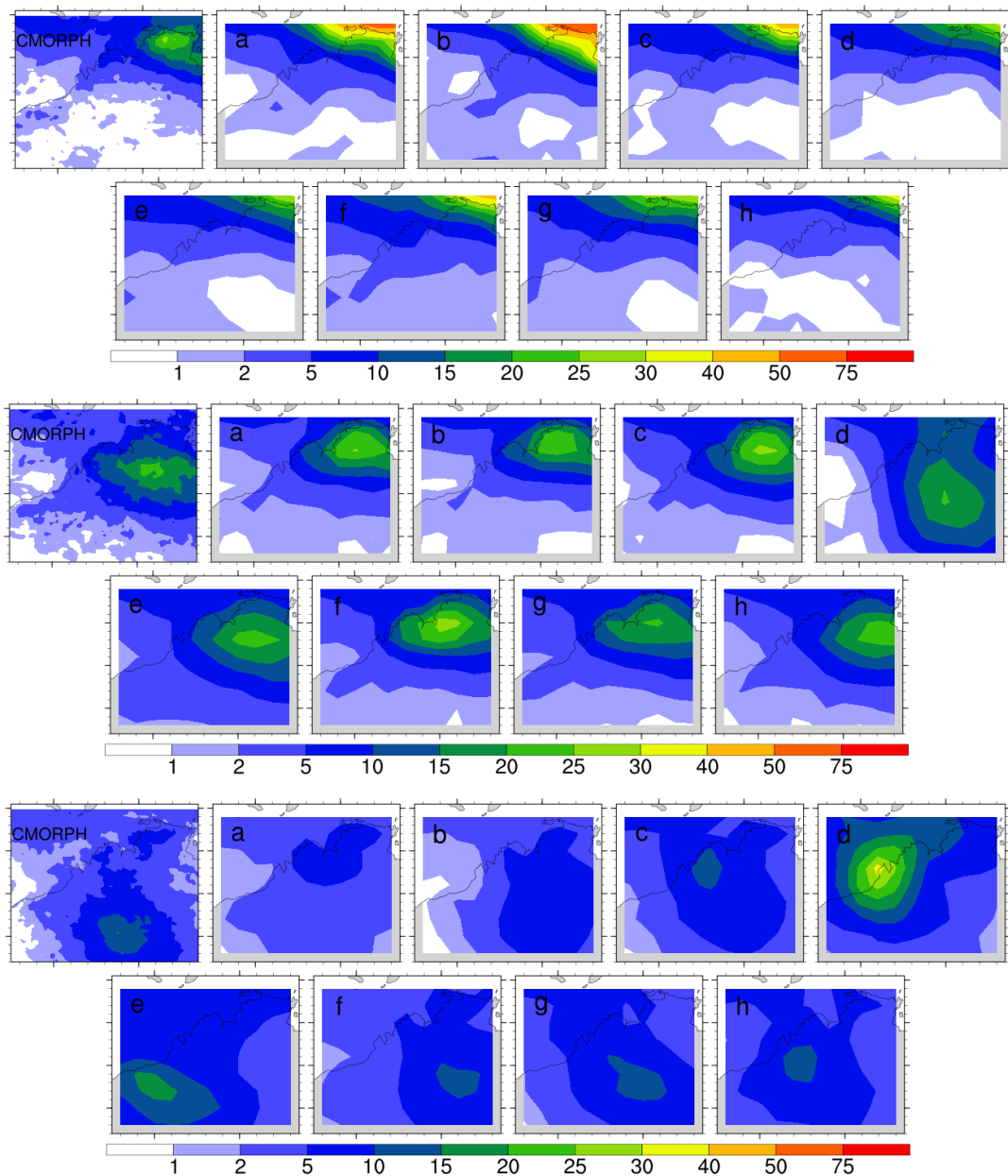


Figure 4.22b: As for Figure 4.11, but for Method III and for Regimes 5 to 7.

frequency than one with a high frequency. Therefore, a separate uncertainty bound for each observed regime allows changes in frequency to be better determined.

Figure 4.23 shows that no model is able to replicate all of the observed rainfall regimes at a frequency within the confidence interval of the observations. Generally, the frequency of Regimes 1 (light rainfall), 4 (rainfall maximum located between the Kimberley and Top End regions) and 5 (rainfall maximum over the Top End) are overestimated in the models. Note that Regime 1 is far more frequent in both observations and models, therefore a relatively

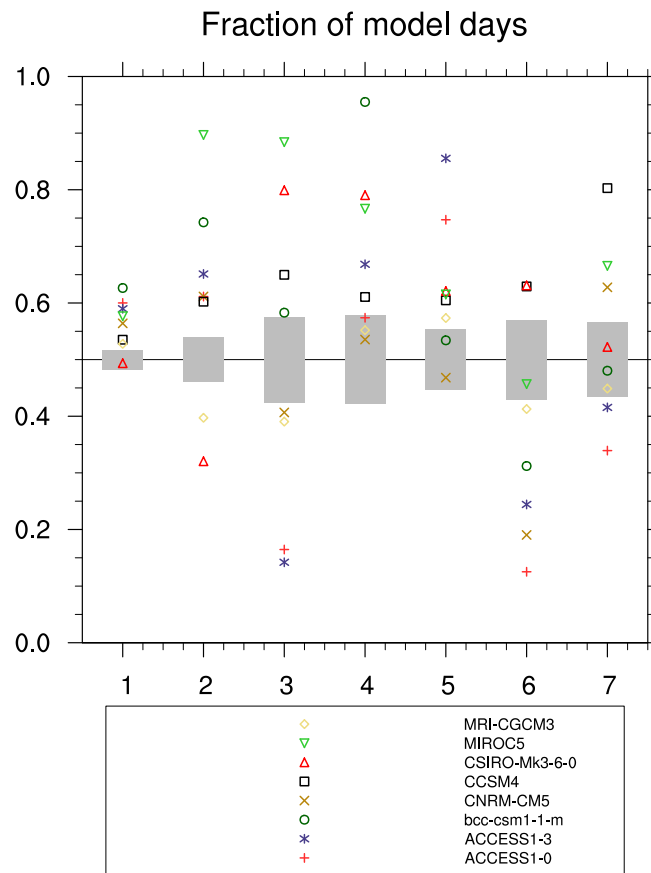


Figure 4.23: Fraction of model days in each regime, plotted for each model. The grey bars show a 95% confidence interval for the ideal fraction (0.5) of model days.

large change in frequency between the model and observations will have a much smaller effect on the model fraction than for the heavier, less frequent regimes. This is taken into account with the smaller confidence interval for this regime. The overestimation of model days in Regime 1 is consistent with the overestimated frequency of this regime found in Sections 4.3.2 and 4.3.3. Since the dataset for clustering contains an equal number of both model and observed days, and models are found to overestimate the frequency of light rainfall, Regime 1 from this method must contain more model days than observed days, and therefore the model fraction is greater than 0.5. Regime 6 is generally underestimated in frequency by the models, which explains the similarity of all of the spatial patterns to the observed Regime 6, since this regime is heavily populated by observed days. The remaining heavy regimes (3 and 7) are overestimated in frequency by some models, but underestimated by others.

When specific models are considered, most models produce some regimes too frequently

and others too infrequently. All regimes from MIROC5 and CCSM4 contain more model than observed days, a result of both these models generally producing rainfall too frequently which agrees with the results in Figure 4.15. In MIROC5, Regime 2 consists of a rainfall peak over the Pilbara rather than the typical Moderate regime pattern, and Regimes 3 and 4 are too intense relative to observations. The significant difference in pattern and intensity implies that the regime is heavily populated by model days, which is confirmed by the fractions given for MIROC5 in Figure 4.23. The two ACCESS models produce Regimes 3, 6 and 7 too infrequently and the others too frequently, with no regime containing model days within the uncertainty bound. The CSIRO model is the only one that produces Regime 1 (light) at the correct frequency with this method (agrees with the results in Section 4.3.3), but the remaining regimes also vary in their frequency. CNRM-CM5 and MRI-CGCM3 produce some heavier regimes which are within the uncertainty bounds of the observations. The remaining regimes from these models are not far outside the uncertainty bounds, which suggest these are the models most able to replicate regimes at the correct frequency.

The mean across regimes of the magnitude of differences between each model fraction from this method and 0.5 can be used as a general overview of the ability of each model to determine regimes with the correct frequency. The larger the difference between the model fraction and 0.5, the greater the difference in frequency between the rainfall pattern in the model and observations, or in the case of fractions greater than 0.5, the greater the deviation in spatial pattern in this method. Thus, a smaller mean means that the model fractions are closer to 0.5, and therefore the model is able to reproduce the spatial patterns and frequency of the regimes more accurately. The difference means for each model are presented in Table 4.7. The models with fractions closest to 0.5 are MRI-CGCM3 and CNRM-CM5, which both have regimes that are either within the uncertainty bounds in Figure 4.23, or not very distant from them. The ACCESS models and MIROC5 are similarly poorly ranked for different reasons - the ACCESS models produce Regimes 3 and 6 at a frequency that is too low, while MIROC5 produces regimes that are too intense, resulting in significant deviation from the observed frequency. The fractions here are considered in the final model ranking, which is discussed in the next section.

Table 4.7: Sum of differences across regimes between model fractions and the ideal fraction of 0.5.

Model	Difference mean	Model	Difference mean
MRI-CGCM3	0.072	bcc-csm1-1-m	0.164
CNRM-CM5	0.110	ACCESS1-0	0.200
CCSM4	0.134	MIROC5	0.207
CSIRO-Mk3-6-0	0.150	ACCESS1-3	0.209

#### 4.4 Discussion: Overall model ranking

A subset of CMIP5 models were assessed for their ability to replicate the observed rainfall regimes and the climatological mean in NW Australia. Almost all models are able to replicate some of the observed rainfall regimes, although many models produced regimes that are not observed. All models produced a Light regime and a range of heavier regimes. However, all models have biases in the climatological mean rainfall, with many producing too much rainfall over ocean regions north of the continent, and too little rainfall over land within 500km of the coast. Some models produce too much rainfall over the entire study region. Almost all models overestimate the frequency of wet days in the region, of which the greatest bias is in the frequency of days in the Light regime. Thus, most models fail to produce the synoptic systems responsible for heavy rainfall in the region.

There is significant difference between models in their ability to replicate the pattern, frequency and intensity of the observed regimes. From Method II (direct clustering), the three models with the smallest sum were CCSM4, MRI-CGCM3 and CNRM-CM5. By inspecting the regimes produced in Method II, we see these three models appear to replicate most of the observed regimes well, although there is some difficulty around the Kimberley and western Top End regions which is a common problem among all models. The maps obtained from Method III also show relatively little difference in the spatial pattern relative to the observations. However, CCSM4 produces far too much rainfall due to producing too many wet days, resulting in the frequency of all regimes being higher than the observations. CNRM-CM5 produces a frequency of the heavy regimes to be similar to the observations as evidenced from Figure 4.23, although fails to replicate the spatial pattern of Regime 6, and produces too many days in the Light regime. MRI-CGCM3 has the weakest bias in the climatological rainfall, and reproduces almost all regimes with frequencies closest to the observations. There is slightly too few heavy regime days, however the difference is small

relative to the other models.

The model ranks for each method based on the metrics described in Section 4.2.2 are presented in Table 4.8. An overall ranking is calculated by summing the ranks based on each individual metric. Using this method, MRI-CGCM3 is the highest ranked model as the climatological mean, regime spatial patterns, wind fields and frequency are all close to the observations relative to the other models, although the seasonal distribution of rainfall is shifted a month later than observed. CNRM-CM5 is also highly ranked with the frequencies of its regimes being close to those observed, although rainfall toward the end of the rainy season is slightly higher than observed. CSIRO-Mk3-6-0 is ranked third for a similar reason despite falling outside the top 3 from Method II and producing rainfall too early in the season. Upon inspection of the regimes from Method II, all of the coastal regimes are replicated well including Regime 3, which some other models fail to produce with the correct spatial pattern. Method III shows that Regime 4 is produced far too frequently, however for this model other regimes are reproduced within the uncertainty bound of the observations. The two ACCESS models are ranked 5th and 6th respectively, with their close rankings likely to be linked to the similar convection and cloud microphysics schemes used in those models.

The poorest performing models from this ranking include MIROC5 and bcc-csm1-1-m. Both models perform poorly since they produce some heavy regimes with too high an intensity, resulting in a larger distance sum in Method II, and a fraction of heavy regimes that is too high in Method III. Both models also produce a rainfall maximum over the Pilbara instead of a Moderate-type regime, and reproduce the wind patterns associated with the heavy regimes poorly.

## 4.5 Conclusion

A set of eight CMIP5 models are assessed for their ability to replicate the observed mean rainfall and observed rainfall regimes over NWA using three methods: projection, independent clustering and combining model and observed data. Each assessment method allows comparison between models and observations, and an overall ranking for these models is determined by considering measures of frequency, intensity and spatial pattern of model rainfall regimes. When considering the mean rainfall, models tend to show positive biases to north

Table 4.8: Table summarising ranks of models based on multiple criteria: capturing mean rainfall, capturing frequency from Method I, distances from Method II, deviations of fractions in Method III.

Model	Ranking					Overall
	Yearly mean	Method I - Frequency	Method I - Winds	Method II - Distance sum	Method III - Model fraction sum	
ACCESS1-0	3	4	6	4	6	<b>5</b>
ACCESS1-3	2	6	3	7	8	<b>6</b>
bcc-csm1-1-m	6	8	5	8	5	<b>7</b>
CCSM4	8	7	2	2	3	<b>4</b>
CNRM-CM5	5	3	4	3	2	<b>2</b>
CSIRO-Mk3-6-0	4	1	7	5	4	<b>3</b>
MIROC5	7	5	8	6	7	<b>8</b>
MRI-CGCM3	1	2	1	1	1	<b>1</b>

of the Australian coastline and in inland areas of the study region, the strength of which vary by model. Models also struggle to replicate the observed rainfall trend over the entirety of the NWA study region, although most do show an increase somewhere within the study region. Most, but not all, of the observed regime spatial patterns are replicated, although generally the models have the most difficulty in replicating regimes responsible for inland rainfall.

Most models produce light rainfall too often, agreeing with previous studies. Regimes responsible for heavy rainfall in coastal areas are too infrequent and too intense in the majority of models. The frequency of TCs is mostly either replicated well or slightly underestimated, with a small number of models either strongly underestimating or overestimating the frequency of TC days. In addition, the majority of models do not reproduce the synoptic patterns responsible for the heavy regimes, although when compared to other models, the ACCESS models perform best at reproducing monsoon lows and MRI-CGCM3 performs best at reproducing mid-latitude waves.

By considering ranking measures that consider each model's ability to replicate the observed mean climate and frequency, intensity and synoptic patterns of observed regimes, an overall ranking for the models is determined. The models ranked as the top 3 are MRI-CGCM3, CNRM-CM5 and CSIRO-Mk3-6-0, which reproduce the observed mean rainfall and observed regimes with frequencies relatively close to the observations. The ranking is a general guide for informing changes to rainfall regimes in a future climate, which will be investigated in the next chapter.

## Chapter 5

# Future projections of rainfall regimes over north-western Australia

### 5.1 Introduction

In Chapters 4, the ability of each model to simulate the observed climate over NWA was determined by ranking their ability to replicate the observed frequency, intensity and spatial pattern of the regimes over the region. The ranking is used to inform future projections of rainfall over north-western Australia, which is the focus of this chapter. This chapter will focus solely on the RCP8.5 emissions scenario, the highest emissions scenario in CMIP5 which considers unabated emissions beyond 2100. Under the RCP8.5 emissions scenario, CMIP5 models tend to have high agreement on changes to precipitation in mid to high latitude regions, and little agreement in parts of northern Australia (Knutti and Sedlacek, 2013). However, taking subsets of the best performing models can increase the level of agreement in rainfall changes. Jourdain et al. (2013) take a subset of 10 best performing CMIP5 models over the Indo-Australian monsoon region based on ability to replicate ENSO and monsoon characteristics. They find that 7 models show significant wetting across northern Australia by the end of the 21st century under the RCP8.5 emissions scenario. Frederiksen and Grainger (2015) use a similar multi-model ensemble employing high-ranking models (based on ability to reproduce the variability in the 500 hPa geopotential height field as per Grainger et al. (2014)) to arrive at a similar conclusion, and find that enhanced north-westerly winds over the summer period are the main driver of this trend. Experiments in CMIP5 models also suggest that TC numbers in the South Indian Ocean are likely to decrease in a future climate

(Knutson et al., 2015; Utsumi et al., 2016), although the trend map produced by Knutson et al. (2015) suggests the change is smaller near the NWA coast.

In chapter 4, the ability of a subset of CMIP5 models to replicate the rainfall regimes over NWA was established. The subset was selected based on availability of TCLV data and resolution. The selected models were able to replicate most, but not all of the spatial patterns associated with the observed regimes, although there are significant biases in the frequency and intensity of the model regimes.

The aim of this chapter is to explain the projected trend in rainfall over NW Australia in terms of the rainfall regimes identified in the previous chapters. This chapter focuses solely on the RCP8.5 scenario to highlight changes to the regimes in the case of unabated carbon emissions. Changes to the mean rainfall under the RCP8.5 scenario are described for each model, before applying the projection and independent clustering methods outlined in the previous two chapters to define the rainfall regimes. Changes to frequency and intensity of each rainfall regime are described, with the aim of using these changes to explain the trend in mean rainfall in each model.

Section 5.2 will outline the data used to consider the RCP8.5 future climate scenario in each model, and the approaches used to determine rainfall regimes in a future climate. In Section 5.3, changes to the climatological mean rainfall are described. Section 5.4 projects the daily rainfall in the RCP8.5 scenario onto each model's independently determined regimes, and decomposes the change in rainfall into changes in frequency and intensity of each regime. Section 5.4.5 describes changes to the synoptic patterns in some important regimes. Section 5.5 describes changes to the spatial patterns when RCP8.5 daily rainfall is clustered independently of the observations, while the final section summarises the main findings of this chapter.

## 5.2 Data and methods

### 5.2.1 Data

Daily precipitation was taken from the same eight CMIP5 models used in the previous chapter, however in this case the model runs corresponding to the years 2070-2099 in the RCP8.5 emissions scenario were used. Details of each model's resolution is provided in Table 4.1. Precipitation data are regridded to  $2.0 \times 2.0$  degree resolution in the same way as in Chapter 4. Tracks of tropical cyclone-like vortices (TCLVs) were again detected using the same method outlined in Section 3.2.3, and removed from the data using the same cyclone removal method outlined in Section 2.1.2, where any day in which a TCLV centre is located within the study region is considered to be a TC day and thus separated from the data. Prior to any regime assignment, dry days (defined as a spatial average  $<0.1 \text{ mm day}^{-1}$ ) are also removed from the data.

### 5.2.2 Future regime determination

Changes to the rainfall for each model under a future climate are assessed in multiple ways. Firstly, changes to mean rainfall and winds in a future climate relative to the model's own current climate are determined. Changes to mean rainfall are calculated as a percentage difference in the annual mean between 2070-2099 and 1970-1999 in each model's historical run. The mean of the 850 hPa winds during the monsoon season (October to March) are also calculated for each model, and the difference in wind speed and direction calculated to indicate changes to the overall flow in a future climate.

Secondly, the rainfall regimes in the future climate are determined and compared to those in the historical period in each model. Two of the three regime assignment methods outlined in Section 3.2.4 are used to classify future rainfall in the models into regimes. The first approach is the projection method (Method 1 in Chapter 3), where rainy days in each model (spatial average  $>0.1 \text{ mm}$  as in previous sections) are projected onto existing regimes. Prior to this chapter, this method involved determining the Euclidean distance between a particular (historical) model day and each of the observed regimes, and placing the day into the regime for which the Euclidean distance is smallest (ie. the "closest" regime). The same approach

is used in this case, except that the daily rainfall from the RCP8.5 run is projected onto the independently determined regimes produced in the model's historical run using Method II in Chapter 4. This method assumes that the spatial patterns produced by rainfall regimes in the future climate will be the same as those in the model's historical period. The advantage of this method is that the fixed definition of the regimes allows changes to the frequency and intensity of each regime to be calculated and interpreted easily. In addition, changes to the synoptic patterns can be determined easily as there is no influence from changes in rainfall spatial patterns. However, the fixed rainfall patterns result in the inability of this method to determine if there are changes in the spatial pattern of regimes. To determine changes in the regime spatial patterns, daily rainfall in the RCP8.5 scenario is also clustered directly, as will be discussed later in this section.

The change in rainfall between the RCP8.5 scenario from 2070-2099 and the historical run (1970-1999) is then decomposed into changes in frequency and intensity contributions from each regime. This is a similar approach to that described in Section 2.1.5, using the expression:

$$\bar{P}_2 - \bar{P}_1 = \sum_{i=1}^N [(f_{2,i} - f_{1,i})P_{1,i} + (P_{2,i} - P_{1,i})f_{1,i} + (P_{2,i} - P_{1,i})(f_{2,i} - f_{1,i})] \quad (5.1)$$

where  $f_i$  represents the frequency of regime  $i$  and  $P_i$  represents its precipitation. In Section 2.1.5, the subscripts 1 and 2 represented the periods 1950-1979 and 1980-2009 respectively. Here they represent the periods 1970-1999 and 2070-2099 in the historical and RCP8.5 model runs respectively. As per Section 2.1.5, the three terms in the sum represent contributions to the trend due to changes in frequency, intensity and the cross terms respectively. The cross terms may be neglected for small changes - which is true for all models considered in this chapter. Since regimes from different models have different spatial patterns, it is difficult to directly compare terms for specific regimes between models. However, regimes labelled 1 and 2 always correspond to patterns closely resembling the observed Light and Moderate regimes, thus regimes 3 to 7 are combined into a single "heavy" regime group to compare between models. Individual regimes are investigated to explain the spatial pattern of the mean rainfall trend in each model.

Changes to synoptic patterns in the RCP8.5 scenario are also examined by calculating composites of the 850 hPa wind fields for each regime at each model's native resolution. Anomalies are calculated relative to the composites of each regime from Method II in Chapters 3 and 4. We choose the result from Method II since the aim of this chapter is to indicate changes in the rainfall regimes and synoptic patterns within each model, rather than compare the synoptic patterns to observation-derived patterns as per Method I.

Daily rainfall in the RCP8.5 scenario is also clustered directly to produce rainfall regimes independent of the historical period, which is the same approach as Method II outlined in Section 3.2.4. This method takes into account any changes to the spatial patterns associated with the regimes, since it is possible that differing spatial patterns may become more dominant in a future climate. The future regimes are matched to their counterparts in the historical period (Method II) by finding the arrangement that minimises the sum of the Euclidean distances across each pair. This is the same approach taken to match historical model regimes from Methods II and III to observations. A detailed example of the matching method is given in Section 3.4.3. In Section 4.3.3, the minimised distance score was interpreted as the general closeness of model regimes to the observations, and was used to rank the ability of models to replicate the observed regimes. In this case, the minimised distance sum is interpreted as the amount of change that will occur to the spatial patterns for the model regimes, so no ranking is needed here.

## **5.3 Trends in mean climate under RCP8.5**

### **5.3.1 Trend in the mean rainfall**

Changes in yearly mean rainfall in 2070-2099 under the RCP8.5 emissions scenario relative to 1970-1999 in the historical period are presented in Figure 5.1 for each model. The maps are ordered from most drying to most wetting, based on the percentage change averaged across the region. The maps show significant variability in the trend in rainfall amongst the models, with ACCESS1.3 and CSIRO-Mk-3-6-0 showing very strong drying of more than 50% over large areas of NWA. ACCESS1.0 shows drying over the ocean, but negligible change over land. In contrast, CNRM-CM5, CCSM4 and MIROC5 show a wetting trend over the region, with wetting centred over the Kimberley region in the former two models.

MIROC5 displays more significant wetting over inland areas. bcc-csm1-1-m shows drying in the far west of the study region, but no significant trend elsewhere. MRI-CGCM3 shows slight wetting in the far south-east of the study region, but little trend elsewhere.

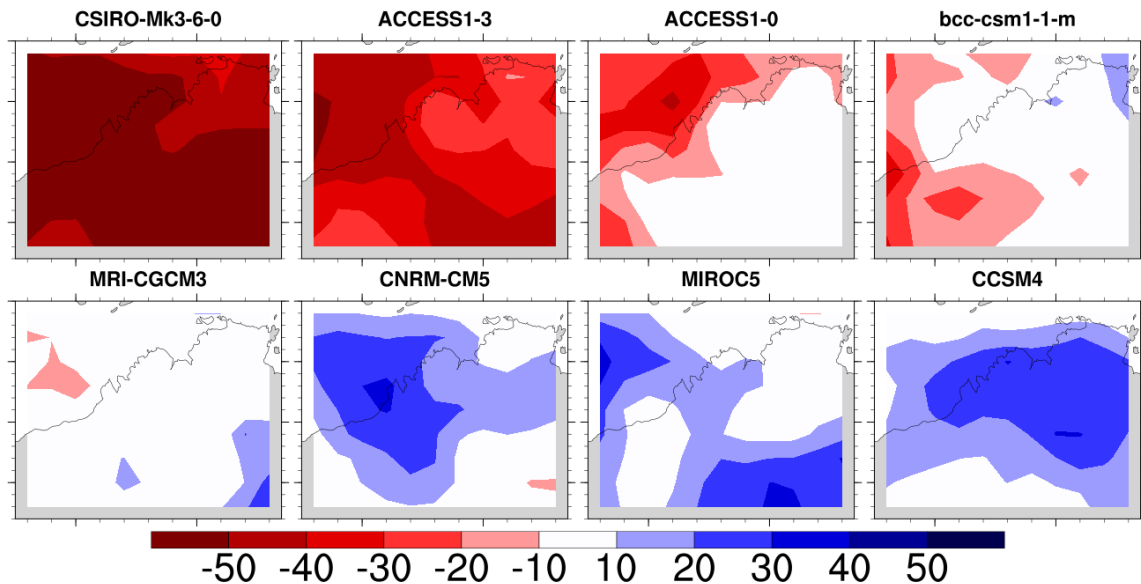


Figure 5.1: Percentage change in rainfall in each model for the years 2070-2099 in the RCP8.5 scenario, relative to 1970-1999 in the historical run. The models are ordered from most drying (top left) to most wetting (bottom right), incrementing left to right.

There is no consistency in rainfall trend across the top three ranked models from Chapter 4 (CNRM-CM5, CSIRO-Mk3-6-0 and MRI-CGCM3), since the three models show significant wetting, drying and little trend respectively. Thus, the choice of high ranking models does not provide consistency in future rainfall predictions over NWA. The variation between high ranking models here agrees with Brown et al. (2016), but is in contrast to Jourdain et al. (2013) and Frederiksen and Grainger (2015), although the ranking used in Chapter 4 is focused on NWA rainfall regimes only, and does not include relationships to ENSO or other large-scale modes of variability.

### 5.3.2 Trend in the mean flow

To illustrate the changes to the mean low-level winds in the CMIP5 models considered in this study, the mean flow at 850 hPa from October to March is calculated in each model. The difference relative to each model's October to March mean flow in the historical period is shown in Figure 5.2. bcc-csm1-1-m shows stronger westerlies over the Maritime Continent,

and weaker easterlies over northern Australia. This appears to be consistent with a southward shift of the monsoon trough, despite there being minimal change to mean rainfall in this model. CCSM4 shows a similar pattern with slightly stronger westerlies to the north of the Australian continent and weaker easterlies over land, but the pattern is consistent with the enhanced rainfall shown in Figure 5.1. In contrast, ACCESS1-3 and CSIRO-Mk3-6-0 show strengthened south-easterlies over northern Australia. This is consistent with a northward shift of the monsoon trough, and in these cases they can explain the sharp reduction in mean rainfall in these models.

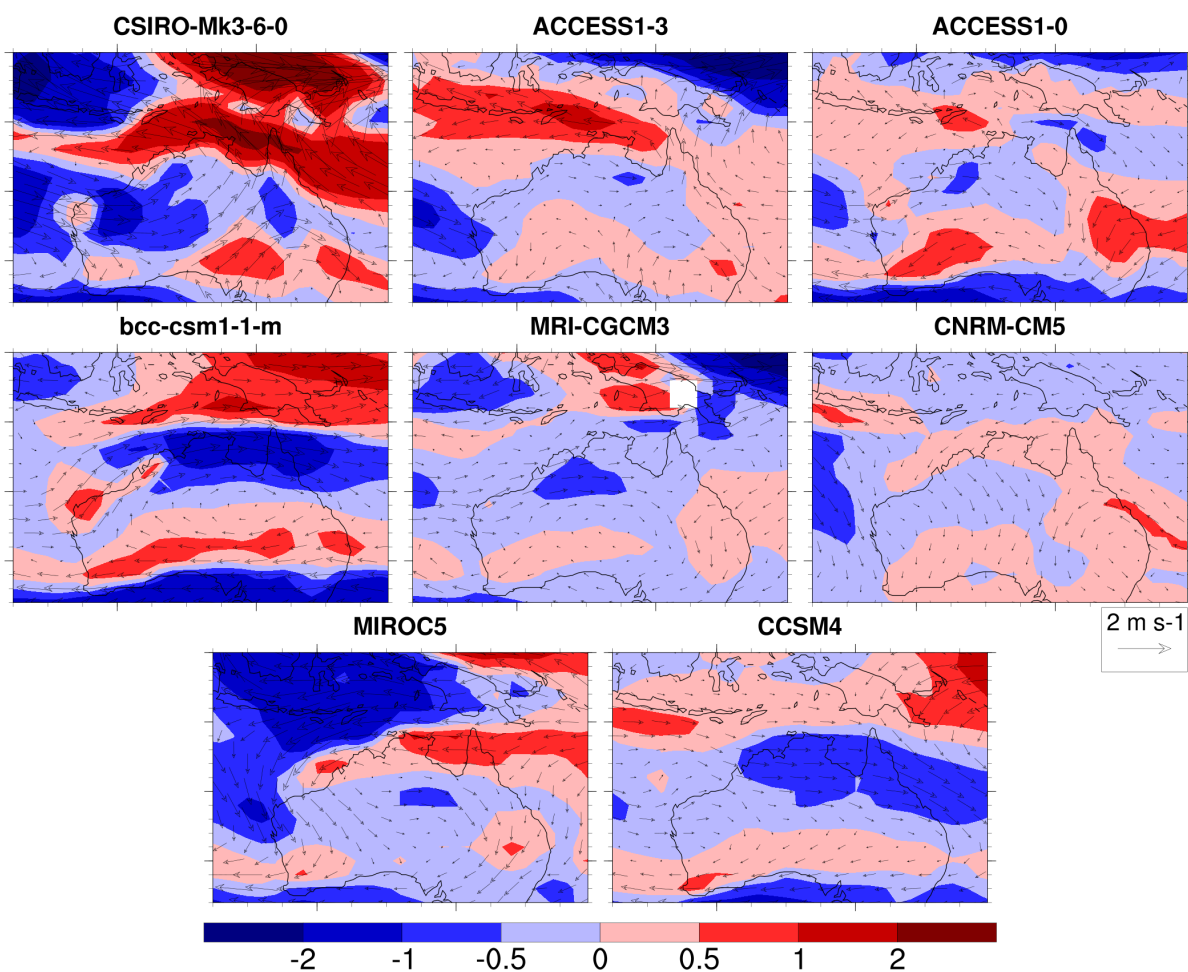


Figure 5.2: Difference in the mean 850 hPa wind fields in each model for October to March, between the RCP8.5 scenario 2070-2099 and the historical period 1970-1999 in each model. Blue shading indicates weaker wind speeds, while red shading indicates stronger wind speeds. Vectors indicate the direction of the change. Shading units are  $\text{m s}^{-1}$ .

MIROC5 shows reduced westerlies over the Maritime Continent and enhanced easterlies over north-eastern Australia. The wind trend pattern also appears to explain little of the

rainfall trend in the region. The remaining models (ACCESS1-0, CNRM-CM5, MRI-CGCM3) show little discernible pattern in the trend in the 850 hPa wind fields.

In summary, the projected changes to the mean winds over the region vary significantly across models, and do not necessarily explain the trend in rainfall. Changes to the rainfall regimes in the models will now be discussed with the aim of explaining the changes in mean rainfall in each model.

## **5.4 Projecting RCP8.5 days to the historical model regimes**

### **5.4.1 Spatial patterns of projected future rainfall regimes**

For each model, daily rainfall from the RCP8.5 scenario for the years 2070-2099 are projected onto the historical regimes determined from direct clustering. Projecting wet days from the RCP8.5 scenario onto the historical model regimes results in spatial patterns that appear highly similar in shape to each model's own historical regimes. As discussed in Section 3.4.2, assigning regimes using this method forces each future rainfall regime to be similar to the existing regimes. To highlight the similarity of the shapes as well as changes to intensity, the difference between the rainfall pattern in the RCP8.5 scenario and the historical period is calculated for each regime and each model. The differences for regimes 3 to 7 and for the TC regimes are shown in both parts of Figure 5.3. The models have been ordered from top to bottom such that more drying models are placed toward the top (based on spatial mean of the difference pattern), gradually changing to the most wetting models at the bottom.

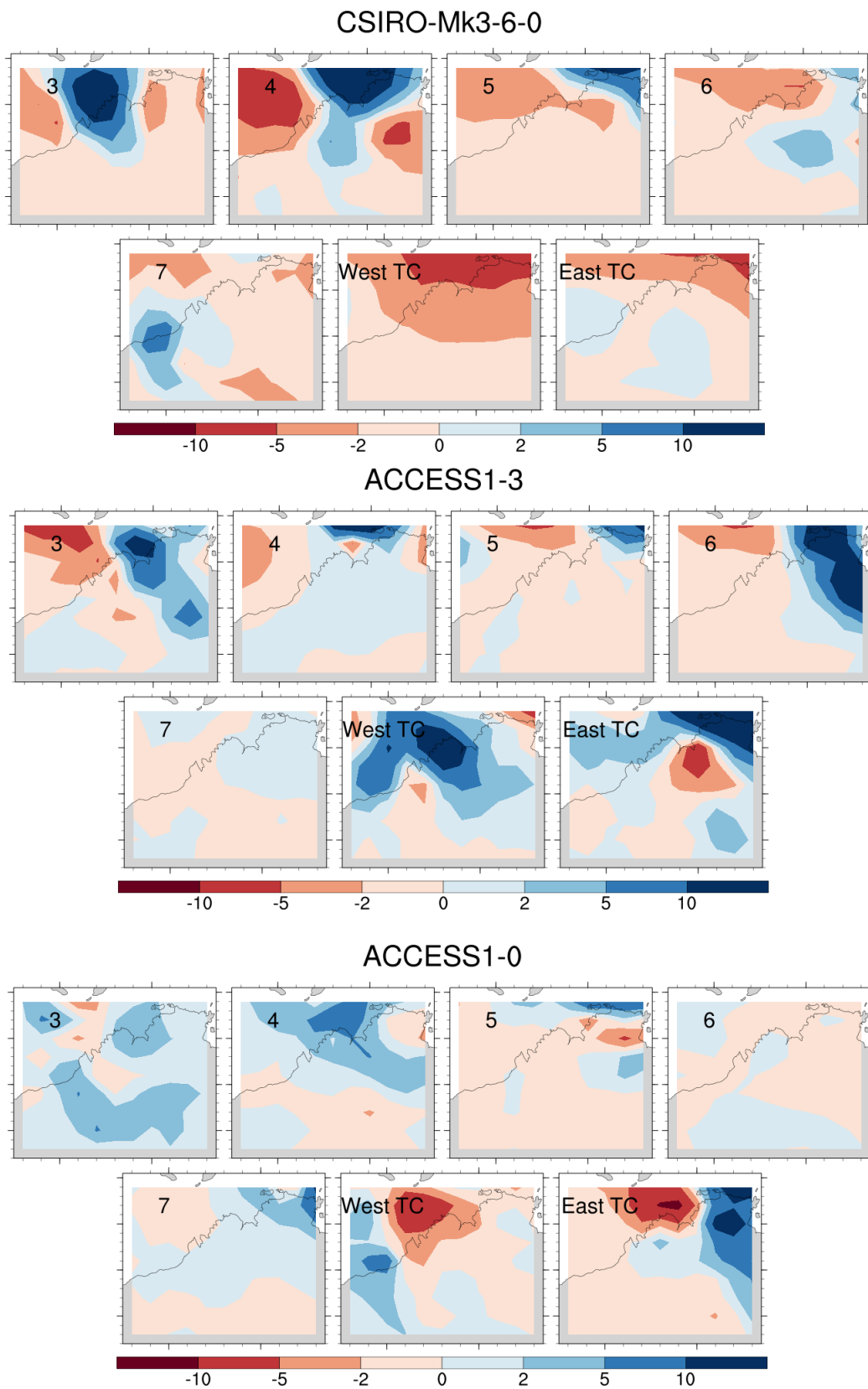


Figure 5.3a: Change in rainfall ( $\text{mm day}^{-1}$ ) for regimes 3 to 7 and the two TC regimes under the RCP8.5 scenario relative to the historical period. The historical regimes are those from the independent clustering method (Method II). The three subfigures together present models in order of most drying to most wetting. The models in this subfigure range from the most drying (top) to the third most drying (bottom).

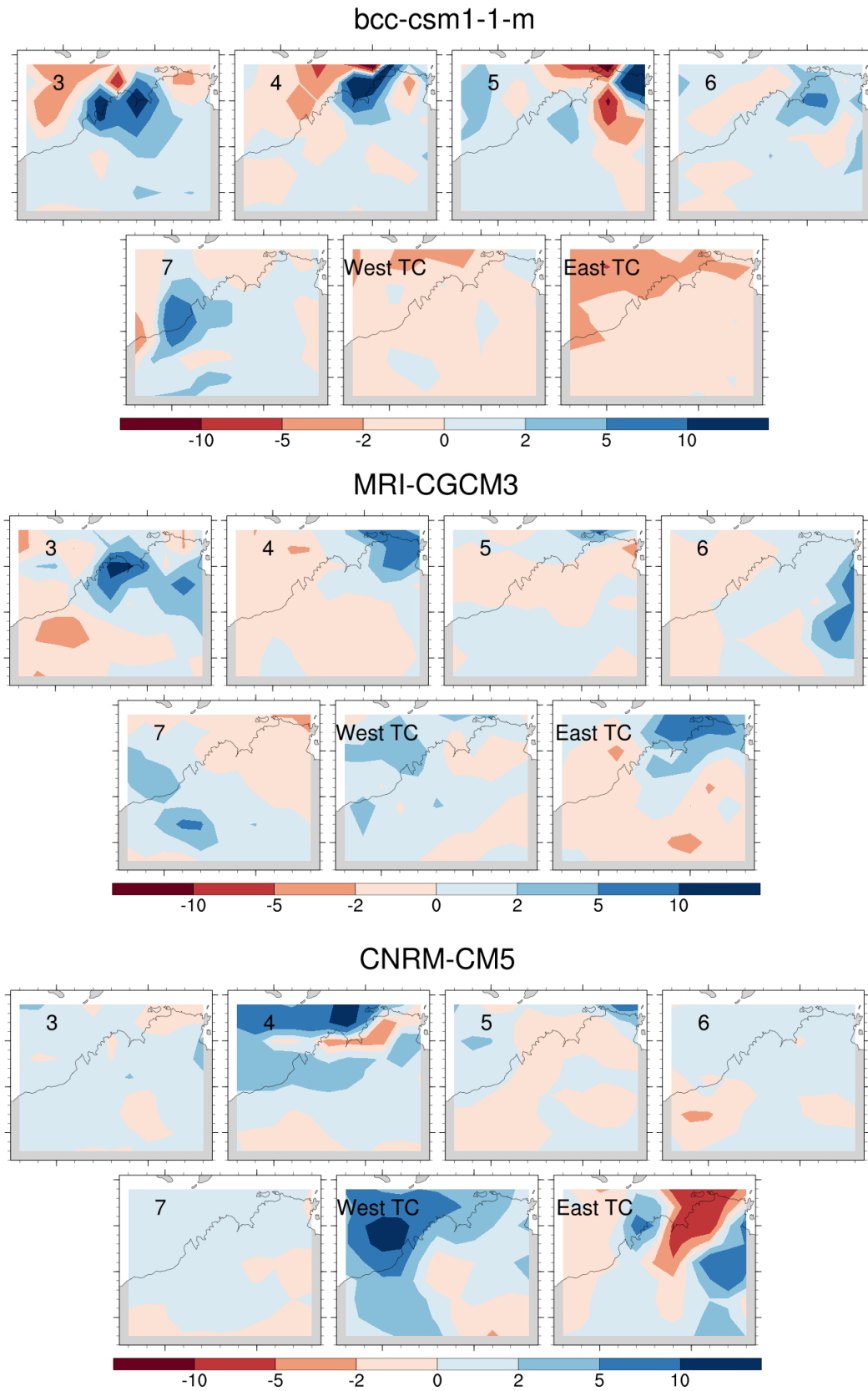


Figure 5.3b: Change in rainfall ( $\text{mm day}^{-1}$ ) for regimes 3 to 7 and the two TC regimes under the RCP8.5 scenario relative to the historical period. The historical regimes are those from the independent clustering method (Method II). The three subfigures together present models in order of most drying to most wetting. The models in this subfigure range from the two models with little trend (top and middle) to third most wetting (bottom).

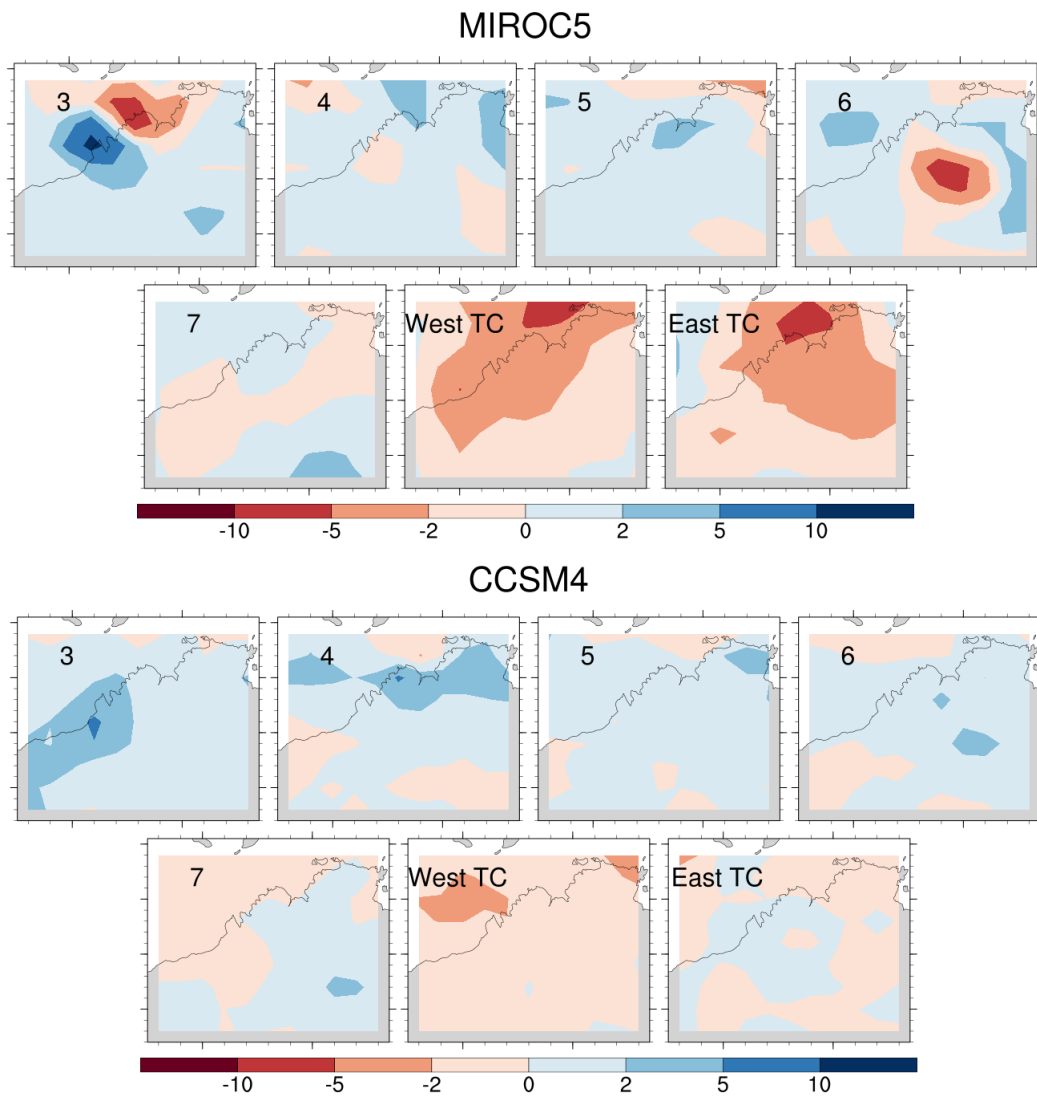


Figure 5.3c: Change in rainfall ( $\text{mm day}^{-1}$ ) for regimes 3 to 7 and the two TC regimes under the RCP8.5 scenario relative to the historical period. The historical regimes are those from the independent clustering method (Method II). The three subfigures together present models in order of most drying to most wetting. The models in this subfigure are the two most wetting models.

In some cases, the changes are strongly positive near each regime's area of maximum rainfall. The location of the strongly positive differences shows that the overall spatial pattern of the regime does not change significantly (see Appendix B for the RCP8.5 regime maps), although the intensity of the regimes increases. In some regimes, there are negative differences located close to positive differences - this is indicative of minor changes to the location of maximum rainfall. More significant changes to location would result in transitions between regimes - this is not the case as is discussed in the next section. For most other cases, the changes in rainfall are small, with no model showing a significant decrease in the change in rainfall in any regime.

As we move from drying to wetting models, there is little difference in the trend in rainfall intensity in most regimes, except for the two most wetting models (CCSM4, MIROC5) that show relatively little change in intensity across all heavy regimes. However, CNRM-CM5 is also a significantly wetting model and does produce intensity increases for Regime 4 and parts affected by TCs. Therefore, changes to intensity tend to depend little on the wetting or drying nature of the models. The influence of intensity changes is covered in more detail later in this section, and in Section 5.4.3.

#### **5.4.2 Frequency and intensity of projected future rainfall regimes**

Changes in the frequency of regimes in the RCP8.5 scenario relative to the historical period for each model are shown in Figure 5.4. The regimes have patterns similar to the historical model patterns, although not necessarily the observed regimes since the rainfall is projected to the independently determined regimes from Method II in the previous chapter. Because each model may produce regimes with spatial patterns that do not resemble the observations, it is inaccurate to attach the same name labels to the model regimes as to the observations. Instead, in a similar way to that shown in Section 4.3.3, the frequencies of all non-cyclone heavy regimes (Regimes 3 to 7) are first grouped together to illustrate their changes. The models have been ordered such that more drying models are placed toward the left of the figure (based on spatial mean of the difference pattern), and more wetting models are placed toward the right.

ACCESS1.3 and the CSIRO model are the two models with the largest increase in the

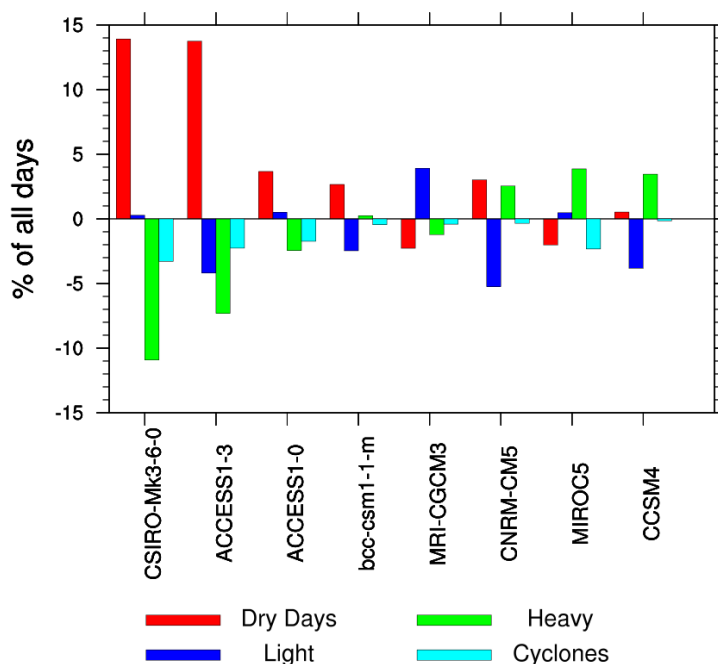


Figure 5.4: Difference in frequency of dry days, light, TC and all heavy regimes in the RCP8.5 scenario (2070-2099) relative to the historical period (1970-1999) in each model. The models are ordered from most drying (left) to most wetting (right).

frequency of dry days. This is consistent with the strong reduction in annual rainfall in Figure 5.1. The reasons for the decrease in wet days are similar for these two models - decreases in the frequency of heavy regimes are most prominent, however for ACCESS1.3 a reduction in the frequency of light days is a larger contributor than for CSIRO-Mk3-6-0.

Most of the remaining models show a less significant increase in the fraction of dry days, thus a reduction in the frequency of wet days. Generally, as we step towards more wetting models, the change in the fraction of dry days becomes smaller and eventually opposite in sign, although CNRM-CM5 shows an increase in dry days despite being a strongly wetting model.

The changes in frequency of groups of regimes vary greatly across the four models that show either wetting or little change in the climatological mean under a future climate. MRI-CGCM3 shows a decrease in the frequency of dry days, however there is also a slightly lower rate of heavy rain regime days which is compensated by an increase in light regime days. These competing factors could partly explain the lack of trend observed in Figure 5.1. MIROC5, one of the most strongly wetting models over land, shows a slight decrease in

the number of dry days and a compensating increase in the number of heavy rainfall days, although a decrease in TC frequency is present. CNRM-CM5 is the other significantly wetting model and shows a counter intuitive increase in dry days, however there is a sharp drop in light days and an increase in heavy rainfall days. CCSM4 also shows a similar pattern, although there is little change in dry days overall. Half of the models in this study project a decrease in the frequency of TC days, while others show almost no change in TC frequency. No model projects a significant increase in TC frequency, which agrees with previous studies (e.g. Lavender and Walsh (2011)).

Figure 5.5 shows the change in frequency of individual heavy regimes, including TCs. The changes to frequency of individual regimes are generally small and similar in sign across heavy regimes in each model, indicating there is relatively little preference for changes to the frequency of individual regimes over others. As noted above, the sum of frequency changes across heavy regimes is more significant, indicating that the consideration of heavy regimes as a group gives an adequate overview of general rainfall changes in the region.

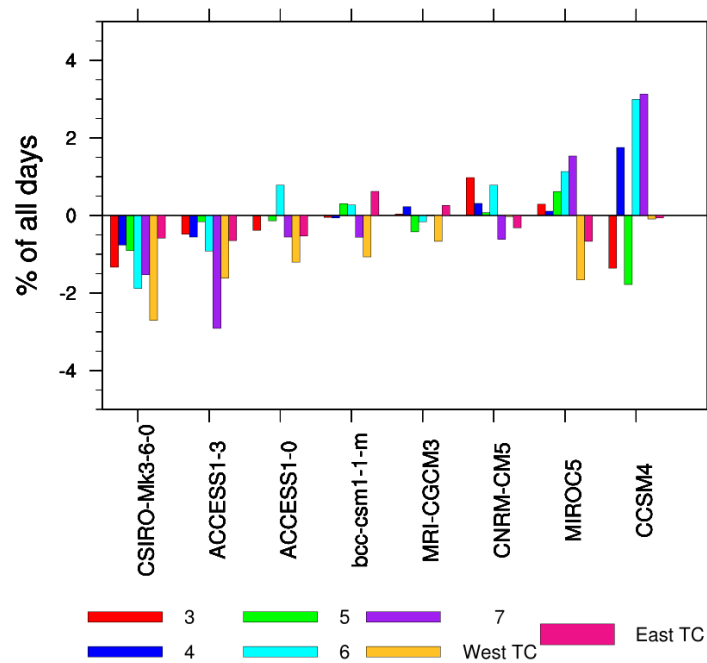


Figure 5.5: As for Figure 5.4, but broken down into individual heavy and TC regimes. Note the change in scale relative to the previous figure.

The difference in the projected changes to frequency across models suggests the mechanisms causing changes in rainfall vary greatly among models. In Section 4.3.2, it was found

that some models often fail to reproduce the circulation patterns responsible for rainfall in the region, and the biases vary across models. The differences in their representation, in addition to other biases in replicating other modes of variability, could lead to differences in future predictions. Since different regimes have different intensities, their contribution to the predicted change in rainfall in each model can be more easily highlighted using a decomposition of mean rainfall, shown in the next section.

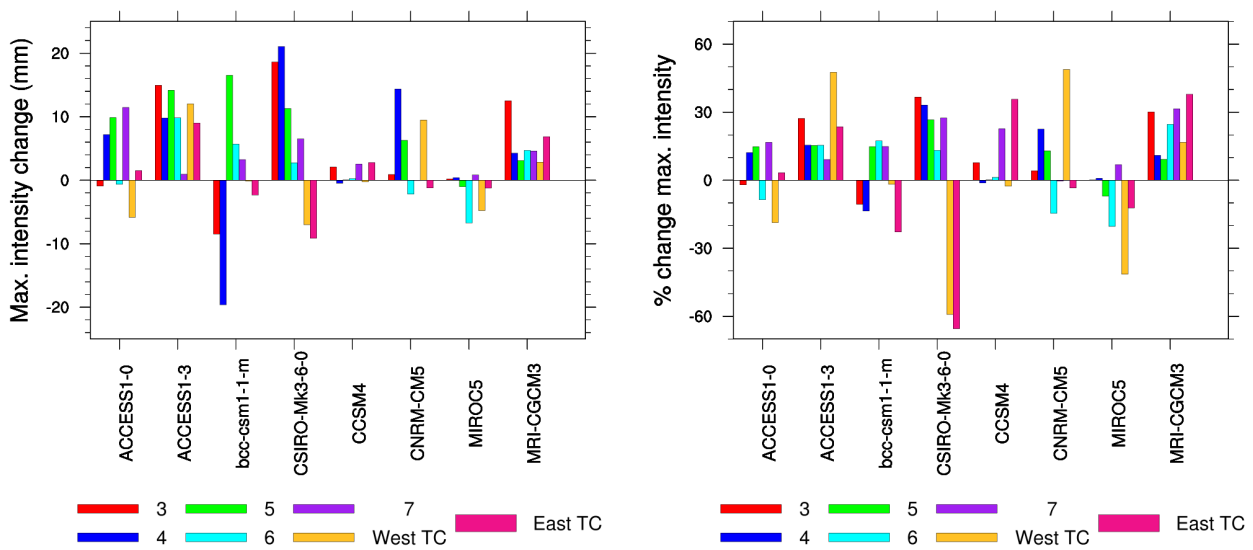


Figure 5.6: (left) Difference in maximum rainfall ( $\text{mm day}^{-1}$ ) between the RCP8.5 projected regimes in each model and their respective historical regimes, for regimes 3 to 7. (right) As for the left panel, but presented as a percentage difference.

Figure 5.6 shows the difference in maximum intensity (value of the point of maximum intensity in the regime) between the RCP8.5 projected regimes and the regimes in the historical period. The change in maximum is different to the changes shown in Figure 5.3, since minor changes in the spatial pattern of regimes result in large changes away from the maximum, while Figure 5.6 calculates the difference in the maximum point only. Almost all models show an increase in the average maximum intensity across all heavy regimes, with the greatest magnitude of increase occurring in the two models with the strongest drying trend, ACCESS1-3 and CSIRO-Mk3-6-0. MRI-CGCM3 also shows a large percentage increase in intensity, which is partly exacerbated by the relatively low intensity of that model's historical heavy regimes (see Section 4.3.3). Conversely, CNRM-CM5 and MIROC5 show relatively little change to the maximum intensity of regimes of less than  $5 \text{ mm day}^{-1}$  in most cases.

bcc-csm1-1-m shows large changes to absolute maximum intensity of Regimes 3, 4 (both decreasing) and 5 (increasing) which manifest as percentage changes of under 20%, due to the very large absolute intensity of the historical regimes. Changes to rainfall intensity in TCs varies greatly across models, with CSIRO-Mk3-6-0 producing a large percentage decrease in rainfall, however this model does not produce realistic TC circulation or rainfall patterns. Of the models that do produce realistic rainfall patterns (ACCESS models, CNRM-CM5 and MRI-CGCM3), there are increases in rainfall intensity in line with other heavy regimes.

The contribution of heavy regimes to changes in rainfall is difficult to ascertain by considering differences only, thus a decomposition method is needed to determine how frequency and intensity differences each contribute to the overall trend. The decomposition is presented and discussed in the next section.

### 5.4.3 Decomposition of rainfall regimes

In the previous section we investigate direct changes in the frequency of groups of rainfall regimes. To determine how the changes in frequency affect the rainfall trend, we decompose the rainfall trend into changes in frequency and intensity of the regime groups. This method is the same as that used in Section 2.4 to study observed trends. The terms in the decomposition are shown in Figure 5.7. The models are arranged from the most drying on the left to the most wetting on the right. The size of the terms will be different to the frequency and intensity changes in the last section since each term incorporates both frequency and intensity of each regime.

In Section 2.4, the most dominant terms driving the observed rainfall increase were the frequency terms for regimes responsible for heavy rainfall. Similarly, for projected changes in rainfall by the end of the 21st century, the most dominant terms overall are the frequency terms for the heavy regimes, although the sign and magnitude vary greatly across models. Despite the changes in frequency of the light regime changing significantly in some models (see Figure 5.4), they are a much smaller contributor to the overall trend due to the low intensity of rainfall in this regime. On the other hand, the high intensity of the heavy regimes results in a large contribution to the rainfall trend from relatively small changes in frequency.

The frequency terms for the heavy regimes are strongly negative for the most drying

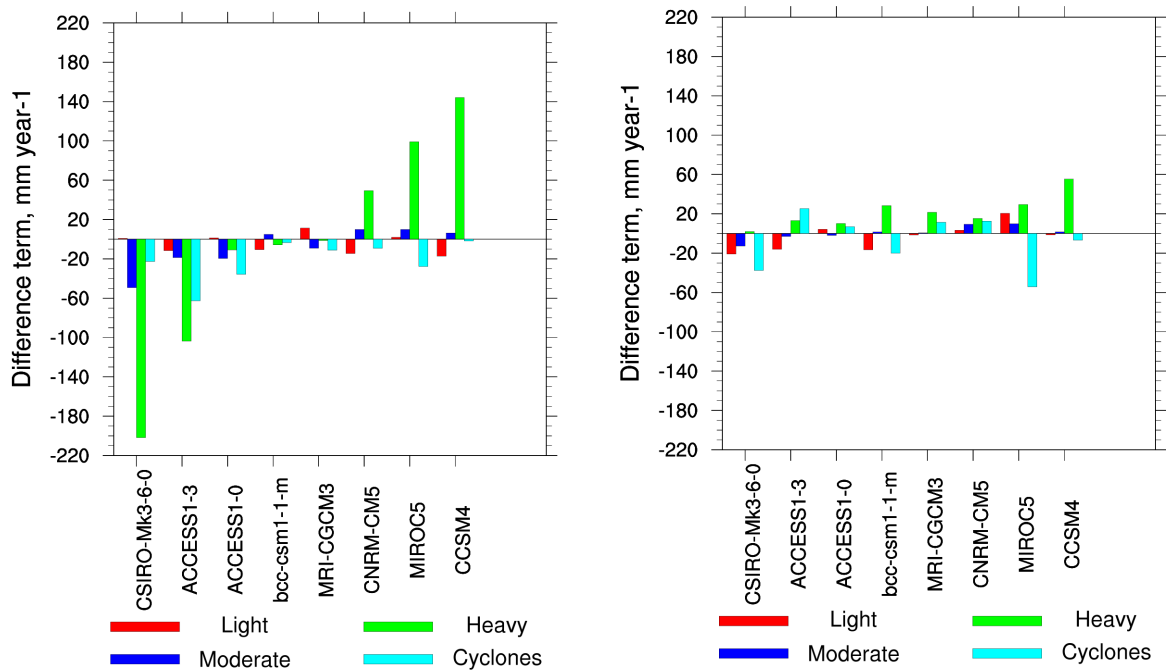


Figure 5.7: Decomposition terms for the contributions to the change in the mean annual rainfall from each regime in each model. Left panel (a) shows changes associated with changes in frequency, right panel (b) shows changes associated with changes in intensity. The models are arranged from most drying (left) to most wetting (right) in each panel.

models, ranging up to strongly positive for the most wetting models. Since no other regime shows a pattern this significant in either the frequency or intensity terms, this shows that the tendency of a model to be drying or wetting over NWA is strongly dependent on changes to the frequency of the heavy rainfall regimes. These are already infrequent regimes, consisting of less than 30% of all days in all models, and less than 10% in some models. Due to their high intensity, small changes in frequency can lead to large changes in mean rainfall. However, the rainfall trend is far less dependent on the frequency of TCs, since the terms are generally smaller than for the remaining heavy regimes except for the ACCESS models and CSIRO-Mk3-6-0 where the frequency terms are of a similar order of magnitude as other heavy regimes (compare to Figure 5.8). The reduced effect of TCs on the rainfall trend in a future climate is in contrast to Chapter 2, where TC frequency was found to be important to the observed rainfall trend. According to the models, changes to rainfall in a future climate depend on changes to the frequency of formation of synoptic systems such as monsoon lows and mid-latitude interactions which are responsible for rainfall in the region.

The right panel of Figure 5.7 shows the second part of the decomposition, corresponding

to contributions from changes in intensity. These intensity terms in the decomposition are much smaller in magnitude than the frequency terms generally, and there is little if any pattern that can explain the difference in the wetting or drying tendency between models. All models show positive intensity terms for the heavy regimes. Thus, all models are showing an increase in intensity of rainfall from structured synoptic systems. CSIRO-Mk3-6-0 shows a negligible increase, while CCSM4 shows the largest increase in the intensity of these regimes. The changes to the intensity of the light and moderate regimes varies among models, although there is a slight tendency for drying models to reduce intensity of the Light regime in a future climate.

Overall, changes to rainfall intensity are not the main drivers of the rainfall trend in any of the models, however there is some consistency in models about how intensity changes in a future climate. The most dominant driver of the projected trend in mean rainfall in all CMIP5 models analysed here tends to be changes in frequency of regimes responsible for heavy rainfall. Changes to TCLV frequency and intensity tend to be much smaller contributors than non-TC regimes. Each model has a different spatial pattern for the projected trend, for example, CNRM-CM5 produces wetting closer to the coast than MIROC5. The difference in these spatial patterns is explained in terms of the decomposition terms next.

#### **5.4.4 Using decomposition to explain trend spatial patterns**

Changes to the mean rainfall in each model under the RCP8.5 scenario have been discussed, however Figure 5.1 shows that some models may show different amounts of wetting or drying in different parts of the study region. We show in Section 5.4.3 that changes to mean rainfall in the models are primarily due to changes in the frequency of the heavy rainfall regimes. In Figure 5.7, the terms for all heavy regimes were combined into a single term for each model. The decomposition terms for each individual regime will now be presented separately, with the aim of explaining each model's spatial pattern of the trend in mean rainfall in Figure 5.1. The decomposition terms for the heavy regimes are shown in Figure 5.8.

Generally, the intensity terms in each model for individual heavy regimes are small and

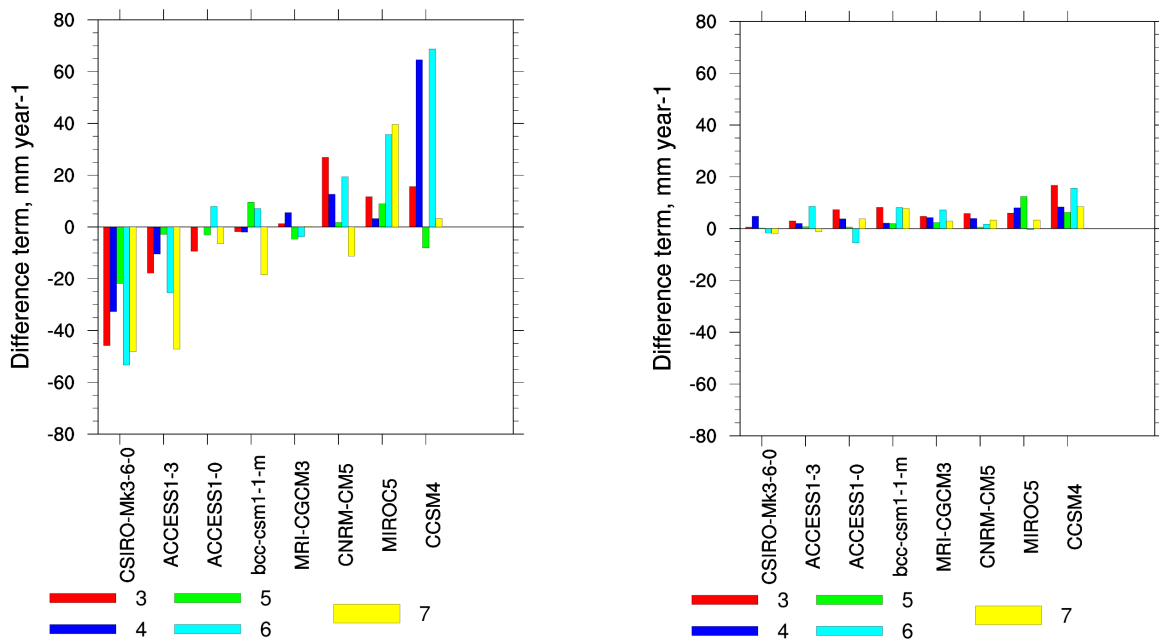


Figure 5.8: Breakdown of heavy regime terms from Figure 5.7. Left panel (a) shows the frequency terms of the decomposition, right panel (b) shows the intensity terms. Note the change in scale compared to Figure 5.7.

positive, and thus do not explain any part of the spatial pattern in the rainfall trend in each model (see Figure 5.1). The strong negative trend in the rainfall in CSIRO-Mk3-6-0 can be explained by a decrease in frequency of all heavy regimes, as well as the Moderate regime. The broad negative trend in ACCESS1-3 can be explained by a sharp decrease in the frequency of TCs, as well as a reduction in Regimes 6 and 7 which, in this model, both have rainfall maxima in the Top End (for regime 7, see patterns in Figure 4.11). Over land, ACCESS1-0 and MRI-CGCM3 have no strong trend in the climatological rainfall, and thus frequency and intensity changes are generally small or cancel out. bcc-csm1-1-m shows greater drying in the far west of the study region, which may be explained by a decrease in the frequency of Regime 7, which corresponds to a rainfall peak in the Pilbara in this model.

The three wetting models (CNRM-CM5, CCSM4 and MIROC5) have different wetting patterns, which are related to changes to specific heavy regimes. CNRM-CM5 shows wetting in the Pilbara and Kimberley regions, which can be explained by increases in the frequency of Regime 3 (Kimberley-type in pattern). CCSM4 shows significant wetting in a large region extending from the Kimberley to inland parts of the Top End, which is explained by the sharp increase in frequency in Regimes 4 and 6 which have maxima in those regions. MIROC5

shows wetting further inland, explained by the increase in frequency of Regimes 6 and 7 (both centred inland). Thus, changes to frequency of individual heavy regimes explain the spatial patterns in the rainfall trend in the future climate scenario.

#### 5.4.5 Changes to circulation patterns

To determine how the circulation patterns associated with the rainfall regimes are changing under the RCP8.5 scenario, composites of 850 hPa wind are calculated for each model. This level is chosen as this most easily characterises the flow associated with most of the regimes. The anomaly relative to the historical period for Regimes 1 and 4 are shown in Figures 5.9 and 5.10. These two regimes are shown as examples of flow under a light regime and a monsoon low-type regime respectively. Composites for the other regimes are provided in Appendix B.

Regime 1, corresponding to the Light regime, is characterised in both observations and the historical period in all models by easterly winds over northern Australia peaking at around 6-8  $\text{m s}^{-1}$  (see Figure 4.8). The anomaly plots in Figure 5.9 show very little change (less than 1  $\text{m s}^{-1}$ ) over northern Australia in the two ACCESS models, CNRM-CM5, MIROC5 and MRI-CGCM3. Some weakening of the easterlies is present in bcc-csm1-1-m and CSIRO-Mk3-6-0, and is more widespread in CCSM4.

Regime 4 corresponds to a rainfall maximum located between the Kimberley and Top End regions. In the observations, this regime is associated with a monsoon low located near the region of maximum rainfall. As described in Section 4.3.2, the ACCESS models are able to replicate the observed wind field more closely than the other models, with 850 hPa wind speeds around the closed low as high as 10  $\text{m s}^{-1}$ . These two models indicate a strengthening of the flow (indicated by red shading in Figure 5.10) on the northern flank of the low, but a weakening on the southern flank. MRI-CGCM3 indicates weakening of the westerly flow over Indonesia, but strengthening over northern Australia. Comparing the RCP8.5 composite to the historical composite for this regime in MRI-CGCM3, the region of low pressure more closely resembles a monsoon low in RCP8.5 than the historical period. Westerly flow north of the monsoon trough also weakens significantly in bcc-csm1-1-m, CCSM4 and CNRM-CM5. The weak cyclonic flow in MIROC5 also further weakens in the future scenario.

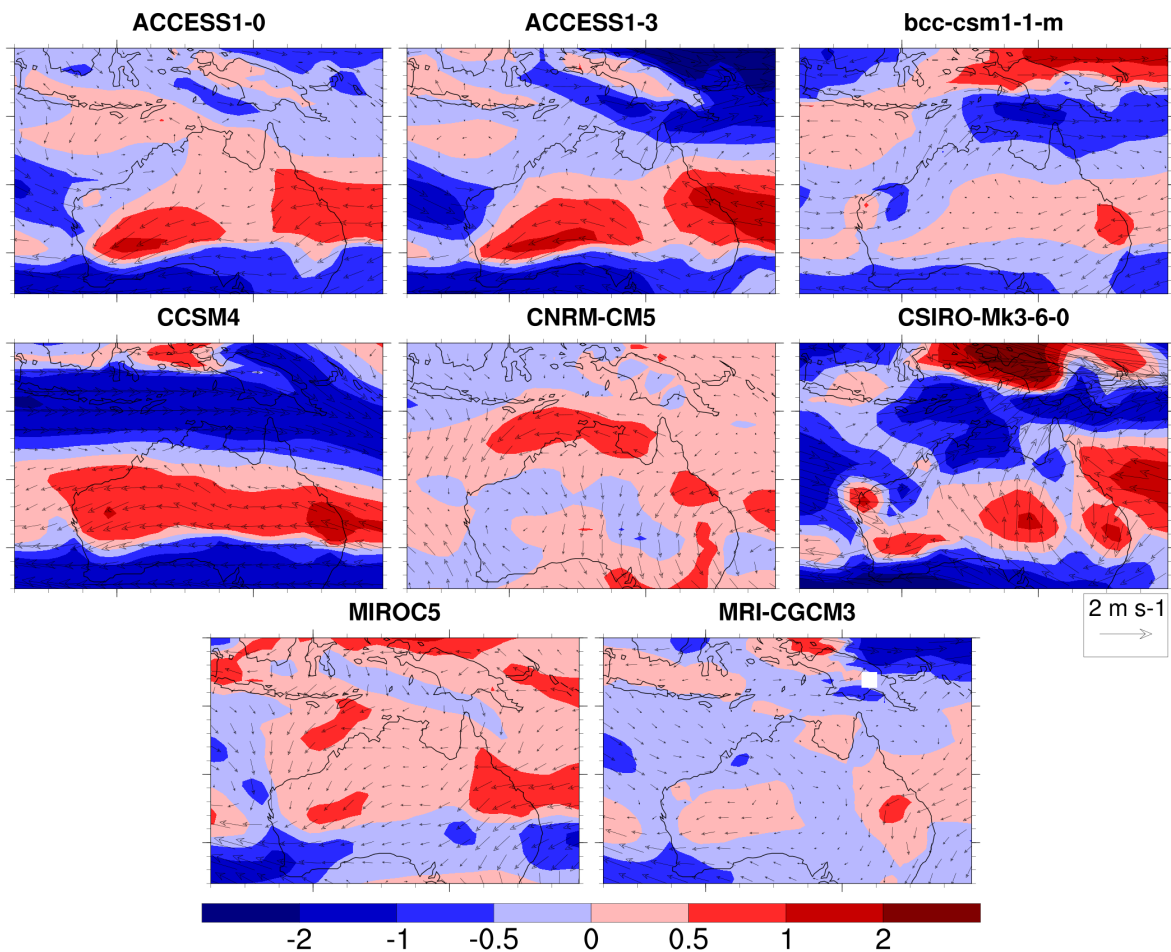


Figure 5.9: 850 hPa wind anomaly for the RCP8.5 scenario for Regime 1 in all models, relative to each model's historical Regime 1. Blue shading indicates weaker wind speeds, while red shading indicates stronger wind speeds.

Projections under the RCP8.5 scenario suggest low-level flow is unlikely to change for the dry and light rainfall regimes. However, for regimes characterised by monsoon lows, there is some difference between models in terms of flow changes in a future climate. However, due to the difficulty of some models in replicating observed synoptic patterns for monsoon low regimes, changes under a future climate must be interpreted with care. The regimes discussed in this section are forced to appear like the historical regimes in each model. The possibility of changes to the regime spatial patterns is discussed in the next section.

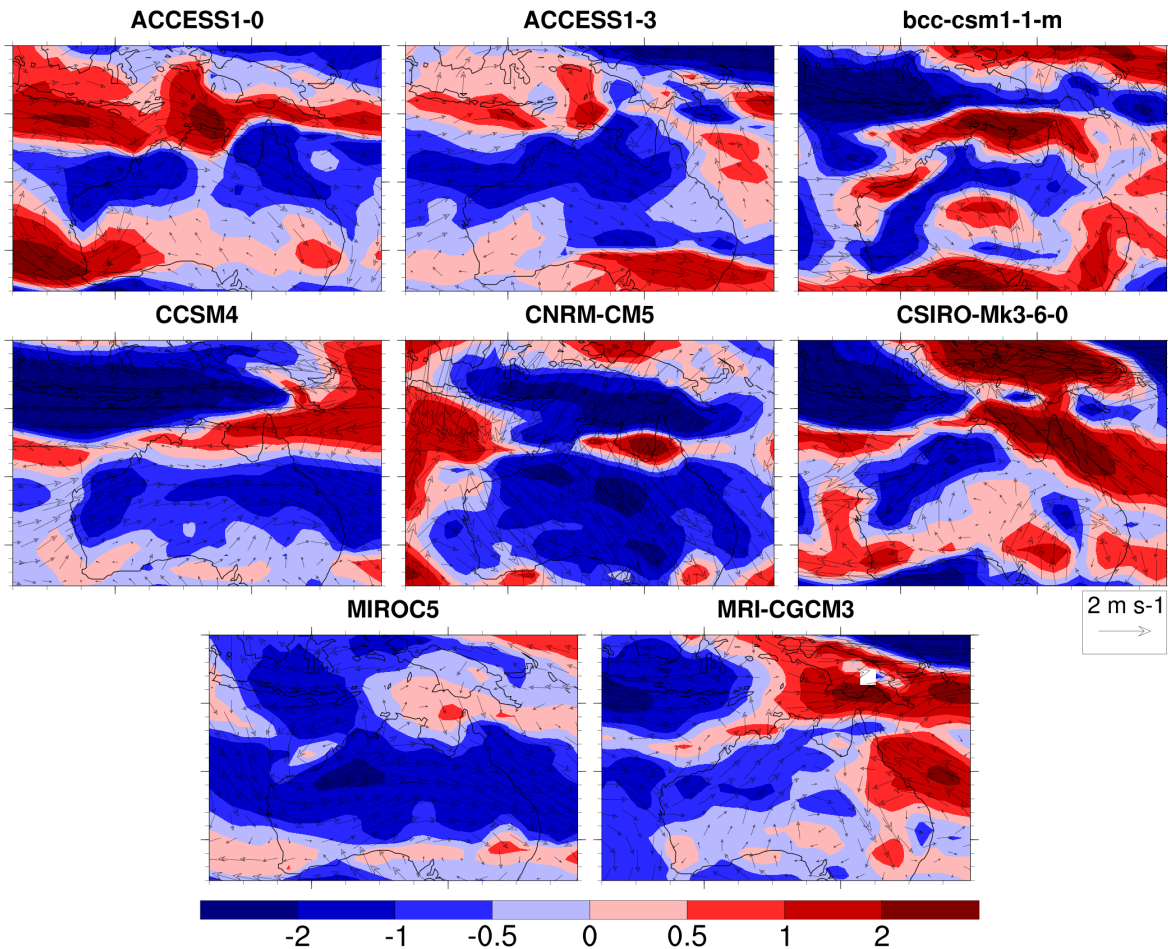


Figure 5.10: 850 hPa wind anomaly for the RCP8.5 scenario for Regime 4 in all models, relative to each model's historical Regime 4. Blue shading indicates weaker wind speeds, while red shading indicates stronger wind speeds.

## 5.5 Independently determined rainfall patterns under a future climate

The previous section describes changes to frequency and intensity of rainfall regimes in each model. However, those regimes are the result of projecting daily rainfall onto historical patterns from each model, and thus they are forced to have the same shape as the historical regimes. To determine whether there are changes to the simulated rainfall patterns in the RCP8.5 scenario, daily rainfall for each model is clustered independently following TCLV and dry day separation, resulting in a set of future rainfall regimes for each model independent of their patterns in the historical period.

The rainfall patterns produced by each model are shown in Figures 5.11 and 5.12. In

each model, the patterns are arranged according to the lowest possible sum of Euclidean distances between these regimes and those from the historical period (see Section 4.3.3 for regimes arranged by number, or Appendix B for regimes arranged by model). The regimes are arranged by model here rather than by regime number as per Section 4.3.3 since the aim is to describe the future scenario in each model, rather than compare representations of specific regimes. Generally, the models continue to produce patterns and intensities corresponding to a light rainfall regime, in addition to multiple heavy regimes located along the coast. However, relative to each model's historical period, there are some differences in rainfall pattern and intensity in most models.

In the historical period, the two ACCESS models have difficulty in producing rainfall in inland areas. In the RCP8.5 scenario presented here, both models present two regimes that have a maximum over the Top End. The mapping appears to have swapped Regimes 6 and 7 in ACCESS1-3 relative to the historical period, and shifted one maximum further south with increased intensity. In addition, the intensity of TC regimes increases, consistent with the result from the decomposition in Figure 5.7. In ACCESS1-0, an Inland type regime emerges from the clustering, which may explain the lack of trend in mean rainfall by counteracting the strong negative trend over coastal areas. CCSM4, CSIRO-Mk3-6-0, MIROC5 and bcc-csm1-1-m produce largely the same patterns as in their historical period, although they have an increased maximum intensity. MIROC5 reproduces all its previous regimes other than Regime 7, which is located much further north. bcc-csm1-1-m no longer produces a Moderate type regime and CSIRO-Mk3-6-0 shifts rainfall slightly northward for Regime 7, consistent with the northward movement of the monsoon circulation in Figure 5.1.

In CNRM-CM5, there are two Top End type regimes in a future climate, while maxima over the Kimberley and Pilbara no longer emerge in a future climate. MRI-CGCM3 produces three regimes with inland rainfall, in contrast to the historical period where there were two with lower intensity (see Figure 4.14). The increase in the number and intensity of inland-based regimes is in contrast to the change in climatological mean found in Figure 5.1, which indicates little change in total rainfall over land areas.

The frequency of the independently determined regimes in each model is shown in Figure

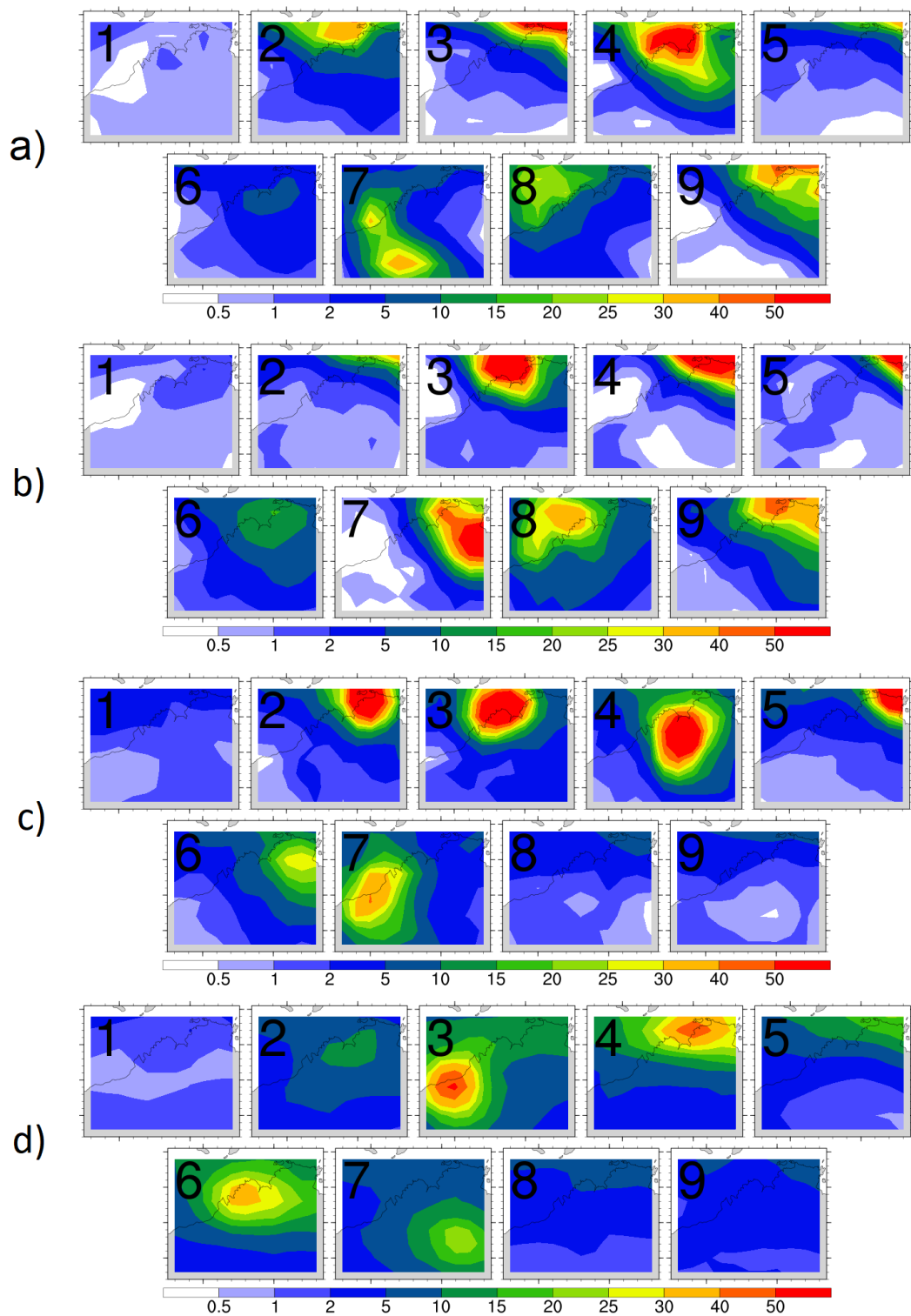


Figure 5.11: The rainfall patterns for the independently determined regimes under the RCP8.5 scenario. Models are ordered as follows from top to bottom: ACCESS1-0, ACCESS1-3, bcc-csm1-1-m, CCSM4. Units are in  $\text{mm day}^{-1}$ .

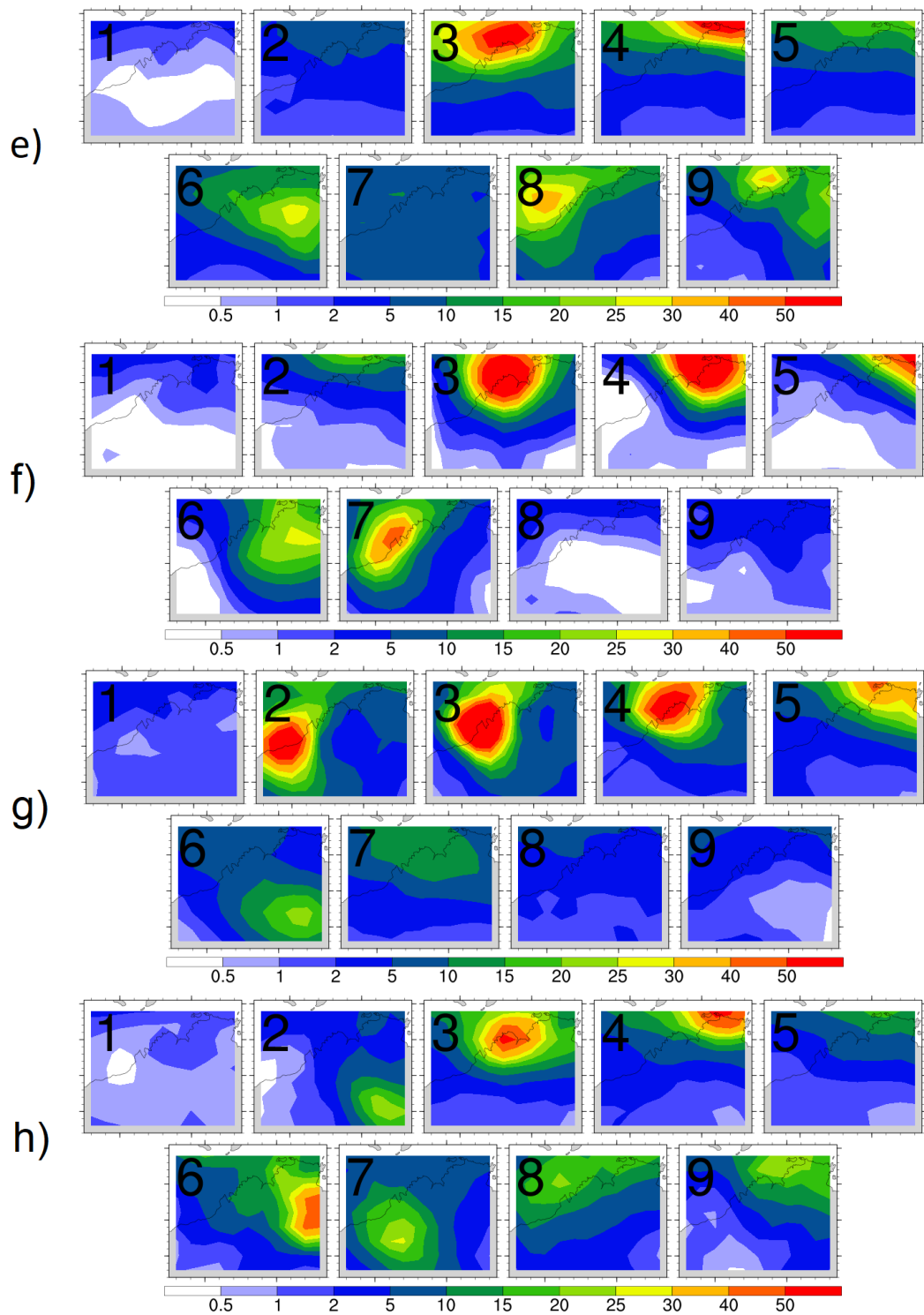


Figure 5.12: As for previous subfigure. Models on this page from top to bottom: CNRM-CM5, CSIRO-Mk3-6-0, MIROC5, MRI-CGCM3.

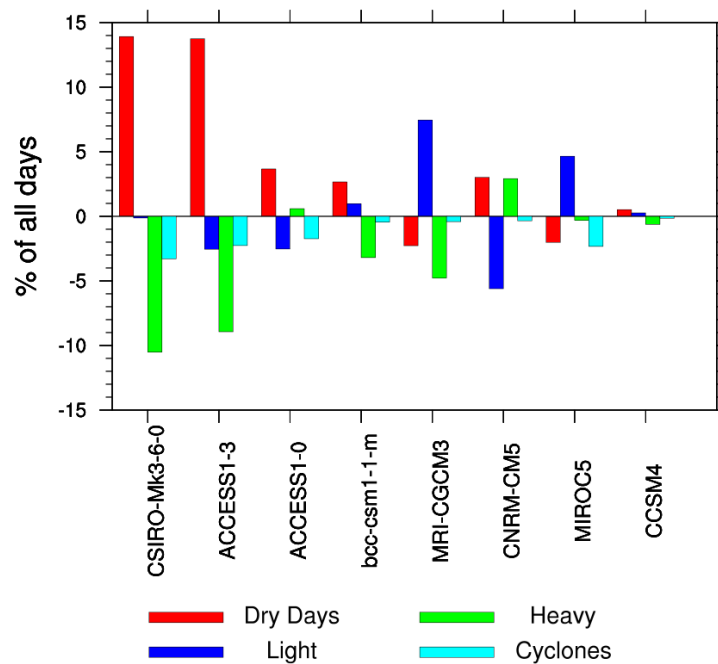


Figure 5.13: Difference in frequency of dry, light, combined heavy and TC regimes in each model between the independently determined regimes in the RCP8.5 scenario and the historical period.

5.13. The regime frequencies are grouped into dry, light and heavy regimes in order to explain the changes to rainfall in a future climate more clearly. Similar to the result determined from the decomposition in Section 5.4.3 and the frequency changes in Figure 5.4, in ACCESS1-3 and CSIRO-Mk3-6-0 there is a sharp reduction in the frequency of heavy regimes including TCs, and a sharp increase in the frequency of dry days. The frequency of these independently determined regimes therefore also explain the projected reduction in rainfall in these models.

For other models, determining changes in rainfall from the independent RCP8.5 regimes is more complex and involves investigating differences in both frequency and intensity of individual regimes. To this end, the frequency and intensity of each of the heavy regimes are presented in Figures 5.14 and 5.15 respectively. In ACCESS1-0, there is an increase in the frequency of total heavy regimes, however Regime 6 in both the historical and RCP8.5 scenarios have maxima less than  $10 \text{ mm day}^{-1}$ . Most of the total change in heavy regime frequency is due to change in this relatively light regime, with the remaining heavy regimes with high maxima (more than  $40 \text{ mm day}^{-1}$ ) decreasing in frequency. These regimes are located close to the coast, which explains the negative projected trend over coastal areas

in this model. Similarly, a sharp decrease in the frequency of regime 7 in bcc-csm1-1-m, corresponding to a rainfall maximum in the west of the region, explains the negative trend in that region. A large change in the frequency of light rainfall days in MRI-CGCM3 at the expense of dry days tends to minimise the trend over the region, agreeing with the result in the previous section for that model.

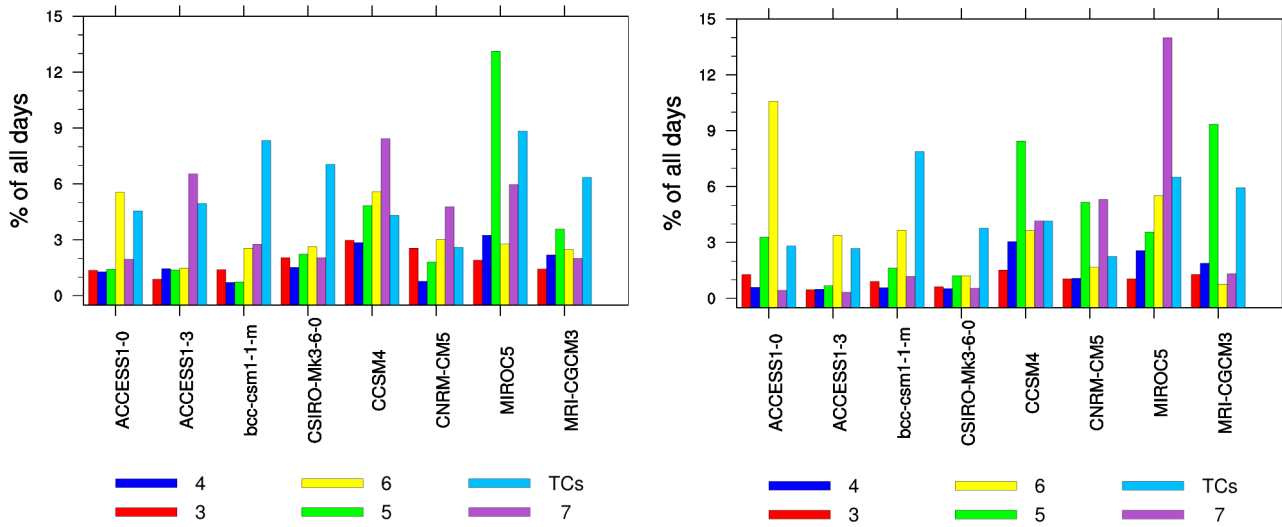


Figure 5.14: (left) Frequency of individual independently determined regimes from the historical period. (right) Same, but for the independently determined regimes under the RCP8.5 scenario.

The wetting trend in the remaining three models have different causes in terms of frequency and intensity changes. In MIROC5, the majority of the rainfall change occurs inland. The RCP8.5 scenario presents a regime (6) with a maximum located further inland than in the historical period (Regime 7 in that period). The inland movement of this regime explains the positive trend in inland areas. In CNRM-CM5, a much higher maximum emerges for Regime 6, with a location agreeing with that of the greatest rainfall change in Figure 5.1. CCSM4 displays almost no change in the frequency of the regimes, in contrast to the increasing trend in total rainfall. There is a marked increase in the maximum intensity of the heavy regimes in this model. The increased intensity is found in the intensity terms of the decomposition in the right panel of Figure 5.7, however the reduction in frequency of heavy regimes is contrasting with the left panel which suggests increases in frequency is the main driver of the trend in this model. The discrepancy is best explained by changes in intensity being the main driver rather than frequency. Increasing intensity of (moderate) daily rainfall

will result in these days being preferentially assigned to heavy regimes in Method I rather than a Moderate or Light type regime. This preferential assignment results in an apparent increase in the frequency of heavy regimes at the expense of moderate days. Similarly, an increase in the frequency of moderate days can result from the transitioning of light days, which explains the frequency terms in Figure 5.7. Thus, changes in rainfall in CCSM4 are highly likely to be due to intensity changes rather than frequency changes. However, this does not necessarily hold true for other models, especially those which have a drying trend as noted above.

Overall, changes to the nature of heavy rainfall regimes generally are the main drivers of the trend in each model. Changes to the spatial pattern or specific regimes may cause spatial differences in the trend pattern. Drying trends tend to be most strongly influenced by decreased frequency of heavy regimes, while wetting trends tend to be caused by a combination of frequency and intensity changes.

Figure 5.15 shows the maximum intensity of the independently determined regimes under the RCP8.5 scenario. Again, since the spatial patterns of the regimes change, it is impossible to directly compare the intensity of specific regimes, however changes to in the intensity of heavy regimes generally can be discussed. When compared to the historical regimes (see Section 4.3.3 the intensity of the heaviest regimes in every model increases. ACCESS1-3 has the largest change in intensity, with two heavy regimes now producing in excess of 120 mm day<sup>-1</sup> on average. Every model has at least one regime with a maximum above 50 mm day<sup>-1</sup>. The increased intensity in all models can therefore partly explain the increase in rainfall in some models. However, the increased intensity is strongly counteracted by reduced frequency of heavy regimes in drying models.

To summarise changes in the spatial patterns of each model's rainfall regimes, the sum of the distances to the historical period are determined in the same manner as was used to match the model regimes to the observations in Section 4.3.3. The distance sums are presented in Table 5.1.

The sums are generally only slightly smaller than those in Table 4.5, suggesting the

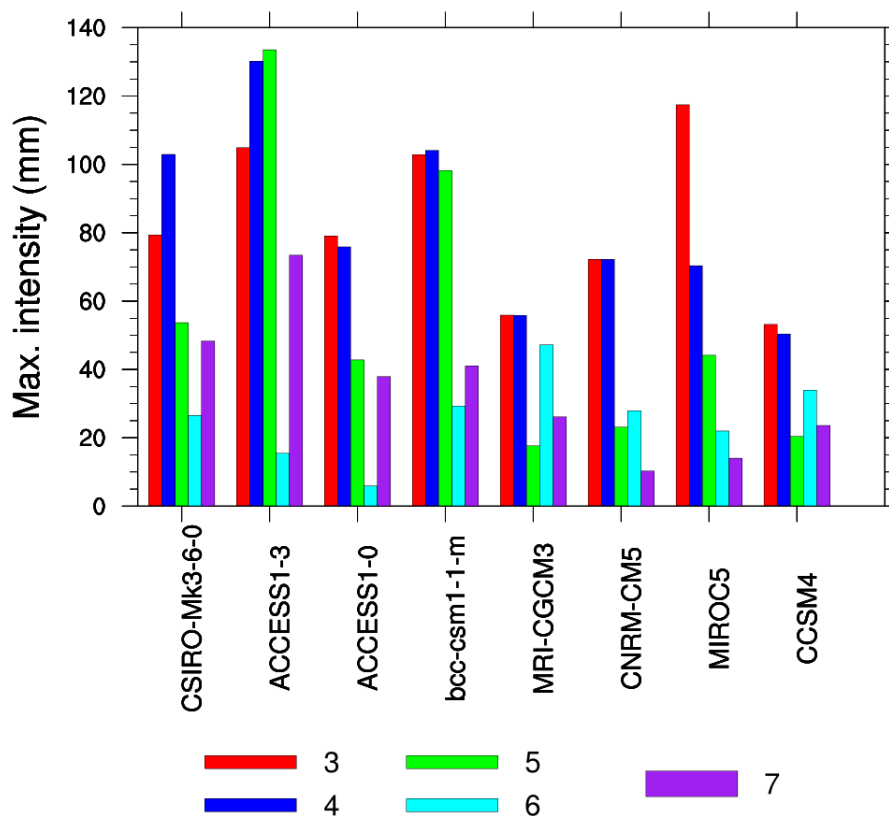


Figure 5.15: Maximum intensity for the heavy regimes under the RCP8.5 scenario across all models.

changes to the regimes in the RCP8.5 scenario are of a similar size to their deviation from the observations. The patterns for CCSM4 are relatively unchanged from the historical period, as indicated by the small distance sum. The range in distance sums across other models suggest there are often significant differences in spatial patterns. In the ACCESS models, inland regimes begin to emerge from the clustering at the expense of coastal regimes. These inland regimes are not produced in the historical period in these models, however they do exist in the observations. The intensity of coastal regimes in MIROC5 and CSIRO-Mk3-6-0 increase significantly, although the spatial patterns are similar to their respective historical

Table 5.1: Distance sums for each model between the RCP8.5 and historical periods.

Model	Distance	Model	Distance
ACCESS1-0	280.8	CSIRO-Mk3-6-0	361.64
ACCESS1-3	516.1	CNRM-CM5	189.8
bcc-csm1-1-m	559.9	MRI-CGCM3	298.1
CCSM4	256.1	MIROC5	436.3

periods. This is in contrast to the previous section where intensity changes are found to be minor.

Changes to spatial patterns here could either result from shifts in the circulation patterns, or be a result of allowing the definition of the regime to change by clustering independently of the historical period. Changes to spatial patterns may also be the result of 7 clusters being an inappropriate choice for the majority of the models. This is one of the main limitations of the approach, where by choosing 7 clusters, we force regimes to exist in the models where they are similar to other regimes. However, choosing an independent number of clusters for all models is difficult and subjective, and thus relies on careful consideration of each model separately.

## 5.6 Discussion and conclusions

Changes to rainfall over NWA in eight CMIP5 models under the RCP8.5 emissions scenario are determined by calculating the percentage change in rainfall, and using two regime assignment methods to determine how rainfall regimes contribute to the mean change under a future climate. The set of CMIP5 models that were assessed in Chapter 4 produce a range of changes to mean rainfall under RCP8.5. The sign and magnitude of the changes do not appear to depend on whether a model represents the observed rainfall well, although it is possible that the convection scheme used by the ACCESS models may lead to a drying trend since it is shared by ACCESS1-0 and ACCESS1-3 (Bi et al., 2013). However, the decomposition shows that changes to the frequency and intensity of specific regimes is different, and the drying trend over land in ACCESS1-3 is not present in ACCESS1-0. Thus, the shared scheme does not appear to cause similarities in the rainfall projection. The lack of relationship between model rank and model projection is in contrast to Jourdain et al. (2013) and Frederiksen and Grainger (2015) who found that a selection of high-ranking models were more consistent in producing wetting over northern Australia. However, the results for MIROC5, CNRM-CM5 and CCSM4 (the three models common to this study and the multi-model ensemble of Frederiksen and Grainger (2015)) are consistent with their findings.

The two regime assignment methods applied to the future rainfall provide differing explanations for the difference in projected rainfall trend across models. The projection method

(Method I) suggests that there are changes to the intensity of heavy regimes in a future climate, but these are less important than changes to the frequency of those regimes, which determine whether a model is drying or wetting. However, by directly clustering the rainfall (Method II) in the RCP8.5 scenario, there is the possibility that changes to regime spatial patterns (in the case of MIROC5) or intensity (for CCSM4) are important drivers in some models. From direct clustering, decreases in the frequency of heavy rainfall regimes and TCs are still the only explanation for decreasing rainfall in the drying models. Due to the high rainfall intensity and low frequency of heavy regimes in all models, small changes in frequency have a large effect on projected annual rainfall, and thus a slight reduction in frequency of heavy regimes in CSIRO-Mk3-6-0 and ACCESS1-3 has resulted in the large decrease in projected rainfall. Despite intensity being a small driver of the overall trend in the models, the agreement on increased intensity suggests that extreme rainfall events (relative to the current climate) are likely to increase in frequency. The models also generally agree on a reduced incidence of TC days in the region, however the contribution of TC frequency changes to the overall trend is minor when compared to other heavy rainfall regimes. This is in contrast to observed changes to rainfall regimes, where changes to TC frequency are more significant (see Chapter 2). The higher maximum rainfall intensity of non-TC regimes when compared to TC regimes could result in higher sensitivity to changes in frequency, and could partially explain the difference in contribution to the trend in the models.

Examination of heavy regimes in the models that replicate the observed synoptic patterns most closely suggests a slight strengthening of the north-westerly flow on the northern flank of the monsoon lows associated with heavy rainfall. The strengthening partially explains the increased intensity of the heavy regimes, since the low-level moisture flux into the systems responsible for the rainfall increases. However, there is little agreement among models since most fail to replicate observed flow patterns associated with the regimes. Most models in this study agree on a weakening of low-level easterly flow to the south of the systems responsible for heavy rainfall, consistent with Held and Soden (2006).

As described, many models produce changes to the spatial patterns of typical rainfall regimes over NWA, of a similar magnitude to the deviation from the observations. In some models, different spatial patterns emerge from the clustering, while some patterns disappear

in other models. The changes to the spatial patterns partially explain the pattern of the projected rainfall change in CNRM-CM5 and MIROC5.

Overall, the models do not agree on the sign or magnitude of the change in mean rainfall, the frequency and spatial pattern of rainfall regimes, or the synoptic patterns associated with the regimes, and thus at this point it is difficult to determine how rainfall will change under a future high emissions scenario over NWA. However, models do agree on a minor increase in intensity in most regimes in a future climate, consistent with observations. Future work should therefore focus on examining how biases in specific models affect the development of the synoptic systems responsible for rainfall in northern Australia.

## Chapter 6

# Summary of key conclusions

### 6.1 Observed rainfall regimes over north-western Australia

In Chapter 2, rainfall regimes over north-western Australia were identified and characterised, with the aim of describing typical rainfall patterns in the region in terms of known synoptic patterns, and describing the observed rainfall trend in terms of these rainfall regimes. It is found that an increase in the frequency of regimes responsible for heavy rainfall mainly drives the increasing trend in rainfall over the region. After separating dry and tropical cyclone (TC) days from the daily rainfall record, six rainfall regimes were identified over north-western Australia (NWA) using K-means clustering on gridded daily rainfall over the period 1950-2010. Two TC regimes were determined based on the location of the TC within the region, giving a total of eight regimes. The eight regimes are classified into four groups based on their wind, potential vorticity, humidity and K-index fields.

The first group, thunderstorm regimes, consist of either isolated or scattered convection with no synoptic forcing, and are responsible for 86% of all rainy days but only 55% of the climatological rainfall in the region. The second group consists of two monsoon low regimes that are responsible for rainfall over the Kimberley and Top End regions of NWA respectively. They constitute 6.5% of all rainy days and contribute 19% of the rainfall in the region. The monsoon low regimes are characterised by isolated potential vorticity anomalies near the point of maximum rainfall, consistent with those identified by Berry et al. (2012). The third group, tropical cyclones (TCs), are responsible for less than 4% of rainy days, but provide around 12% of spatially averaged rainfall over the region, consistent with Jiang and Zipser

(2010) who found a similar percentage of rainfall is provided by TCs. This study considered only spatially averaged rainfall over the region and not specific stations, thus the percentage is likely to be higher in some locations within the region, which would be consistent with Ng et al. (2015) who found TCs can be responsible for up to 40% of rainfall at some stations in NWA. The last group, mid-latitude interactions, are characterised by mid-latitude Rossby waves refracted equatorward over NWA, and are responsible for 3.7% of rainy days and 12.8% of rainfall in the region, centred over the Pilbara and far inland regions of NWA.

By decomposing the change in rainfall into changes in frequency and intensity of individual regimes in 1980-2009 compared to 1950-1979, we find that the frequency of regimes responsible for heavier rainfall (monsoon lows, TCs, mid-latitude interactions) has increased at the expense of days with isolated thunderstorms. We determined that the greatest contributor to the overall trend is an increase in tropical cyclones in the Pilbara region, however this trend may be exaggerated by the difficulty of detecting TCs in the pre-satellite era. Changes in intensity of the rainfall regimes in the second period relative to the first were found to be negligible, except for the thunderstorm regimes, where there is a slight increase. The outcome that frequency changes in heavy regimes, especially TCs, are more important than rainfall intensity changes is at odds with some previous studies that found little change in TC numbers (Ren and Leslie, 2015), or that rainfall intensity changes are more important than frequency changes (Emori and Brown, 2005), although the increase in the frequency of monsoon lows agrees with Lavender and Abbs (2013).

Extreme rainfall days have been increasing in frequency over the period 1950-2010, consistent with the mean rainfall trend. TCs and monsoon lows are most likely to be responsible for extreme rainfall, although a regime consisting of widespread thunderstorms without synoptic forcing is also responsible for a significant fraction of extreme days per year.

## 6.2 Evaluating rainfall over north-western Australia in CMIP5 models

### 6.2.1 Methods for assigning regimes to model rainfall

Chapters 3 and 4 focused on evaluating the ability of CMIP5 models to replicate observed rainfall regimes over NWA, with the aim of understanding model biases over the region before determining changes to regimes in a future climate. Differences in the spatial pattern, frequency, and intensity of rainfall regimes between models and observations were established. To this end, three regime assignment methods were developed to assess the spatial patterns, frequency and intensity of rainfall in models over the region. We first started by developing and testing the methodology on a single CMIP5 model, ACCESS1-0, before using metrics based on the methodology to rank a subset of models based on their ability to reproduce the pattern, frequency and intensity of observed regimes. Three methods to assign regimes to model daily rainfall were developed.

Method I (projection) assigns daily model rainfall a regime based on the minimum Euclidean distance to an observed regime. This method forces the model regimes to have the same spatial pattern as the observations, and therefore allows direct comparison of frequency and synoptic patterns. Thus, from Method I, differences in frequency and pattern correlations for wind fields were used as metrics for model ranking. However, Method I does not allow the possibility of the model to produce differing spatial patterns.

Method II (direct clustering) clusters model rainfall with no input from observations, allowing the typical rainfall patterns in the model to be determined. Unlike Method I, this allows the rainfall spatial patterns in each model to be different to observed regimes, however frequency and intensity differences relative to observations cannot be easily determined since we would be comparing the frequency of different patterns. In Method II, model regimes are matched (paired) to observed regimes by arranging them such that the sum of Euclidean distances over all pairs is minimised (see Section 3.2.4 for an example). This sum is a measure of general closeness of model regimes to observed regimes, and is used as another model ranking measure.

Method III (hybrid clustering) clusters an equal amount of both model and observed data in one dataset. The spatial pattern of resulting regimes is based on a fraction of both model and observed days. A model that perfectly reproduces the observed regimes should result in each regime containing approximately 50% model days. A deviation from 50% determines whether the model fails to reproduce an observed regime, or produces a regime that is not observed, and such deviations are used as an additional ranking metric. Overall, this method concisely shows the differences in spatial pattern and frequency of model and observed regimes.

## 6.2.2 Model evaluation

In Chapter 4, a set of eight CMIP5 models were assessed for their ability to replicate the observed mean rainfall and observed rainfall regimes, with MRI-CGCM3, CNRM-CM5 and CSIRO-Mk3-6-0 the three best ranked models. When considering the mean rainfall, models tend to show positive biases north of the Australian continent and in inland areas of the study region, the strength of which vary by model. Models do not replicate the observed rainfall trend over the Australian continent, although most show an increase somewhere within the study region.

Most, but not all, of the observed regime spatial patterns are replicated, although generally the models have the most difficulty in replicating regimes responsible for inland rainfall since most independently determined regimes (from Method II) in each model either have a weak maximum inland or no regime with an inland maximum at all. Most models produce light rainfall too often, agreeing with previous studies (Stephens et al., 2010). Regimes responsible for heavy rainfall in coastal areas are too infrequent and too intense in the majority of cases. The frequency of TCs over the region is mostly either replicated well or slightly underestimated, with a small number of models either strongly underestimating or overestimating the frequency of TC days. However, the positions of the storm tracks are poorly replicated in some models, with too many TC days in the western half of the study region and too few in the eastern half. In addition, the majority of models struggle to reproduce the synoptic patterns responsible for the regimes responsible for heavy rainfall, although when compared to other models, the ACCESS models perform best at reproducing monsoon lows

and MRI-CGCM3 performs best at reproducing mid-latitude waves.

By considering ranking measures that consider each model's ability to replicate the observed mean climate and frequency, intensity and synoptic patterns of observed regimes, an overall ranking for the models is determined. The models ranked as the top 3 are MRI-CGCM3, CNRM-CM5 and CSIRO-Mk3-6-0 which reproduce the observed mean rainfall and observed regimes with frequencies relatively close to the observations. These top ranked models are different to those found as high ranking by Frederiksen and Grainger (2015) or Jourdain et al. (2013), although their studies did not use some of the high-ranking models used in this study. The ranking is considered to be a general guide for informing changes to rainfall regimes in a future climate.

### **6.3 CMIP5 rainfall over north-western Australia: Considering a future climate**

In Chapter 5, potential changes to rainfall regimes over NWA in the eight CMIP5 models under the RCP8.5 emissions scenario are determined. While changes vary greatly across models, any changes are mainly driven by frequency changes to regimes responsible for heavy rainfall. The percentage change in rainfall was calculated over the region, and two of the three regime assignment methods developed in Chapter 3 were used to determine how rainfall regimes change under a future climate. Method I (projection) was used to determine changes to the frequency, intensity and low-level flow relative to each model's regimes in the historical period, while Method II (direct clustering) enabled changes to regime spatial patterns to be determined.

Changes to mean rainfall vary greatly among models, indicating little agreement across models as in previous studies (e.g. Knutti and Sedlacek (2013)) The ability of a given model to replicate the observed climate in the historical period does not affect the sign or magnitude of the rainfall change since the top 3 models produce different changes to mean rainfall in 2070-2099 relative to 1970-1999. However, by decomposing the changes in rainfall in each model into changes in individual regimes, we find that future changes in rainfall in each model are mostly driven by changes in frequency of regimes causing heavy rainfall.

However, in some wetting models such as CCSM4, intensity changes may be a greater driver than frequency changes. The spatial pattern of the change in the region in each model can normally be explained by changes in the frequency of individual heavy regimes (for example, in bcc-csm1-1-m, a reduction in the frequency of a regime with a maximum in the Pilbara results in a negative trend there), or by changes in spatial pattern of rainfall regimes (for example, in MIROC5, an inland movement of a heavy regime results in a positive trend in the south-east of the study region). In all models, changes to TC frequency are less important to the overall trend than changes in frequency of other regimes, which is in contrast to Chapter 2 where TC frequency changes were the most important driver of the overall rainfall trend in NWA. The reduction in rainfall intensity of TCs in the models relative to other regimes may be partially responsible.

Almost all models show an increase in intensity of the heavy regimes, which in some models is associated with a strengthening of north-westerly flow into the systems responsible for heavy rainfall. The increased intensity of heavy regimes is strongly counteracted by a reduction in the frequency of these regimes in models that predict a drying climate. The spatial patterns of regimes may also change with climate change in the models, with details dependent on the model. Most models predict a reduction in the incidence of TC days, agreeing with some previous studies predicting reduction in TC numbers (Utsumi et al., 2016; Knutson et al., 2010). Across the eight models, changes to intensity of rainfall from TCs varies, but of those models which correctly produce the TC rainfall and wind pattern, a slight increase in intensity is noted, agreeing with Utsumi et al. (2016). Overall, there is very little agreement between models on how mean rainfall will change under a future climate, however there is some agreement on an increase in rainfall intensity per regime. Future work should therefore focus on examining how biases in specific models affect the development of the synoptic systems responsible for rainfall in northern Australia, and potentially involve downscaled studies to understand changes to the frequency and intensity of systems including TCs.

In this work, the regime assignment methods enabled comparison of rainfall regimes between model and observed rainfall, or between future and current climates within CMIP5 models. The methods provide an additional perspective on assessing how well models replicate observed climate, since multiple rainfall patterns resulting from different synoptic sys-

tems can be approached at once, and multiple models can be assessed and ranked with simple metrics. With an understanding of regimes in the observed climate, the methods can be used to compare fields other than rainfall at higher or lower resolution, and can be used to inform climate projections on a regional scale.

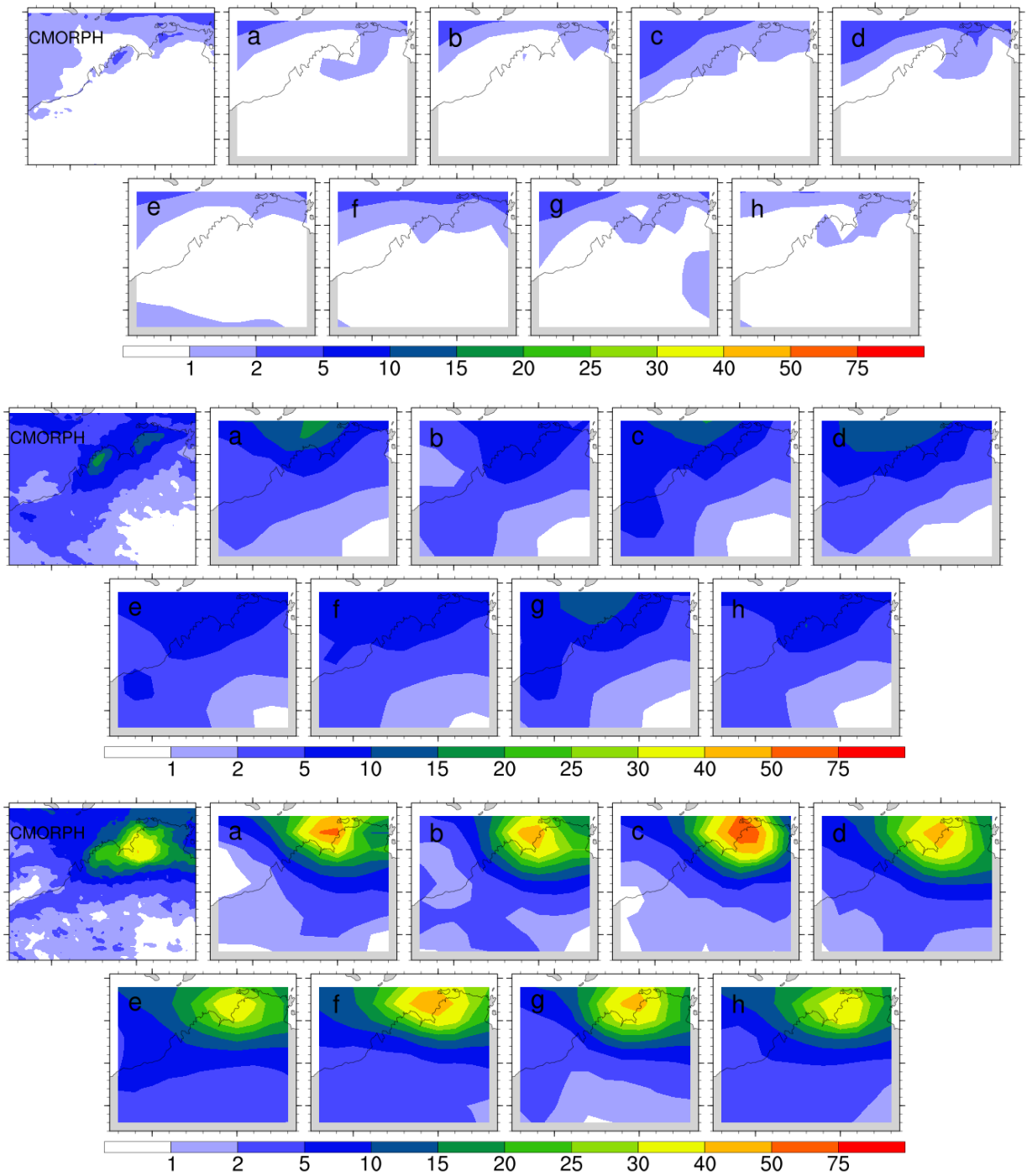
## **Appendix A**

# **CMIP5 historical regimes - full details of spatial patterns and wind fields**

### **A.1 Projected regimes (method 1) - Spatial patterns**

Method 1 assigns daily rainfall in the models to regimes by projecting daily rainfall from each CMIP5 model to the observed regimes. Details of how this method is applied are provided in Section 3.2.4. The rainfall spatial patterns are provided in the figures below, arranged by regime to illustrate the similarity of the model patterns to the observed patterns when this method is used. Regimes 3, 7 and the TC regimes are omitted since they are already shown in Chapter 4.

Appendix A. CMIP5 historical regimes - full details of spatial patterns and wind fields



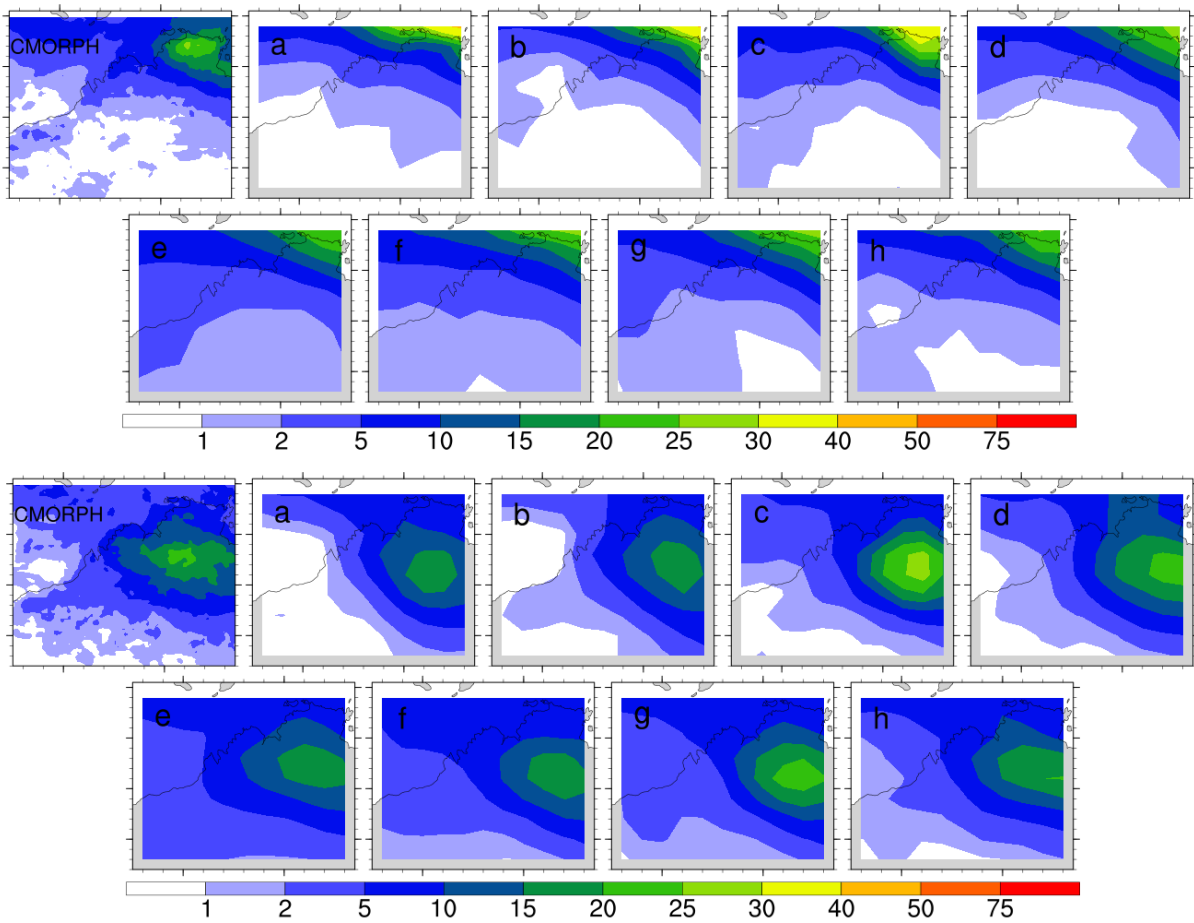


Figure A.1b: Spatial patterns for all regimes from the projection method, except regimes 3 and 7 which are in Figure 4.5 in Section 4.3.2. The first panel shows the spatial pattern in CMORPH, and the subsequent panels show each model. Labelling is as follows: a) ACCESS1-0, b) ACCESS1-3, c) bcc-csm1-1-m, d) CSIRO-Mk3-6-0, e) CCSM4, f) CNRM-CM5, g) MIROC5, h) MRI-CGCM3. Note the change in colour scale relative to figures in Chapter 3. Units are in  $\text{mm day}^{-1}$

As described in Section 4.3.2, the spatial patterns in the models look highly similar to the observations, with only minor changes in intensity. However, this is a direct result of using this method since regimes are assigned based on closeness to pre-existing regimes, and as such the mean of all days which are closest to a given regime will produce a mean close to that observed.

## A.2 Projected regimes (method 1) - 850 hPa and 500 hPa wind fields

The 850 hPa and 500 hPa wind fields for the projected regimes are provided below. The 850 hPa wind fields for regimes 1 and 3 are not given here, as they can be found in Section 4.3.3. Dry days are defined the same way whether method 1 or 2 is used, and a description of dry days will be given here.

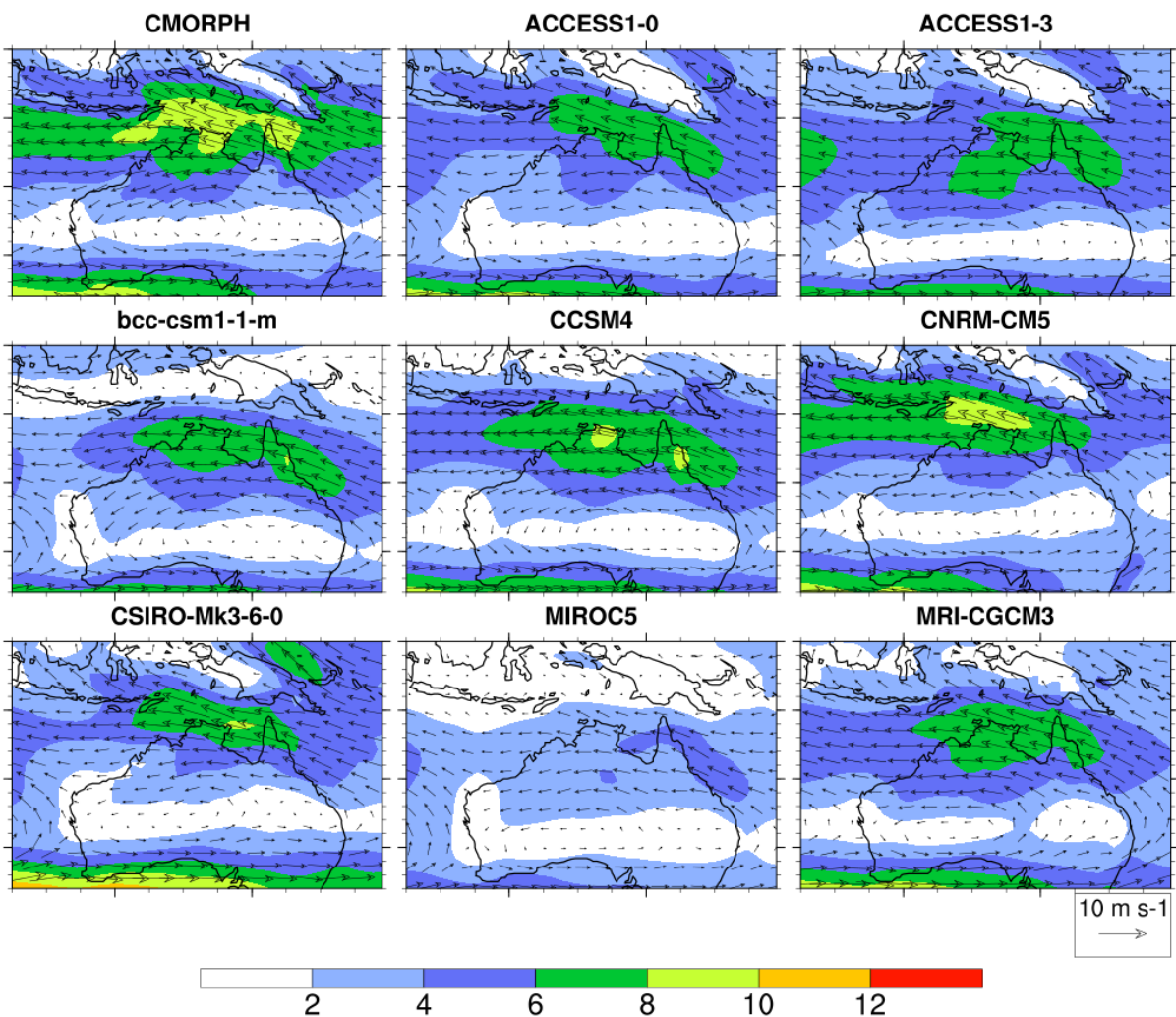


Figure A.2: 850hPa wind composites for dry days in each model.

In the observations, dry days are characterised by south-easterlies over northern Australia. This pattern is replicated relatively well by all models, however the wind speeds are too weak

for MIROC5, a similar bias to regime 1. The winds tend to be more easterly in CCSM4 and CNRM-CM5.

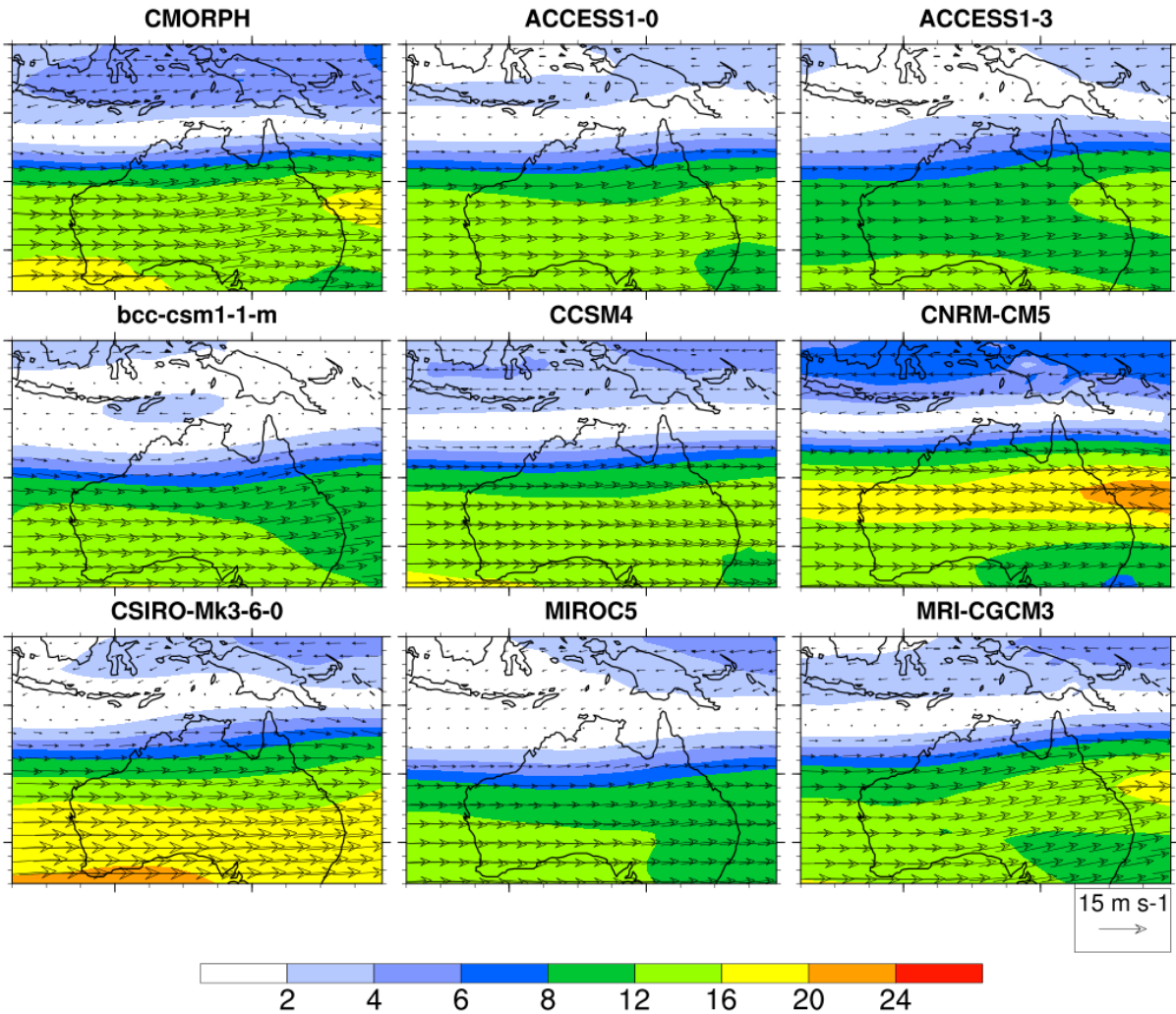


Figure A.3: 500hPa wind composites for dry days in each model

The dry days composites include a large number of days from the austral winter, since this is the dry season over northern Australia. A northward movement and strengthening of the subtropical jet occurs in both models and observations. Some variation in wind speed exists across models, however the pattern is replicated well.

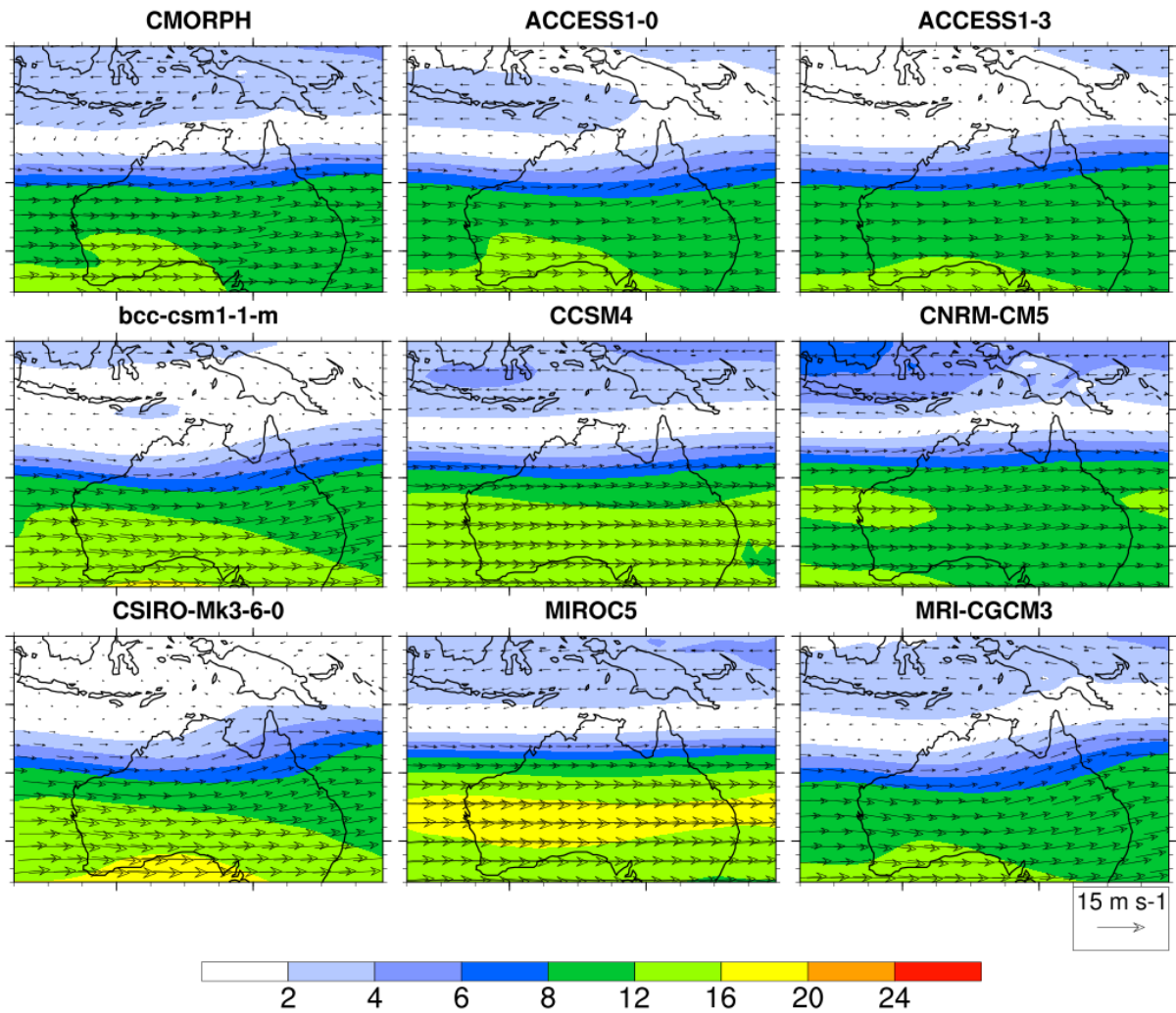


Figure A.4: 500hPa wind composites for regime 1 in each model

Regime 1, which corresponds to light rainfall in both observations and the models (see rainfall patterns in the previous section), is typical of the build-up season where isolated thunderstorms develop in a slightly more unstable atmosphere. The seasonal spread of days in this regime results in the jet being weaker and located further south. This is captured in all models well, with some slight variation in wind speed.

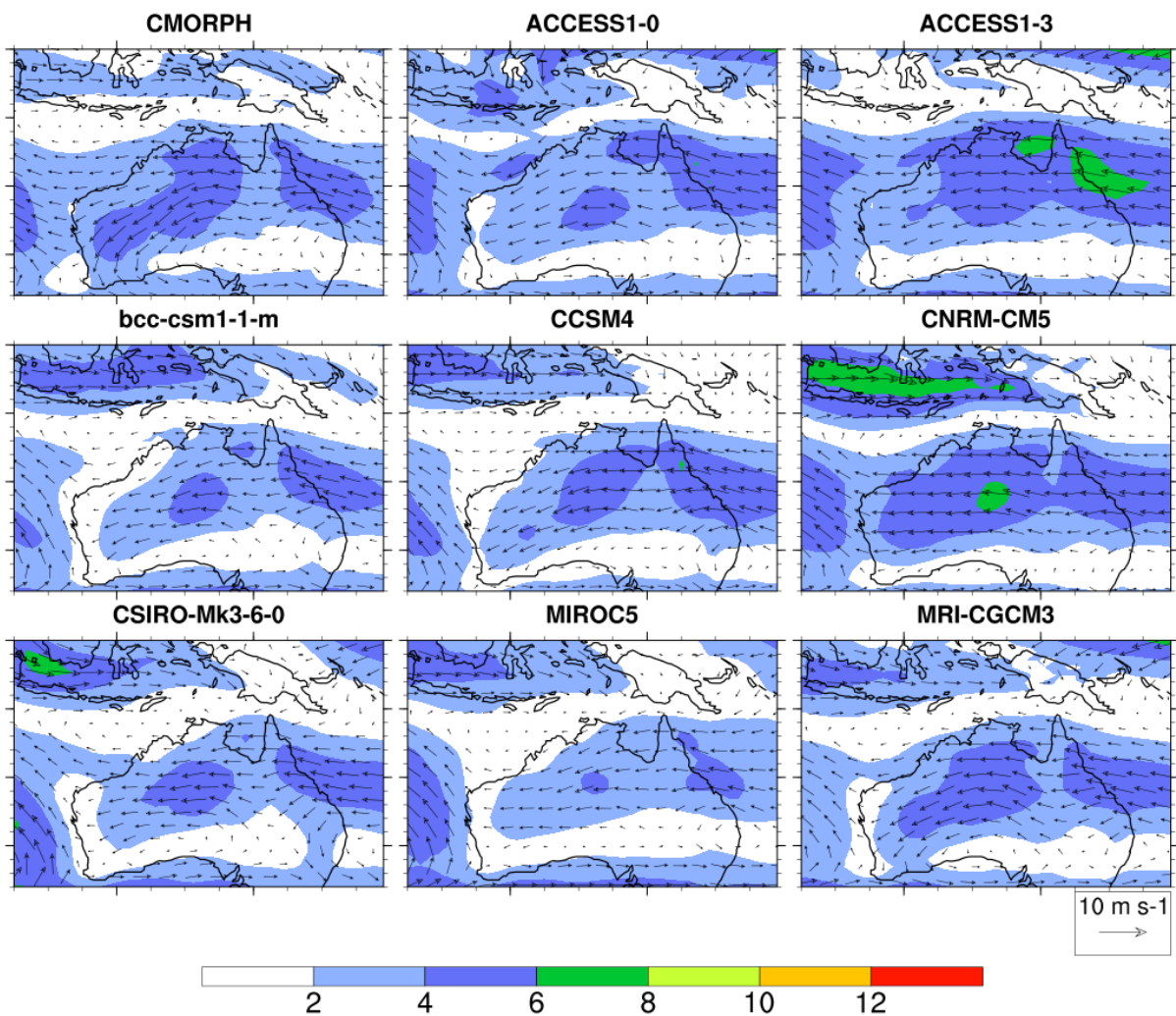


Figure A.5: 850hPa wind composites for regime 2 in each model.

Regime 2, which corresponds to moderate rainfall, is characterised in the observations by weak low-level easterlies. Similar to the composites for regime 1 and dry days, the general wind pattern is replicated well in the models chosen in this study with variations in wind speed across models.

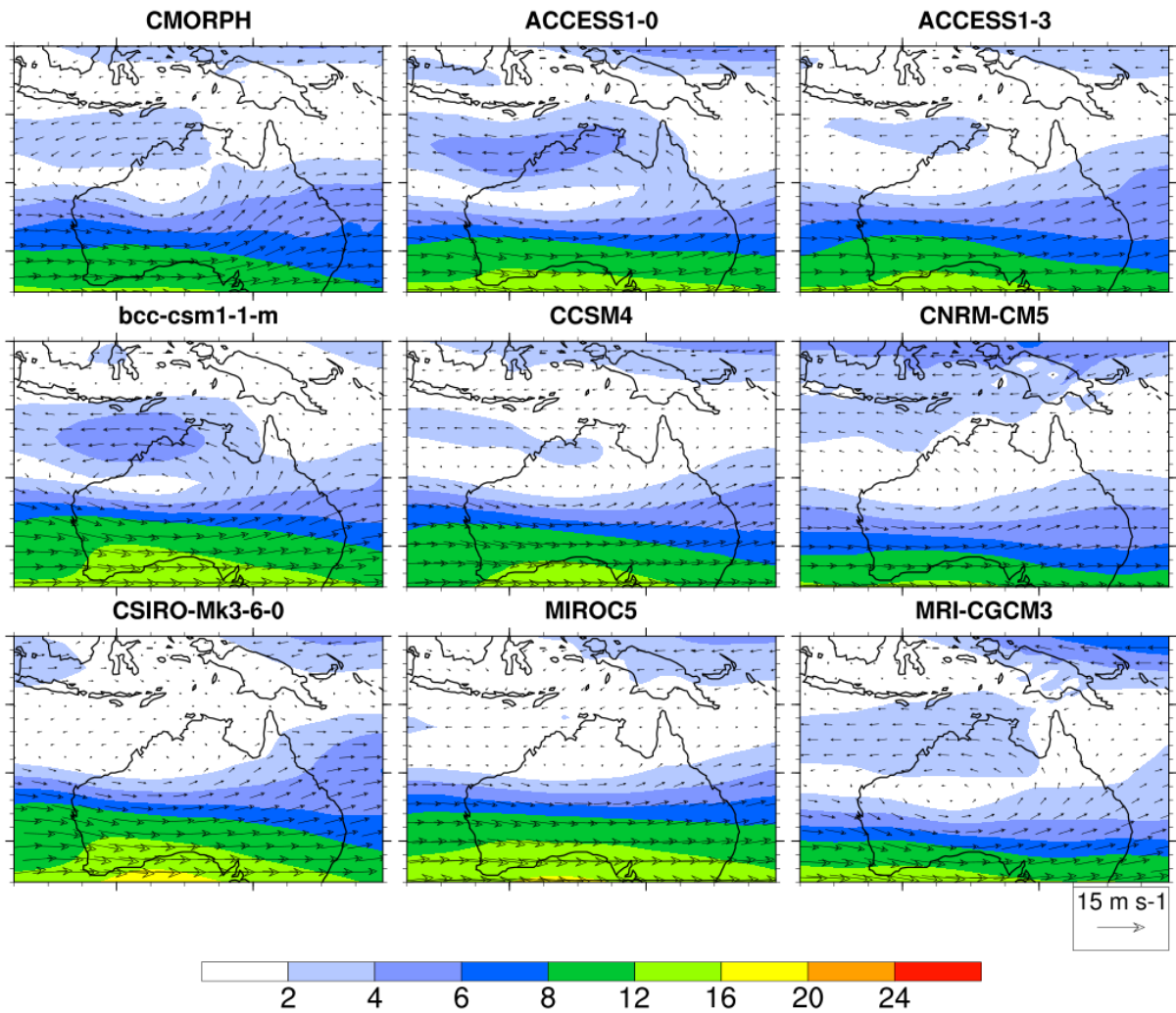


Figure A.6: 500hPa wind composites for regime 2 in each model.

The 500 hPa circulation in regime 2 in the observations is characterised by anticyclonic flow over inland areas of NWA. This pattern is replicated well by all models except CSIRO-Mk3-6-0 and MIROC5, which produce a dip in the jet, but little evidence of a full anticyclonic circulation. Of the models that do replicate the mid-level anticyclone, the wind speed on the northern side varies, with bcc-csm1-1-m producing easterlies on the northern side that are too strong.

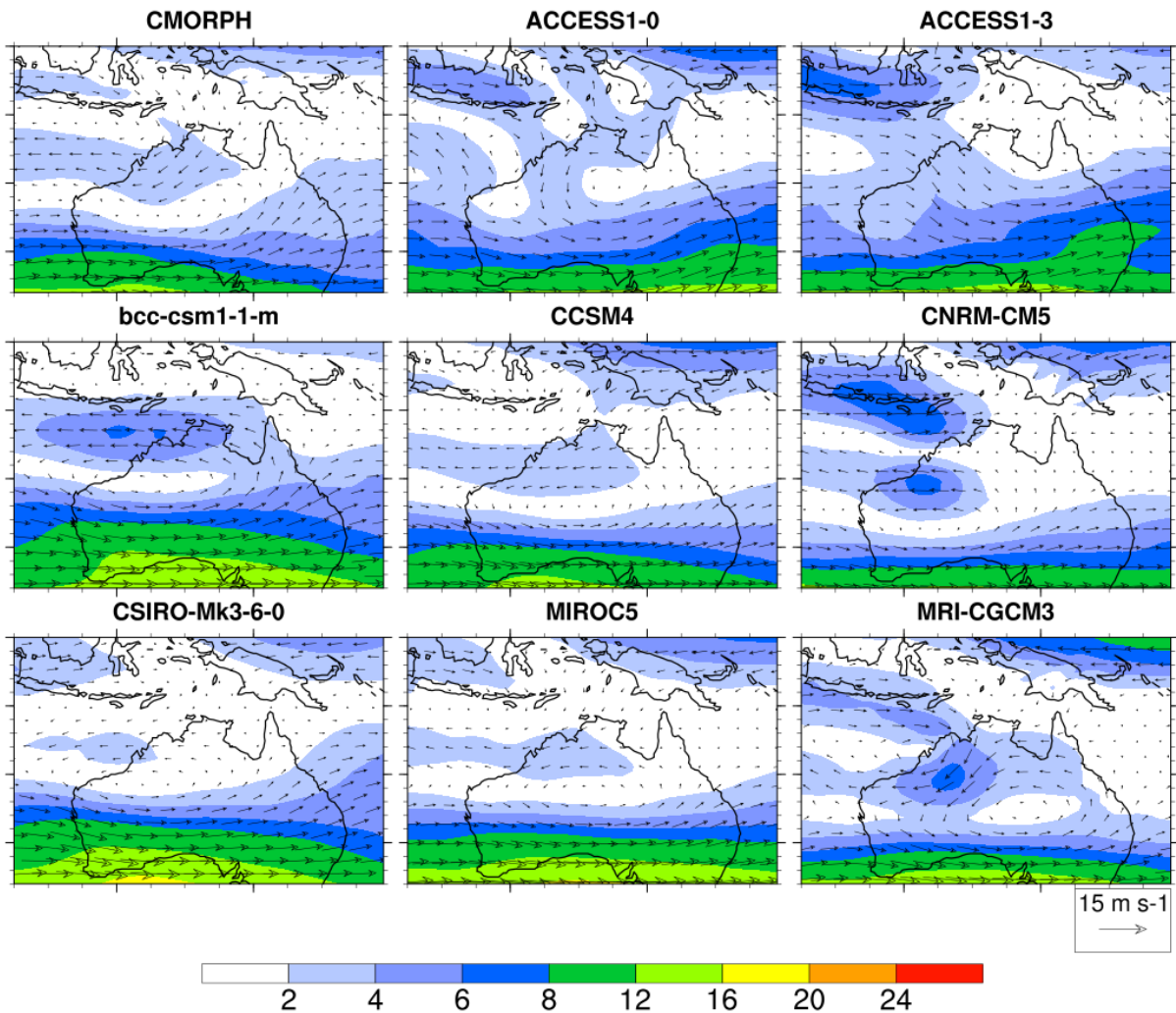


Figure A.7: 500hPa wind composites for regime 3 in each model.

Regime 3 consists of rainfall over the Kimberley region, and in observations is characterised by a closed circulation typical of a monsoon low. Only MRI-CGCM3 has a closed circulation in the upper level structure, with most other models failing to replicate any sort of closed circulation. CNRM-CM5 shows weak convergence similar to the monsoon trough type system noted in Figure 4.9. ACCESS1-3 shows deeper north-westerly winds over the region of maximum rainfall, with the shape of the circulation resembling a wave-like pattern. The remaining models show an anticyclone over central Australia with little other evidence of a closed cyclonic circulation, suggesting the heavy rainfall is the result of localised deep convection rather than having synoptic influence.

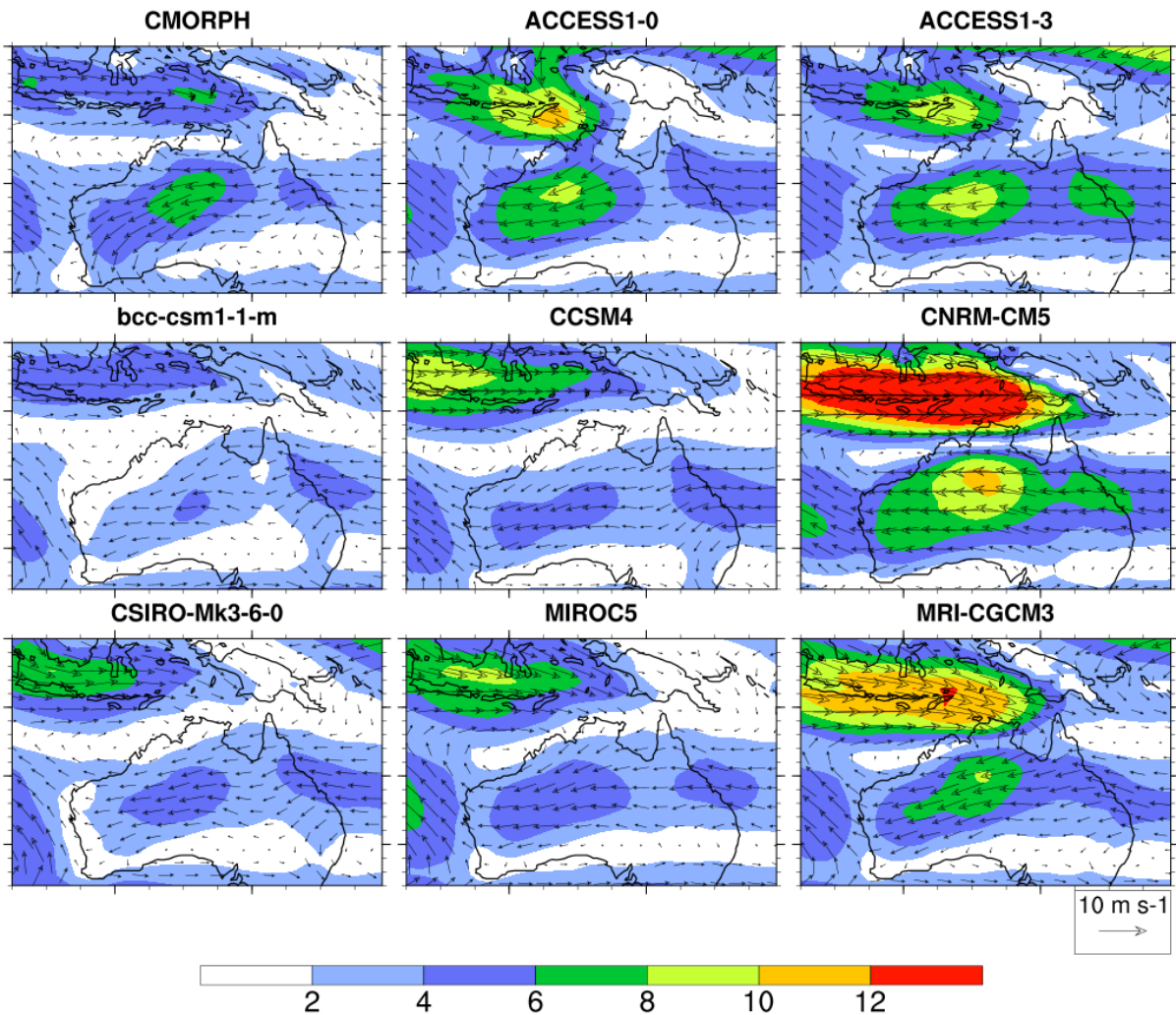


Figure A.8: 850hPa wind composites for regime 4 in each model.

Regime 4 is characterised in the observations by a rainfall maximum located between the Kimberley and Top End regions (see above rainfall maps), and low-level cyclonic circulation close to the region of maximum rainfall. The biases in the models resemble those described for regime 3 in Section 4.3.2, where the ACCESS models and MRI-CGCM3 produce a closed low, CNRM-CM5 and CCSM4 produce a monsoon trough with winds that are too strong and too weak respectively, and bcc-csm1-1-m and CSIRO-Mk3-6-0 produce very little pattern. The only notable difference between the wind fields for this regime and regime 3 are that the centre of the circulation has shifted in line with the change of location of the rainfall maximum.

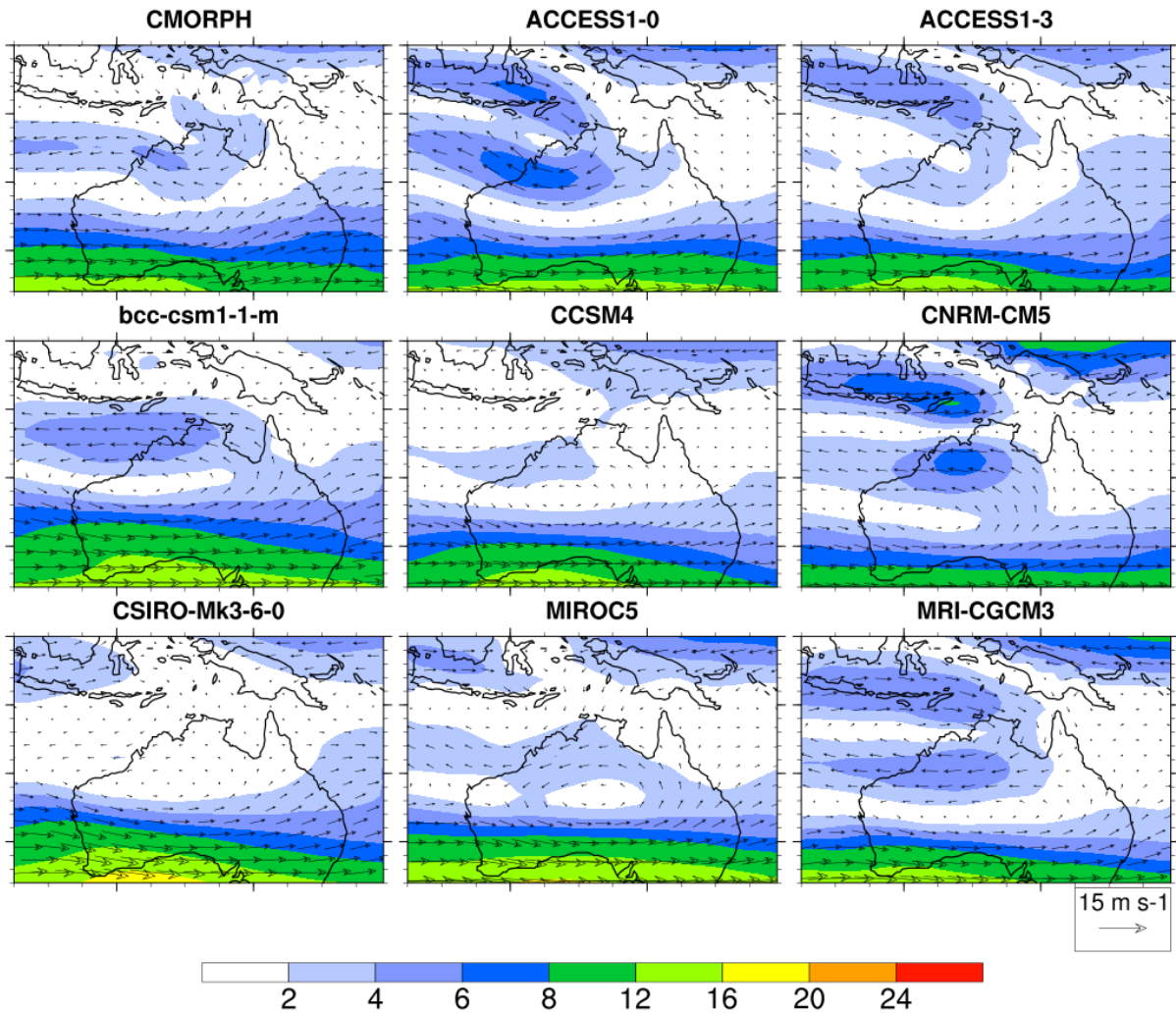


Figure A.9: 500hPa wind composites for regime 4 in each model.

Similar to regime 3, the observed regime 4 is characterised by a closed circulation in the mid levels typical of a monsoon low. The model biases for this regime are similar to that of regime 3, but the ACCESS models are able to replicate the closed circulation more closely. The winds around the trough in CNRM-CM5 are slightly stronger than for regime 3.

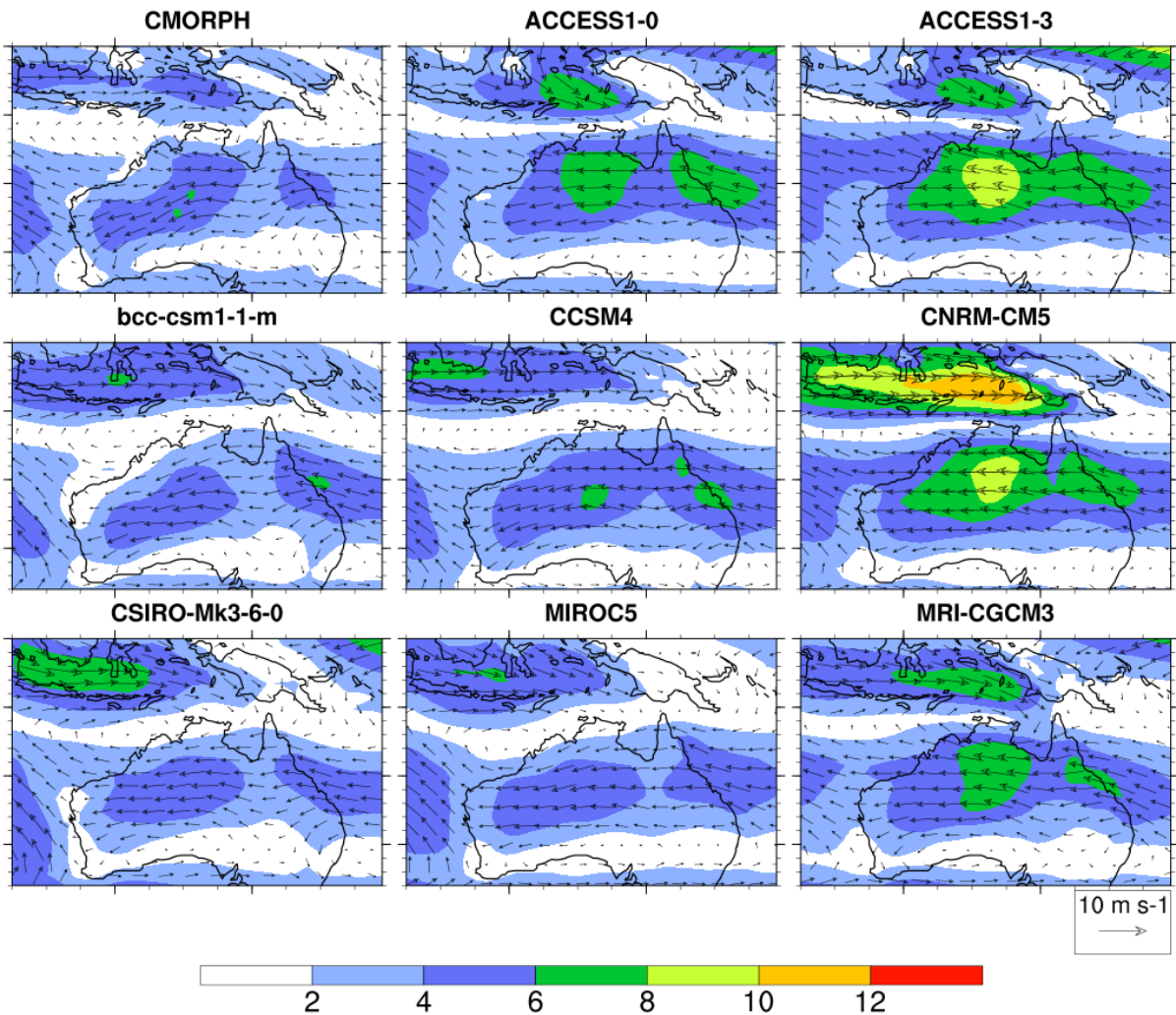


Figure A.10: 850hPa wind composites for regime 5 in each model.

Regime 5 is considered to be another monsoon low-type circulation in the observations. The biases in each model for regime 5 are highly similar to those for regimes 3 and 4. The wind speeds for the circulation in all models are weaker than for regimes 3 and 4, and thus more closely resemble the observations.

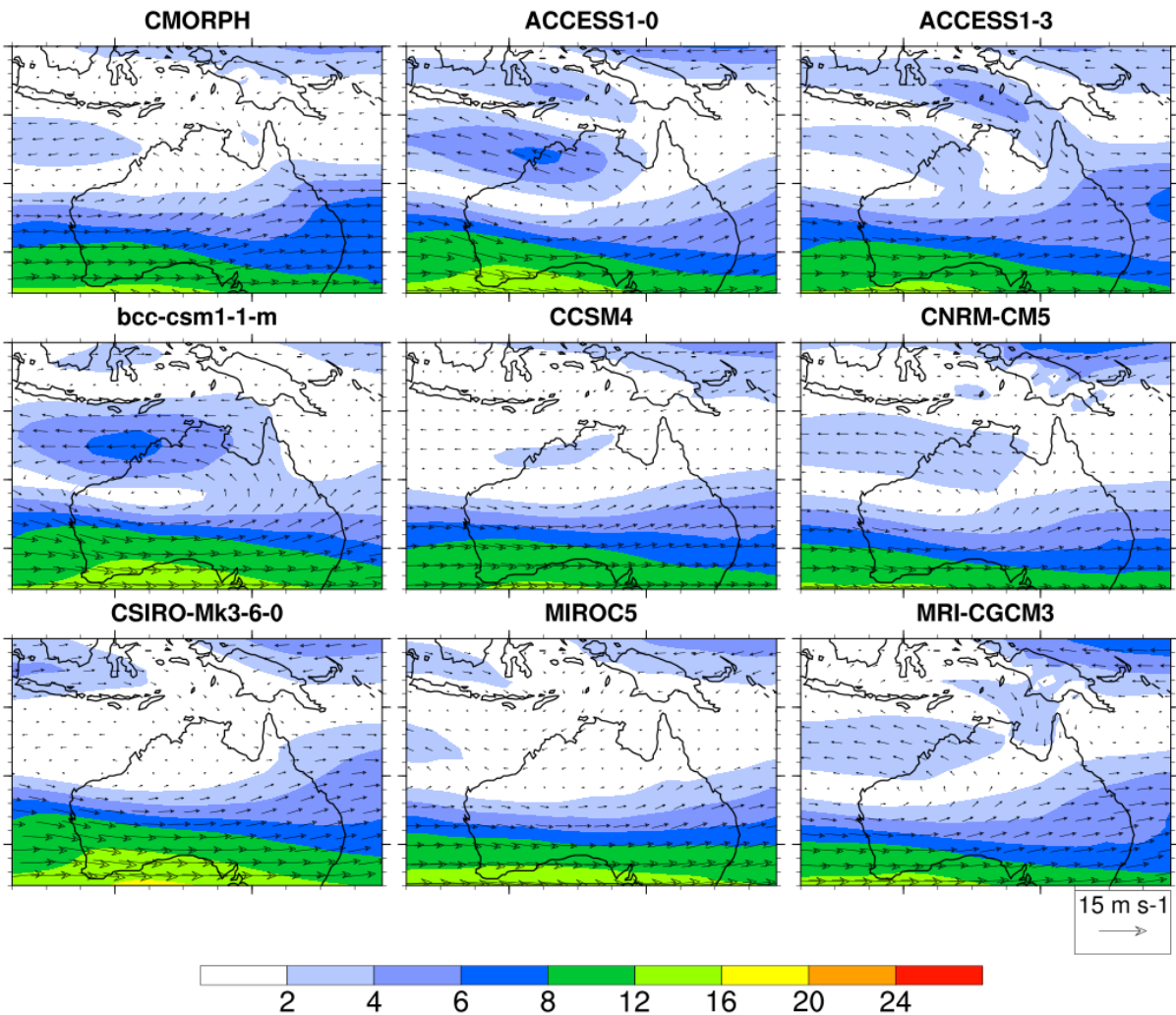


Figure A.11: 500hPa wind composites for regime 5 in each model.

At the 500 hPa level, the structure in many models is the same as for regime 4. The wind speeds are much weaker for MRI-CGM3, but a closed circulation is still evident. ACCESS1-3 and CNRM-CM5 show little evidence of a closed low or convergence at this level.

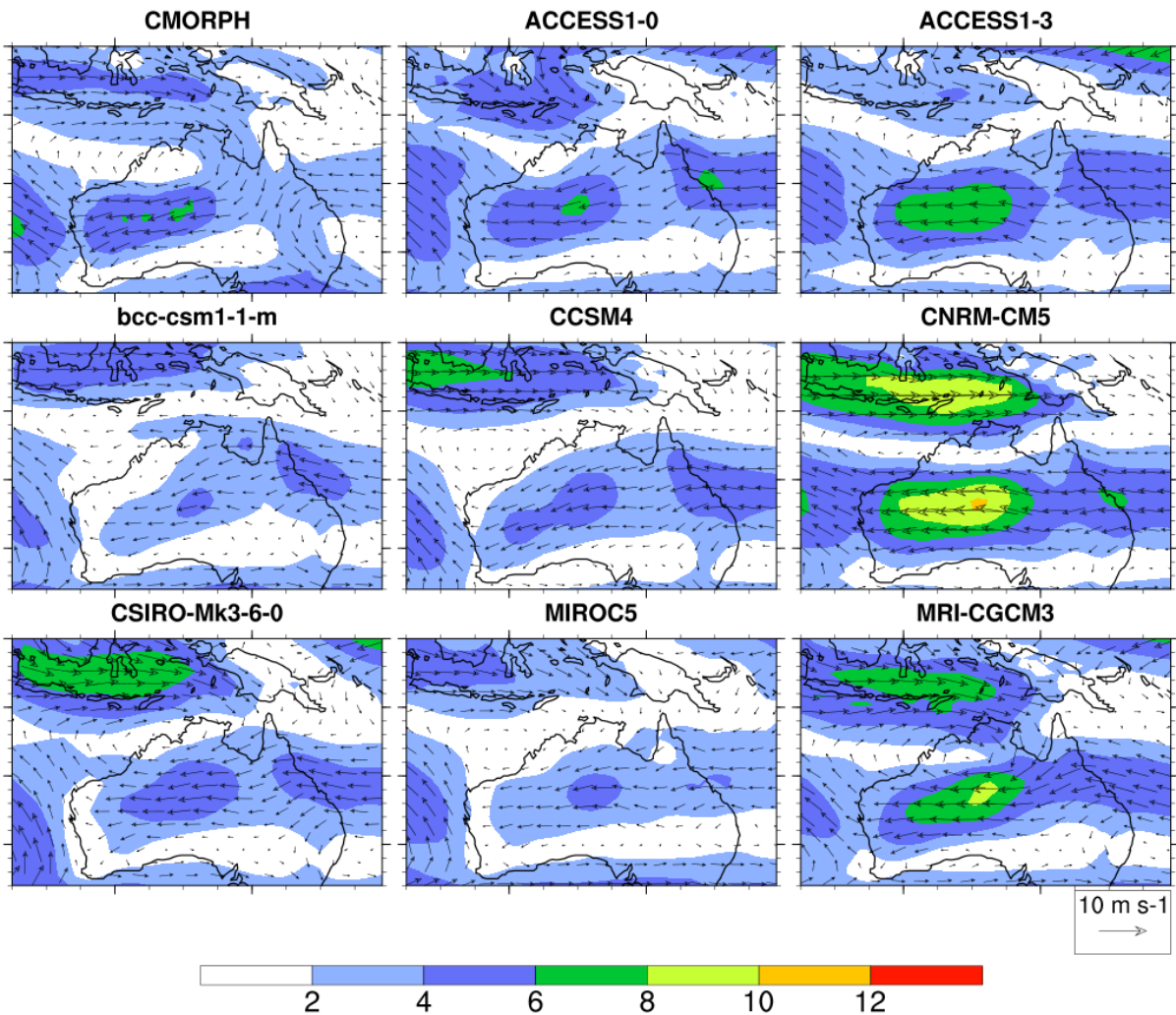


Figure A.12: 850hPa wind composites for regime 6 in each model.

Regime 6 in the observations consists of a rainfall maximum inland of the Top End region, and is characterised by a broad cyclonic circulation at 850 hPa. The closed circulation is replicated well by ACCESS1-3 and MRI-CGCM3, with some evidence of a closed low in CSIRO-Mk3-6-0 and ACCESS1-0. CNRM-CM5 again produces a convergence line consistent with a monsoon trough, similar to the previous regimes. CCSM4, MIROC5 and bcc-csm1-1-m again show little evidence of a closed circulation.

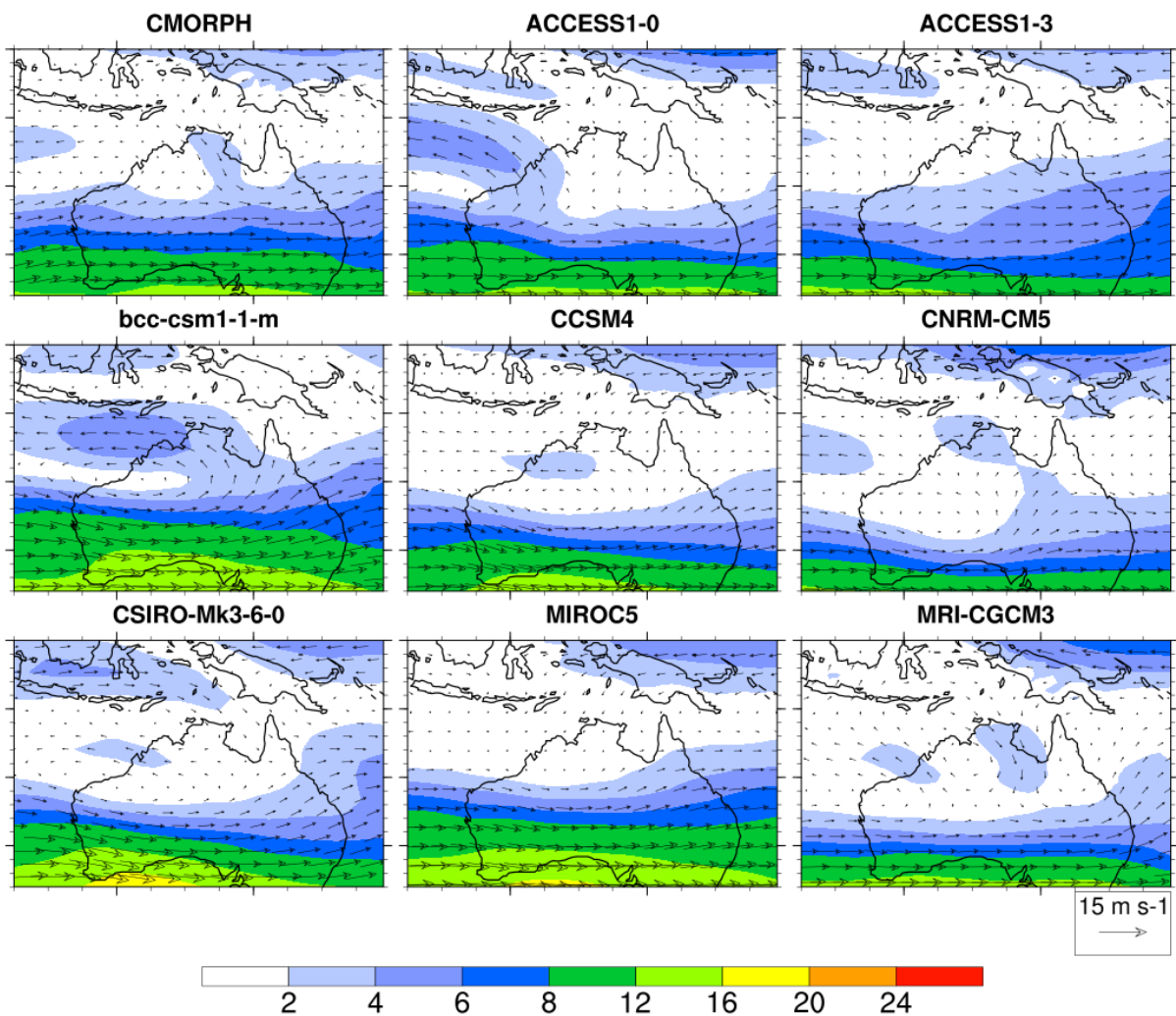


Figure A.13: 500hPa wind composites for regime 6 in each model.

The circulation at 500 hPa over the region for regime 6 is weak in regime 6. As for previous regimes, bcc-csm1-1-m and CCSM4 show an anticyclone over western and central Australia respectively, again showing little evidence of synoptic forcing. The remaining models show very little evidence of a closed circulation.

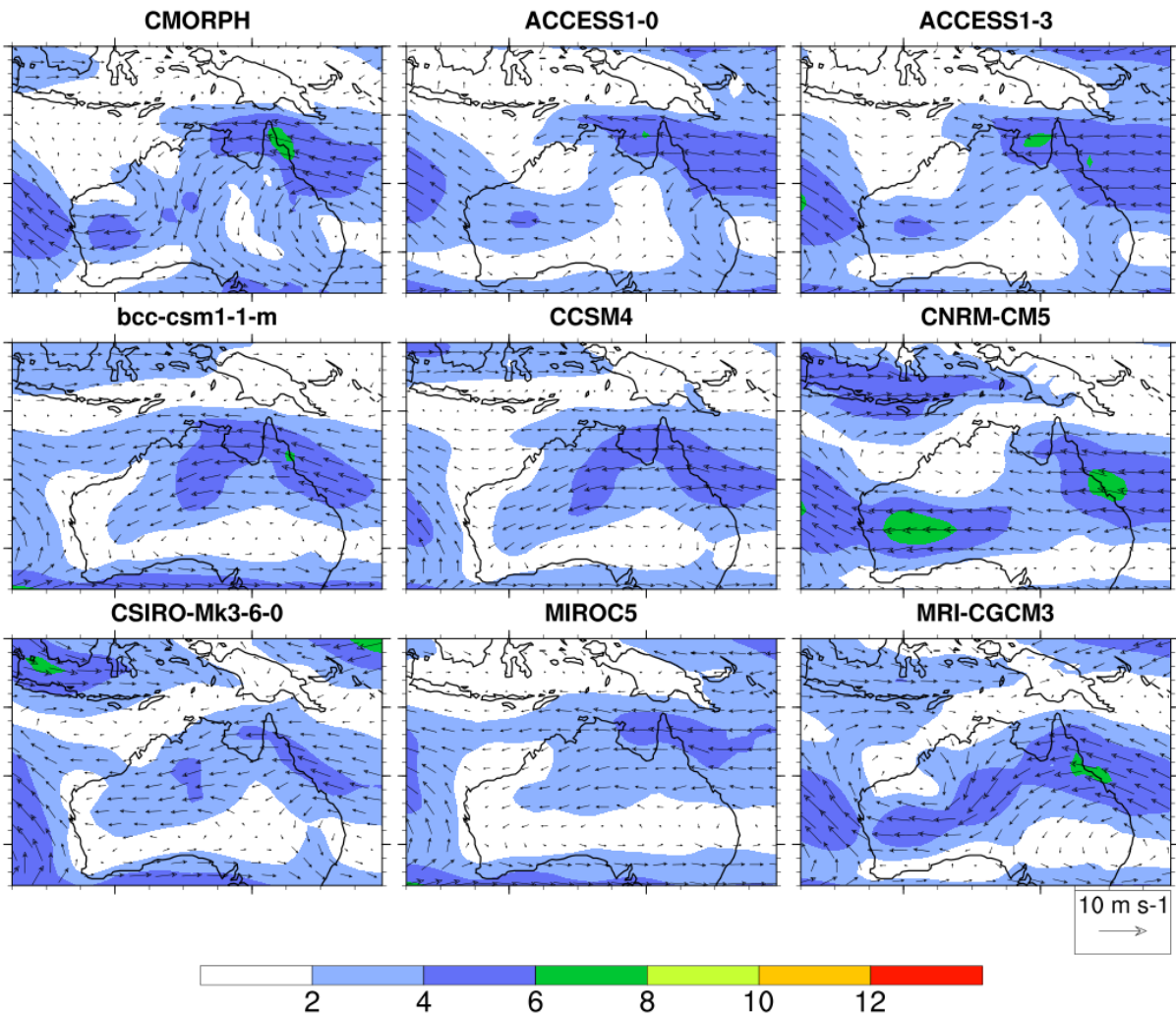


Figure A.14: 850hPa wind composites for regime 7 in each model.

Regime 7 in the observations is defined by rainfall far inland, in the south of the study region. The low level flow is relatively weak, but there is evidence of an easterly trough over the west coast of Australia, and an anticyclone centred on the east coast. This pattern is replicated in most models, although the exact shape varies between models. Only MIROC5 shows little pattern in the flow.

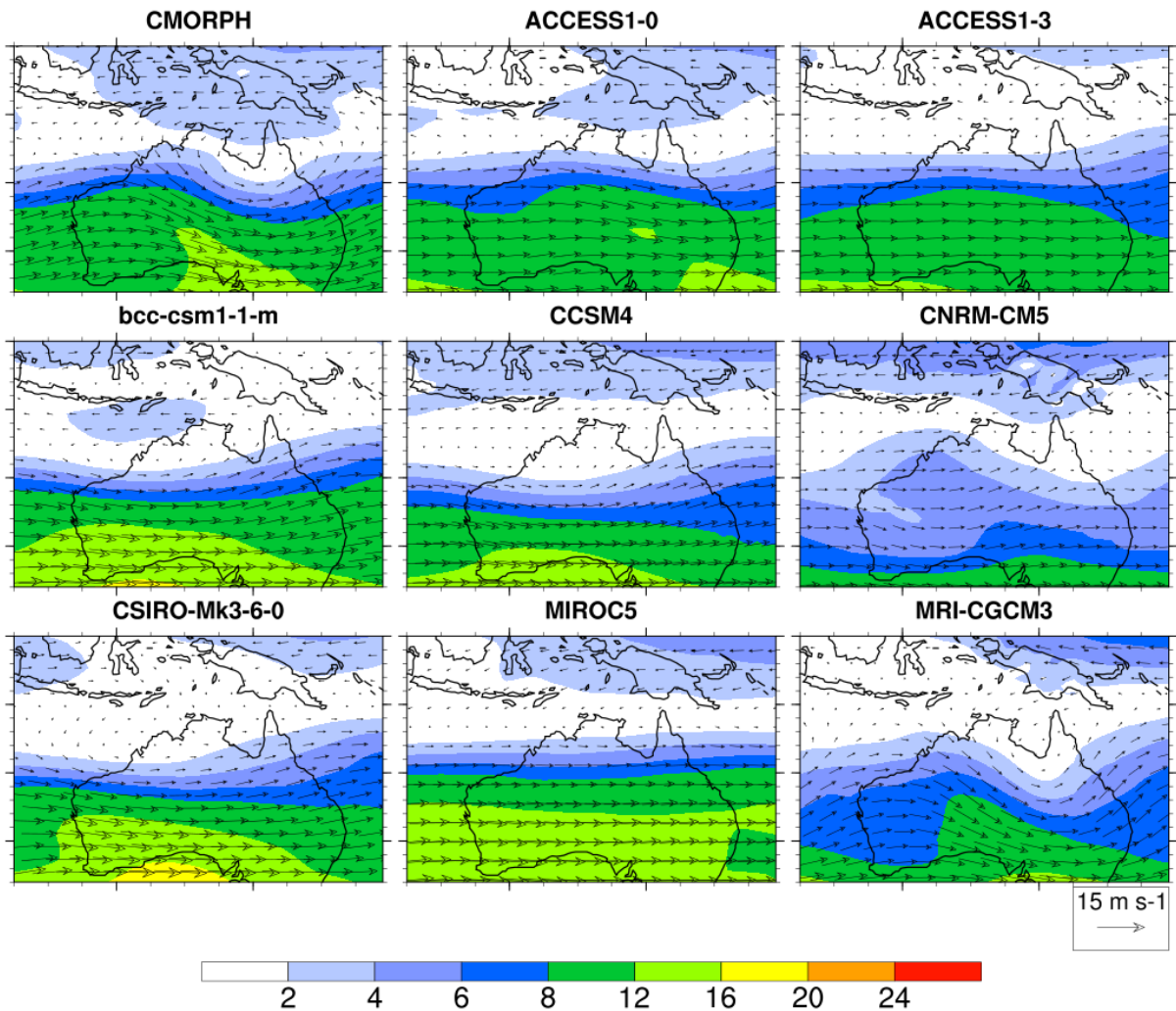


Figure A.15: 500hPa wind composites for regime 7 in each model.

The 500 hPa flow in regime 7 in the observations shows a mid-latitude wave pattern amplifying over the study region. This pattern appears to be poorly replicated in most models aside from MRI-CGCM3, however the ability of models to replicate the mid-latitude Rossby waves responsible for the rainfall is best assessed using the 250 hPa meridional wind, which is presented in Section 4.3.2.

### **A.3 Independently determined regimes (method 2) - 850 hPa and 500 hPa wind fields**

In Section 4.3.3, the rainfall patterns for independently determined regimes are shown. The 850 hPa and 500 hPa wind fields for these regimes are provided below. The 850 hPa wind fields for regimes 4 and 7 are not given here, as they are already given in Section 4.3.3. Dry days are defined the same way whether method 1 or 2 is used, thus since the dry days composites are presented earlier in the Appendix, there is no need to present them again here.

From this method, regimes 1, 3, 4 and 5 in each model appear highly similar in rainfall spatial pattern to their counterparts in the observations, and thus the wind patterns deviate very little from the same regime from the projection method. Most of the differences for these regimes compared to method 1 arise from differences in wind speed.

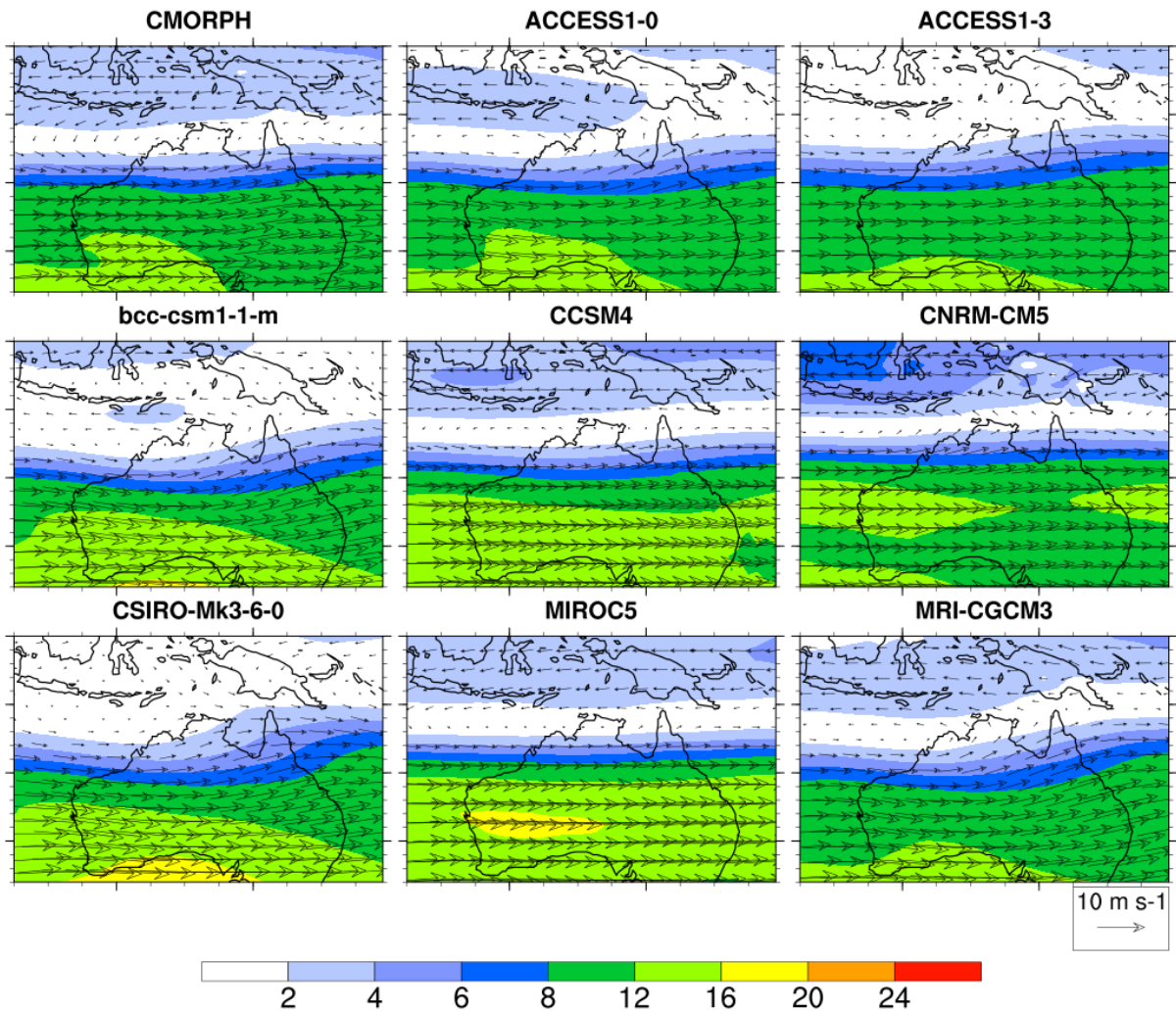


Figure A.16: 500 hPa wind composites for regime 1 in each model

Regime 1, which corresponds to light rainfall in both observations and the models (see rainfall patterns in the previous section), is typical of the build-up season where isolated thunderstorms develop in a slightly more unstable atmosphere. Since the light rainfall regime is captured well in the models, there is essentially no difference between these composites and those determined from regime 1 using the projection method.

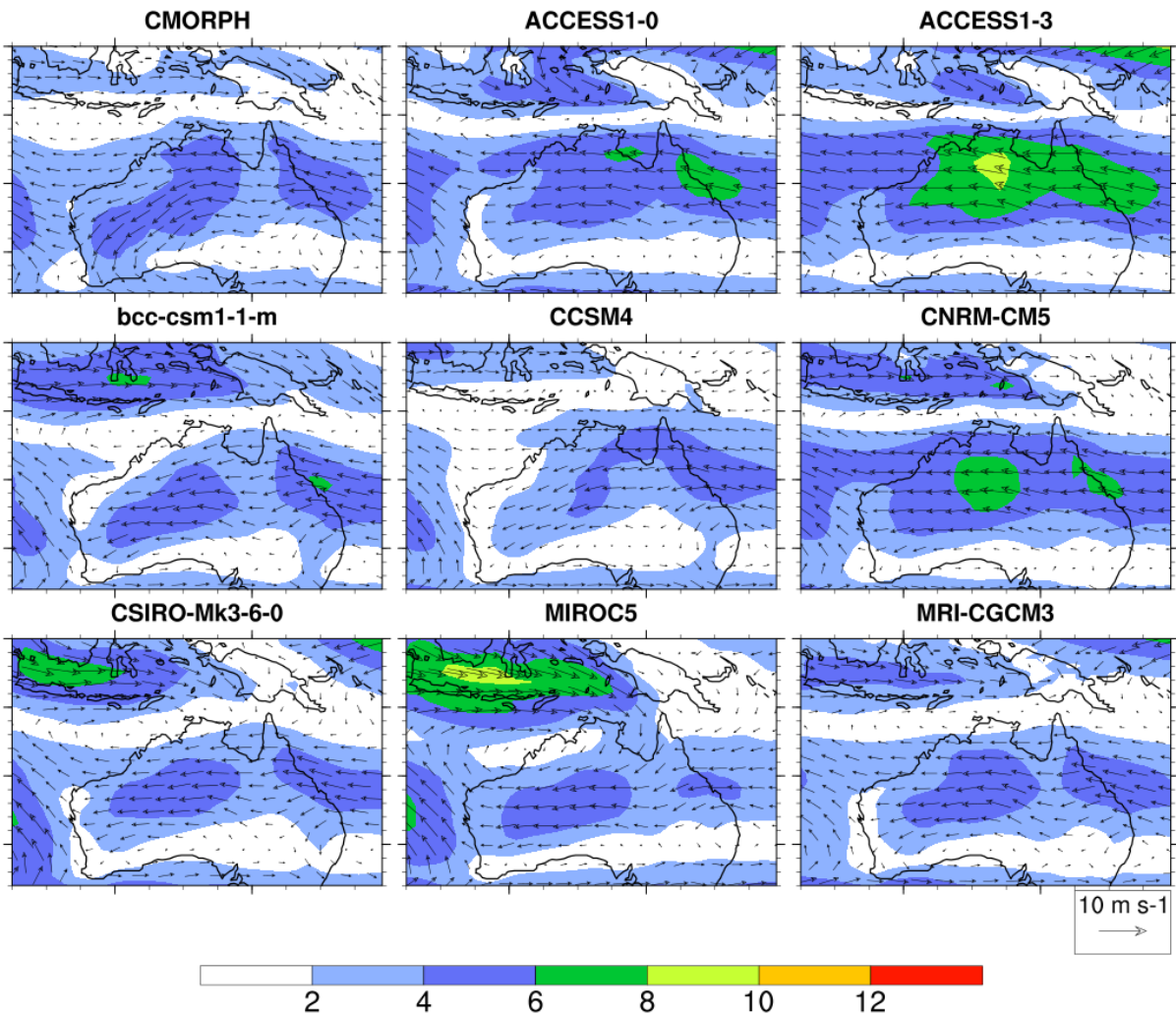


Figure A.17: 850hPa wind composites for regime 2 in each model.

Regime 2, corresponding to days with moderate rainfall, is characterised in the observations by weak low-level easterlies. Similar to the composites for regime 1 and dry days, the general wind pattern is replicated well in the models chosen in this study. However, the speed is too strong in the ACCESS models and CNRM-CM5, and too weak in MIROC5.

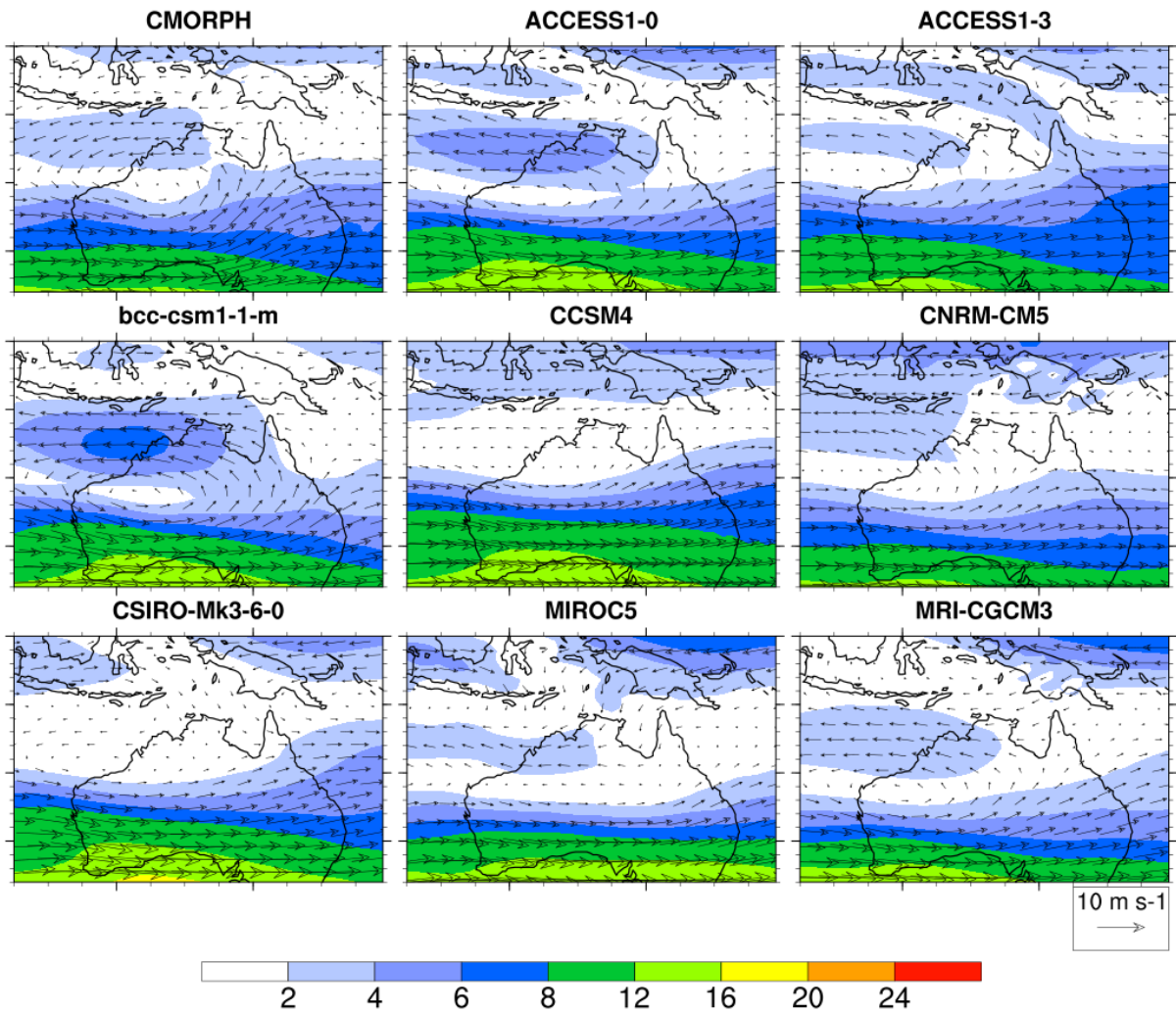


Figure A.18: 500hPa wind composites for regime 2 in each model.

The 500 hPa circulation in regime 2 in the observations is characterised by anticyclonic flow over inland areas of NWA. This pattern is replicated well by all models except CSIRO-Mk3-6-0 and CCSM4, which produce a dip in the jet, but little evidence of a full anticyclonic circulation. Of the models that do replicate the mid-level anticyclone, the wind speed on the northern side varies, with bcc-csm1-1-m producing easterlies on the northern side that are too strong.

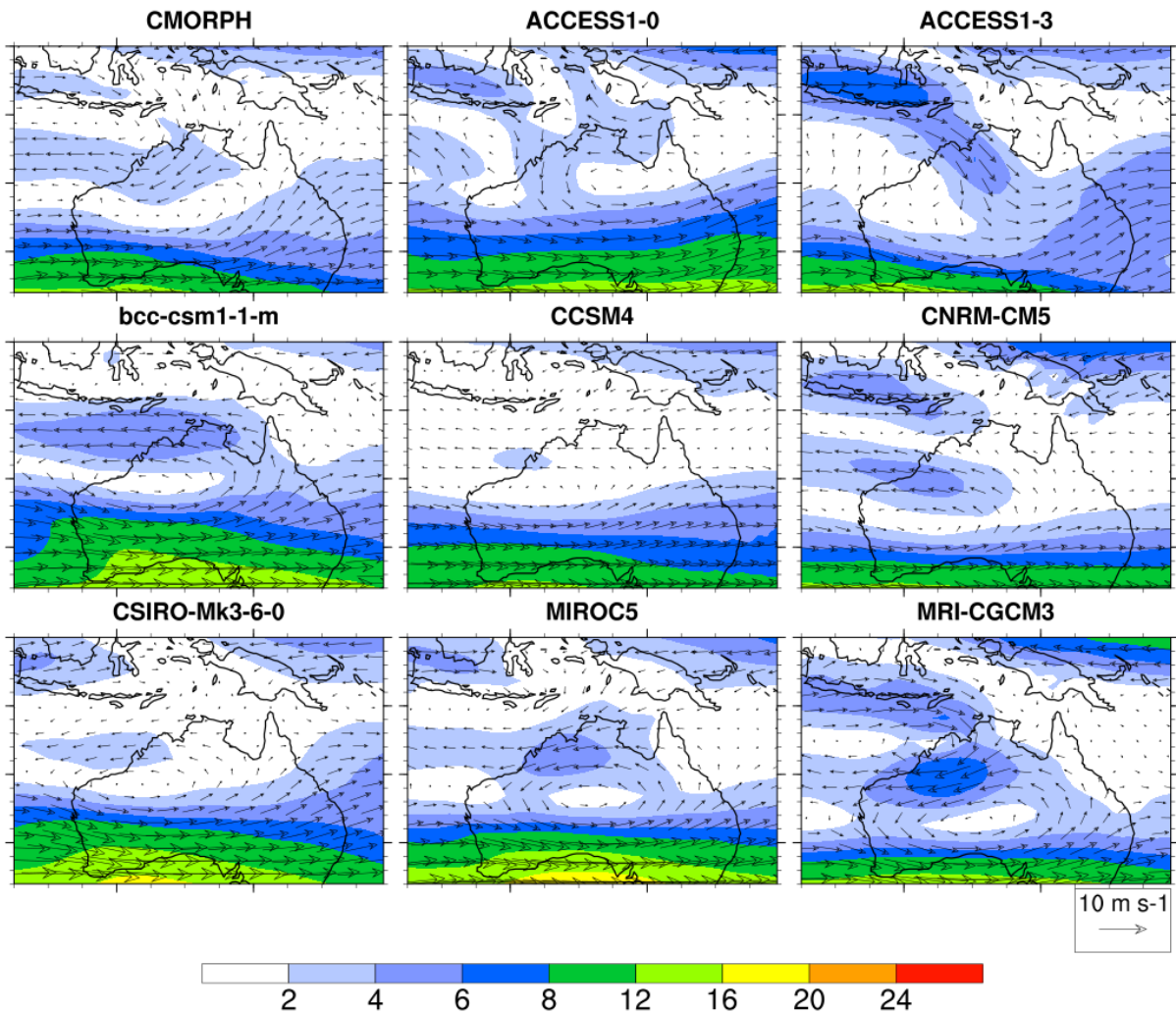


Figure A.19: 500hPa wind composites for regime 3 in each model.

Regime 3 consists of rainfall over the Kimberley region, and in observations is characterised by a closed circulation typical of a monsoon low. The model biases in the wind pattern are the same as those for regime 3 from the projection method, with the ACCESS models and MRI-CGCM3 producing a closed low similar to the observations, CNRM-CM5 and CCSM4 producing a convergence line, MIROC5 producing a broad, weak low and the remaining two models (CSIRO-Mk3-6-0, bcc-csm1-1-m) showing little evidence of a closed circulation.

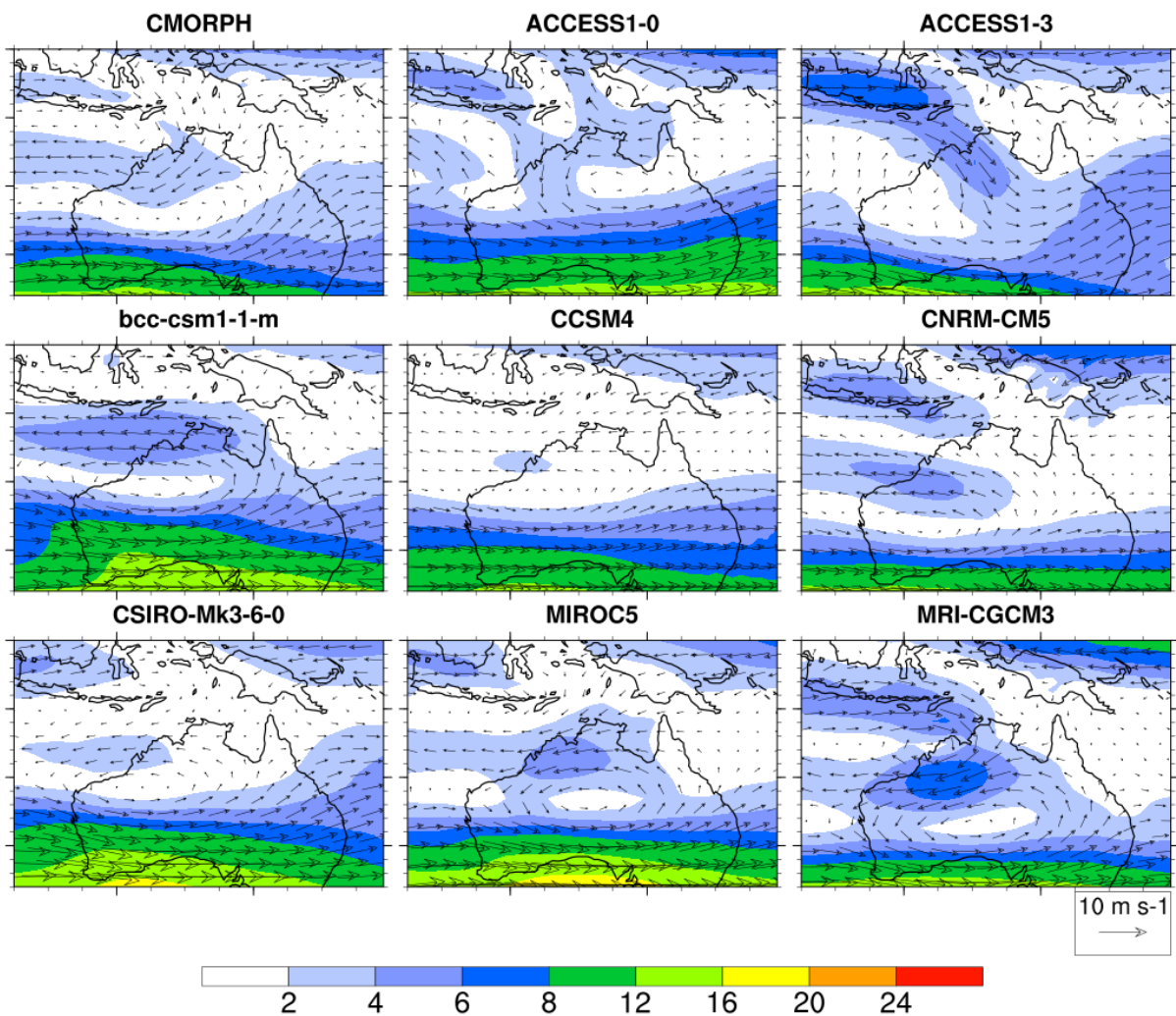


Figure A.20: 500hPa wind composites for regime 3 in each model.

In terms of the 500 hPa winds, only MRI-CGCM3 has a closed circulation in the upper level structure, with most other models failing to replicate any sort of closed circulation. CNRM-CM5 shows weak convergence similar to the monsoon trough type system noted in Figure 4.9. ACCESS1-3 shows deeper north-westerly winds over the region of maximum rainfall, with the shape of the circulation resembling a wave-like pattern. The remaining models show an anticyclone over central Australia, suggesting the heavy rainfall is the result of localised deep convection rather than having synoptic influence.

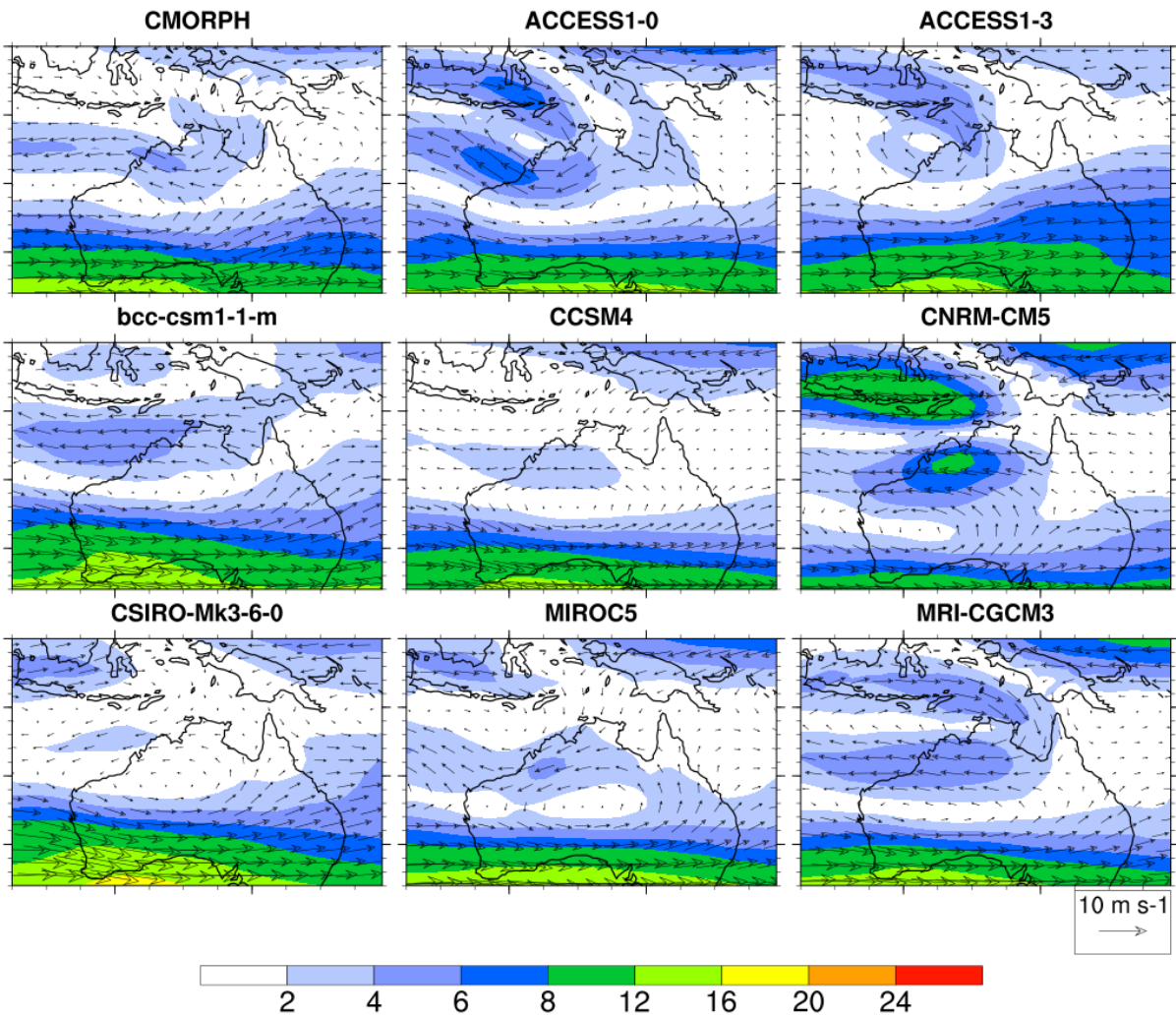


Figure A.21: 500hPa wind composites for regime 4 in each model.

Similar to regime 3, the observed regime 4 is characterised by a closed circulation in the mid levels typical of a monsoon low. The model biases for this regime are similar to that of regime 3, but the ACCESS models are able to replicate the closed circulation more closely. The winds around the trough in CNRM-CM5 are stronger than for regime 3.

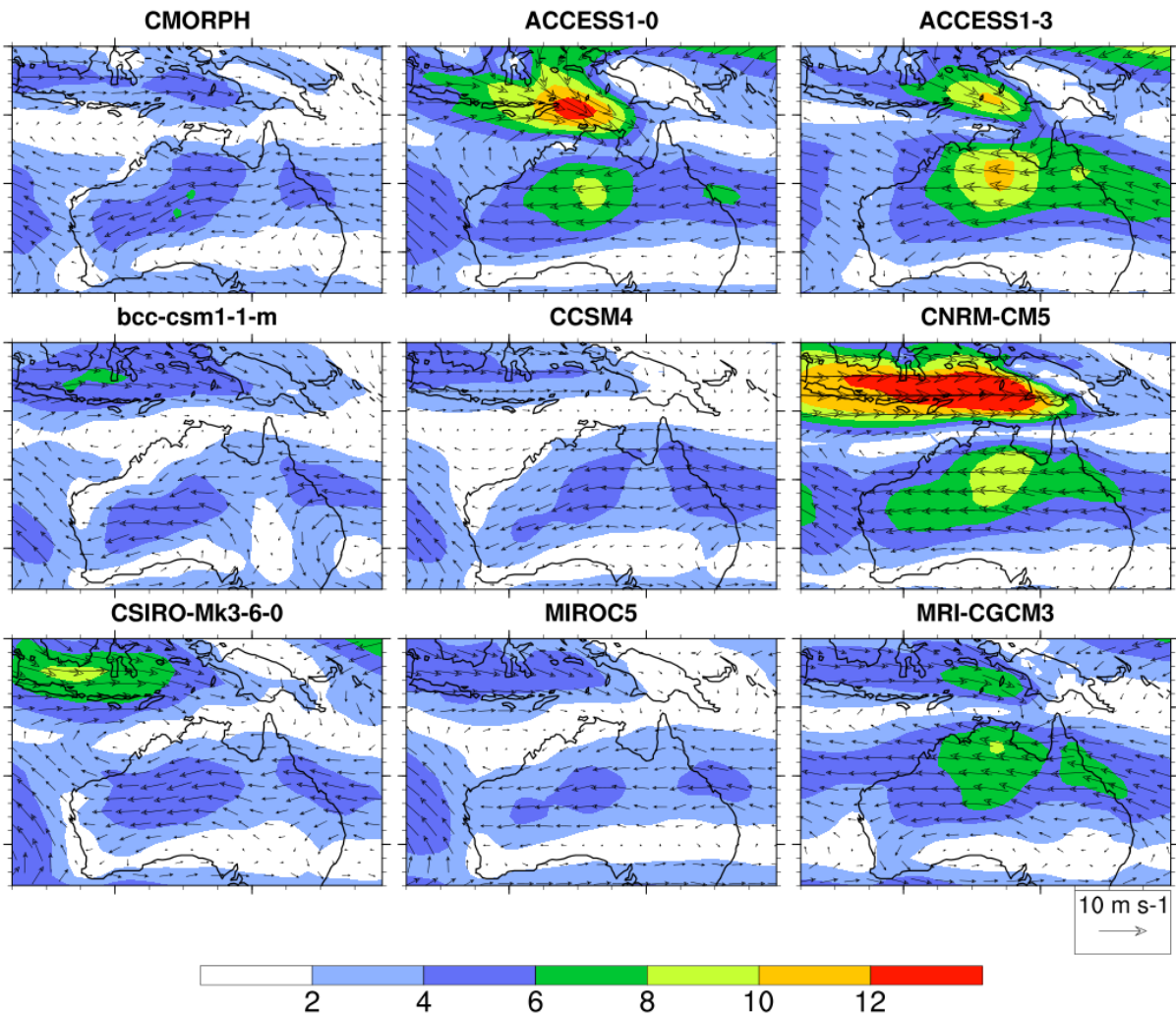


Figure A.22: 850hPa wind composites for regime 5 in each model.

Regime 5 is considered to be another monsoon low-type circulation in the observations. The biases in each model for regime 5 are highly similar to those for regimes 3 and 4. The wind speeds for the circulation in ACCESS1-0 are stronger than in the previous two regimes, while it is weaker for MRI-CGCM3.

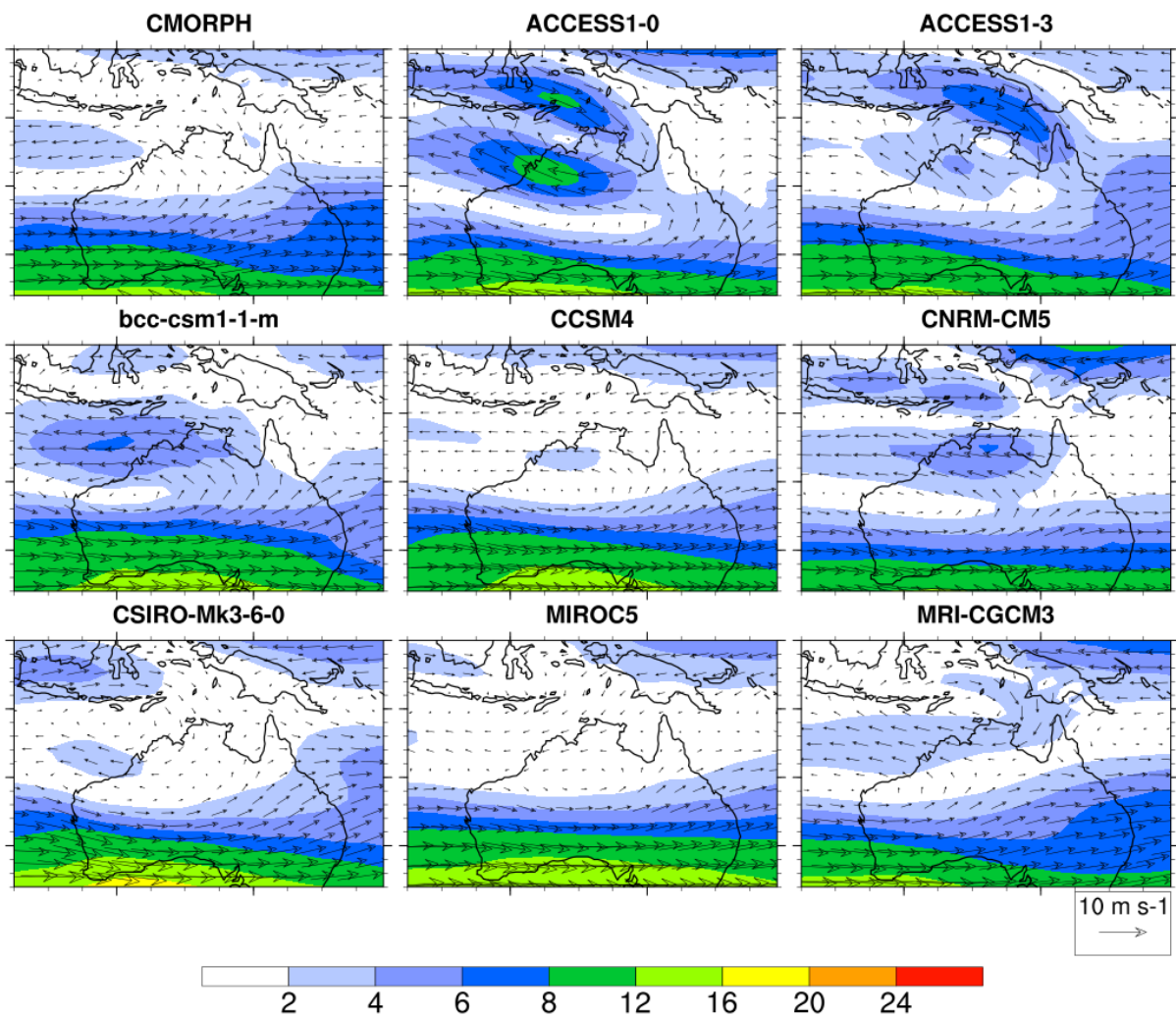


Figure A.23: 500hPa wind composites for regime 5 in each model.

At the 500 hPa level, the structure in each model for regime 5 is the same as for regime 4. The wind speeds are much weaker for MRI-CGM3, but a closed circulation is still evident.

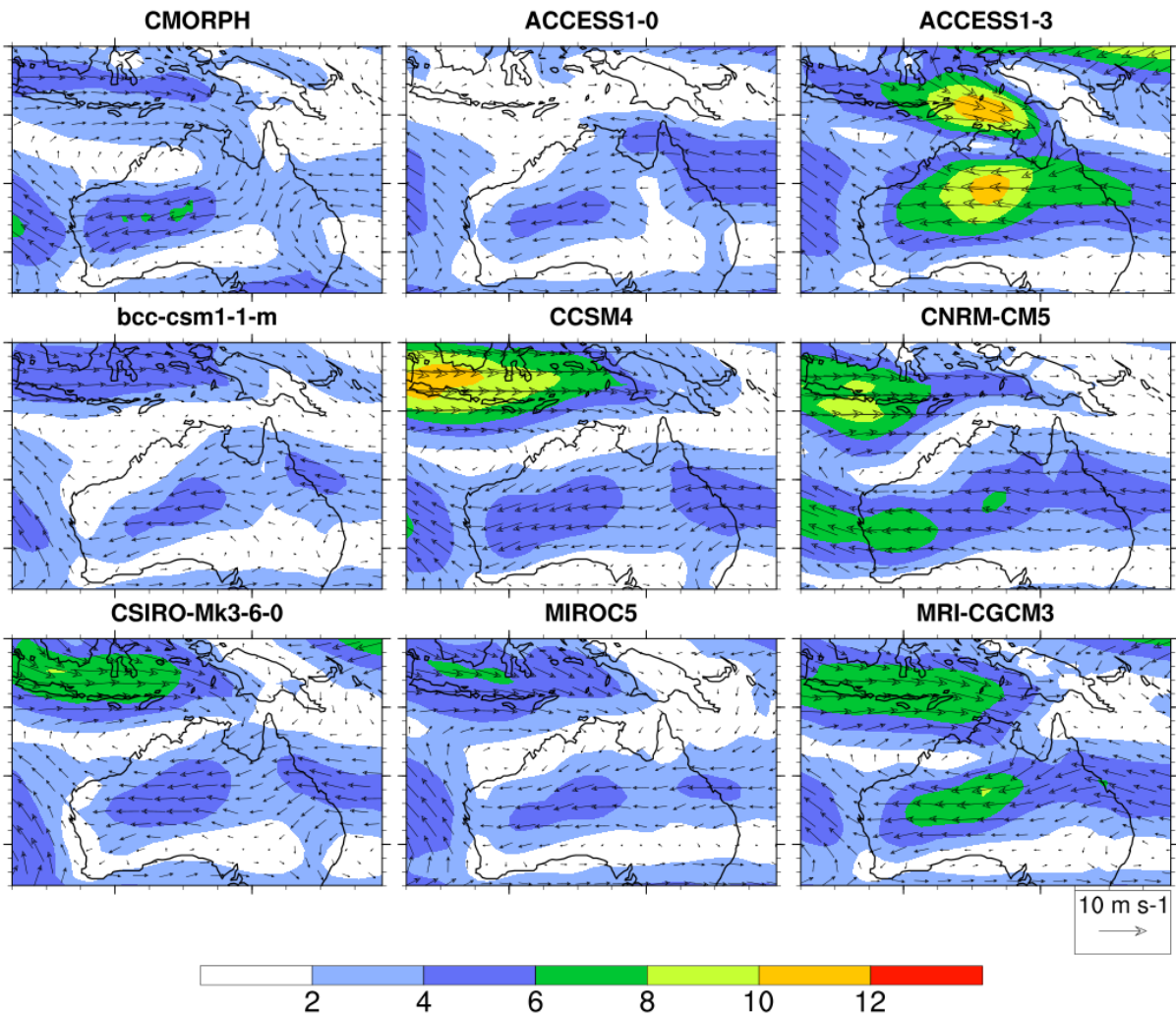


Figure A.24: 850hPa wind composites for regime 6 in each model

Regime 6 in the observations consists of rainfall inland of the Top End region, and is characterised by a broad low-level cyclonic circulation. However, ACCESS1-3 and CNRM-CM5 produce regimes with the maximum in a different location (see Figure 4.12). ACCESS1-3 produces a rainfall maximum over the eastern Top End, and associates it with a strong monsoon low. CNRM-CM5 produces a weak maximum over the Pilbara, which is associated with a broad, weak trough along the coast.

Of the remaining models that do replicate the observed rainfall pattern, many fail to replicate the wind fields associated with the observed rainfall pattern. In this case ACCESS1-

0 fails to replicate the observed monsoon low circulation, which is partly due to the weak rainfall maximum. CSIRO-Mk3-6-0 and CCSM4 show some evidence of a weak cyclonic circulation, indicating some ability to replicate the pattern. MRI-CGCM3 reproduce the system with wind speeds that are higher than the observations, with the centre located too far east in ACCESS1-3. MIROC5 and bcc-csm1-1-m show almost no sign of a closed circulation.

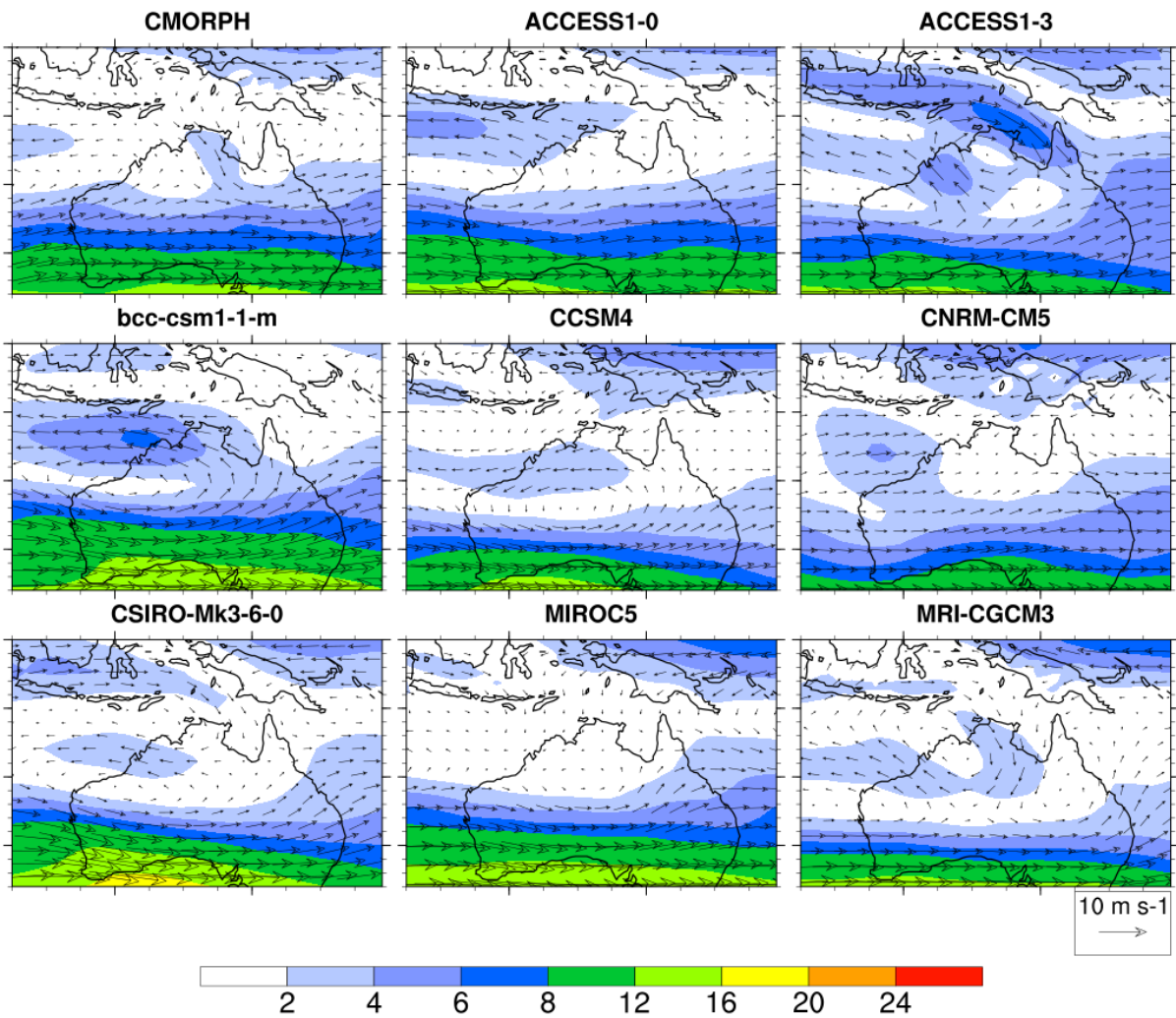


Figure A.25: 500hPa wind composites for regime 6 in each model.

The circulation at 500 hPa for regime 6 is weak in the observations, suggesting the forcing generally occurs at low levels. ACCESS1-3 shows a strong cyclonic circulation similar to the previous heavy regimes, indicating the nature of the circulation for this regime is highly

similar to the other heavy regimes. As for previous regimes, bcc-csm1-1-m and CCSM4 show an anticyclone over western and central Australia respectively, again showing little evidence of synoptic forcing. The remaining models show very little evidence of a closed circulation.

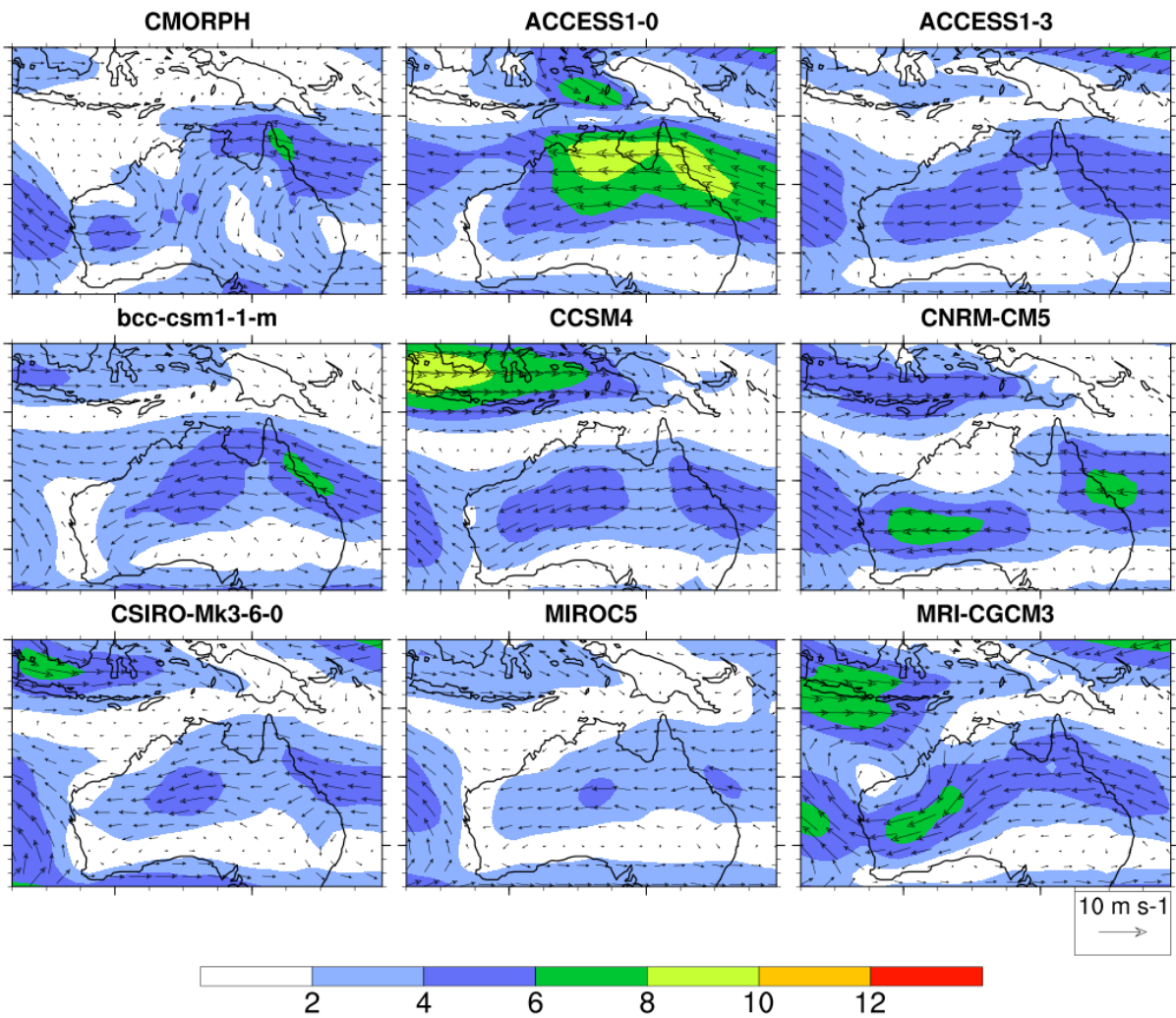


Figure A.26: 850hPa wind composites for regime 7 in each model.

Regime 7 in the observations is defined by rainfall far inland, in the south of the study region. However, the two ACCESS models fail to produce an inland maximum, and instead produce regimes with maxima close to the coast. In addition, bcc-csm1-1-m and CSIRO-Mk3-6-0 produce maxima that are located in the Pilbara, too far west. MRI-CGCM3 produces a cyclonic circulation over the Pilbara, which most closely resembles the observed pattern. The remaining models show little evidence of a closed circulation or trough which could

explain rainfall in the region. ACCESS1-0 produces a convergence line just north of the continent, explaining the offshore maximum in this regime.

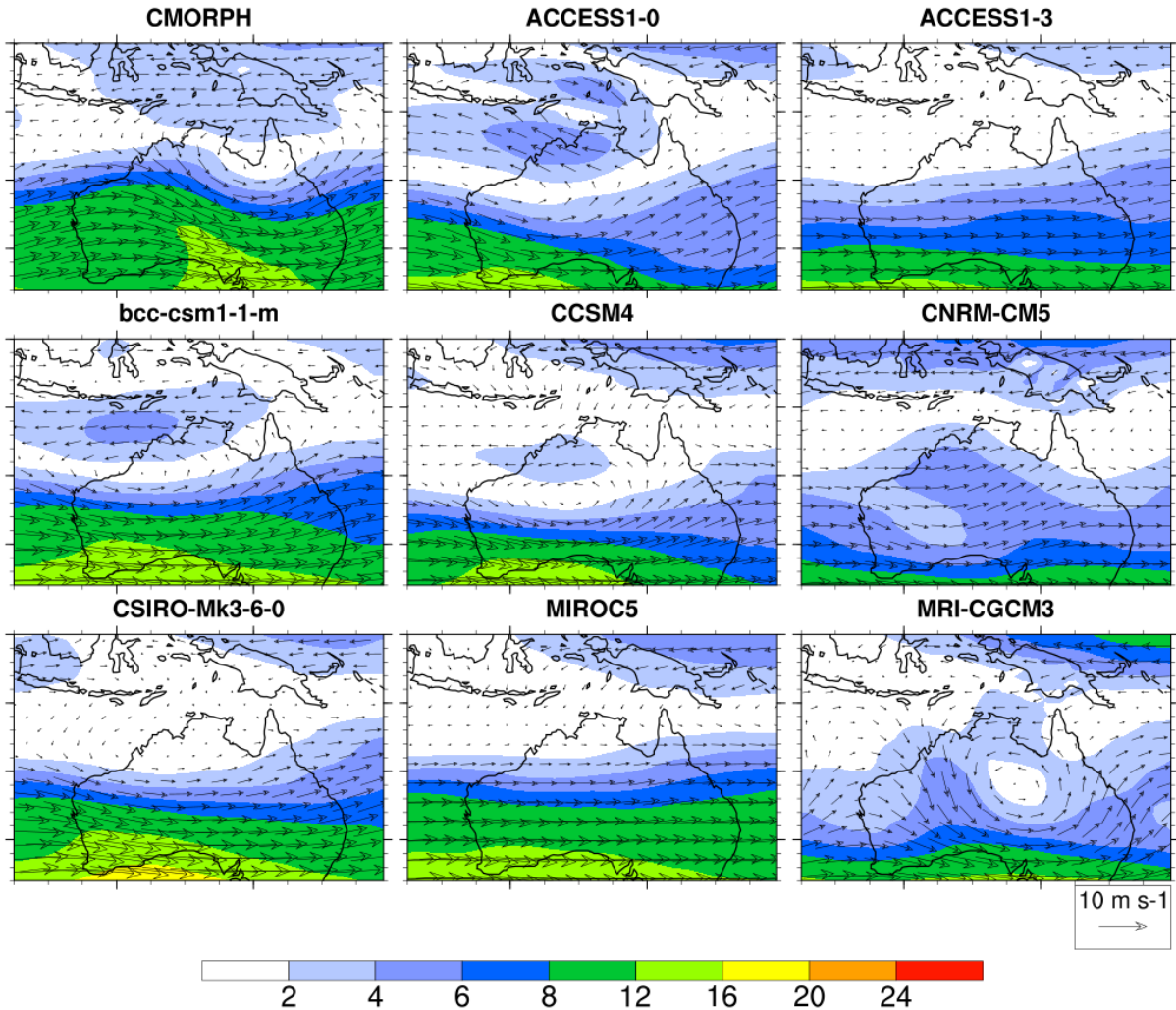


Figure A.27: 500hPa wind composites for regime 7 in each model.

In the observations, the main synoptic-scale characteristic for regime 7 is the mid-latitude wave pattern amplifying over the study region. This pattern is only clearly replicated in the 500 hPa winds by MRI-CGCM3, however as previously described, the Rossby wave pattern is most evident in the 250 hPa meridional wind composites, presented in Figure 4.18.

## A.4 Tropical cyclone wind fields

TC regimes are defined by determining the mean rainfall of all the days for which a TCLV is present in either the west or east part of the study region. These days were removed from the remaining data before applying any of the regime assignment methods covered in Chapters 3 to 5. The flow for the East Cyclone regime is in the main part of Chapter 4. The composites for the West Cyclone regime for each model is given here. The patterns in each model are very similar to the East Cyclone regime, with the low centre simply shifted westward.

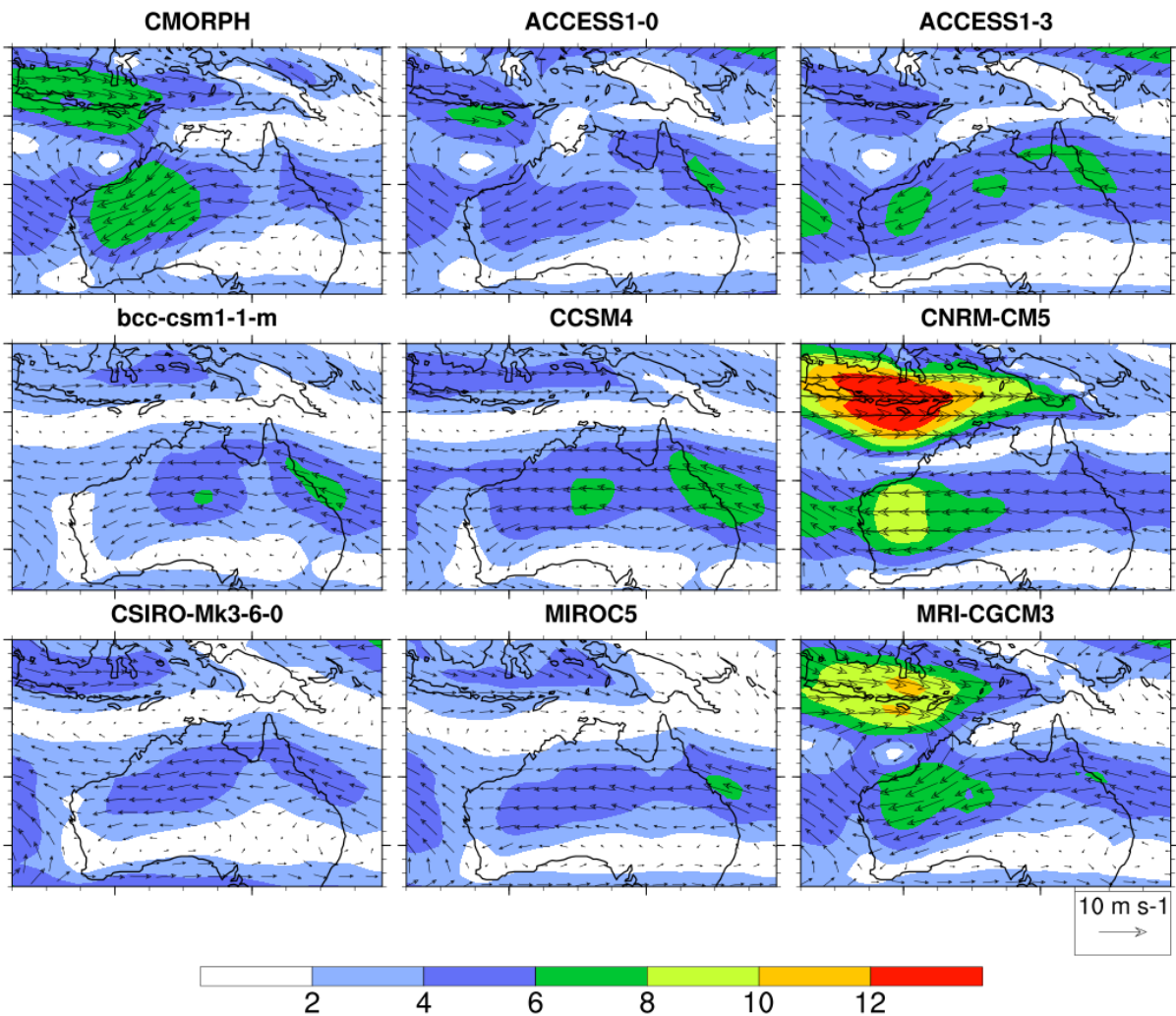


Figure A.28: 850hPa wind composites for regime 8 (western TCs) in each model.

## Appendix B

# CMIP5 RCP8.5 regimes - details of rainfall patterns and wind fields

### B.1 Projected future regimes - rainfall patterns

The projection method (method 1) is applied to daily rainfall under the RCP8.5 scenario. Rainfall under this scenario is projected to each model's independently determined regimes, since the aim is to understand how the model regimes evolve under future climate change.

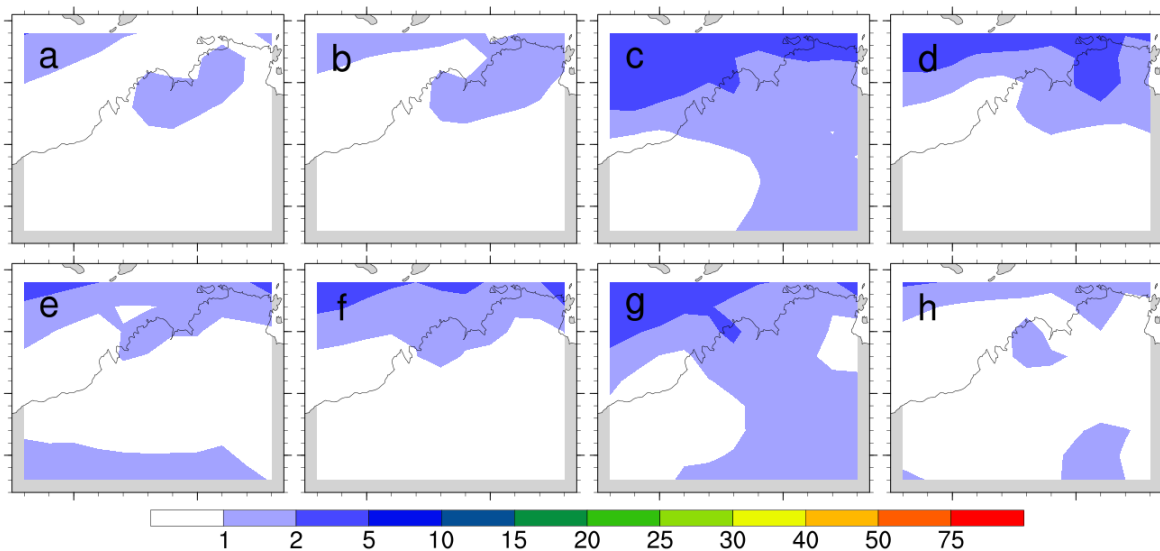


Figure B.1a: Rainfall spatial patterns for regime 1 from projecting RCP8.5 rainfall to each model's independent regimes.

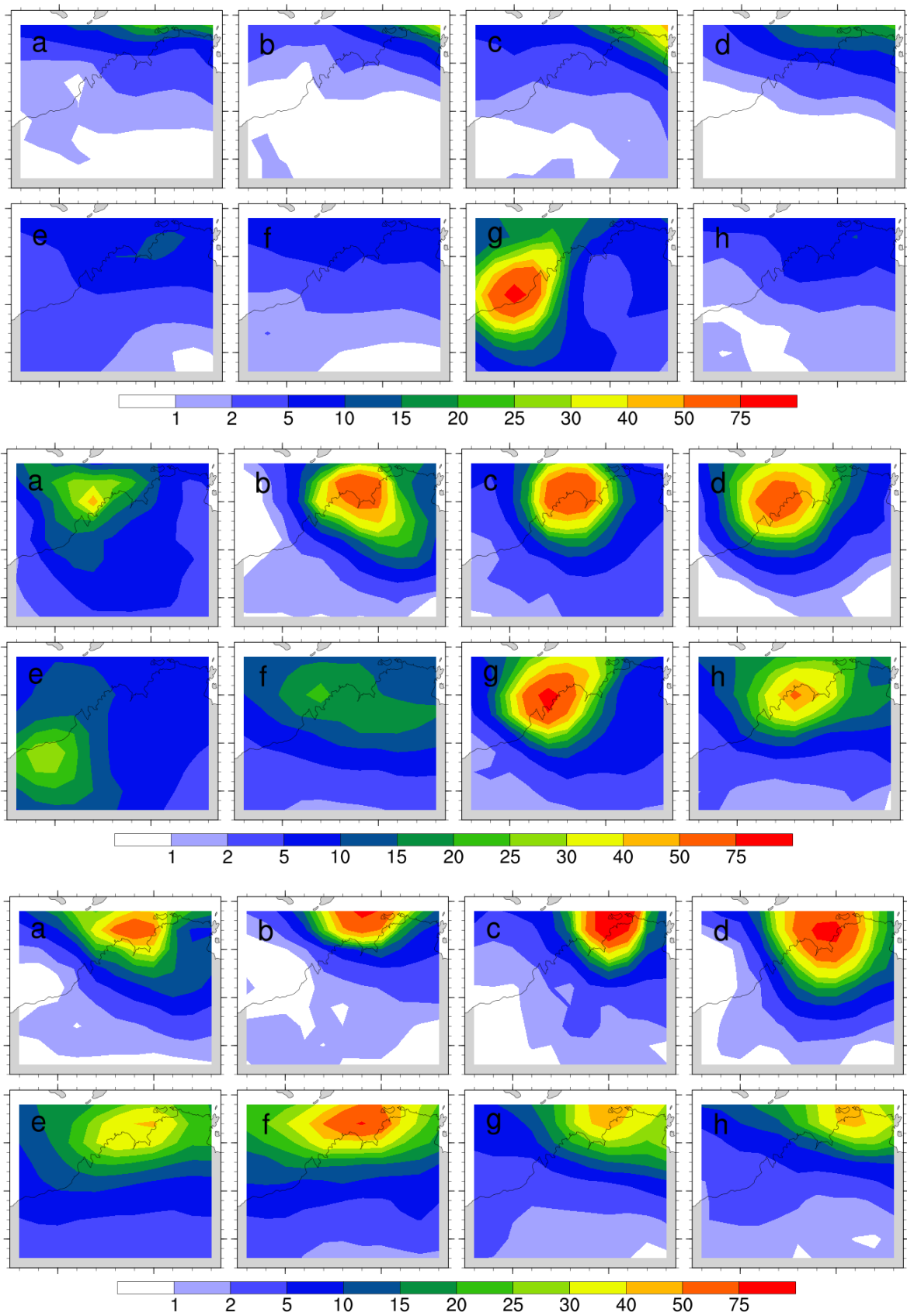


Figure B.1b: As before, for regimes 2 (top) to 4 (bottom).

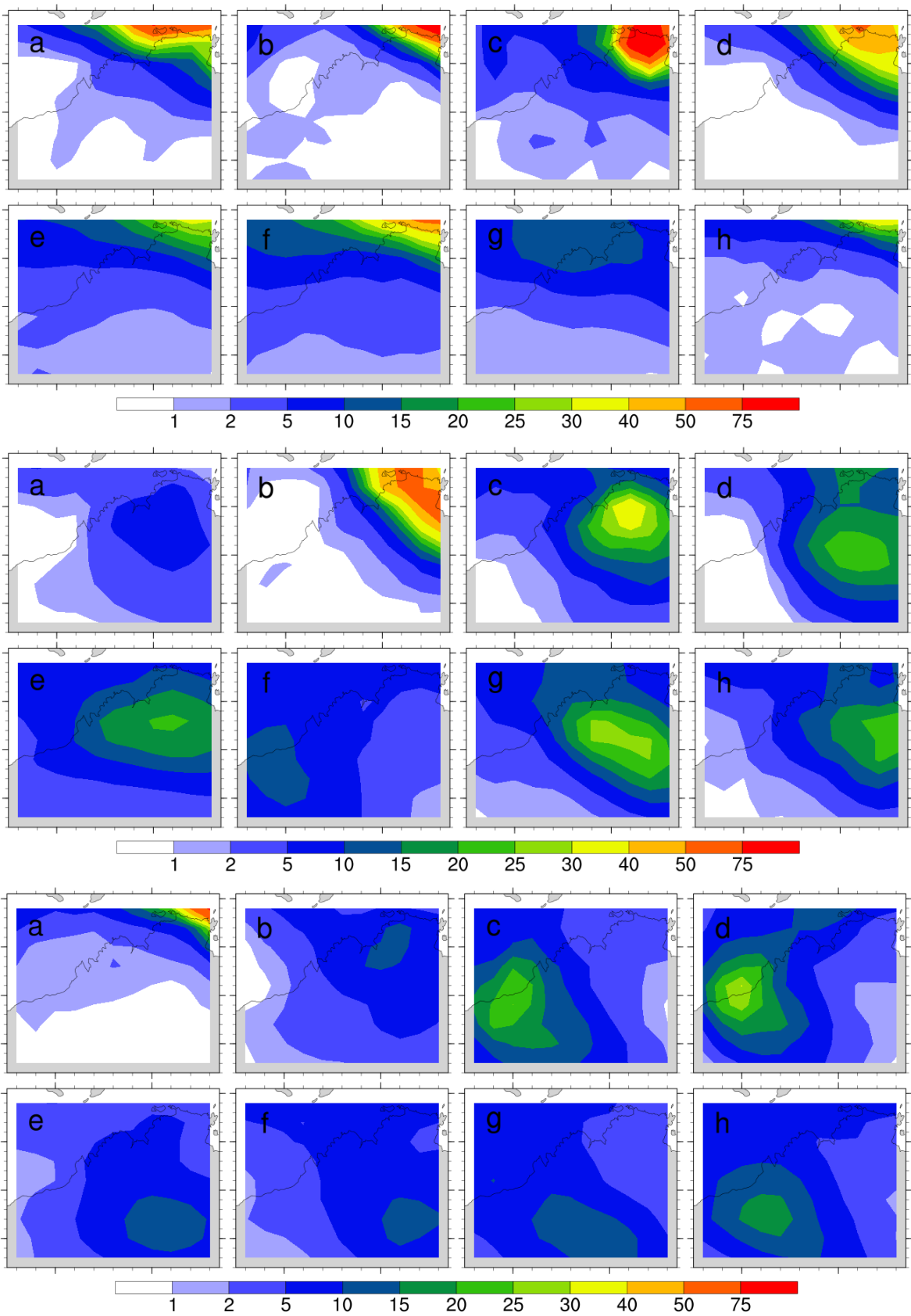


Figure B.1c: As before, for regimes 5 to 7.

When these plots are compared to those in Figures 4.11 to 4.13, we see the spatial

patterns for each regime and model are very similar to those from the historical period. The changes we note in Figure 5.3 are therefore mainly intensity changes, with only slight changes in spatial pattern.

## **B.2 Future regimes from projection method - wind anomalies**

The 850 hPa wind anomalies for each RCP8.5 projected regime relative to the historical period are given below. Regimes 1 and 4 are not shown since they are already shown in Section 5.4.5. In each plot, red shading indicates strengthening of wind speed, while blue indicates a reduction in wind speed. The vectors indicate the direction of the change. For instance, an east pointing vector on blue shading indicates a westerly anomaly, corresponding to a weakened easterly.

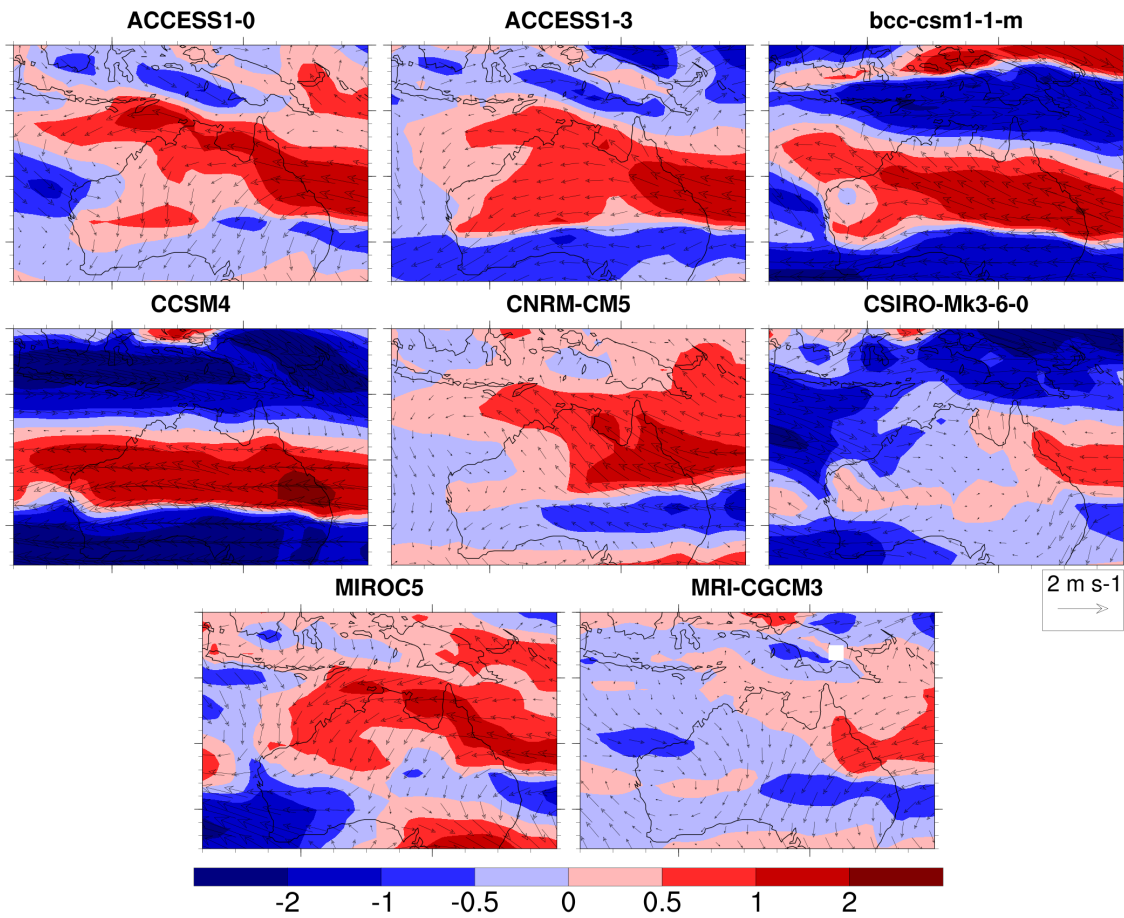


Figure B.2: 850 hPa wind anomalies for dry days in the RCP8.5 scenario relative to the historical period in each model

The low level flow for dry days shows strengthening south-easterlies over northern Australia in the ACCESS models, CNRM-CM5 and MIROC5, indicative of an expansion and strengthening of the Hadley circulation. CCSM4 and bcc-csm1-1-m show strengthened westerlies over central Australia with weakened westerlies to the north of the continent, suggesting the band of strongest winds has moved southward. CSIRO-Mk3-6-0 and MRI-CGCM3 show little change over the continent, but CSIRO-Mk3-6-0 shows severe weakening of the winds over the Indian Ocean.

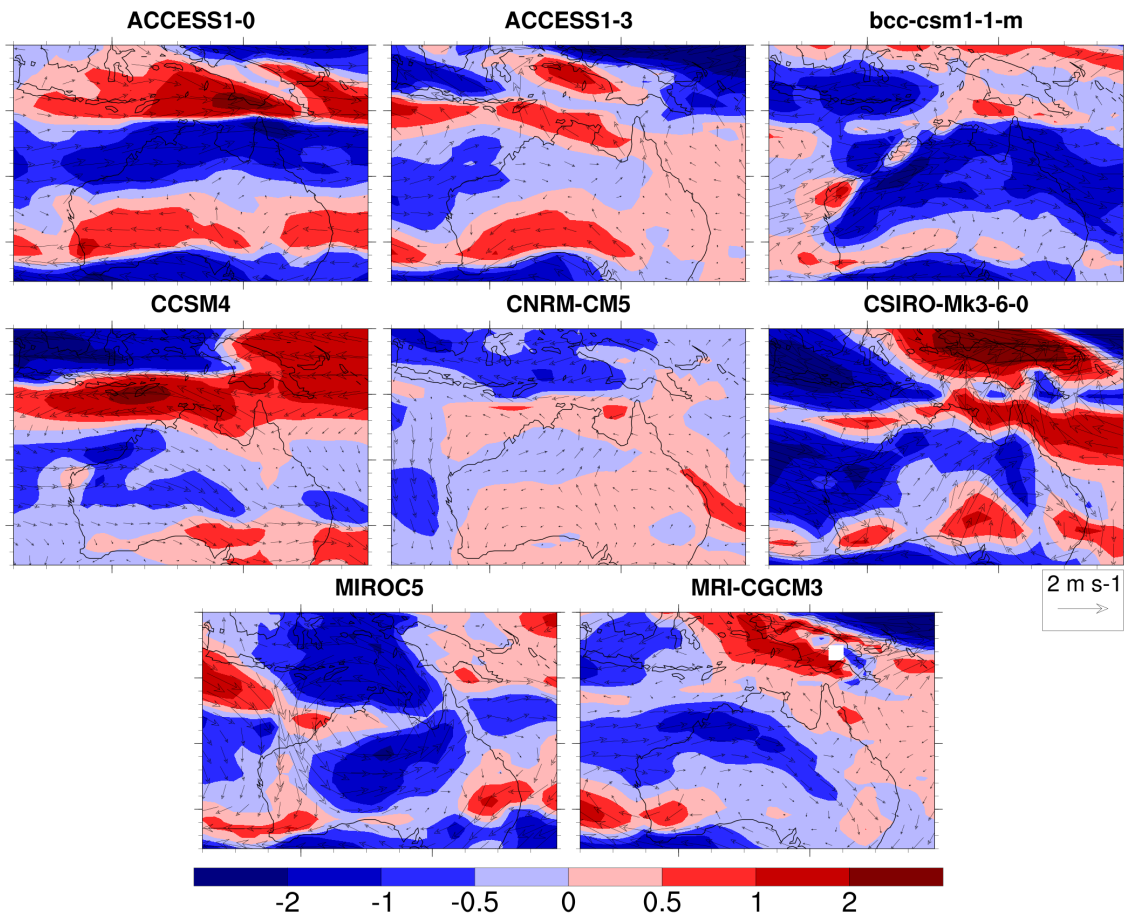


Figure B.3: 850 hPa wind anomalies for regime 2 in the RCP8.5 scenario relative to the historical period in each model

Regime 2 corresponds to moderate rainfall over northern Australia in most models, except MIROC5 where there is a more intense rainfall maximum located over the Pilbara. Weakening easterlies over inland regions are present in ACCESS1-0, bcc-csm1-1-m, CSIRO-Mk3-6-0 and MRI-CGCM3, although the shape of the anomaly plot varies across models. ACCESS1-3 shows slightly stronger convergence just north of the continent, while CCSM4 shows a strengthening of the southeasterlies over northern Australia. CNRM-CM5 shows little change. MIROC5, which produces a rainfall maximum over the Pilbara, is characterised in the historical period by a weak cyclonic circulation that becomes virtually non-existent in the future scenario, as shown by the anticyclonic anomaly above.

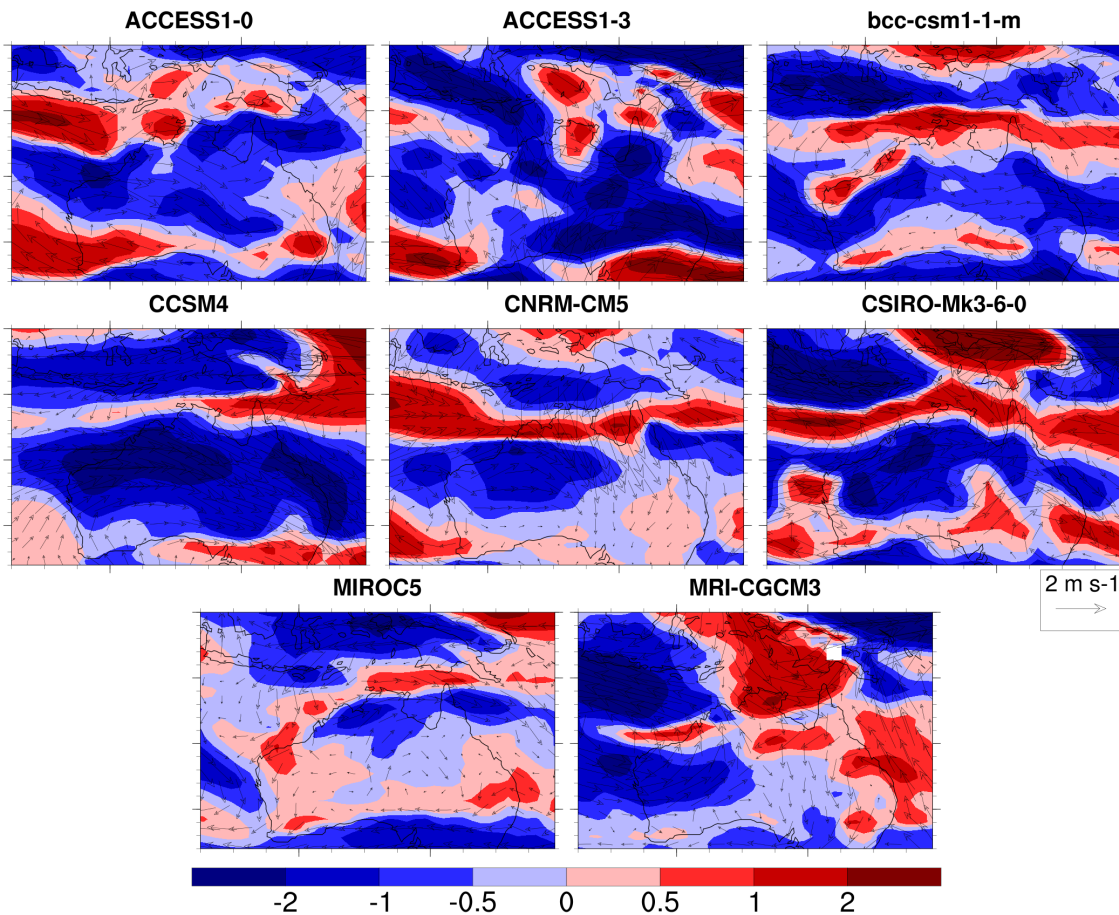


Figure B.4: 850 hPa wind anomalies for regime 3 in the RCP8.5 scenario relative to the historical period in each model

Regime 3 corresponds to a rainfall maximum located near the Kimberley region, except in CCSM4 where it is located over the Pilbara (see Figure 4.11). The monsoon low responsible for the rainfall in the historical period is well replicated in the ACCESS models and MRI-CGCM3. In ACCESS1-0, there is a strengthening of winds on the northern flank of the low, with a weakening on the southern flank. ACCESS1-3 and MRI-CGCM3 show a weakening of the entire low, shown by the anticyclone in the anomaly plots. bcc-csm1-1-m and CSIRO-Mk3-6-0 show enhanced easterlies just north of the continent, indicative of a northward movement of the monsoon trough, which agrees with the change in the mean flow over the monsoon period shown in Section 5.3. CCSM4 shows a significant weakening of the flow over central Australia and over the Maritime Continent. CNRM-CM5 shows a band of

strengthened westerlies, flanked on the south by weakened easterlies and on the north by weakened westerlies. Overall, this shows a southward movement of the monsoon trough in this model.

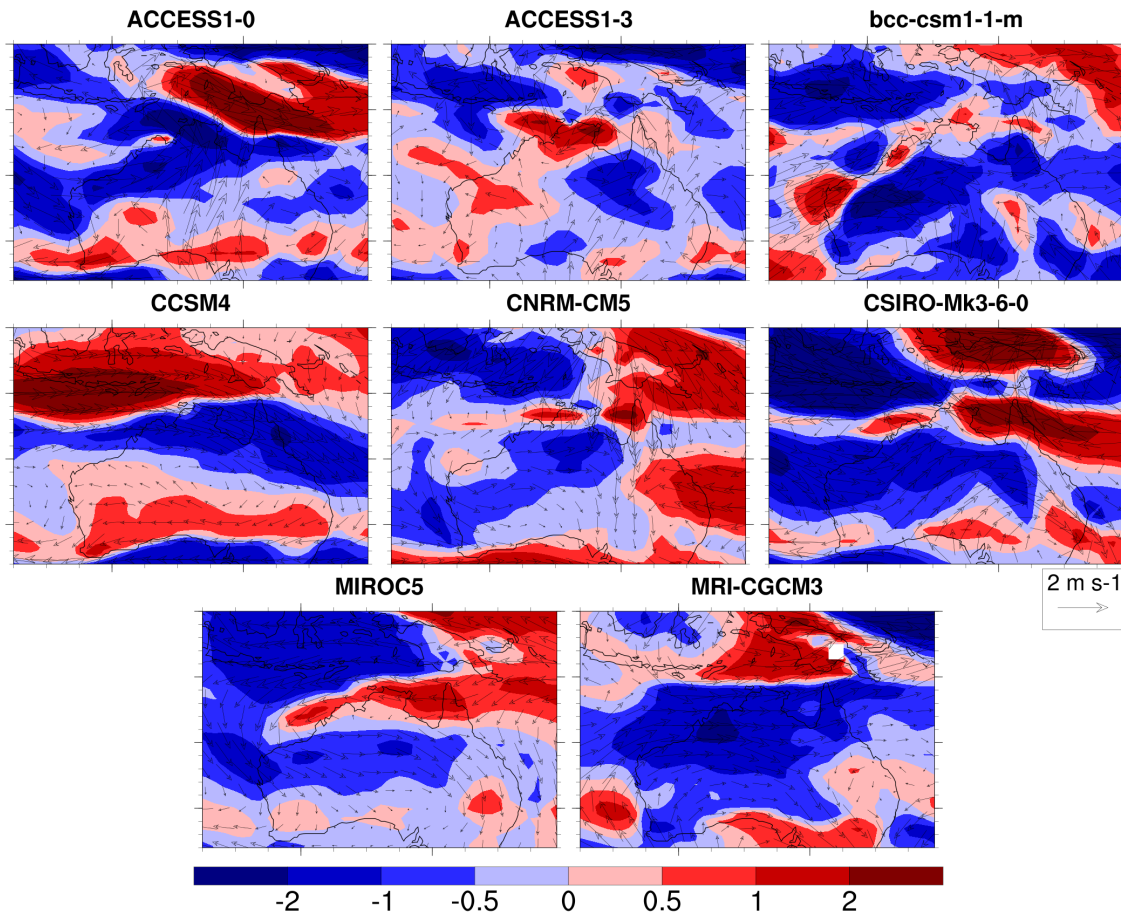


Figure B.5: 850 hPa wind anomalies for regime 5 in the RCP8.5 scenario relative to the historical period in each model

Regime 5 corresponds to a rainfall maximum over the Top End in all models, although the location and intensity of the central maximum varies. CCSM4 and MRI-CGCM3 show a weakening of the easterlies over the continent and strengthening of westerlies to the north of the continent in a similar way to previous regimes in the ACCESS models. ACCESS1-0 here appears to show a weakening of the southerlies over the Top End, however in the historical period the winds in that region are easterly. By comparing the historical and RCP8.5 composites, we note an eastward shift of the monsoon low in the future climate.

Strengthened easterlies are present in MIROC5. The remaining models show relatively little pattern that can explain any changes in rainfall.

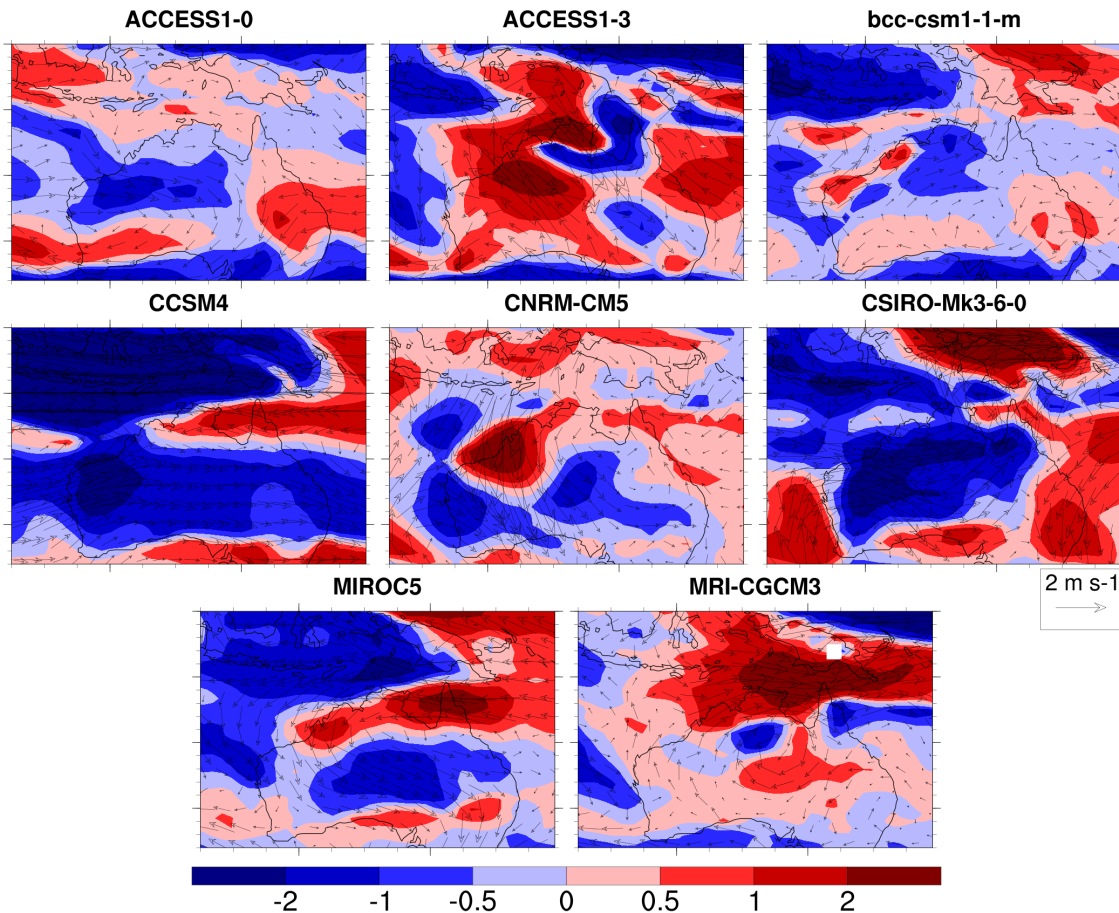


Figure B.6: 850 hPa wind anomalies for regime 6 in the RCP8.5 scenario relative to the historical period in each model

Regime 6 is defined in most models (and observations) by a rainfall maximum just inland of the Top End. MRI-CGCM3 produces strong increase in the strength of the westerly inflow into the low. CCSM4, MIROC5 and CSIRO-Mk3-6-0 show a similar weakening of the easterlies over the continent that have been observed in previous regimes, although these models have difficulty in replicating the wind fields responsible for rainfall in this regime. CNRM-CM5 produces a rainfall maximum over the Pilbara instead of inland from the Top End, but shows a strengthening of the circulation responsible for this rainfall. ACCESS1-3 produces a second rainfall maximum over the Top End for this regime, with higher intensity

than the historical period which is partly explained by enhanced circulation shown by the region of increased wind speed.

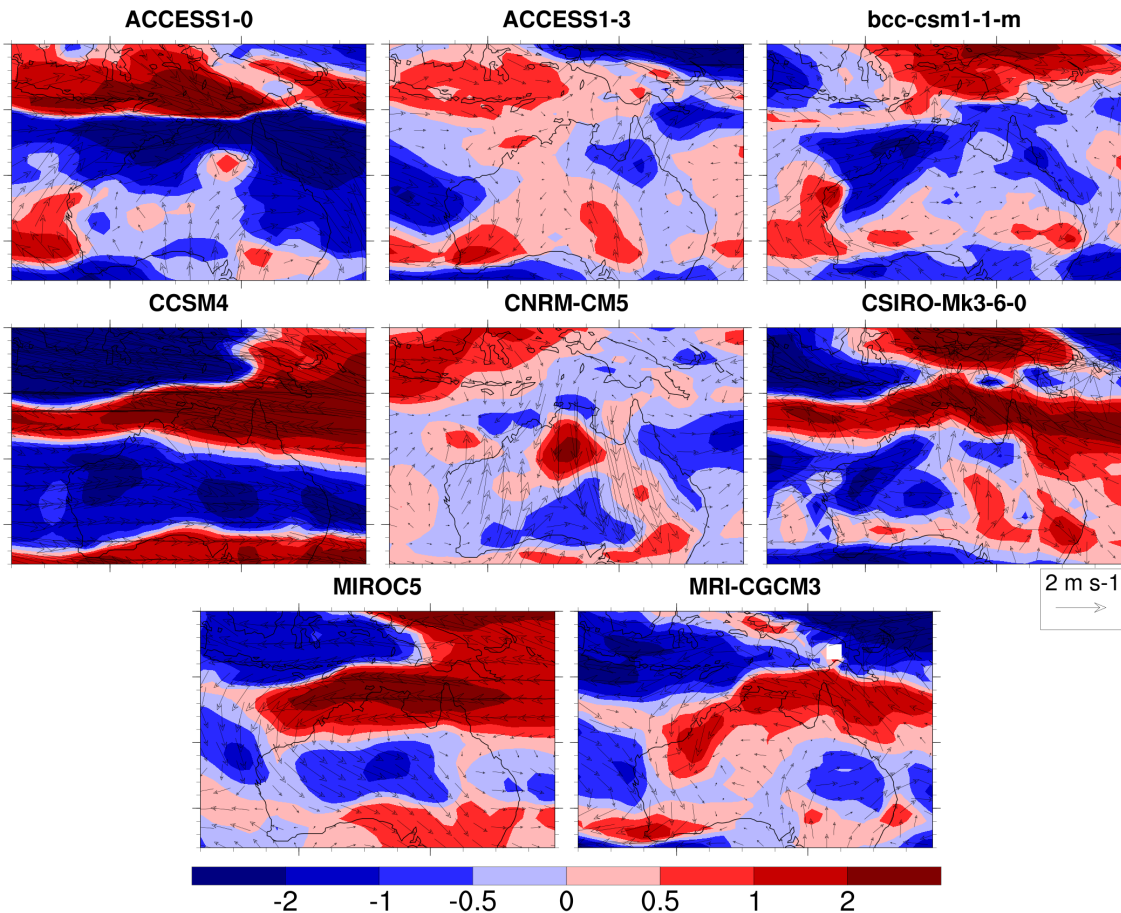


Figure B.7: 850 hPa wind anomalies for regime 7 in the RCP8.5 scenario relative to the historical period in each model

Regime 7 consists of a rainfall maximum either over the Pilbara or inland regions in most models, except in the ACCESS models where rainfall is located over the Top End. The 850 hPa wind fields do not adequately show the dynamics of the mid-latitude waves responsible for observed rainfall over this region, and thus any changes here say little about changes to the regimes. However, for ACCESS1-0 with the rainfall maximum offshore, the northern flank of the convergence line has enhanced winds with the southern flank having lower wind speeds.

## Bibliography

- Ackerley, D., Berry, G., Reeder, M. J., Jakob, C., and Schwendike, J. Summertime precipitation over northern Australia in AMIP simulations from CMIP5. *Quarterly Journal of the Royal Meteorological Society*, 141:1753–1768, 2015.
- Bengtsson, L., Botzet, M., and Esch, M. Hurricane-type vortices in a general circulation model. *Tellus*, 47(2):175–196, 1995.
- Berry, G., Reeder, M. J., and Jakob, C. Physical mechanisms regulating summertime rainfall over northwestern Australia. *Journal of Climate*, 24:3705–3717, 2011.
- Berry, G., Reeder, M. J., and Jakob, C. Coherent synoptic disturbances in the Australian monsoon. *Journal of Climate*, 25:8409–8421, 2012.
- Berry, G. J. and Reeder, M. J. The Dynamics of Australian Monsoon Bursts. *Journal of the Atmospheric Sciences*, 73(1):55–69, 2016.
- Bi, D., Dix, M., Marsland, S. J., O'Farrell, S., Rashid, H. A., Uotila, P., Hirst, A. C., Kowalczyk, E., Golebiewski, M., Sullivan, A., Yan, H., Hannah, N., Franklin, C., Sun, Z., Vohralik, P., Watterson, I., Zhou, X., Fiedler, R., Collier, M., Ma, Y., Noonan, J., Stevens, L., Uhe, P., Zhu, H., Griffies, S. M., Hill, R., Harris, C., and Puri, K. The ACCESS coupled model: description, control climate and evaluation. *Australian Meteorological and Oceanographic Journal*, 63(1):41–64, 2013.
- Brown, J. R., Moise, A. F., Colman, R., and Zhang, H. Will a Warmer World Mean a Wetter or Drier Australian Monsoon? *Journal of Climate*, 29(12):4577–4596, 2016.
- Catto, J., Jakob, C., and Nicholls, N. The influence of changes in synoptic regimes on north Australian wet season rainfall trends. *Journal of Geophysical Research*, 117:1–9, 2012.

Christensen, J. H., Kanikicharla, K. K., Aldrian, E., An, S.-I., Albuquerque Cavalcanti, I. F., de Castro, M., Dong, W., Goswami, P., Hall, A., Kanyanga, J. K., Kitoh, A., Kossin, J., Lau, N.-C., Renwick, J., Stephenson, D. B., Xie, S.-P., Zhou, T., Abraham, L., Ambrizzi, T., Anderson, B., Arakawa, O., Arritt, R., Baldwin, M., Barlow, M., Barriopedro, D., Bia-sutti, M., Biner, S., Bromwich, D., Brown, J., Cai, W., Carvalho, L. V., Chang, P., Chen, X., Choi, J., Christensen, O. B., Deser, C., Emanuel, K., Endo, H., Enfield, D. B., Evan, A., Giannini, A., Gillett, N., Hariharasubramanian, A., Huang, P., Jones, J., Karumuri, A., Katzfey, J., Kjellstrom, E., Knight, J., Knutson, T., Kulkarni, A., Kundeti, K. R., Lau, W. K., Lenderink, G., Lennard, C., Leung, L.-y. R., Lin, R., Losada, T., Mackellar, N. C., Magana, V., Marshall, G., Mearns, L., Meehl, G., Menendez, C., Murakami, H., Nath, M. J., Neelin, J. D., van Oldenborgh, G. J., Olesen, M., Polcher, J., Qian, Y., Ray, S., Reich, K. D., Rodriguez de Fonseca, B., Ruti, P., Screen, J., Sedlacek, J., Solman, S., Stendel, M., Stevenson, S., Takayabu, I., Turner, J., Ummenhofer, C., Walsh, K., Wang, B., Wang, C., Watterson, I., Widlansky, M., Wittenberg, A., Woollings, T., Yeh, S.-W., Zhang, C., Zhang, L., Zheng, X., and Zou, L. Climate Phenomena and their Relevance for Future Regional Climate Change. In Stocker, TF and Qin, D and Plattner, GK and Tignor, MMB and Allen, SK and Boschung, J and Nauels, A and Xia, Y and Bex, V and Midgley, PM, editor, *Climate Change 2013: The Physical Science Basis*, pages 1217–1308. Cambridge Univ. Press, The Pitt Building, Trumpington St, Cambridge CB2 1RP, Cambs, England, 2014. ISBN 978-1-107-05799-9; 978-1-107-66182-0.

Clark, S., Reeder, M. J., and Jakob, C. Rainfall regimes over northwestern Australia. *Quarterly Journal of the Royal Meteorological Society*, 144(711, B):458–467, 2018.

Davidson, N., McBride, J., and McAveney, B. The onset of the Australian monsoon during winter monex - synoptic aspects. *Monthly Weather Review*, 111(3):496–516, 1983.

Davidson, N. E., Tory, K. J., Reeder, M. J., and Drosowsky, W. L. Extratropical - Tropical interaction during onset of the Australian monsoon: Reanalysis diagnostics and idealized dry simulations. *Journal of the Atmospheric Sciences*, 64(10):3475–3498, 2007.

Dee, D. P., Uppala, S. M., Simmons, A. J., Berrisford, P., Poli, P., Kobayashi, S., Andrae, U., Balmaseda, M. A., Balsamo, G., Bauer, P., Bechtold, P., Beljaars, A. C. M., van de Berg, L., Bidlot, J., Bormann, N., Delsol, C., Dragani, R., Fuentes, M., Geer, A. J., Haimberger, L., Healy, S. B., Hersbach, H., Holm, E. V., Isaksen, L., Kallberg, P., Koehler,

- M., Matricardi, M., McNally, A. P., Monge-Sanz, B. M., Morcrette, J. J., Park, B. K., Peubey, C., de Rosnay, P., Tavolato, C., Thepaut, J. N., and Vitart, F. The ERA-Interim reanalysis: configuration and performance of the data assimilation system. *Quarterly Journal of the Royal Meteorological Society*, 137(656, A):553–597, APR 2011.
- Dowdy, A. J. Long-term changes in Australian tropical cyclone numbers. *Atmospheric Science Letters*, 15(4):292–298, 2014.
- Emanuel, K. A. Downscaling CMIP5 climate models shows increased tropical cyclone activity over the 21st century. *Proceedings of the National Academy of Sciences of the United States of America*, 110(30):12219–12224, 2013.
- Emori, S. and Brown, S. J. Dynamic and thermodynamic changes in mean and extreme precipitation under changed climate. *Geophysical Research Letters*, 32:1–5, 2005.
- Evans, S., Marchand, R., and Ackerman, T. Variability of the Australian Monsoon and Precipitation Trends at Darwin. *Journal of Climate*, 27(22):8487–8500, 2014.
- Feng, J., Li, J., and Xu, H. Increased summer rainfall in northwest Australia linked to southern Indian Ocean climate variability. *Journal of Geophysical Research-Atmospheres*, 118(2):467–480, 2013.
- Flato, G., Marotzke, J., Abiodun, B., Braconnot, P., Chou, S. C., Collins, W., Cox, P., Driouech, F., Emori, S., Eyring, V., Forest, C., Gleckler, P., Guilyardi, E., Jakob, C., Kattsov, V., Reason, C., Rummukainen, M., AchutaRao, K., Anav, A., Andrews, T., Baehr, J., Bindoff, N. L., Bodas-Salcedo, A., Catto, J., Chambers, D., Chang, P., Dai, A., Deser, C., Doblas-Reyes, F., Durack, P. J., Eby, M., de Elia, R., Fichet, T., Forster, P., Frame, D., Fyfe, J., Gbobaniyi, E., Gillett, N., Fidel Gonzalez-Rouco, J., Goodess, C., Griffies, S., Hall, A., Harrison, S., Hense, A., Hunke, E., Ilyina, T., Ivanova, D., Johnson, G., Kageyama, M., Kharin, V., Klein, S. A., Knight, J., Knutti, R., Landerer, F., Lee, T., Li, H., Mahowald, N., Mears, C., Meehl, G., Morice, C., Msadek, R., Myhre, G., Neelin, J. D., Painter, J., Pavlova, T., Perlwitz, J., Peterschmitt, J.-Y., Raisanen, J., Rausser, F., Reid, J., Rodwell, M., Santer, B., Scaife, A. A., Schulz, J., Scinocca, J., Sexton, D., Shindell, D., Shiogama, H., Sillmann, J., Simmons, A., Sperber, K., Stephenson, D., Stevens, B., Stott, P., Sutton, R., Thorne, P. W., van Oldenborgh, G. J., Vecchi, G., Webb, M., Williams, K., Woollings, T., Xie, S.-P., and Zhang, J. Evaluation of Climate

- Models. In Stocker, TF and Qin, D and Plattner, GK and Tignor, MMB and Allen, SK and Boschung, J and Nauels, A and Xia, Y and Bex, V and Midgley, PM, editor, *Climate Change 2013: The Physical Science Basis*, pages 741–866. Cambridge Univ. Press, The Pitt Building, Trumpington St, Cambridge CB2 1RP, Cambs, England, 2014. ISBN 978-1-107-05799-9; 978-1-107-66182-0.
- Frederiksen, C. S. and Grainger, S. The role of external forcing in prolonged trends in Australian rainfall. *Climate Dynamics*, 45:2455–2468, 2015.
- Gent, P. R., Danabasoglu, G., Donner, L. J., Holland, M. M., Hunke, E. C., Jayne, S. R., Lawrence, D. M., Neale, R. B., Rasch, P. J., Vertenstein, M., Worley, P. H., Yang, Z.-L., and Zhang, M. The Community Climate System Model Version 4. *Journal of Climate*, 24 (19):4973–4991, OCT 1 2011.
- George, J. *Weather Forecasting for Aeronautics*. Academic Press, 1960.
- Grainger, S., Frederiksen, C. S., and Zheng, X. Assessment of Modes of Interannual Variability of Southern Hemisphere Atmospheric Circulation in CMIP5 Models. *Journal of Climate*, 27(21):8107–8125, 2014.
- Held, I. M. and Soden, B. J. Robust responses of the hydrological cycle to global warming. *Journal of Climate*, 19(21):5686–5699, 2006.
- Hoang, L. P., Reeder, M. J., Berry, G., and Schwendike, J. Coherent potential vorticity maxima and their relationship to extreme summer rainfall in the Australian and north African tropics. *Journal of Southern Hemisphere Earth Systems Science*, 66:424–440, 2016.
- Holland, G. Interannual variability of the australian summer monsoon at darwin - 1952-82. *Monthly Weather Review*, 114(3):594–604, 1986.
- Hurley, J. V. and Boos, W. R. A global climatology of monsoon low-pressure systems. *Quarterly Journal of the Royal Meteorological Society*, 141:1049–1064, 2015.
- Jiang, H. and Zipser, E. J. Contribution of tropical cyclones to the global precipitation from eight seasons of TRMM data: Regional, seasonal, and interannual variations. *Journal of Climate*, 23:1526–1537,1539–1543, 2010.

- Jones, D. A., Wang, W., and Fawcett, R. High-quality spatial climate data-sets for Australia. *Australian Meteorological and Oceanographic Journal*, 58(4):233–248, 2009.
- Jourdain, N. C., Sen Gupta, A., Taschetto, A. S., Ummenhofer, C. C., Moise, A. F., and Ashok, K. The Indo-Australian monsoon and its relationship to ENSO and IOD in reanalysis data and the CMIP3/CMIP5 simulations. *Climate Dynamics*, 41(11-12):3073–3102, 2013.
- Joyce, R. J., Janowiak, J. E., Arkin, P. A., and Xie, P. Cmorph: A method that produces global precipitation estimates from passive microwave and infrared data at high spatial and temporal resolution. *Journal of Hydrometeorology*, 5:487–503, 2004.
- King, A. D., Alexander, L. V., and Donat, M. G. The efficacy of using gridded data to examine extreme rainfall characteristics: a case study for Australia. *INTERNATIONAL JOURNAL OF CLIMATOLOGY*, 33(10):2376–2387, AUG 2013.
- Knapp, K. R., Kruk, M. C., Levinson, D. H., Diamond, H. J., and Neumann, C. J. The International Best Track Archive for Climate Stewardship (IBTrACS): Unifying Tropical Cyclone Data. *Bulletin of the American Meteorological Society*, 91(3):363+, 2010.
- Knutson, T. R., Sirutis, J. J., Zhao, M., Tuleya, R. E., Bender, M., Vecchi, G. A., Villarini, G., and Chavas, D. Global projections of intense tropical cyclone activity for the late twenty-first century from dynamical downscaling of cmip5/rcp4.5 scenarios. *Journal of Climate*, 28(18):7203–7224, 2015.
- Knutson, T. R., McBride, J. L., Chan, J., Emanuel, K., Holland, G., Landsea, C., Held, I., Kossin, J. P., Srivastava, A. K., and Sugi, M. Tropical cyclones and climate change. *NATURE GEOSCIENCE*, 3(3):157–163, MAR 2010.
- Knutti, R. and Sedlacek, J. Robustness and uncertainties in the new CMIP5 climate model projections. *Nature Climate Change*, 3(4):369–373, 2013.
- Krakauer, N. Y. and Fekete, B. M. Are climate model simulations useful for forecasting precipitation trends? hindcast and synthetic-data experiments. *Environmental Research Letters*, 9(2):024009, 2014.
- Kuleshov, Y., Fawcett, R., Qi, L., Trewin, B., Jones, D., McBride, J., and Ramsay, H. Trends

- in tropical cyclones in the South Indian Ocean and the South Pacific Ocean. *Journal of Geophysical Research-Atmospheres*, 115, 2010.
- Kumar, S., Merwade, V., III, J. L. K., and Niyogi, D. Evaluation of temperature and precipitation trends and long-term persistence in cmip5 twentieth-century climate simulations. *Journal of Climate*, 26(12):4168–4185, 2013.
- Lavender, S. L. and Walsh, K. J. E. Dynamically downscaled simulations of Australian region tropical cyclones in current and future climates. *Geophysical Research Letters*, 38, 2011.
- Lavender, S. L. and Abbs, D. J. Trends in Australian rainfall: contribution of tropical cyclones and closed lows. *Climate Dynamics*, 40:317–326, 2013.
- Manabe, S., Holloway, J., and Stone, H. Tropical circulation in a time-integration of a global model of the atmosphere. *Journal of the Atmospheric Sciences*, 27(4):580–&, 1970.
- Mapes, B. and Houze, R. A. An integrated view of the 1987 Australian monsoon and its mesoscale convective systems. I: Horizontal structure. *Quarterly Journal of the Royal Meteorological Society*, 118:927–963, 1992.
- Moise, A., Wilson, L., Grose, M., Whetton, P., Watterson, I., Bhend, J., Bathols, J., Hanson, L., Erwin, T., Bedin, T., Heady, C., and Rafter, T. Evaluation of CMIP3 and CMIP5 Models over the Australian Region to Inform Confidence in Projections. *Australian Meteorological and Oceanographic Journal*, 65(1):19–53, 2015.
- Murakami, H. and Sugi, M. Effect of model resolution on tropical cyclone climate projections. *SOLA*, 6:73–76, 2010.
- Murphy, Jr., M. J., Siems, S. T., and Manton, M. J. Regional Variation in the Wet Season of Northern Australia. *Monthly Weather Review*, 144(12):4941–4962, 2016.
- Narsey, S., Reeder, M. J., Ackerley, D., and Jakob, C. A Midlatitude Influence on Australian Monsoon Bursts. *Journal of Climate*, 30(14):5377–5393, 2017.
- Ng, B., Walsh, K., and Lavender, S. The contribution of tropical cyclones to rainfall in northwest Australia. *International Journal of Climatology*, 35(10):2689–2697, 2015.
- Nguyen, K. and Walsh, K. Interannual, decadal, and transient greenhouse simulation of tropical cyclone-like vortices in a regional climate model of the South Pacific. *Journal of Climate*, 14(13):3043–3054, 2001.

- Pascale, S., Lucarini, V., Feng, X., Porporato, A., and Hasson, S. U. Analysis of rainfall seasonality from observations and climate models. *Climate Dynamics*, 44(11-12):3281–3301, 2015. Copyright - Springer-Verlag Berlin Heidelberg 2015; Document feature - ; Last updated - 2015-07-01.
- Pope, M., Reeder, M. J., and Jakob, C. Regimes of the north Australian wet season. *Journal of Climate*, 22:6699–6715, 2009.
- Ramsay, H. A., Leslie, L. M., Lamb, P. J., Richman, M. B., and Leplastrier, M. Interannual variability of tropical cyclones in the Australian region: Role of large-scale environment. *Journal of Climate*, 21:1083–1103, 2008.
- Raut, B., Jakob, C., and Reeder, M. J. Rainfall changes over south-western Australia and their relationship to the southern annular mode and ENSO. *Journal of Climate*, 27:5801–5814, 2014.
- Reeder, M. J. and Smith, R. K. Mesoscale meteorology. In Karoly, D. J. and Vincent, D. G., editors, *Meteorology of the Southern Hemisphere*, pages 201–241. American Meteorological Society, 1998.
- Ren, D. and Leslie, L. Changes in tropical cyclone activity over northwest Western Australia in the past 50 years and a view of the future 50 years. *Earth Interactions*, 19:1–24, 2015.
- Rotstayn, L. D., Cai, W., Dix, M. R., Farquhar, G. D., Feng, Y., Ginoux, P., Herzog, M., Ito, A., Penner, J. E., Roderick, M. L., and Wang, M. Have Australian rainfall and cloudiness increased due to the remote effects of Asian anthropogenic aerosols? *Journal of Geophysical Research*, 112:D09202, 2007.
- Rotstayn, L. D., Collier, M. A., Dix, M. R., Feng, Y., Gordon, H. B., O'Farrell, S. P., Smith, I. N., and Syktus, J. Improved simulation of Australian climate and ENSO-related rainfall variability in a global climate model with an interactive aerosol treatment. *International Journal of Climatology*, 30(7):1067–1088, 2010.
- Shi, G., Cai, W., Cowan, T., Ribbe, J., Rotstayn, L., and Dix, M. Variability and trend of north west Australia rainfall: Observations and coupled climate modeling. *Journal of Climate*, 21:2938–2959, 2007.

- Smith, I. An assessment of recent trends in Australian rainfall. *Australian Meteorological Magazine*, 53:163–173, 2004.
- Smith, I., Wilson, L., and Suppiah, R. Characteristics of the north Australian rainy season. *Journal of Climate*, 21:4298–4311, 2008.
- Stephens, G. L., L'Ecuyer, T., Forbes, R., Gettelman, A., Golaz, J.-C., Bodas-Salcedo, A., Suzuki, K., Gabriel, P., and Haynes, J. Dreary state of precipitation in global models. *Journal of Geophysical Research-Atmospheres*, 115, 2010.
- Suppiah, R. The Australian Summer Monsoon - A Review. *Progress in Physical Geography*, 16(3):283–318, 1992.
- Taschetto, A. S. and England, M. H. An analysis of late twentieth century trends in Australian rainfall. *International Journal of Climatology*, 29(6):791–807, 2009.
- Utsumi, N., Kim, H., Kanae, S., and Oki, T. Which weather systems are projected to cause future changes in mean and extreme precipitation in cmip5 simulations? *Journal of Geophysical Research: Atmospheres*, 121(18):10,522–10,537, 2016. 2016JD024939.
- Vitart, F., Anderson, J., and Stern, W. Simulation of interannual variability of tropical storm frequency in an ensemble of GCM integrations. *Journal of Climate*, 10(4):745–760, 1997.
- Voltaire, A., Sanchez-Gomez, E., Salas y Melia, D., Decharme, B., Cassou, C., Senesi, S., Valcke, S., Beau, I., Alias, A., Chevallier, M., Deque, M., Deshayes, J., Douville, H., Fernandez, E., Madec, G., Maisonnave, E., Moine, M.-P., Planton, S., Saint-Martin, D., Szopa, S., Tyteca, S., Alkama, R., Belamari, S., Braun, A., Coquart, L., and Chauvin, F. The CNRM-CM5.1 global climate model: description and basic evaluation. *Climate Dynamics*, 40(9-10, SI):2091–2121, 2013.
- Walsh, K. J. E., Fiorino, M., Landsea, C. W., and McInnes, K. L. Objectively determined resolution-dependent threshold criteria for the detection of tropical cyclones in climate models and reanalyses. *Journal of Climate*, 20(10):2307–2314, 2007.
- Walsh, K., Nguyen, K., and McGregor, J. Fine-resolution regional climate model simulations of the impact of climate change on tropical cyclones near Australia. *Climate Dynamics*, 22(1):47–56, 2004.

- Wardle, R. and Smith, I. Modeled response of the Australian monsoon to changes in land surface temperatures. *Geophysical Research Letters*, 31(16), 2004.
- Watanabe, M., Suzuki, T., O'ishi, R., Komuro, Y., Watanabe, S., Emori, S., Takemura, T., Chikira, M., Ogura, T., Sekiguchi, M., Takata, K., Yamazaki, D., Yokohata, T., Nozawa, T., Hasumi, H., Tatebe, H., and Kimoto, M. Improved Climate Simulation by MIROC5. Mean States, Variability, and Climate Sensitivity. *Journal of Climate*, 23(23):6312–6335, 2010.
- Xin, X.-G., Wu, T.-W., Li, J.-L., Wang, Z.-Z., Li, W.-P., and Wu, F.-H. How Well does BCC\_CSM1.1 Reproduce the 20th Century Climate Change over China? *Atmospheric and Oceanic Science Letters*, 6(1):21–26, 2013.
- Yukimoto, S., Adachi, Y., Hosaka, M., Sakami, T., Yoshimura, H., Hirabara, M., Tanaka, T. Y., Shindo, E., Tsujino, H., Deushi, M., Mizuta, R., Yabu, S., Obata, A., Nakano, H., Koshiro, T., Ose, T., and Kitoh, A. A New Global Climate Model of the Meteorological Research Institute: MRI-CGCM3-Model Description and Basic Performance. *Journal of the Meteorological Society of Japan*, 90A(SI):23–64, 2012.